

GEOMETRICAL ANALYSIS OF CENTRIFUGAL FORCE GENERATING ELECTRODE FOR THERMAL ADDITIVE CENTRIFUGAL ABRASIVE FLOW MACHINING PROCESS

A Thesis submitted in the partial fulfilment of requirement for the

Doctor of Philosophy

in

**The Department of
MECHANICAL ENGINEERING**

Submitted

By

Anant Bhardwaj

(2K19/PHDME/501)

Under the Supervision of

Prof. Rajiv Chaudhary

Dr. Krovvidi Srinivas



Department of Mechanical, Production & Industrial Engg. and Automobile Engg.

Delhi Technological University

Shahbad Daultpur, Main Bawana Road

Delhi-110042, India



DELHI TECHNOLOGICAL UNIVERSITY

Shahbad Daulatpur, Main Bawana Road

Delhi-110042 (India)

DECLARATION

I hereby declare that thesis entitled “**Geometrical Analysis of Centrifugal Force Generating Electrode For Thermal Additive Centrifugal Abrasive Flow Machining**” submitted by me in fulfillment of the requirement for the degree of Doctor of Philosophy to Delhi Technological University (Formerly Delhi College of Engineering) is a record of bona fide work carried out by me under the supervision of Dr. Rajiv Chaudhary, Professor, Department of Mechanical Engineering, Delhi Technological University and Dr. Krovvidi. Srinivas, Assistant Professor, Department of Mechanical Engineering, Delhi Technological University.

I further declare that the work reported in this thesis has not been published and will not be submitted, either in part or in full, for the award of any other degree or diploma in any other Institute or University.

(ANANT BHARDWAJ)

Roll No: 2K19/PHDME/501

Department of Mechanical Engineering

Delhi Technological University

Delhi - 110042



DELHI TECHNOLOGICAL UNIVERSITY

Shahbad Daulatpur, Main Bawana Road

Delhi-110042 (India)

CERTIFICATE

This is to certify that the work embodied in the *Thesis* entitled “**Geometrical Analysis of Centrifugal Force Generating Electrode For Thermal Additive Centrifugal Abrasive Flow Machining**” is a record of bona fide research work carried out by **Mr. Anant Bhardwaj (2K19/PhDME/501)** in fulfillment of requirements for the award of degree of **Doctor of Philosophy in Mechanical Engineering** specialization in **Production Engineering**. He has worked under our guidance and supervision and has fulfilled the requirement which, to our knowledge, have reached the requisite standard for submitting the thesis.

The results in this thesis have not been submitted in part or full at any other University or Institute for the award of any degree or diploma.

(Dr. Rajiv Chaudhary)

Professor
Mechanical Engineering Department
Delhi Technological University
Delhi-110042 (India)

(Dr. Krovvidi Srinivas)

Assistant Professor
Mechanical Engineering Department
Delhi Technological University
Delhi-110042 (India)



DELHI TECHNOLOGICAL UNIVERSITY

Shahbad Daulatpur, Main Bawana Road

Delhi-110042 (India)

ACKNOWLEDGEMENT

Firstly, I would like to express my gratitude to my Supervisors **Prof. Rajiv Chaudhary** and **Dr. Krovvidi Srinivas** for their pertinent support of my Ph.D. study and related research, for their patience, motivation and immense knowledge. Their valuable guidance and mentorship helped me in all the time of research and thesis writing.

Beside my supervisors, I would like to thank **Prof. S.K Garg**, DRC Chairman and HOD, Department of Mechanical Engineering for his valuable suggestions and encouragement. I am extremely thankful to **Prof. R.C Singh**, **Prof. Qasim Murtaza**, **Prof M.S Ranganath**, **Prof R.S Mishra**, **Dr. Sanjay Kumar**, **Dr. N yuvraj** and **Dr. Manjunath K** of Department of Mechanical Engineering, **Dr. Jayasimhadri. M** of Department of Applied Physics, Delhi Technological University for their constant encouragement.

I am extremely thankful to **Mr. Lakhan Kada**, **Mr. Roshan Kumar**, **Mr. Rahul. N. Mool**, **Mr. Sandeep Singh**, **Mr. Tekchand**, **Mr. Netram**, **Mr. Deepak**, **Mr. Virender kumar Sharma**, **Mr. Prince Sah**, **Mr. Sunil Kumar**, **Mr. Lallan Sinha**, **Mr. sanjay singh duhan**, **Mr. Rajesh Bohra**, **Mr. kishan** and **Mr. Manish** of department of mechanical engineering for their help. I would also like to thank **Mr Gagan Sharma** and **Mr Anurag** of Applied physics department of DTU for their help in testing.

I always got constant encouragement from **Prof. R.S Walia**, HOD PIED PEC Chandigarh and **Dr. Parvesh Ali**, Assistant Professor, GBU Greater Noida for their motivation during my Ph.D. I am extremely thankful to **Mr. Bandla Sheshvenkat Naidu**, **Mr Vinay Yadav**, **Mr Gaurav Mishra** and **Ms. Durvesh** for their constant support and help during my experimental and writing work and providing moral support.

I am indebted to my father **Dr. Ashutosh Bhardwaj** and mother **Mrs. Sarita Rani** for their encouragement. I am extremely thankful to my brother **Mr. Madhav Kant Bhardwaj** for creating amicable environment at the domestic front such that I would be able to concentrate on my work. I also express my sincere thanks to my fellow Ph.D. friends for their constant encouragement.

Lastly I would like to thank My uncle **Prof. Girish Kumar Sharma** who motivated me for Ph.D and dedicate this Thesis to my grandfather **Late Prof. V.K Sharma** who is a source of constant motivation for me.

Anant Bhardwaj

PREFACE

In this thesis titled “**Geometrical Analysis of Centrifugal Force Generating Electrode for Thermal Additive Centrifugal Abrasive Flow Machining Process**” the effect of geometry centrifugal force generating electrode on the material removal and percentage improvement in surface finish is analyzed. The thesis includes modelling and simulation along with the experimentation with different CFG electrode and a novel spline shape electrode with the curved blade is proposed.

Chapter 1 includes the description of abrasive flow machining along with its hybrids develop so far. The chapters discuss about the TACAFM process which is the latest hybrids of AFM along with its process parameters, advantages and the novelty of the work.

Chapter 2 compiles the accounts of various research work on abrasive flow machining and its applications. The accounts describing the hybridization, development of media, fixture and tooling, mathematical modelling and the industrial application of the process is highlighted. The chapter is concluded with the research gap followed by the objectives of the present study.

Chapter 3 contains the detail description of the experimental setup including the equipment’s ratings, functions and the dimensions of the different CFG electrodes and the workpiece. The chapter also contains the detail description of the fixture used for holding the workpiece and also contains methodology adopted for the investigations.

Chapter 4 deals with the media used in the TACAFM process. The chapter deals with the preparation of media and its property. The proposed media is a mixture of polymer, gel and abrasives. The chapter deals with the preparation of polymer, gels and media and also study their requisite rheological property using the rheometer. The FTIR analysis of the proposed media is done for the analysis of polymeric linkage of the media.

Chapter 5 involves the modeling and simulation to check the feasibility of different shape of electrode for the TACAFM process. The TACAFM process with different electrode geometry is analyzed on ANSYS Fluent to justify the spark formation and to analyze the flow parameters. The variation of pressure and temperature on the brass workpiece is analyzed which gave the idea of material removal for the TACAFM process and the temperature distribution validates the spark formation.

Chapter 6 involves the experimentation to analyse the effect of the different electrode geometry on the material removal and on the surface finish of the workpiece during the

TACAFM process. The experiments are designed on the basis DOE based on RSM Methodology. The chapter discussed RSM methodology and process parameters used in the TACAFM process. The Discussion about parameters affecting the material removal and percentage improvement in surface finish is also discussed in this chapter.

Chapter 7 includes the results of the various tests performed on the finished workpiece machined by the TACAFM with the help of spline shape electrode with the curved blade. The chapter discuss the morphology of finished brass surface with the help of optical micrograph taken by optical microscope, surface roughness plot taken by Taylor Hobson tallysurf, SEM image taken from scanning electron microscope, X ray diffraction and the EDAX plot. The chapter also discuss the advantage of the new proposed CFG electrode with curved blade over the conventional spline shape electrode with straight blade and also validates the experimentation process.

Chapter 8 includes the overall conclusions of the study and includes key points of the literature review, media preparation, modelling and simulation, experimental analysis and the results and validation section. The chapter also discussed about the future scope of the study in brief.

The report is concluded with the list of references referred during the investigation and the list of publication achieved from the present work.

List of Figures

Figure 1 Non-Conventional Machining processes	2
Figure 2 Variants of AFM 2(i) One-way AFM 2 (ii) Two – way AFM (iii) Orbital AFM	3
Figure 3 Different hybrids of AFM (i) Magnetic force assisted AFM (ii) Ultrasonic vibrations (iii) Centrifugal force assisted abrasive flow machining process (iv) Rotational AFM	5
Figure 4 Hybrids of AFM (i) Drill-bit guided AFM (ii) electrochemical AFM (iii) Helical AFM (iv) Hybrid of Electrochemical and centrifugal force assisted AFM	5
Figure 5 Hybrid of centrifugal and magnetic force assisted AFM (ii) Mechanism of Thermal Additive Centrifugal Force Assisted AFM	6
Figure 6 Geometrical Shape of the electrode (i) Straight spline electrode (ii) Triangular shape electrode (iii) square shape electrode (iv) spline shape electrode with curved blade	9
Figure 7 Major area of Literature review of AFM process.....	11
Figure 8 Schematic diagram of experimental setup.....	28
Figure 9 Experimental setup	29
Figure 10 EDM Power supply and EDM Controller (ii) 3-Phase Induction Motor with Power Drive (iii) Fixture with terminal (iv) Conventional AFM Setup (v) Side view	31
Figure 11 Detail description of Nylon fixture.....	32
Figure 12 Proposed Electrodes Spline electrode with straight blade (ii) Spline electrode with curved blade (iii) triangular electrode (iv) brass workpiece (v) Top view of spline electrode with curved blade (vi) Square electrode	33
Figure 13 Fixture and equipment (i) and (ii) detail of fixture used (iii) Precision Balance (iv) Taylor Hobson Tally surf.....	34
Figure 14 Methodology used in the investigations	36
Figure 15 Compact Rheometer for viscosity	39
Figure 16 Engine oil based gel sample	42
Figure 17 Viscosity Vs Shear rate for engine oil	44
Figure 18 Shear stress vs Shear rate for engine oil	45
Figure 19 Transformer oil based gel	46
Figure 20 Viscosity vs Shear rate for transformer oil.....	47
Figure 21 Shear stress vs shear rate for transformer oil.....	48
Figure 22 hydrocarbon oil based gel.....	49
Figure 23 Viscosity Vs shear rate for hydrocarbon oil	51

Figure 24 Shear stress Vs Shear rate for hydrocarbon oil.....	52
Figure 25 Different samples of Gel (i) Hydrocarbon oil sample gel (ii) Engine oil sample Gel (iii) Transformer oil sample gel (iv) Setup for gel preparation	53
Figure 26 Viscosity vs shear rate for polymer	56
Figure 27 Shear Stress vs Shear rate for polymer	57
Figure 28 Preparation of Media (i) Equipment used for the preparation (ii) preparation of polymer (iii) preparation of gel (iv) mixing of polymer and gel by hand (v) mixing of abrasive particle (vi) Freshly prepared media for TACAFM process.	58
Figure 29 Viscosity vs shear rate for the media.....	60
Figure 30 Shear stress with respect to shear rate	60
Figure 31 FTIR analysis of the Prepared Media	61
Figure 32 Solid Model of Workpiece on CREO Parametric	65
Figure 33 Solid Model of Media used in investigation.....	66
Figure 34 Solid Model of square electrode used in investigation.....	67
Figure 35 Solid Model of Triangular electrode used in investigation	68
Figure 36 Solid Model of Spline Shape Electrode with straight blade used in investigation.....	69
Figure 37 Solid Model of spline shape electrode with curved blade used in investigation.....	70
Figure 38 Square shape CFG electrode assembly.....	71
Figure 39 Triangular shape CFG electrode Assembly.....	72
Figure 40 Triangular shape CFG electrode assembly.....	73
Figure 41 Spline shape CFG electrode Assembly	73
Figure 42 Schematic diagram of square shape electrode.....	75
Figure 43 Schematic diagram for triangular shape electrode	75
Figure 44 Mechanism of spark formation for spline shape electrode with curved blade	76
Figure 45 Mechanism of TACAFM process with square electrode	76
Figure 46 Mechanism of TACAFM Process with triangular electrode	77
Figure 47 Geometry of the square shape electrode in design modular in Ansys Fluent	78
Figure 48 Geometry of the triangular shape electrode in design modular in Ansys Fluent	78
Figure 49 Geometry of the square shape electrode in design modular in Ansys Fluent	79
Figure 50 Meshing of electrode assembly	80
Figure 51 Meshing of workpiece	81
Figure 52 Meshing of square shape electrode.....	81
Figure 53 Meshing of square shape electrode with the workpiece	82
Figure 54 Meshing of spline shape electrode.....	82

Figure 55 Meshing of spline shape electrode with the workpiece	83
Figure 56 Meshing of triangular shape electrode.....	83
Figure 57 Meshing of triangular shape electrode with workpiece.....	84
Figure 58 ANSYS Fluent Setup.....	85
Figure 59 Boundary condition highlighting inlet, outlet, workpiece and the CFG electrode..	86
Figure 60 Boundary condition for the Stationary wall	87
Figure 61 Conversion curve showing Energy, continuity, X,Y and Z velocity trends on residual Vs iterations curves	88
Figure 62 Pressure distribution for the straight spline electrode at stationary condition.....	89
Figure 63 Temperature distribution over the workpiece with straight spline electrode at stationary conditions	90
Figure 64 Pressure distribution over the workpiece with Spline shape electrode with straight blade at rotation of the electrode.....	91
Figure 65 Temperature distribution over the workpiece by spline electrode with straight blade during the rotation of CFG electrode at 100 rpm	92
Figure 66 Conversion curve of spline electrode with curved blade.....	93
Figure 67 Pressure distribution over the workpiece by spline shape electrode with curved blade at stationary condition.	94
Figure 68 Temperature distribution over the workpiece by the Spline shape electrode with curved blade during the stationary condition of the electrode	95
Figure 69 Streamline pattern of the media for spline shape electrode.....	96
Figure 70 Pressure distribution inside the media with spline shape electrode.....	97
Figure 71 Temperature distribution inside the media with the spline shape electrode.....	98
Figure 72 Pressure distribution over the workpiece due to spline electrode with curved blade at 100 rpm rotation.....	99
Figure 73 Temperature distribution over the workpiece by the spline shape electrode with the curved blade at 100 rpm rotation of the electrode	99
Figure 74 Streamline pattern of the spline shape electrode with curved blade at 100 rpm rotation	100
Figure 75 Temperature distribution inside the media during the 100 rpm rotation of the spline shape electrode with the curved blade	101
Figure 76 Pressure difference inside the media with spline shape electrode with curved blade at 100 rpm rotation of the electrode	102
Figure 77 Conversion curve for square shape electrode at stationary condition	103

Figure 78 Pressure distribution over the workpiece by square shape CFG electrode at the stationary condition.....	104
Figure 79 Temperature distribution of the square shape CFG electrode at the stationary condition of the electrode.....	105
Figure 80 Stream line distribution of the media in TACAFM process with square shape CFG electrode at stationary condition of CFG electrode	106
Figure 81 Pressure distribution inside the media with square shape electrode at stationary condition of the electrode during the TACAFM process.....	107
Figure 82 Temperature distribution inside the media with square shape electrode at stationary condition of the electrode during the TACAFM process.....	107
Figure 83 Conversion curve for rotation of the square electrode	108
Figure 84 Pressure distribution over the workpiece by TACAFM process by square shape electrode with 100 rpm rotation of the electrode	109
Figure 85 Temperature distribution over the workpiece by TACAFM process by square shape electrode with 100 rpm rotation of the electrode.	110
Figure 86 Stream line distribution of the media in TACAFM process with square shape CFG electrode at the rotation of 100 rpm of CFG electrode	111
Figure 87 Pressure distribution inside the media with square shape electrode at 100 rpm rotational condition of the electrode during the TACAFM process	111
Figure 88 Temperature distribution inside the media with square shape electrode at 100 rpm rotation	112
Figure 89 Conversion curve for triangular electrode at stationary conditions.....	113
Figure 90 Pressure distribution over the workpiece at TACAFM process by the triangular shape CFG electrode at stationary condition	114
Figure 91 Temperature distribution over the workpiece by triangular shape CFG electrode at stationary condition.....	115
Figure 92 stream line pattern of the media flow in TACAFM Process by triangular shape CFG electrode at stationary condition	115
Figure 93 Temperature distribution inside the media during the TACAFM process at stationary condition of the CFG electrode.	116
Figure 94 Pressure distribution inside the media during the TACAFM process at stationary condition of the CFG electrode.....	117
Figure 95 Conversion curve for triangular electrode at rotation of 100 rpm.	118

Figure 96 Pressure distribution over the workpiece at TACAFM process by the triangular shape CFG electrode at rotation of CFG electrode at 100 rpm.....	119
Figure 97 Temperature distribution over the workpiece by triangular shape CFG electrode at rotation of CFG electrode at 100 rpm	119
Figure 98 stream line pattern of the media flow in TACAFM Process by triangular shape CFG electrode at 100 rpm of the CFG electrode	120
Figure 99 Pressure distribution inside the media during the TACAFM process at stationary condition of the CFG electrode.....	121
Figure 100 Temperature distribution inside the media during the TACAFM process at stationary condition of the CFG electrode.	121
Figure 101 Response surface Methodology flow chart	124
Figure 102 Actual Vs Predicted Value for MR.....	129
Figure 103 Perturbation curve for MR.....	129
Figure 104 Effect of shape of electrode on material removal	130
Figure 105 Effect of Supply current on the material removal	131
Figure 106 Effect of Duty Cycle on material removal.....	132
Figure 107 Effect of rotational speed on material removal	132
Figure 108 Effect of supply current and electrode type on material removal.....	133
Figure 109 Effect of Duty cycle and electrode on material removal	134
Figure 110 Effect of rotational speed and electrode on material removal	135
Figure 111 Effect of duty cycle and supply current on material removal.....	135
Figure 112 Effect of Rotational speed and supply current on Material removal	136
Figure 113 effect of rotational speed and duty cycle on material removal.....	137
Figure 114 Predicted and experimental value for the percentage improvement in surface finish	139
Figure 115 Perturbation curve for the percentage improvement in surface finish.....	140
Figure 116 Effect of type of electrode on percentage improvement in surface finish.....	141
Figure 117 Effect of supply current on the percent improvement in surface finish	141
Figure 118 Effect of Duty cycle on the percentage improvement in the surface finish	142
Figure 119 Effect of rotational speed on the percentage improvement in surface finish	143
Figure 120 Effect of type of electrode and supply current on the percentage improvement in surface finish.....	143
Figure 121 Effect of duty cycle and electrode on the percentage improvement in surface finish	144

Figure 122 Effect of electrode and rotational speed on percentage improvement in surface finish	145
Figure 123 Effect of supply current and duty cycle in percentage improvement in surface finish	145
Figure 124 Effect of supply current and rotational speed on percentage improvement in surface finish.....	146
Figure 125 Effect of duty cycle and rotational speed on percentage improvement in surface finish	147
Figure 126 Comparison of material removal of TACAFM process with different shape of CFG electrodes.....	151
Figure 127 Comparison of percentage improvement in surface finish of TACAFM process with different geometry of CFG electrode.....	151
Figure 128 Micrograph without polishing (a) and (b) 100 X magnification, (c) and (d) 200 X magnification	153
Figure 129 Polished micrograph (a) and (b) 100 X magnification (c) and (d) 200 X magnification	154
Figure 130 Polished Structure with etchant (a) and (b) 100X magnification (c) and (d) 200X magnification	155
Figure 131 Image of Brass surface (i) Un finished Surface (ii) Finished surface (iii) Uniform Spark Marks (iv) Finished Surface	156
Figure 132 XRD Pattern of the workpiece (i) before finishing (ii) After finishing.....	157
Figure 133 EDAX of the workpiece (a) Area of consideration (b) Graph highlighting the peak of the constituent element (c) table showing the weight percent of the constituent elements	158
Figure 134 Surface roughness plots (a), (b) and (c) plots before machining (d),(e) and (f) plots after machining.....	159
Figure 135 Material removal mechanism of electrode (a) spline shape electrode with straight blade (b) mechanism of material removal with primitive tool (c) Top view of the spline shape electrode with curve blade (d) Mechanism of material removal by proposed electrode	161

List of Tables

Table 1	Technical Specification of the equipment.....	35
Table 2	Property of Rheometer	40
Table 3	Engine oil viscosity trends	42
Table 4	Viscosity trend for transformer oil	46
Table 5	Viscosity trends for hydrocarbon oil.....	50
Table 6	Viscosity data for Polymer.....	55
Table 7	Viscosity data corresponding to rheometer.....	59
Table 8	Meshing details	80
Table 9	Materials and their Property	85
Table 10	Boundary conditions	87
Table 11	Factor levels of CCD.....	125
Table 12	Model Analysis	125
Table 13	Analysis of Response in RSM CCD methodology	125
Table 14	Scheme and results of Central Composite Design	126
Table 15	ANOVA for Quadratic model for MR	128
Table 16	ANNOVA table for the percentage improvement in surface finish.....	138
Table 17	Optimal Values and results	148

Table of Contents

DECLARATION	i
CERTIFICATE	ii
ACKNOWLEDGEMENT	iii
PREFACE	iv
List of Figures	vi
List of Tables	xii
Abstract.....	xvi
Chapter 1. Introduction	1
1.1. Background	1
1.2. Abrasive Flow Machining	3
1.3. TACAFM Process	6
1.4. Process Parameters of TACAFM Process	7
1.5. Effect of Geometry of CFG Electrode	8
1.6. Proposed Novel Electrode	9
1.7. Motivation for this research work	10
Chapter 2. Literature Review	11
2.1. Background	11
2.2. Literature review	12
2.3. Recent development in AFM	25
2.4. Research Gap	27
2.5. Research objective	27
Chapter 3. Experimental Setup Electrode and Fixture Development.....	28
3.1. Experimental Setup	28
3.2. Conventional AFM setup.....	29
3.3. Three- Phase Induction Motor	30
3.4. Frequency control Power drive.....	30
3.5. EDM controller and Power supply	30
3.6. Fixture	30
3.7. CFG Electrode and the workpiece.....	32
3.8. Measurement of Surface Roughness and Material Removal	33
3.9. Methodology.....	36
Chapter 4. Media Preparation and Characterization.....	38
4.1. Introduction	38
4.2. Viscosity	38
4.3. Elasticity	38

4.4.	Viscoelasticity.....	38
4.5.	Viscosity Measurement.....	39
4.6.	Constituent of the Media.....	40
4.7.	Preparation of gel	41
4.8.	Engine oil.....	41
4.9.	Transformer oil	45
4.10.	Hydrocarbon oil.....	49
4.11.	Selection of Gel material and preparation.....	52
4.12.	Preparation of polymer.....	54
4.13.	Preparation of Media	57
4.14.	FTIR of Media	61
Chapter 5. Computational Modelling of TACAFM Process		63
5.1.	Background	63
5.2.	Effect of flow parameter	64
5.3.	Extrusion Pressure	64
5.4.	Media Flow Rate	64
5.5.	Abrasive Concentration	64
5.6.	CFG electrode rotation.....	64
5.7.	Solid Modelling of TACAFM Process	65
5.7.1.	Workpiece	65
5.7.2.	Media	66
5.7.3.	Centrifugal Force Generating Electrode	66
5.8.	Assembly of the CFG different shaped CFG electrode.....	70
5.9.	Analysis of TACAFM process	77
5.10.	Meshing of TACAFM Process	79
5.11.	ANSYS Fluent setup	84
5.12.	Boundary conditions	85
5.13.	Simulation Results.....	88
5.13.1.	Spline Shape electrode with straight blade	89
5.13.2.	Spline shape electrode with curved blade	93
5.14.	Square shape CFG electrode.....	102
5.14.	Triangular shape CFG electrode.....	112
Chapter 6. Experimentation.....		123
6.1.	Background	123
6.2.	Response Surface Methodology	123
6.3.	Effect of Process parameters on Material Removal	127

6.4. Effect of Process Parameters on percentage improvement in Surface finish	137
6.5. Confirmation Experiment.....	147
Chapter 7. Results, Discussion and validation	150
7.1. Background	150
7.2. Morphology of Finished Brass Surface	152
7.2.1. Optical Micrograph	152
7.2.2. SEM Images.....	155
7.2.3. X-Ray Diffraction	156
7.2.4. EDAX analysis	157
7.3. Surface Roughness Plots	158
7.4. Advantage of Curved spline shape electrode over straight blade.....	159
Chapter 8. Conclusion and Future Scope of Work.....	163
8.1. Conclusions	163
8.2. Future Scope	166
References	167
Research Publications in SCI/SCIE Journals.....	180
Publication in scopus/ peer review.....	180
Conferences attended	180

Abstract

Abrasive flow machining (AFM) is one of the prominent method to finish the hollow intrinsic surface which are hard to reach by the conventional tools. The process has significant applications but low machining time is the major limitation of the process. To limit this various hybrid have developed and Thermal additive centrifugal abrasive flow machining (TACAFM) is the new name in the list. The TACAFM process uses the advantage of heat energy produced by the spark and the centrifugal force assisted abrasive flow machining process for enhancing the material removal through melting and erosion process. The spark is generated due to the EDM effect produced by supplying pulse DC supply between the workpiece and centrifugal force generating (CFG) electrode placed coaxially between the hollow workpiece whose internal surface is to be machined. This CFG electrode plays vital role in the efficient working of TACAFM process. The media containing the abrasive acts as a dielectric and supports the spark formation. The present investigation deals with the improvement of TACAFM process by improving CFG electrode, fixture design, media and by analyzing computational model of TACAFM process. The initial CFG electrode used in the process is spline shape electrode with straight blade. To improve the working efficiency of the process different geometrical shape of CFG electrode (rectangular, triangular, spline shape with straight blade, spline shape with curve blade) is proposed in this investigation. The experiments were performed on brass workpiece and the media with desirable property is prepared. Different base oil including (transformer oil, engine oil and Hydrocarbon oil) were studied using rheometer and hydrocarbon oil was chosen for media preparation on the basis of viscosity analysis. ANSYS Fluent is used to analyze the spark generation and study the flow parameters. The experimental results were analyzed using central composite design based on response surface methodology. The electrode type, supply current, duty cycle and the rotational speed of electrode is taken as the process parameter and their effect of material removal and percentage improvement in surface finish is analyzed. The simulation results were in agreement with the experimental results. The investigation showed that the spline shape electrode with curved blade showed maximum MR with significant improvement in percentage improvement in surface finish. The morphological study of brass showed the machining marks and spark proof. The different XRD pattern and EDAX also highlights the spark generation process.

Chapter 1. Introduction

In this chapter various machining process are discussed and the prominent Abrasive Flow Machining Process for machining of the internal surfaces is brought into the picture. The chapter also discussed the development of hybrids form of AFM along with the advantage of novel TACAFM process and the motivation behind choosing the topic. The chapter also includes process parameters involves in the development of novel TACAFM process and background for selecting the proposed electrode.

1.1. Background

The present era is an era of manufacturing and more precisely finishing. The term manufacturing is an old concept which has historical evidence. The term machine is associated with the mechanized system which got popularized during the industrial revolution took place in England. The initial phase of the manufacturing and machining processes were attributed to the development of the weapons of warfare (artillery, guns, canon and the bullets) and the modes of transportation which broadly includes shipbuilding and railways. Considering the brief background, on the basis of application, the manufacturing process may be divided into primary manufacturing and secondary manufacturing. Primary manufacturing includes manufacturing application that is based on forming, casting techniques and the powder metallurgy, which aims to provide basic shapes and size as per the industrial requirements. The other group is the secondary manufacturing which broadly includes the machining process aiming for dimensional accuracy, close tolerances and desired surface finish. The processes involve in this group are machining operation by conventional and non-conventional processes. The term conventional and non-conventional energy resources are based on the contact between the tool and the workpiece. Here the tool is harder than the workpiece and the machining operation takes place due to the relative motion between the tool and workpiece. The nonconventional manufacturing process involves conventional machine tools operation like milling, turning, drilling, shaping is some example. Considering non-conventional machining process, the main parameter is the non-contact between the tool and the workpiece. This involves the inclusion of mechanical, electrical, electrochemical energy processes, thermochemical and the combination of these processes to get the desire shape and dimensional tolerances.

Figure 1 demonstrate the basic classification of the non-conventional machining processes. The classification is based on the basic mechanism, sources of intermediate energy, transfer energy

medium and the energy processes. The non-conventional machining processes are classified on the basis of available energy sources which includes mechanical, electrochemical, chemical and thermos-electric energy, the process based on mechanical energy involves Mechanical Counter Grinding, Ultrasonic machining, abrasive jet machining. When we consider electrochemical energy, the prominent examples are electrochemical grinding (ECG), electrochemical machining (ECM). When energy based on the chemicals are consider, then chemical machining and chemical etching is the prominent machining processes. Thermoelectric energy interactions involve processes like electrical discharge machining (EDM), electron beam machining (EBM), laser beam machining (LBM) when the basic mechanism of material removal is vaporization while ion beam machining and plasma arc machining is used when the basic mechanism is erosion (**Jain et al. 2009**).

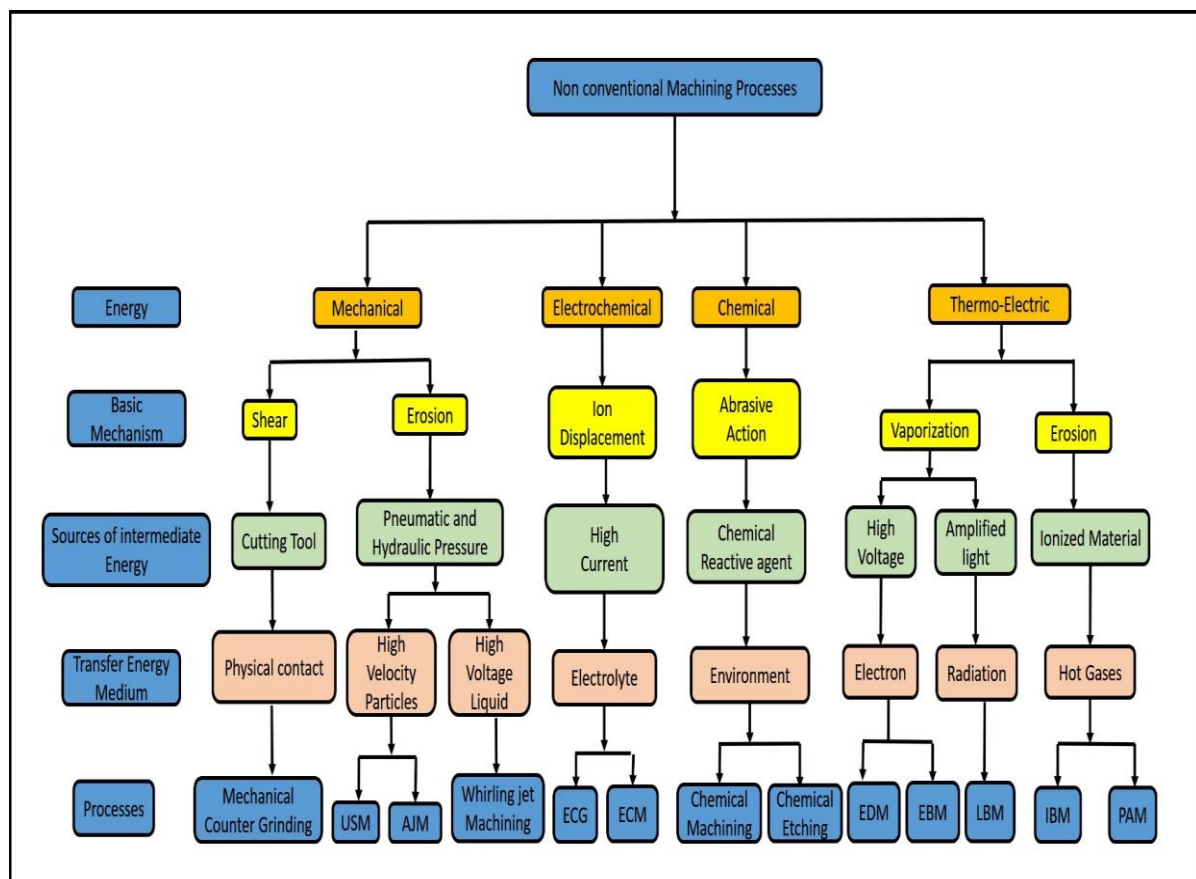


Figure 1 Non-Conventional Machining processes

The above listed modern machining technique find their applications in recent machining processes for the machining of metals, non-metals, alloys and the composites. But when it comes to machining of internal surfaces, abrasive flow machining (AFM) is the aggressor. As the machining of hollow intrinsic part is difficult when we consider conventional machining

tool like lapping, honing and the surface finishing operations. This is because of the inability of the conventional tool to finish the desired internal surface of the tool.

1.2. Abrasive Flow Machining

Abrasive flow machining is a non-conventional machining process which uses an abrasive based media for machining the internal surface of the workpiece. The conventional abrasive flow machining process involves the finishing of internal surface through the abrasion process due to interaction of the abrasive particles present in the media and the wall of the workpiece. The media consist of polymer, abrasive and gel which together makes it a viscous medium capable of holding the abrasive for the finishing process. The workpiece whose internal surface is to be finished is placed co-axially between the upper and lower cylinder through which the media is flows due to the pressure difference. On the basis of the configuration, there are three variants of AFM which are one-way AFM, two- way AFM and the orbital AFM. Figure 2 shows the various variants of TACAfm process. Figure 2 (i) shows the one way AFM where the extrusion media is extruded in one direction, figure 2 (ii) shows the two way AFM where the media is extruded from the lower side to the upper side and vice-versa and figure 2 (iii) shows the orbital AFM where low amplitude vibrations are provided to the media which enhances the interaction of the media particle with the wall of the workpiece, which enhances the MR and provides desired surface finish.

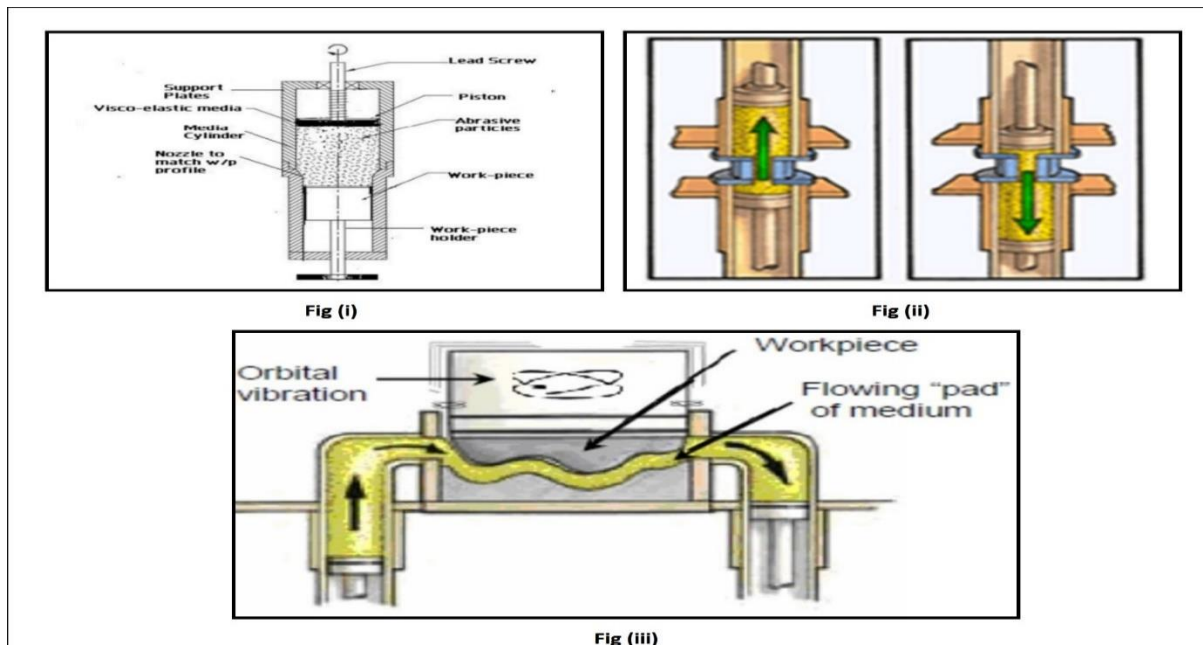


Figure 2 Variants of AFM 2(i) One-way AFM 2 (ii) Two – way AFM (iii) Orbital AFM (Bhardwaj et al. 2019).

Though AFM provides finishing upto nano level but low MR and considerable machining time is the major limitation of the process. To cater this limitation of AFM different hybrids are developed which includes centrifugal force-assisted AFM (**Walia et al. 2006**), helical AFM (**Brar et al. 2013**), ultrasonic AFM (**Sharma et al. 2015**), drill-bit guided AFM (**Sankar et al. 2009**), rotational AFM (**Sankar et al. 2010**), magnetic force assisted AFM (**Singh et al. 2002**), electrochemical force assisted AFM (**Dabrowski et al. 2006**), hybrid of centrifugal and magneto force assisted AFM (**Singh et al. 2015**), Hybrids of centrifugal and electrochemical force assisted AFM (**Vaishya et al. 2015**) and the thermal additive centrifugal abrasive flow machining process (**Ali et al. 2020, 2022**). In centrifugal force assisted AFM, an extra centrifugal force is provided when a rotating rod is co-axially placed along the workpiece. This rotating rod provides circular motion to the media which in turn results in the increase in the dynamic number of active abrasive particles resulting in the increase in the enhancement of MR. The similar concept takes place for the helical and drill-bit guided AFM where the rotating helical rod provides centrifugal action along with the restricted passage of the media flow which increases the MR. In rotational AFM the workpiece is given rotation instead of the rod which results in the finishing process. The magnetic force assisted AFM use the magnet surrounding the workpiece. These magnets the attracts the media particles which contains carbonyl particles in the media resulting in the abrasion process. The advantage of magnetic force assisted AFM and the centrifugal force assisted AFM is clubbed in the hybrid of magneto and centrifugal AFM. When the media is made alcoholic by adding sodium iodide and potassium iodide, then anodic dissolution of the workpiece takes place. This process is called electrochemical force assisted AFM. When electrochemical force assisted AFM clubs with the centrifugal action of the workpiece, the process is called hybrids of electrochemical and centrifugal force assisted AFM. The latest hybrid of AFM is TACAFM process where the media is converted to dielectric by adding the kerosene and hydrocarbon based media. Also the gap between the electrode and the workpiece is made very less up to 0.1 mm. The electrode is given negative supply through pulsed DC and the workpiece is made positive. Thus the machining takes place due to the spark generation and the abrasion process of the centrifugal force generating electrode.

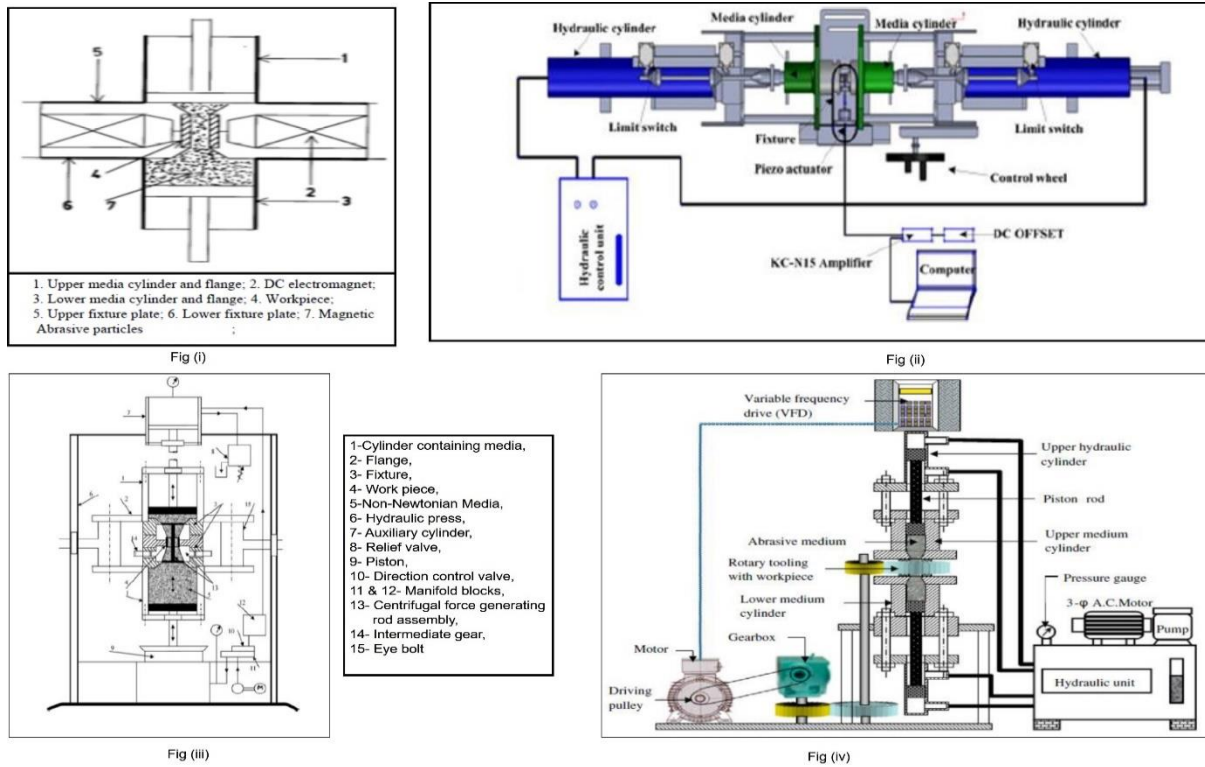


Figure 3 Different hybrids of AFM (i) Magnetic force assisted AFM (ii) Ultrasonic vibrations (iii) Centrifugal force assisted abrasive flow machining process (iv) Rotational AFM (Bhardwaj et al. 2019)

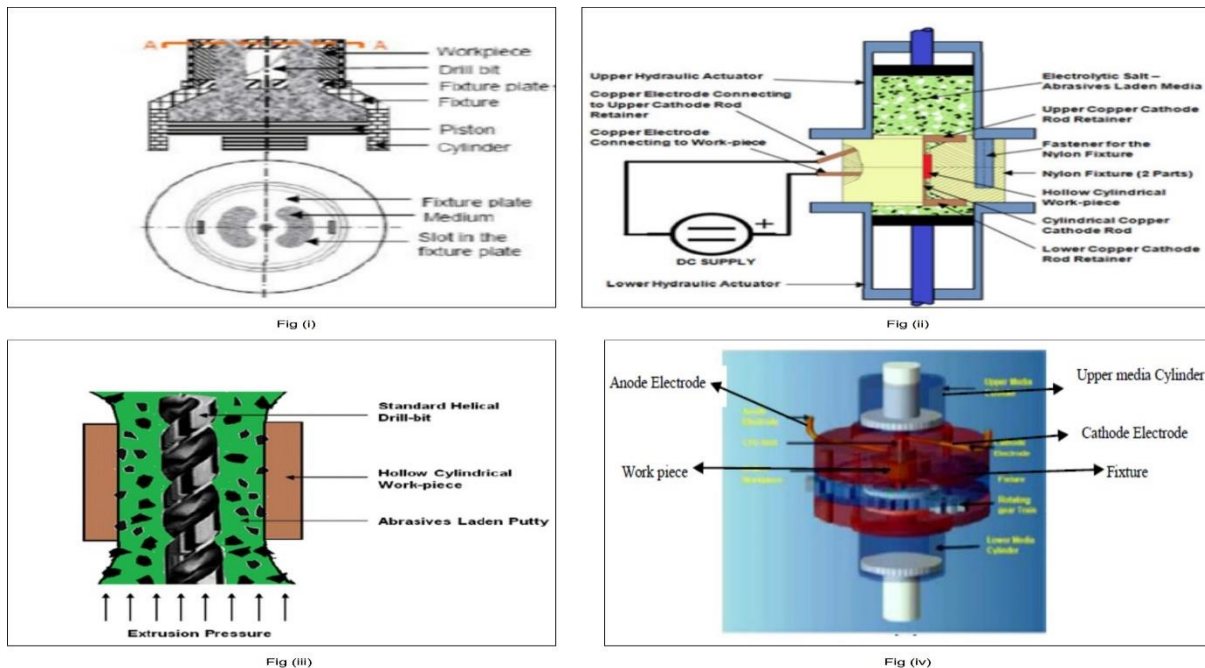


Figure 4 Hybrids of AFM (i) Drill-bit guided AFM (ii) electrochemical AFM (iii) Helical AFM (iv) Hybrid of Electrochemical and centrifugal force assisted AFM (Bhardwaj et al. 2019)

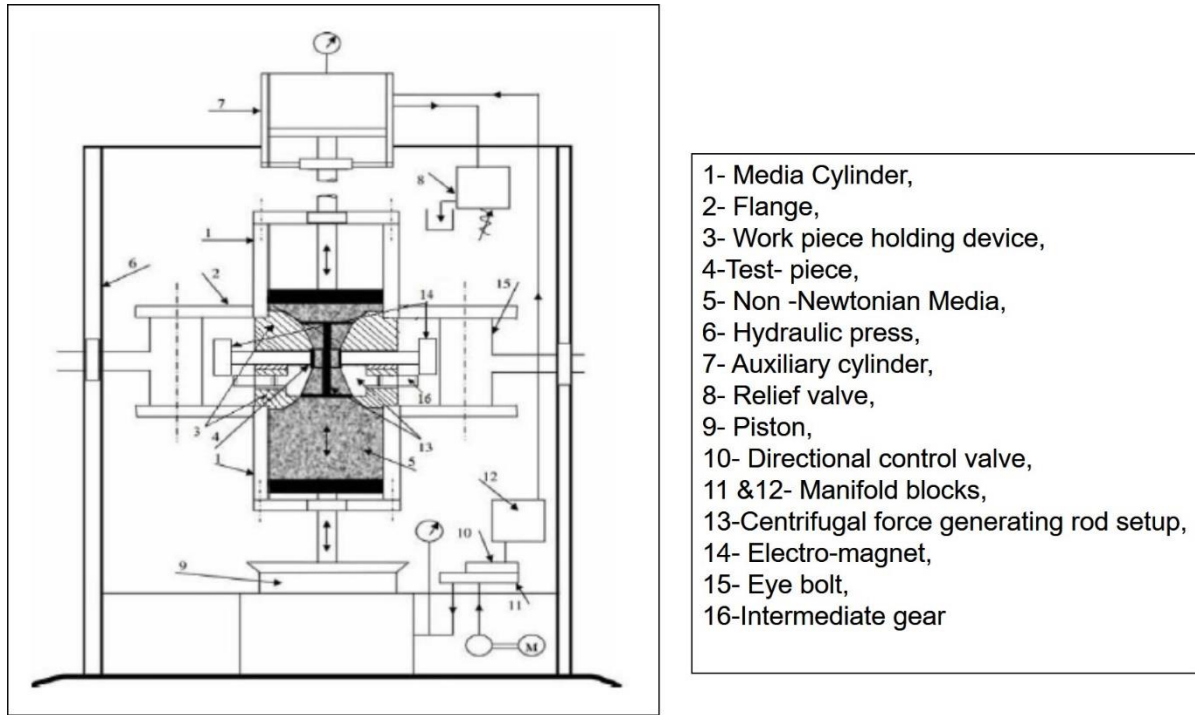


Fig (i)

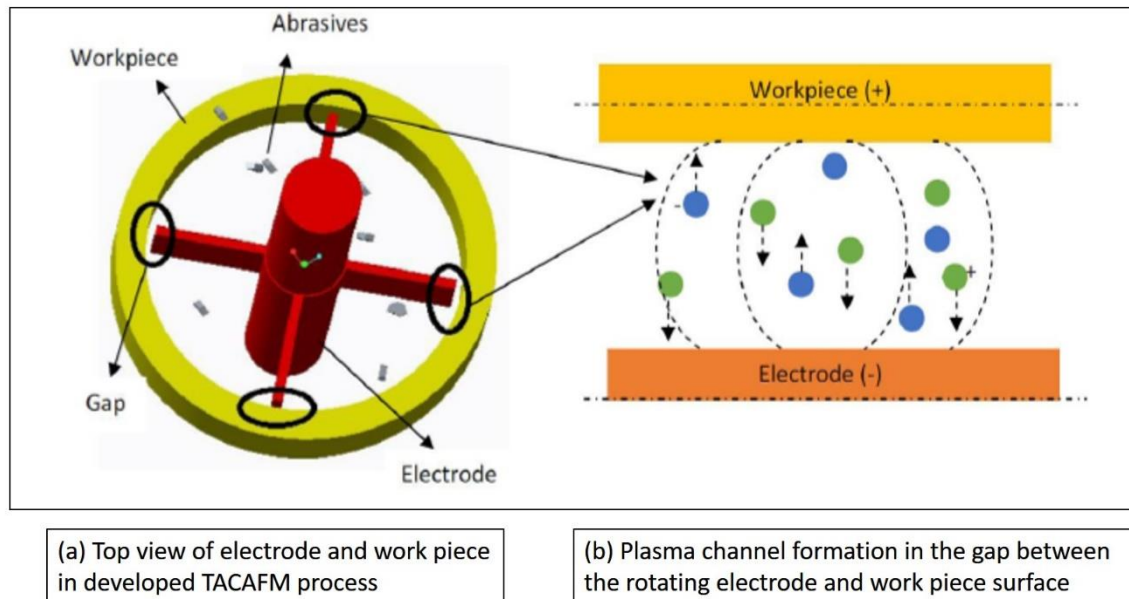


Fig (ii)

Figure 5 Hybrid of centrifugal and magnetic force assisted AFM (ii) Mechanism of Thermal Additive Centrifugal Force Assisted AFM (Ali et al. 2022)

1.3. TACAAM Process

TACAAM (Ali et al. 2020) is a recent hybrid of AFM that uses the advantage of spark energy produced due to the EDM effect, centrifugal force due to the centrifugal force generating (CFG) electrode and the axial force due to the extrusion of media. The process combines CFAAFM, the spark EDM process, and the conventional AFM process (extrusion of media containing

abrasive, polymer and gel). The requisite gap required for the spark formation between the CFG electrode and the workpiece is maintained by the EDM controller and the EDM power supply provides the pulse direct current (DC) that initiates the spark's spark formation. Figure 5 (ii) shows the arrangement of electrodes placed coaxially between the hollow cylindrical workpiece whose internal surface is to be machined. The electrode and workpiece assembly is enclosed by the media cylinder in which a highly viscous media containing abrasives, polymer and gel is extruded within the internal surface of the workpiece due to pressure difference. This extrusion of media results in the abrasion action of abrasive on the internal surface of the workpiece resulting in the MR. The material removal process is further strengthened by the rotation of the electrode which develops centrifugal action on the media particle increasing the dynamic number of abrasive particles near the wall of the workpiece. During the TACAFM process the pulsed DC supply is provided between the electrode and the workpiece and a very small gap of about 0.1 to 1 mm is maintained. This pulsed DC supply along with a very small gap results in the spark formation due to the EDM effect and the thermal energy is added to the process which results in MR through melting. Hence an effective machining takes place by the combination of abrasion and melting mechanism. When the pulsed DC is supplied between the terminals, containing the workpiece with positive polarity and the CFG electrode having negative polarity, the electrons on the electrodes tend to move towards the workpiece surface due to the similar repulsive nature of similar polarity. These electrons strike the media particles resulting in ionisation of the media particles and with the increases in the current, the electrons increase, resulting in the formation of plasma channels. As the concentration of ions becomes significantly large, this plasma channel transforms into a spark. The spark is generated uniformly around the three gaps between the electrode and the workpiece and results in the MR through the process of melting and erosion from the surface of the workpiece. Figure 5 (ii) highlights the mechanism of spark formation. Figure 5 (ii) (a) shows the top view of the spark formation by showing the top view of the electrode and workpiece inside the fixture. Figure 5 (ii) (b) shows the plasma formation mechanism and the spark formation in the media. The development of TACAFM process enhances surface finish and provides less machining time which is the major limitation of the conventional AFM.

1.4. Process Parameters of TACAFM Process

The TACAFM process consists of combination of EDM and centrifugal force assisted AFM, thus the individual process parameters of both these process comes into account. For the spark EDM process, the supply current and the duty cycle are the prominent parameters while for the

TACAFM process, the abrasive concentration, abrasives mesh size, types of abrasive, media flow rate, extrusion pressure of the media cylinders, geometry of the CFG electrode and the rotational speed of the CFG electrode are the prominent factor which effects the surface finish and the MR in the TACAFM process.

1.5. Effect of Geometry of CFG Electrode

The geometry of the centrifugal force generating electrode plays a vital role in the working of TACAFM process as it does 2 tasks. Firstly, it provides restrictive path in the direction of the media flow. This restrictive path increases pressure on the workpiece and also increases the dynamic number of active abrasive particles and increases the workpiece abrasive interactions which enhances the MR. Also the rotation of the centrifugal force generating electrode provide centrifugal action to the media which results in the increase in the MR. The third most prominent function of the electrode is that it acts as an anode which results in the spark generation. The spark generated results material removal through melting and ablation and result in more material removal. Also the rotation of the electrode results in the uniform spark travel along the surface of the workpiece. Thus electrode geometry plays a vital role in the material removal process.

The present study involves the analysis of TACAFM process with different electrode geometry which includes triangular electrode, square electrode, spline shape electrode. Each type of electrode has its specific advantage. The square shape electrode gives uniform spark distribution (**Walia et al. 2006**) while the triangular electrode gives maximum surface roughness with same extrusion pressure (**Walia et al. 2006**). The spline shape electrode contains longitudinal grooves which provides a suitable path for the media flow (**Walia et al. 2008**). The initial investigation on the TACAFM process was done with the spline shape electrode with the straight blade. The present investigation also proposes a novel spline shape electrode with the curved blade. Figure 6 shows the shapes of the various CG electrode in the present study.

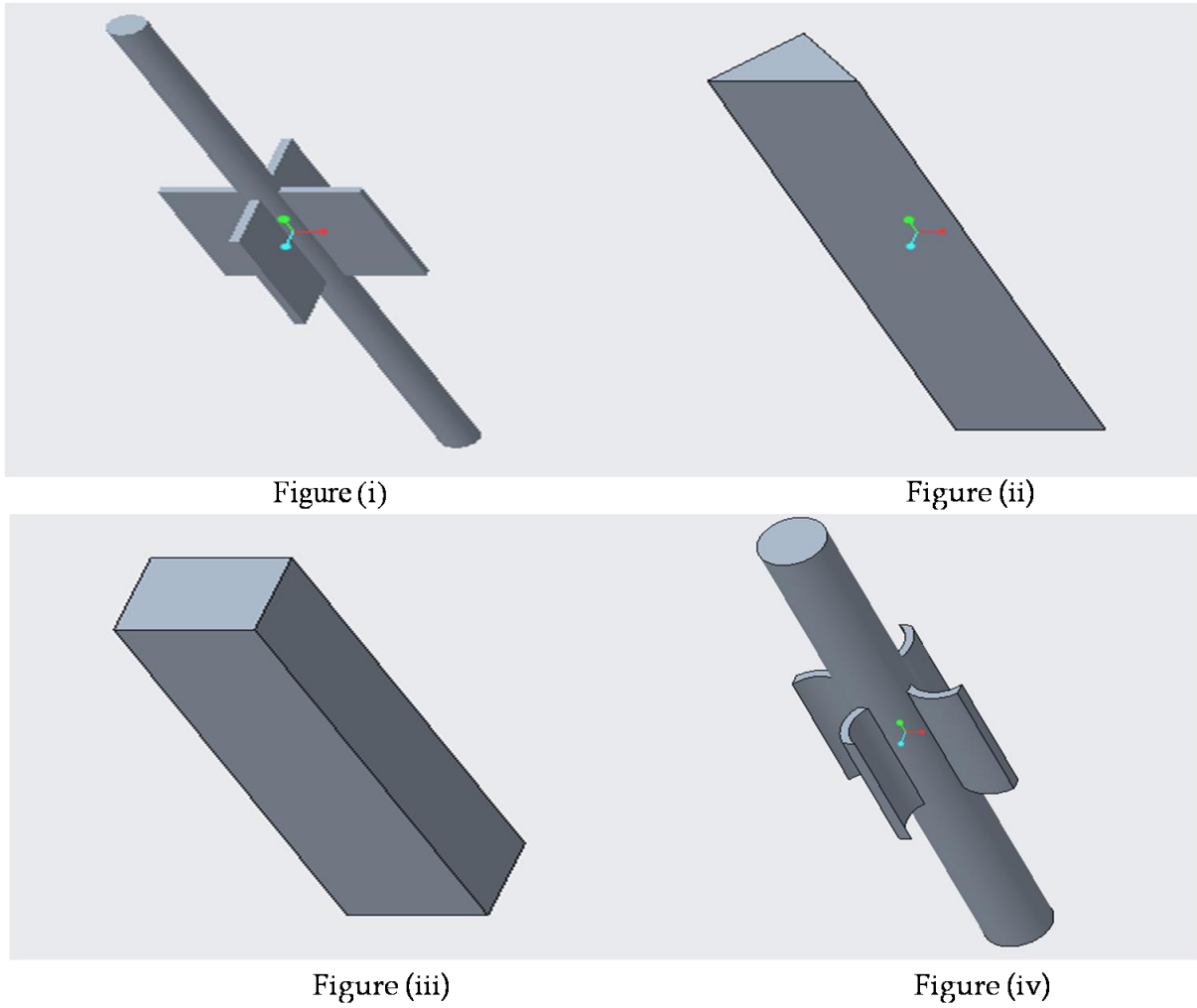


Figure 6 Geometrical Shape of the electrode (i) Straight spline electrode (ii) Triangular shape electrode (iii) square shape electrode (iv) spline shape electrode with curved blade
Thus to overcome the issue of low MR of conventional AFM process, the TACAFM came into the picture and to improve its process efficiency, the researchers proposed a novel shaped electrode which enhances MR, improves surface quality and provides ease in the fabrication and cost of the initial CFG electrode used in the TACAFM process.

1.6. Proposed Novel Electrode

The researcher proposed a novel spline shape electrode with the curved blade to enhance the material removal process of the TACAFM process. The CFG electrode provides the centrifugal action in the media which results in the increase in the resultant force by which the abrasive particles strike on the surface of the workpiece. This resultant force is increase due to the combined action of the Coriolis force, weight of abrasive and also due to the conventional extrusion process. The curvature effect on the proposed electrode results in proper mixing of abrasive particle with the media particle and increases the dynamic number of active abrasive

particles near the workpiece. Also the curvature effect increases the static pressure in the media which in turn increases the cutting forces of the abrasive on the wall of the workpiece.

1.7. Motivation for this research work

In the modern era, the requirement of products for better functional performance and dimensional accuracy along with the aesthetic value has significantly increased leading to the emergence of non-conventional finishing processes. Abrasive Flow Machining possess advantage of machining internal surfaces of hollow workpiece but the limitation of low MR and large machining time predominates. To cater this limitations various hybrids were developed in which TACAFM is the most recent hybrid. The working of centrifugal force generating electrode highly depends on the shapes of CFG electrode. But the centrifugal force generating electrode required for the TACAFM process involves a complex manufacturing process. Thus there is dire need to improve the geometry of the CFG electrode along with the other process parameters which may influence the performance of the TACAFM process.

Summary

- 1. Abrasive Flow Machining is a prominent process for finishing of hollow internal surfaces of the workpiece.**
- 2. Process find its application in major areas including aerospace, automobile, biomedical and ancillary and piping's. Also the in providing mirror like finish in industrial components like gears, finishing of additively manufactured and FDM parts and removal of recast layer in EDM, LBM and in IBM process.**
- 3. To cater the limitation of Low MR, hybridization of AFM is required. TACAFM is the latest hybridization of AFM which includes the advantage of electrical discharge machining (EDM) and centrifugal force assisted abrasive flow machining process (CFAAFM).**
- 4. The geometry of the centrifugal force generating (CFG) electrode is a prominent parameter for improving material removal in TACAFM process. Thus improvement in geometry of CFG electrode results in the enhancement of MR of TACAFM process.**

Chapter 2. Literature Review

This chapter compiles the accounts of various research work on abrasive flow machining and its applications. The accounts describing the hybridization, development of media, fixture and tooling, mathematical modelling and the industrial application of the process is highlighted. The chapter is concluded with the research gap followed by the objectives.

2.1. Background

Abrasive flow machining is non-conventional finishing process which uses a non-Newtonian fluid for the material removal process. The media used in process contains abrasive, polymer and gel which provides the desired property to the media to carry out abrasion process for the material removal process. In the present investigation, the literature review has been separately carried out for the various sub section of the AFM process which includes, different hybrids of AFM, development of media and its property, fixturing and the media flow path, effect of process parameters on material removal and the various applications of AFM and its hybrids processes. Figure 7 describes the major areas of the AFM process consider for the literature review in the present study.

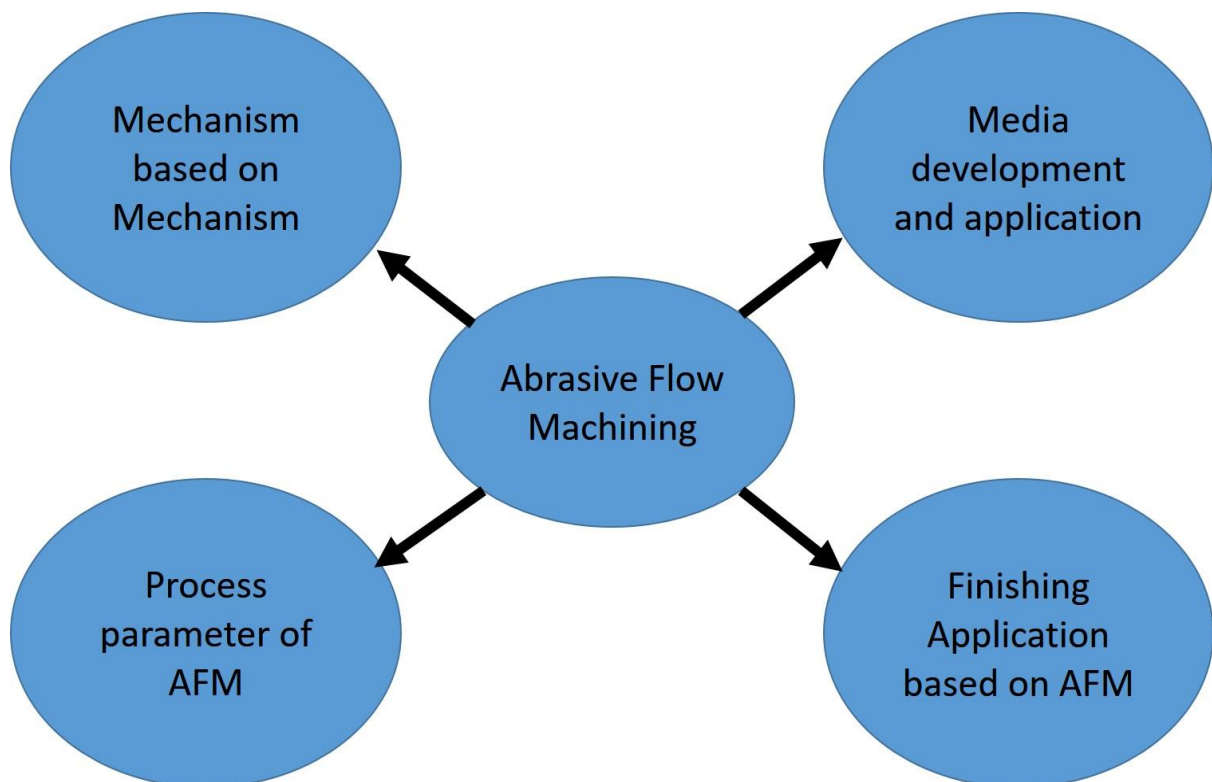


Figure 7 Major area of Literature review of AFM process

2.2. Literature review

The present study compiles the major areas of the AFM process which involves its application in the finishing process, its hybridization, development of flow parameters, application of the process parameters of the AFM and the simulation and mathematical model for the material removal analysis of the developed AFM process.

Crochet et al. (1985) carried out numerical simulation for the analysis non Newtonian viscous flow of the media in the TACAFM process. The researcher realized that a there the numerical computation would lead to good understanding of the behavior of the media and its rheological property along with the deep understanding of the material removal process.

William and Rajkumar (1989) study the machining process of the conventional AFM process and jotted various machining parameters of the process. The researchers analyzed the effect of various process parameter on the material removal and the surface finish. The researcher found that the surface finish and the material removal of the workpiece significantly varies with the material of the workpiece and is different for different material with same process parameters. The researcher also highlighted that the extrusion pressure and the viscosity of the media plays a vital role in the material removal process.

Rhodes et al. (1996) jotted the application of conventional AFM process for the finishing of cylindrical heads an highlighted the cost and technical efficiency of the conventional AFM process for this purpose and highlights its improved functional effectiveness and significant reduction in the hazardous emissions during the finishing of cylindrical heads by conventional AFM process.

Petri et al. (1998) used the concept of artificial neural network model paired with heuristic search algorithm for the computation of surface finish and the change in dimensions during the conventional AFM process. The proposed model gave satisfactory result and highlighted the key points of the computational modelling of the AFM process.

Jain and Jain (1999) did simulation followed by the experimental validation to analyze the trend of material removal and the profile surface finish using the conventional AFM process. The researcher claimed that the media viscosity is the prominent parameter for achieving surface finish and material removal. The researchers found that the media generally contains the abrasive grains which are randomly orientated in the media depending upon its concentration in media. The researcher found that the experimental results were in line with

the simulation results with abrasive concentration, abrasive particles 'size, pressure and the number of cycle as the prominent machining parameters.

Singh and Shan (2002) proposed the concept of magneto AFM process which enhances the material removal capacity of the conventional AFM process by considering the advantage of magnetic action on the AFM media. The researcher claimed that the material removal is significantly improved when the magnetic field is applied around the workpiece. The researcher also claimed that the magnetic field intensity is the prominent parameter which affects both the material removal and the percentage improvement in the surface finish.

Singh et al (2002) analyzed the wear and material removal process of magnetic force assisted AFM over the brass and aluminum workpiece. The researchers observed the material removal and the wear of the workpiece with the help of SEM images. The researchers also jotted the effectiveness of AFM process on the brass workpiece compared to the aluminum workpiece. The researcher claimed that the media flow rate does not affect the material removal significantly compared to the material type and also the magnetic field does not significantly affect the percentage improvement in surface finish compared to the material removal.

Gorana et al (2004) emphasized on the material removal mechanism of the conventional AFM process. The researchers proposed the mechanism of material removal based on the cutting force and the active grain density. The researcher performed the experiments and analysed the cutting force's axial and radial component using a dynamometer. The researcher also computed the force ratio and highlighted its linear relationship with the surface finish.

Jha and Jain (2004) proposed magnetorheological Abrasive Flow polishing based on the rheological property of the media. The researchers performed experiment on the stainless steel workpiece by varying different magnetic intensity. The researchers claimed that increasing the magnetic field intensity decreases the surface finish as there is a reduction in the depth of grinding impression in the surface.

Walia et al. (2006) (a) applied the centrifugal effect in the media by introducing a centrifugal force generating electrode for the computation of the material removal and the percentage improvement in the surface finish. The researchers claimed that the application of the CFG rod co-axially between the hollow workpiece leads to the increase in the number of active particles near the wall of the workpiece. Further it was observed that about 80 percent of the machining time is reduced when the centrifugal force generating electrode is introduced with the conventional AFM process.

Walia et al. (2006) (b) used Ansys® to apply the finite element method for the computation of media characteristic in centrifugal force assisted abrasive flow machining process. The researcher analysed the various flow parameters including stresses, velocity and the pressure developed on the workpiece during the media flow. The distribution of pressure and velocity is in line with the literature trend with pressure values maximum at the inlet and minimum at the outlet. The velocity reached its maximum value at the centrifugal force generating electrode and steadily decreases with the flow.

Walia et al. (2006) (c) analysed the process parameters during centrifugal force assisted abrasive flow machining using experimental and validation by Taguchi's method. The researchers designed experiment by taking conventional process parameters like rotational speed of CFG rod, grit size of the abrasive and the extrusion pressure. The researchers found that the surface is significantly affected by the pressure of extrusion and the rotational speed of the CFG rod. Also the significant improvement in the surface finish in less number of cycle is observed when the advantage of centrifugal force is added with conventional AFM process.

Gorana et al (2006) analysed the cutting force in the abrasive flow machining process by considering the single abrasive particle. The researcher performed experiments to analyse the effect of axial, radial and active grain density on the material removal. The researcher concluded that the grain density significantly affects the material removal of the AFM process.

Gorana et al (2006) (b) simulated the abrasive flow machining process using a kinematic model. The researchers selected the conventional process parameters including grain size, grain density and the concentration of the abrasive particle, cutting force on the grain, grain spacing and the initial surface roughness of the workpiece. The researchers observed a significant improvement in the material removal with the variation in the pressure of extrusion and concentration of the abrasive. Also the two parameters significantly affect the grain density of the abrasive used in the workpiece.

Dabrowski et al. (2006) used the advantage of electrochemical machining with the conventional AFM process. The researchers added electrolyte (potassium iodide) in the media. The workpiece is made cathode and the container is made anode. Thus the machining takes place by the dissolution of the ions in the polymeric electrolyte. The researchers reported a significant improvement in the surface finish compared to the conventional AFM process.

Tzeng et al. (2007) reported a self-modulating abrasive media consisting of adjustable fluidity and viscosity during the finishing process. The media is used to machine SUS304 micro

channels made by wire EDM process. The researchers used machining time, extrusion pressure, concentration and size of the abrasive as the finishing parameters. Further the researchers reported that the surface roughness of the workpiece significantly decreases when the coarse abrasive are used in place of the fine abrasive media particles.

Wang and Weng (2007) developed a silicon based rubber media for conventional abrasive flow machining process to finish an EDM generated surface. The researcher claimed that the proposed media provides a better surface roughness when in use compared to the conventional polymer base media of the conventional AFM process. Also the researcher claimed that the proposed media showed the significant improvement in the process efficiency of conventional AFM as a constant working temperature is maintained in the media. The researcher also observed that the surface integrity is much better in case of the finer media particle compare to coarser one.

Wani et al. (2007) magnetic abrasive flow machining process and study the surface roughness of the finish work piece. The researcher analysed the FEM based model to study the pressure based magnetic abrasive brush. The simulation results were validated with the experiment and the experimentation results were in line with the simulation results and the researcher also claimed that the magnetic pressure increases with the magnetic flux density.

Fang et al (2007) analyse the abrasive movement pattern during the AFM process and highlighted the sliding, rubbing and the rolling motion of the abrasive which results in the material removal process. The finishing may be achieved by the individual process or by the combination of the movement. The researchers also commented that the hardness of the workpiece, particle size and the normal load are prominent parameter affecting wear of the workpiece.

Das et al. (2008) analysed the rheological property of the media used in the magnetic force assisted abrasive flow machining and magnetic abrasive finishing process and highlighted the role of axial pressure while considering the media as the Bingham plastic. The researcher concluded that increasing CIP particle in the media establishes a strong magnetic field connection resulting in the higher material removal.

Walia et al. (2008) (a) described the active number of abrasive particle during the conventional AFM process and highlighted the increase in the number of active particle when the centrifugal force generating electrode is introduced in the system. The experiments were also performed

to validate the mathematical results resulting in an increase in the material removal for the CFAAFM process which is in line with the mathematical model.

Walia et al. (2008) (b) discussed the morphology of finished brass workpiece when the finishing of CFAAFM takes place. The researcher performed XRD and computed the residual stresses of the finished workpiece and suggested that the CFAAFM does not affect the surface microlayer of the workpiece and there is an increase in the value of residual stress of the workpiece along with the microhardness.

Walia et al. (2009) used a rotating CFG rod for the improvement in the MR. The researcher claimed that the desired surface finish is obtained at the lesser number of cycle compared to the conventional AFM process when CFAAFM is used with the other parameter kept constant.

The impact of media temperature on the effectiveness of the abrasive flow machining process was investigated by Fang et al. (2009). The studies were conducted using a test rig and conventional AFM equipment. Steels A 36, 1045, and AISI 1080 were used to create the specimens. The experimental findings demonstrated that when temperature increased, the media's viscosity dropped. The number of cycles causes the media's temperature to rise. The results of the trials showed that when the number of cycles was greatly increased, the removal of material and the surface roughness decreased, which further impacted the system efficiency.

Drill bit guided abrasive flow machining (DBG-AFF) is the term given by Sankar et al. (2009) to the process of rotating the media through the drill bit along the bit's axis for a higher rate of finishing. The abrasive particles are forced to reorganize randomly through the helical path by the drill bit. The dynamic number of abrasive particles was enhanced as a result. The AISI 1040 and AISI 4340 workpiece were used in experiments for both the AFM and DBG-AFF processes. It was discovered that the drill bit guided AFM technique produced improved surface quality and MR.

AFM processes that use centrifugal force to remove material can be predicted using an analytical model, which was proposed by Walia et al. (2009) (b) and validated by experimental data. According to the authors, the movement path of the abrasive particles as they pass through the workpiece can be used to forecast the angle of indentation and striking velocity of the abrasive particles. The important parameters for material removal were the number of cycles, abrasive grit size, extrusion pressure, and CFG rotating speed.

The application of conventional AFM principles to the finishing of advanced ceramic materials was investigated by Uhlmann et al. (2009). The outcome showed that surface finish improved

throughout the first finishing period. Because ceramic material is ductile, the smooth surface is extended throughout the material removal process. This procedure softened the edges of micro cracks and the grain boundaries.

In order to combine abrasive and ferromagnetic particles, Wang and Lee (2009) created a novel abrasive medium using silicone gel. The issue of environmental contamination and the recycling of abrasive particles in the media was lessened by this kind of media. The researcher polished a cylindrical rod made of mild steel material using gel abrasives in the magnetic finishing procedure. The chuck retained the cylindrical rod, allowing it to vibrate and revolve in an axial direction.

Using an AFM method, Kar et al. (2009) produced a novel media based on a viscoelastic carrier and studied its rheological properties and fine finishing. The materials used to make this kind of media were butyl and natural rubber. The rheological properties of the media are significantly influenced by temperature, frequency, creep time, and shear rate, according to the experimental data.

Rotational Abrasive Flow Machining was created by Sankar et al. (2010). In this method, the media reciprocated between the two hydraulic cylinders while the entire tooling was rotated by external means. To determine the ideal parameters for changing roughness, experiments were conducted on Al alloy and Al alloy/SiC MMCs under varying extrusion pressure and medium composition. Additionally, the impact of workpiece rotation on material removal has been examined by the researchers.

Mali and Manna (2010) used the AFM approach to polish the cylindrical surface of an Al/15% weight Al/SiCp - MMC workpiece. This material is significant to the automotive, space, and machining industries. The impact of the factors on surface finish and material removal was examined by the researchers. To determine the impact of AFM parameters, a mathematical model was developed for various Ra values and material removal rates. The experimental results showed that the AFM method could finish the component, however spoilage of surface finish was discovered if the process parameters were not appropriately regulated.

A brand-new polishing method called the Electrochemomechanical polishing technique was presented by Jang et al. (2010). The electrochemical anodic reaction on the conductive workpiece in the electric field was used in this method. The features of the reaction in an electrolytic solution were examined during the tests using GC specimens. The experimental

findings provided information on the electrochemical oxidation reactions that affected the GC specimens and correlated with variations in current.

A novel carrier media was created by Rajesha et al. (2010) as a substitute technique for the finishing step of the abrasive flow machining process. Thermogravimetric analysis (TGA) and Fourier transform infrared (FTIR) were used to characterize this recently produced medium. By taking into account the abrasive concentration, extrusion pressure, media viscosity, and flow rate as the variable parameters and material removal and surface quality improvement as the responses, the medium's performance was examined. This newly created medium, which was based on an ester, could tolerate temperatures as high as 71°C without losing any of its properties. According to the experimental results, surface finish and material removal are significantly improved by using this kind of media.

The Ultrasonic AFM technique was developed by Sharma et al. (2011) to improve surface integrity and material removal. The vibrations in the ultrasonic range were applied to the workpiece surface in a normal direction. The vibrations that were supplied were in the 5–20 KHz and 10–50 μm ranges, respectively, with a high frequency and low amplitude. A piezo-actuator and specially made fixture were used to apply this frequency and amplitude. The relative speed of the abrasive particles contacting the workpiece surface was enhanced by the vibrations.

Sankar et al. (2011) employed several co-polymer-based media, such as plasticizer, abrasives, and soft styrene butadiene-based polymer, for the AFM process' finishing. The generated media's static and dynamic rheological characteristics were examined by the researcher. Al alloys and MMCs were used in the Rotational AFM Process tests. In comparison to material removal and surface roughness improvement, the impact of rheological parameters such as shear stress, percent viscous component, stress relaxation modulus, and storage modulus was investigated. The experimental result revealed that material removal increases in tandem with an increase in yield shear stress. The surface roughness first progressively rose before beginning to decrease as a result of the strong radial force applied by the media.

A parametric investigation was carried out by Bahre et al. (2012) to ascertain the impact of lead time and medium pressure on surface integrity. The workpiece chosen by the researcher was an AISI 4140 automobile steel that is often used. Using an axial force sensor, the impact of the medium pressure on the machined item was also investigated. The testing results showed that there was a noticeable improvement in surface finish after 15 cycles of the AFM technique.

Singh and Walia (2012) combined the magnetic effect with abrasive flow machining and adjusted the parameters to remove material more efficiently, increasing process productivity. Based on the experimental data, the researchers concluded that the magnetic field had a major impact on the removal of material. The maximum removal of material was reached at 0.4 Tesla of magnetic flux density, with some fluctuations in the result seen up to 0.6 Tesla of magnetic flux density.

In order to improve material removal in the AFM process, Brar et al. (2013) created the Helical AFM technique. The media flow channel was designed with a typical helical drill bit, and the media passed via the drill's flutes. A centrifugal force was created in the media flow channel by the media's movement along the curvature path, increasing the number of abrasive particles in the media and improving material removal. According to the experimental findings, material removal using helical AFM was 2.5 times greater than that of conventional AFM. Drill bit contribution to material removal was 89.74%.

A workable method for guaranteeing integration of the ideal configuration of media, machine, and geometry during the optimization of the AFM process was provided by Howard and Cheng (2013). The average roughness, edge form, and the process conditions that led to their achievement in test piece geometry are the two main explanatory variables that the researcher suggested selecting. Through CFD simulation and machining trials on the intricate work components, its approach and implementation were examined and validated. This technique used an optimized machine design to increase the process's capabilities and efficiency.

A novel media based on styrene butadiene rubber was created by Gao et al. (2013), and DF-101S was utilized to characterize it. The fluidity and stability of the novel media at high temperatures were examined. ZYGO and MLLD60 were used to measure the surface characteristics of the novel media during the experiments. The outcomes demonstrated that the recently created medium had excellent fluidity and high temperature stability, making it suitable for use in the AFM finishing process.

Schmitt and Diebels (2013) introduced a model for non-Newtonian media, and using COMSOL Multiphysics, additional simulation of the Abrasive Flow Machining process was carried out after key parameters were determined. The nodes that were shown on the domain boundary were shifted properly and in response to the local shear rate.

In order to shorten processing time, Wan et al. (2014) compared zero order semi mechanistic and simple approaches for the two-way AFM process. The outcome demonstrated that the zero

order methodology will be helpful for internal passage analysis when the cross section along the media flow path shows little to no fluctuation.

In 2014, Kenda et al. used an abrasive flow machining procedure to finish a plastic gear. The stability and longevity of the plastic gear teeth were increased by polishing their surface. According to the experimental results, it was a good substitute for hand polishing processes when it came to finishing. The benefits of employing the AFM method included reduced finishing time, consistent surface quality, and no harm to the tooth's profile.

Wang et al. (2014) created a novel AFM approach by giving the media helical tunnels to improve the abrasive particle's intermixing during the media flow. The surface finish and material removal were enhanced by this method. According to the experimental results, helical passageways resulted in a 76% improvement in surface finish, compared to a 60% improvement in the original circular route.

Elastic abrasive particles were employed by Sooraj and Radhakrishnan (2014) to provide extremely fine finishing on the workpiece's internal surfaces. In the case of elastic abrasives, the abrasive particles are embedded with elastomeric balls that can conform to the surface of the workpiece and polish the surface profile finely without affecting its shape. To compute material removal, a mathematical model was created, and experiments were used to validate it. An experiment plan based on response surface methodology with central composite design was implemented. For the surface finish, the effects of axial pressure, abrasive grain size, and elastic abrasive longitudinal stroke velocity were investigated. Based on the experimental results, it was discovered that the surface finish was significantly impacted by the interplay between axial pressure and cutting velocity.

Ibrahim et al. (2014) used the Taguchi approach to optimize the parameters for material removal and % improvement in surface roughness. These parameters were stroke length, pressure, number of cycles, abrasive concentration, and abrasive particle size. The experimental findings demonstrated that the abrasive concentration was significant for the removal of material, and the stroke length was the most significant parameter for the percentage improvement in surface roughness. The surface polish and material removal percentage improvements were judged to be 91.39% and 96.4%, respectively, by the researcher.

In a single machining technique, Swat et al. (2014) reported an optimal process control using a combination of variable piston pressure levels. Better finishing was achieved in less time with this technique. The specimen that the researcher utilized for finishing was made of AISI 4140,

a material that is frequently used in automobiles. Moreover, the researcher created a force model based on axial force measurements made during the research process. According to the experimental results, homogeneous surface roughness was obtained at a minimum of 40 MPa extrusion pressure, as opposed to 70 MPa.

Electrochemical assisted Abrasive Flow Machining (also known as hybrid AFM/ECM) was introduced by Brar et al. (2015). Material removal in this developed method happened as a result of both the ECM effect and abrasion. In order to remove the substance, the researcher further refined the procedure settings. The experimental findings demonstrated that the amount of material removed was greatly influenced by the following parameters: voltage, electrode size, extrusion pressure, molal concentration of salt, and abrasive particle size. Because it uses the workpiece as the anode and the cathode as the electrode, this method can be used to prismatic geometries.

Gupta and Chahal (2015) optimized the electro-chemically assisted abrasive flow machining process's voltage, number of cycles, molal concentration, and rotating rod diameter in order to remove material. According to the experimental results, the voltage had the largest impact on material removal (i.e., 43.35%), followed by the molal concentration (i.e., 32.72%). The rotating rod's diameter (i.e., 8.02%) had the least impact on material removal.

In 2015, Mittal et al. completed Al/SiC MMCs by utilizing an Abrasive Flow Machining technique and conducted experiments using a Taguchi L27 array. According to the experimental results, the extrusion pressure significantly influenced the rate of material removal and the percentage improvement in surface roughness. According to the research, this procedure can be used to polish surfaces created by the EDM process and can also repair faults that were created during the EDM process. The workpiece material was also discovered to be a major response parameter. It was discovered that when SiC was first raised, the material removal rate reduced, but as SiC content rose, it increased even more.

Venkatesh et al. (2015) (a) used ultrasonic aided abrasive flow machining to complete bevel gear finishing made of EN8 steel. Using a CFD approach, the researchers demonstrated a finite element simulation to examine the behavior of media during EN8 steel finishing. It was also investigated how the media's temperature, pressure, and velocity affected the workpiece's length. The outcome shown that, as compared to traditional abrasive flow machining, ultrasonic aided abrasive flow machining significantly increased the bevel gear's surface polish and

removal of material. The outcomes showed that the ultrasonic frequency was a crucial factor in improving surface quality and removing material.

A computational method was employed by Venkatesh et al. (2015) (b) to examine the behavior of the media during the Ultrasonic assisted Abrasive Flow Machining procedure. The media effect on the responses (fluid pressure, fluid velocity profile, fluid temperature distribution, and wall shear on the workpiece surface) at various machining settings was determined using a simulation program. For the simulation, a three-dimensional model of UAAFM was created. The simulation's outcome showed that an abrasive particle striking the surface at an angle of " θ " greatly altered the fundamental mechanism and increased process efficiency.

Vaishya et al. (2015) combined the usage of centrifugal aided abrasive flow machining with electrochemical machining. The researcher examined the effects of process variables, such as voltage, salt molar concentration, rpm, etc., on the responses, or material removal and percentage improvement in surface finish, based on the Taguchi experimental design. This method was employed with a low operating extrusion pressure of 6 MPa in order to preserve the geometric tolerances of the delicate components and shield them from harm. According to the experimental results, material removal in AFM assisted by centrifugal force and electrochemistry was similar to that of other hybrid procedures.

Dong et al. (2015) looked into the relationship between media flow pressure, material removal rate, and machining quality by studying the machining mechanism of abrasive flow machining. The normal pressure operating on the inner surface of the circular tube and the wall sliding velocity were modelled by the researcher. In Abrasive Flow Machining, the material removal rate for the highly viscoelastic media was calculated. The outcome of the experiment demonstrated a direct relationship between the wall sliding velocity and the abrasive media's characteristics. The wall sliding velocity increases as the abrasive flow and viscosity increase.

Bremerstein et al. (2015) looked at how much abrasive media was worn both before and after finishing using abrasive flow machining. To investigate the impact of abrasive wear on the machining process reactions, the medias were tested on the workpiece under comparable settings. According to the experimental results, the particle size, shape, and composition of the abrasive media were what caused the AFM process's efficiency to decline.

Fu et al. (2016) used the Abrasive Flow Machining procedure to complete the blisk uniformly. Blisk's consistent blade surface roughness had a major role in enhancing the aero-engine's performance. Blisk's surface polish was challenging to produce consistently because of high

geometric interferences resulting from its complicated structure. With varying mesh sizes and mass percentages of abrasive particles, researchers investigated an experimental prototype blisk with straight blades using both numerical and experimental simulation techniques. The experiment's findings demonstrated that while the entire blades' surface finish increased following the AFM process of polishing, the leading and trailing edges' surrounding areas had rougher surfaces overall.

The first outcome of a project to translate the concept to metallic materials was reported by Uhlmann et al. (2016) in order to meet the automotive industry's need for intersecting holes. A functional association between the chosen parameters and the inner contour work results was developed. The findings demonstrated that while flow velocity and shear rate increased cutting rate, they decreased grain retaining capacity.

An attempt to model the force created in the AFM process during finishing was made by Singh et al. (2016). By calculating the forces, the researcher provided a simulation of the work piece's final roughness profile. According to the experimental results, surface roughness enhanced together with an increase in stroke count. It resulted from more roughness peaks being sheared off as the number of strokes increased. Surface finish improved as a result of increasing radial and axial forces acting on the work piece surface as the extrusion pressure increased.

Kumar et al. (2016) finished a cast iron workpiece using alumina and carbon nanotubes combined as abrasive particles. CNTs were created using the CVD method, and TEM was used to characterize them. In order to examine the impact on material removal and surface quality improvement, the amount of CNT was increased while maintaining constant values for the other parameters. Surface finish and material removal significantly improved as a result of this.

As the raceways of larger bearing rings with an outer diameter of 200 mm or more are grounded and then assembled in developing nations, Wu and Gao (2016) polished large bearing ring raceways using an AFM method. In the industrialized world, these were completed by high frequency whetstone oscillation. According to the AFM process experiment results, the surface roughness is reduced by the AFM polishing method from a value of $0.4\ \mu\text{m}$ to $(0.1-0.2\ \mu\text{m})$. The lubricating oil coating was greatly conducive due to the new surface topology and roughness created by the AFM polishing technique.

Abrasive Flow Rotary Machining is a new hybrid method that Marzban and Hemmati (2017) developed. In this improved method, the abrasive media's reciprocation motion was removed, and the workpiece was rotated in addition to spin motion for improved reaction. This process's

machinery and tools are straightforward and capable of finishing the components. Using experiments based on the Taguchi design, the process performance was examined. Following the experimentation, the Artificial Neural Network approach was used to construct and model the influence of the process factors. It was discovered that the developed method removed material in a manner akin to that of abrasive flow machining while also saving the abrasive particles in the media.

A multiscale multi-physics simulation based model was suggested by Cheng et al. (2017) to mimic the AFM process towards component form and control of dimensional accuracy. The COMSOL environment was used to carry out the simulation process. Trial experiments were carried out to assess the outcomes and validate the simulation. Simulation and experiment findings demonstrated the effectiveness of this approach for accuracy control and blade profile prediction.

To save costs and forecast results faster, Kheradmand et al. (2017) developed a numerical simulation on Magnetorheological fluid finishing. Both the base fluid and the abrasive particles were present in the media. The focus of the study was on surface roughness variation and hydrodynamic characteristics. It was discovered from the simulation results that the gravity effect was causing the tangential velocity to be unequal in the cross section.

Singh et al. (2017) used the AFM method to polish the aluminum alloys. When compared to the traditional AFM technique, the aluminum alloy required less finishing force to be applied by the abrasive media. Additionally, a simulation model that predicts the finishing force and surface roughness change in the AFM process was proposed using ANSYS POLYFLOW. According to the testing results, finishing force increased in tandem with an increase in extrusion pressure. The ΔRa improved in line with this. The outcomes of the simulation and the experiments were in good accord.

Li et al. (2017) used abrasive flow machining to examine the 90-degree elbow part's polishing quality. At various flow incidence angles, the researcher examined wall shear force and dynamic pressure. It was discovered that the increased inlet pressure boosted the polishing uniformity and effect. According to the testing results, raising the input angle can help achieve surface uniformity during finishing. The best polishing result was obtained at an input angle of 0° – 5° .

Using additive manufacturing techniques such as selective laser melting, electron beam melting, and combined chemical-abrasive flow polishing for produced Inconel 625

components, **Mohammadian et al. (2018)** attempted to increase the surface quality. These methods were employed by the researcher to address the two surface issues—significant surface roughness and texture and semi-welded particles. Semi-welded particles could contaminate an engine part's fluid system, yet a rough surface could make fluid flow problematic. Results from the experiment showed that semi-welded particles could be entirely eliminated and surface integrity could be enhanced by applying the Chemical – Abrasive Flow Polishing procedure.

Li et al. (2018) used an abrasive flow machining process to complete a 90-degree elbow pipe. They next investigated the numerical modelling of the elbow portion completed using solid-liquid two-phase flow. The distribution of dynamic pressure and turbulent kinetic energy for the elbow channel at various inlet velocities was examined by the researcher. An analysis was conducted to determine how well the elbow component finishing procedure worked. According to the simulation results, the dynamic pressure increased gradually and tended to reach its maximum value at the curved section of the flow when it occurs at the same inlet velocity condition. It subsequently became flat at the exit part.

Wei et al. (2019) combined the material removal model for a single abrasive with the statistical model of active abrasives to present a novel predictive model for the material removal in the abrasive flow machining process. Two experiments were carried out by the researcher to calibrate the material removal model. In the studies carried out for validation, the experimental result indicated an error of 6.4% and 6.9%. The findings demonstrated that the projected model could predict the relationship between the distribution of material removal and the cross section of a complex flow channel.

2.3. Recent development in AFM

AFM has emerged as an effective solution when we consider the Nano finishing and machining application. To improve the process efficiency of the AFM and its hybrids form, many scholars researched on the media development. **Ali et al. (2016)** improved the machining efficiency of the AFM process by adding CNT (carbon nano tube) with the media particles. **Ali et al. (2020)** proposed that the CNT particles present in the media accelerates the abrasion process which further results in the enhancement of material removal. **Basha et al. (2023)** developed and experimented polymer based media for the finishing of pure copper using AFM process. **Yadav et al. (2019)** reported the requisite property of the AFM media and highlighted its application in the AFM process. **Dixit et al. (2021)** synthesised Xanthan Gum based abrasive media and use it on the conventional AFM process and highlighted its successful application in the

material removal process. **Zhang et al. (2020)** prepared a novel water based media for the polishing application in the AFM process. **Ahmed et al. (2021)** reported the successful synthesis of Al_2O_3 and SiO_2 based magnetic abrasive for the machining of titanium alloy using AFM and Magnetic force assisted AFM process. Zhang et al. (2022) discussed about the rheological behaviour and material removal mechanism of the media. Li et al. (2023) highlighted the temperature variation in silicon based media for AFM process. Basha et al. (2023) finished the workpiece made of selective laser melting using the polymer based media. Zhuang et al. (2023) developed a new elastic media for the machining of titanium alloy. Feng et al. (2020) discussed novel magnetic compound fluid slurry for the polishing of the internal surface of the workpiece. Srinivas et al. (2019) developed the viscoelastic media for the magnetic abrasive finishing and magnetic force assisted AFM process. Ansari et al. (2023) developed media with the help of ground tire rubber and highlighted its successful application.

Apart from the development of media, the AFM found its application in the machining of additively manufactured part, Kuma et al. (2020) highlighted the finishing of additively manufactured part using AFM, Wahab et al. (2022), Han et al. (2020) and ganeshan et al. (2022) described the successful application of the AFM on additively manufactured and 3D printed parts.

Mohseni-Mofidi et al. (2022) developed mathematical model to improve the finishing mechanism of AFM process. **Manjunath et al. (2020)** used AFM process for the finishing of aluminium propeller. **Rajender et al. (2020)** develop novel fixture for the finishing process. **Fu et al. (2019)** develop new modelling method for the finishing of hollow internal surface. Many scholars work on the computational and simulation technique to analyse the metal cutting mechanism of the conventional AFM process (**Ahmed et al (2017)**, **Bhardwaj et al. (2019)** and Quacquarelli et al. (2022)). **Gautam et al. (2020)**, **Kumar et al (2022)** used taguchi technique and grey relation technique to optimize process parameters of AFM. Many scholars used magnetic based abrasive to achieve the desired finishing and highlighted the mechanism of material removal and surface improvement process, **sharma et al. (2023)**, used viscoelastic magnetic media for machining of AFM process, Choopani et al (2022) developed magnetorheological abrasive flow finishing process for the improvement of material removal in AFM process. and Thus the scope of AFM is wide and finds its application in the modern day finishing processes. And there is a dire need to improve the process of material removal.

Ali et al. (2020) developed a latest hybrid of AFM which is TACAFM process which resulted in the improvement of material removal process using the advantage of material removal by

spark and the surface finishing process of the workpiece. The present investigation deals in the improvement of material removal mechanism of the TACAFM process.

2.4. Research Gap

The following research gap are observed, after going through the literature review.

1. The Material Removal of Abrasive Flow Machining is very low and hence there is a need to develop new and improve the existing hybridization process.
2. The Modeling and Simulation of flow parameters related to media is in initial stage and needed to be develop.
3. There is a need for optimization of process parameters for the improvement of component quality point of view.
4. Detailed study on rheological properties of various media developed are still in the Initial stage.

2.5. Research objective

From the above mentioned research gaps, the present investigation aims to improve in TACAFM hybrid process of AFM with following objectives-

1. Improvement in design and development of the Thermal Additive Centrifugal Abrasive Flow Machining process which enhanced material removal along with surface finish of work surface.
2. Development of new abrasive laden polymer media for hybrid thermal additive centrifugal AFM process and study their rheological properties.
3. To study the effect of shape of the centrifugal force generating electrode along with other parameters on the material removal in TACAFM (Thermal Additive Centrifugal Abrasive Flow Machining).
4. Multi-response optimization of newly proposed TACAFM process.
5. Modeling of flow parameters of newly proposed TACAFM process.

Summary

- 1. AFM is prominent process when comes to finishing of internal surfaces**
- 2. Media development, material removal mechanism, process parameters and the applications of AFM are the major areas of the research in AFM.**
- 3. Low material removal and considerable machining time is the key limitation of AFM process.**
- 4. There is a need for the development of new hybrid of AFM.**

Chapter 3. Experimental Setup Electrode and Fixture Development

This chapter contains the detail description of the experimental setup including the equipment's ratings, functions and the dimensions of the different CFG electrodes and the workpiece. The chapter also contains the detail description of the fixture used for holding the workpiece and also contains methodology adopted for the investigations.

3.1. Experimental Setup

The proposed TACAFM process is the combination of conventional AFM (including the extrusion of media), centrifugal force assisted abrasive flow machining process (it includes the rotation of the electrode) and the thermal effect (due to generation of spark). Thus to achieve this process, various equipment was individually combine together to produce the TACAFM process. The conventional AFM setup facilitates the reciprocation of the media. For the centrifugal force assisted AFM, 3 phase induction motor with the frequency control power drive is used. To facilitates the addition of the thermal energy through spark EDM power supply and EDM power controller is used which controls the supply current and the duty cycle. Figure 8 shows the schematic diagram of the experimental setup and figure 9 shows the actual.

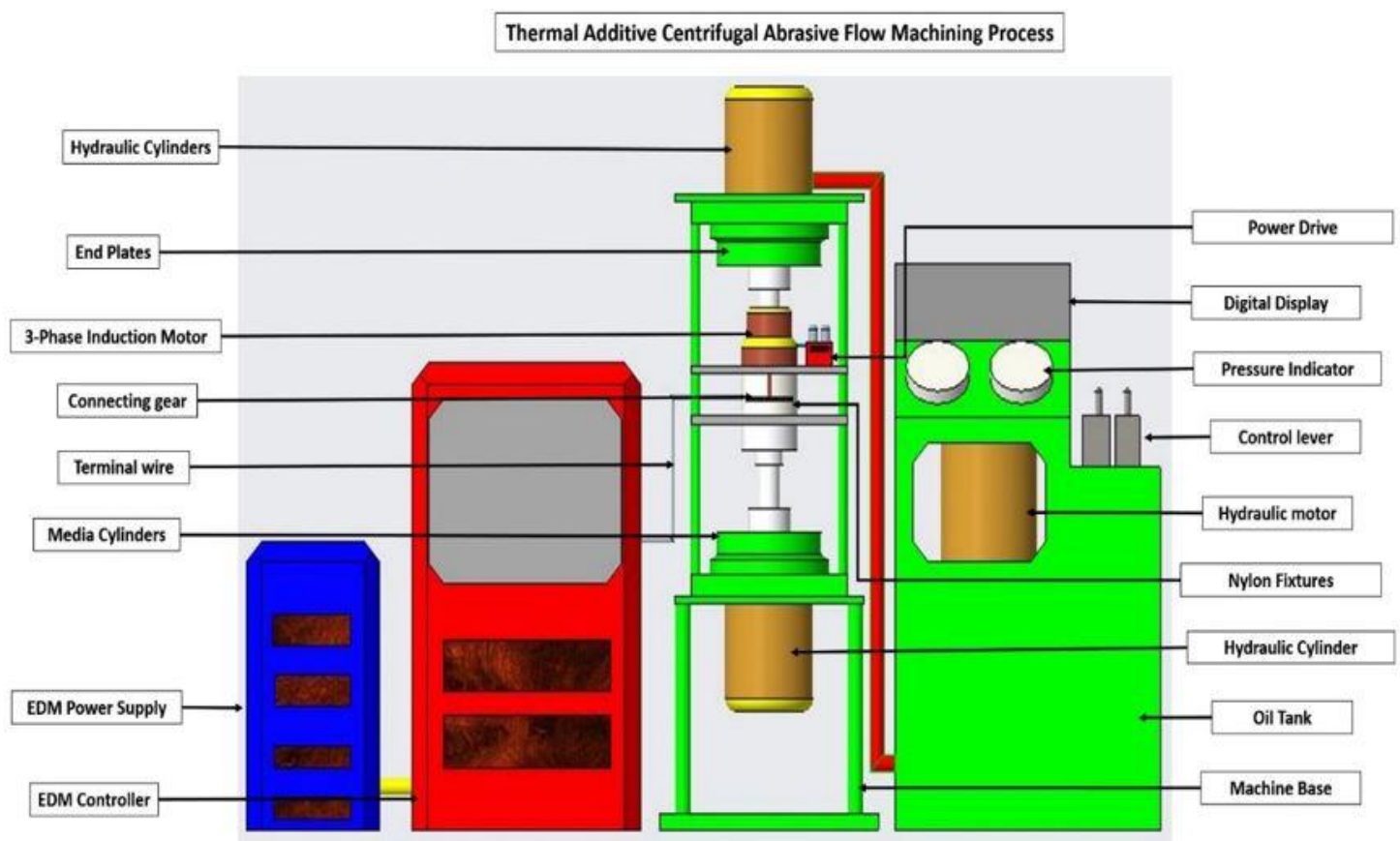


Figure 8 Schematic diagram of experimental setup



Figure 9 Experimental setup

3.2. Conventional AFM setup

AFM involve the extrusion of media due to the pressured difference from the upper cylinder to the lower cylinder and vice-versa. The AFM setup contains machine frame which holds and support the machine. The conventional AFM setup consist of hydraulic power pack whose function is to provide back and forth movement of the piston in the hydraulic cylinders. The components of hydraulic cylinder are motor, reservoir, filter and hydraulic pump with hydraulic circuit. The maximum working pressure for the hydraulic power pack is 210 kg/cm^2 . To facilitate the extrusion of media, the hydraulic cylinders are placed at the upper and the lower end of the machine. The next component of the conventional AFM setup is hydraulic cylinder, which are co-axially placed opposite to each other. The hydraulic cylinders are connected to the barrel which consist of the media that is driven by piston. The piston is driven by the hydraulic power pack through the hydraulic drive. The barrel is connected to the cylinder head at the upper side and the gland at the bottom side. Thus the hydraulic cylinder acts as a mechanical actuator which drives the media through the pressure difference. The diameter of the bore of the hydraulic cylinder is 130 mm and the length of the stroke is 96 mm. The hydraulic cylinders are connected to the media cylinder in which the prepared media is stored. The maximum volume of the media cylinder is 290 cm^3 . In order to facilitates the extrusion pressure, the control levers are used for the upward and lower movement of the piston, Pressure indicators and the pressure control valve are used control the pressure flow.

3.3. Three- Phase Induction Motor

To facilitate the rotation of the electrode, 3 Phase induction motor is used. A gear is mounted on the shaft of the induction motor, which is coupled with the intermediate gear and this intermediate gear is coupled with the gear present in the fixture which rotates the centrifugal force generating electrode. The of the induction motor is 1 HP and the maximum rotational speed of 800 rpm may be achieved. The three phase voltage in the electrical grids connect the motor which creates a rotating magnetic field which controls the rotational speed of the gear mounted on the shaft.

3.4. Frequency control Power drive

The frequency control power drive is used to vary the speed of the 3-Phase induction motor. The device consists of digital display, frequency regulator and the start and stop button. The power rating of the power drive is 0.75 KW / 1 HP with the input voltage of 200 to 240 V per phase.

3.5. EDM controller and Power supply

To generate the spark, the requisite gap between the electrode and the workpiece is to be maintained with the adequate potential difference between the workpiece and the rotating electrode. The EDM power supply is used to supply the pulsed DC. The power supply converts 3 phase main supply into the pulse DC supply. The EDM power supply sense the potential difference between the cathode and anode and directs the controller to sense the gap between the cathode and anode. When the requisite gap is achieved, the controller generates the spark between the rotating electrode and the internal surface of the workpiece. The current rating is 25 Ampere with voltage of 415 V with 50 Hz frequency and the 3 KVA power. Figure 10 shows the detail view of the various components of the experimental setup used in the investigations.

3.6. Fixture

The fixture is used to hold the workpiece and electrode assembly and also guides the media through the hollow workpiece. The material for the fixture is nylon as it is non-conducting material. The fixture was divided into three parts which are upper part, middle part and the lower part. The upper part contains the terminal, middle part holds the workpiece while the lower part includes the gear arrangement for the rotation of the electrode. The fixture included bearings, gears for electrode rotation, work piece, electrode and terminals for power supply. The fixture was made of Nylon, consisted two terminals for positive and negative power supply. Workpiece was attached to the positive power supply while rotating gear was attached

to the negative supply. The fixture was also used to hold the workpiece and to guide the media.

Figure 11 shows the schematic diagram of the fixture used in the investigation.

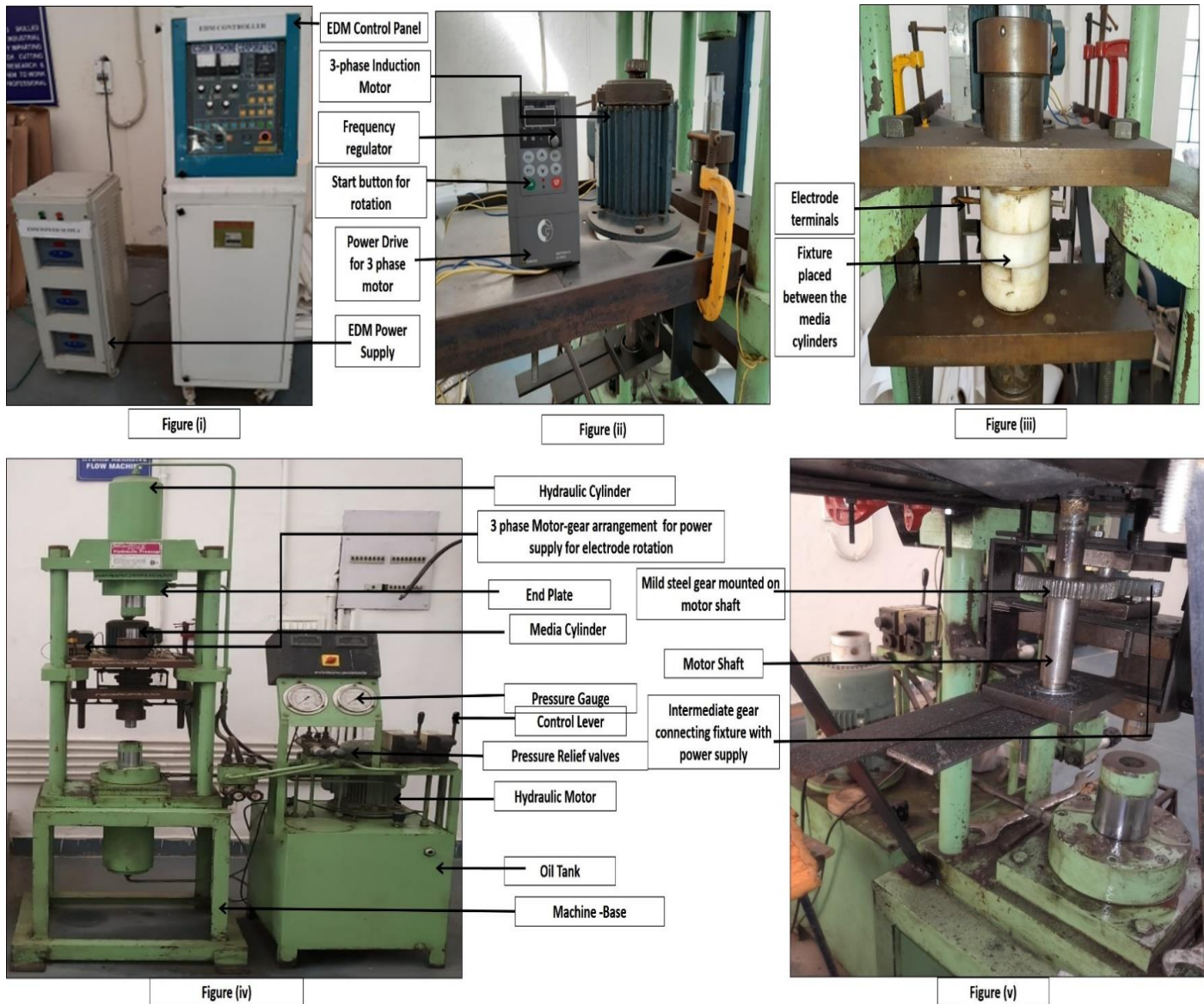


Figure 10 EDM Power supply and EDM Controller (ii) 3-Phase Induction Motor with Power Drive (iii) Fixture with terminal (iv) Conventional AFM Setup (v) Side view

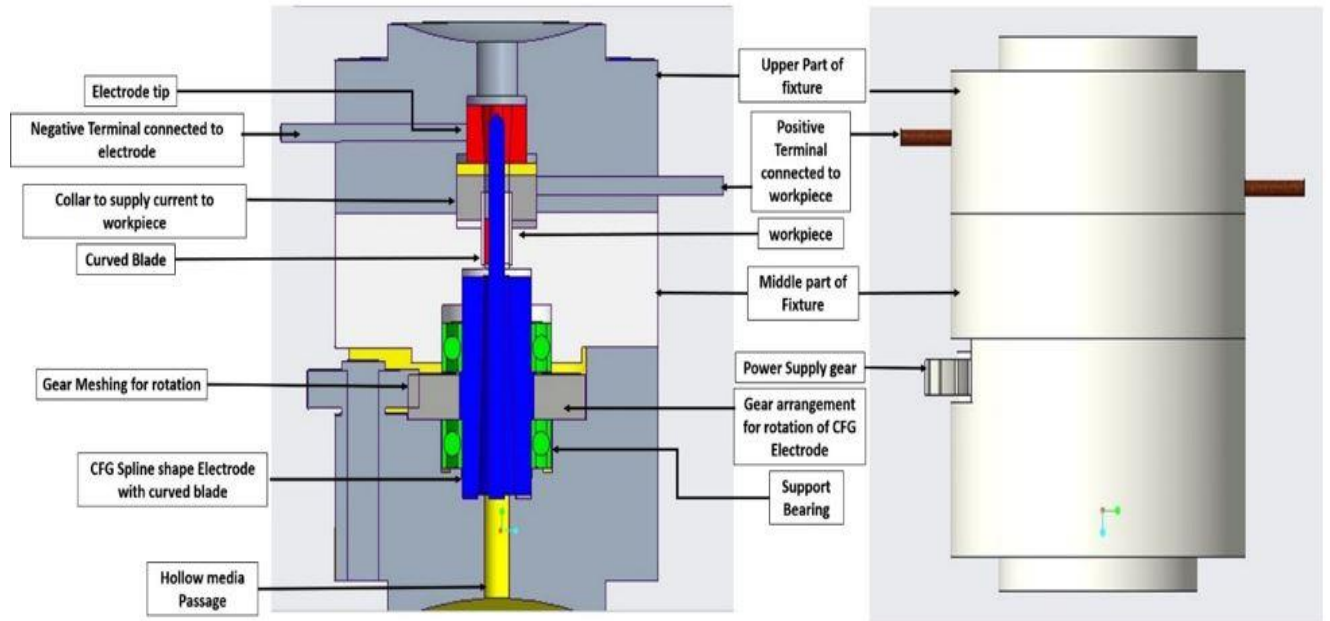


Figure 11 Detail description of Nylon fixture

3.7. CFG Electrode and the workpiece

The researchers selected hollow cylindrical brass workpiece for the investigation with the internal diameter of 8 mm and the outer diameter of 10 mm. the height of the workpiece is taken as 16 mm. In order to compliance with the finishing of internal surface of the workpiece, the dimension of the CFG electrode is so selected that it is coaxially placed within the internal surface of the workpiece and also a minimum gap of 0.1 to 0.9 mm is maintained while rotating the electrode. The another point of consideration is that there should be minimum area for the flow of media so that a constrictive path may be formed which further increases the machining pressure on the workpiece. Keeping these things in view the researcher used various shape of electrode to study their effect on MR and $\% \Delta R_a$. The different shapes used were square electrode, triangular electrode and the spline shape electrode. The spline shape electrode used was with straight fin but a novel spline shape electrode with the curved fin was also used the investigation. The dimension for the square electrode is 5.62 mm. For triangular electrode the dimensions are taken as 6.8 mm and for the spline electrode with straight fin, the inner dimension is taken as 4 mm and the outer dimension is taken as 7.95 mm. For the spline shape electrode with the curved fin, the radius of the electrode is taken as 1.35 for inner curved and for the outer curve of the blade it I taken as 1.5 mm. Figure 12 shows the details of various electrode and the workpiece used in the experimentation.

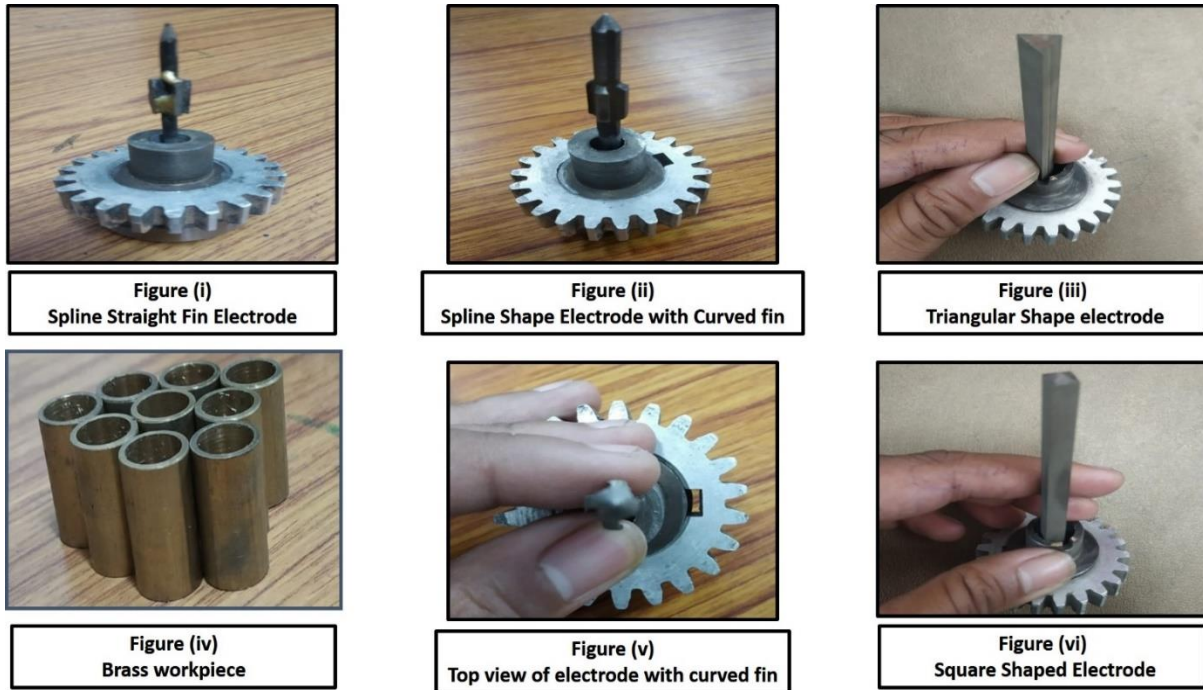


Figure 12 Proposed Electrodes Spline electrode with straight blade (ii) Spline electrode with curved blade (iii) triangular electrode (iv) brass workpiece (v) Top view of spline electrode with curved blade (vi) Square electrode

3.8. Measurement of Surface Roughness and Material Removal

The surface roughness of the internal surface of the workpiece is measured before and after machining with the help of Taylor Hobson Talysurf. The name of the talysurf is TAYLOR HOBSON SURTRONIC 3+ and the precision is 0.01 micrometre. For the computation of the material removal, change in weight before and after the finishing is taken into the consideration. Figure 13 shows the arrangement of workpiece and CFG electrode in the fixture along with its detail view. Figure also highlights the taylor hobson talysurf and the precision weight balance machine. Table 1 highlights the detail of the technical specification of the equipment used in the investigation.

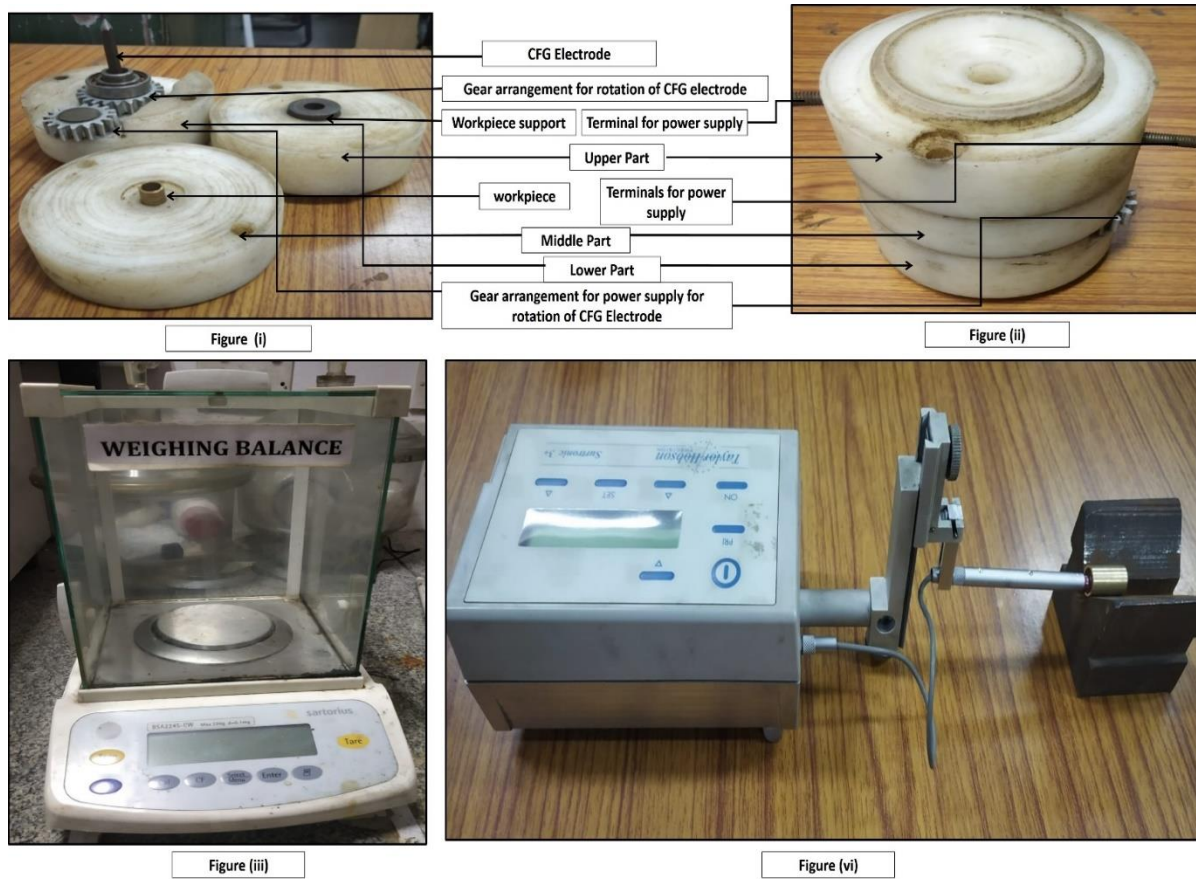


Figure 13 Fixture and equipment (i) and (ii) detail of fixture used (iii) Precision Balance (iv) Taylor Hobson Tally surf

Table 1 Technical Specification of the equipment

Sr. No	Equipment	Description
1	Conventional-AFM Setup	<ul style="list-style-type: none"> • The maximum working pressure is 20 MPa. • The maximum media flow rate is 290 cm³/min • Extrusion of media from upper cylinder to lower cylinder. • Controls the working pressure for machining. • Support the fixture and the workpiece.
2	Three-Phase Induction Motor	<ul style="list-style-type: none"> • Rotation of CFG electrode with the requisite speed. • Maximum rotation speed of the electrode is 800 rpm. • Maximum Power rating 1 horse power.
3	Power Drive	<ul style="list-style-type: none"> • Controls the rotation of the electrode • Regulates the frequency of the 3 phase induction motor. • Power rating 0.75 KW/HP. • Input voltage for the single phase 200 to 240 Volt
4	EDM-Power supply	<ul style="list-style-type: none"> • Pulse DC supply for TACAFM Process • Maximum current rating 25 Ampere. • Power supply – 415, 3 Phase and 50 Hz
5	EDM-Controller	<ul style="list-style-type: none"> • It Maintains the optimum gap between the workpiece and electrode for spark generation. • Controller is based on the microprocessor. • Maximum power 3 KVA.
6	Strait spline CFG Electrode	<ul style="list-style-type: none"> • Mild steel electrode is used for investigation • The inner diameter is 4 mm. • The diameter of the blade spread is 7.95 mm and the width of blade is 2mm.
7	Curved Spline CFG electrode	<ul style="list-style-type: none"> • Mild steel electrode is used for investigation • The internal dimension of the electrode is 4 mm diameter and the outer diameter of the blade is 7.95 mm. • The radius of the inner curve for the curved blade is 1.35 mm and for • The outer curve of the blade is 1.5 mm
8	Triangular shape CFG Electrode	<ul style="list-style-type: none"> • Mild steel electrode is used for investigation • Equilateral triangle is considering for analysis. • 6.8 mm length of side for minimum area of media flow.
9	Square shape CFG Electrode	<ul style="list-style-type: none"> • Mild steel electrode is used for investigation. • The length of the side is 5.62 mm.
10	Workpiece	<ul style="list-style-type: none"> • Hollow Brass workpiece • Outer Diameter 10 mm, Inner Diameter 8 mm, height 16 mm.
11	Fixture	<ul style="list-style-type: none"> • Consist of Nylon Material • Consist of three parts. • Middle part holds the workpiece. • Lower part consists of the CFG electrode and gearing arrangement. • Upper part holds the terminals and workpiece support

3.9. Methodology

The figure 14 shows the flow chart explaining the methodology used in the present study, which aims to highlight the effect of the appropriate electrode which maximize the MR with optimum surface finish.

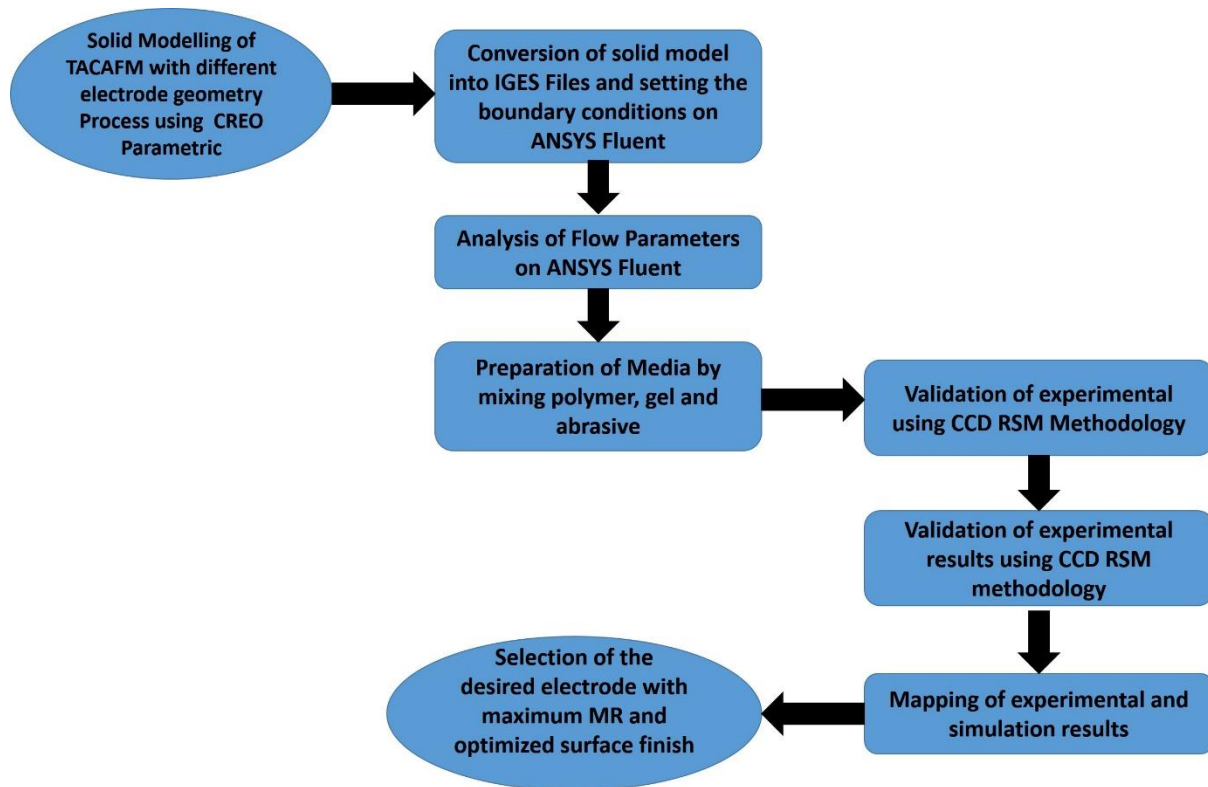


Figure 14 Methodology used in the investigations

The present investigation involves the study of effect of various centrifugal force generating electrode geometry on the TACAFM process with the help of simulation using ANSYS Fluent and with the help of experimental validation using central composite design with response surface methodology. The initial model of the experimental is modelled on the actual dimension on CREO parametric software and the proposed model is transferred to the ANSYS Fluent with the help of the IGES files. The modelled was developed using adequate boundary condition and the analysis is repeated with each electrode separately. The flow parameters were analyzed and the computation of MR and the spark generation were predicted using pressure and temperature computation over the workpiece.

Once the simulation results were analyze the next step was of experimentation. For the experimentation, the viscous media is prepared by mixing the gel, polymer and the abrasive particle. The gel and the polymer were separately prepared using the hydrocarbon oil and the stoichiometric mixing of the components is done for the preparation of the media. Once the

media is prepared the workpiece and the requisite electrode are arranged in the fixture which is kept in the proposed TACAFM setup as discussed in the previous section. The experiments were performed on the prepared DOE formed using the RSM methodology.

The initial and final surface roughness of the internal surface of the workpiece before and after machining is tested using the Taylor hobson tallysurf and the percentage improvement in surface finish is computed. Similarly, the material removal MR is computed by the computation of the change in weight before and after the machining process. The value of the material removal (MR) and the percentage improvement in surface finish ($\% \Delta R_a$) is computed using different values of the process parameters arranged in the DOE, prepared using RSM. The process parameters involve in the study is the type of electrode, supply current duty cycle and the rotational speed. Thus the main purpose of the study is to analyze the effect of electrode on the MR and $\% \Delta R_a$.

The machined workpiece is analyze using the SEM and the XRD analysis of the finished workpiece. The machining pattern of the finished workpiece were analyze using different electrode geometry and the suitable electrode geometry is chosen for which the maximum MR and at the optimized $\% \Delta R_a$. The next chapter will deal with the media preparation and its property for the working of TACAFM process.

Summary

- 1. The TACAFM setup consists of various equipment which caters the conventional extrusion along with the setup, rotation of the electrode and the spark by the EDM.**
- 2. Four different type of electrode is used for the experimentation and suitable electrode with requisite machining capabilities is selected.**
- 3. The fixture is made up of nylon material to avoid the conductive effect of DC and is modified suitably for the adjustment of proposed CFG electrodes.**

Chapter 4. Media Preparation and Characterization

The present chapter deals with the media used in the TACAFM process. The chapter deals with the preparation of media and its property. The proposed media is a mixture of polymer, gel and abrasives. The chapter deals with the preparation of polymer, gels and media and also study their requisite rheological property using the rheometer. The FTIR analysis of the proposed media is done for the analysis of polymeric linkage of the media.

4.1. Introduction

The conventional AFM process is used to finish the internal, intrinsic and hard to reach the surface of the hollow workpiece. The machining occurs due to the abrasion process present in the media. The media plays a vital role in the machining process. This media holds the abrasive particle particles during the machining process. Also the media plays a suitable environment for the spark generation in the TACAFM process. The requisite property of the media is discussed in the subsequent sections.

4.2. Viscosity

Viscosity of the media plays a crucial role in the functioning of TACAFM process as it is responsible for the holding of the abrasive particle during the machining process. Viscosity arises due to the internal friction obtained between the layers of the flowing fluid. More precisely the internal friction is generated due to the intermolecular forces between the neighboring particles of the fluid moving with different velocity. Generally ideal fluids possess zero viscosity but in the AFM process non-Newtonian media is used. This type of fluid follows the power law where the stress is not directly proportional to shear stress.

4.3. Elasticity

Elasticity is the property of the material to regain its original shape when the deforming force is removed. In case of the media, media elasticity refers to the elastic nature or property of a fluid substance. Fluid elasticity means how idle the liquid is on exerting pressure on the fluid to compact its volume or extend it. When more pressure applies, the fluid volume will decrease. Thus the media used in the TACAFM process should follow the elastic nature.

4.4. Viscoelasticity

Viscoelasticity is a property of materials that display both viscous and elastic properties when subjected to deformation in continuum mechanics and materials science. When a stress is applied, viscous materials like water resist shear flow and strain linearly with time. Stretching elastic materials causes them to stretch, yet if the stress is removed, they instantly return to their original shape. Viscoelastic materials display time-dependent strain because they combine

features of each of these characteristics. Viscosity, on the other hand, results from the diffusion of atoms or molecules within an amorphous material, whereas elasticity often results from bond stretching along crystallographic planes in an ordered solid. For the abrasive based finishing, viscoelasticity is the prominent requisite property.

4.5.Viscosity Measurement

The viscosity trend of the media is measured using the compact rheometer. Figure 15 shows the compact rheometer used in the investigation and table 2 shows the property. The rheometer works on the newton law of viscosity which shows the viscosity trends of with shear stress and shear rate. The samples of the base oil used for the computation of the gel which are hydrocarbon oil, transformer oil, engine oil, the base oil used for the polymer which is silicon oil are tested under the similar condition on the rheometer. The working temperature of the sample was kept at the ambient temperature with initial value of 27.74 degree Celsius. The gap between the plates is kept as 1 mm with the force of 8.65 N force on the sample. The shear rate is calculated on the logarithmic scale with the 0.1 to 100 1/s. The time interval between the values were kept 10 s and total 31 points were analysed with the total duration of 310.0 s. The range of the shear stress taken for the consideration are 100 to 1000 MPa.



Figure 15 Compact Rheometer for viscosity

Table 2 Property of Rheometer

Sr.No	Property	Description
1.	Weight of Machine	42 Kg
2.	Size	444 mm width 687 mm height 586 mm thickness
3	Temperature of operations	15-35 degree Celsius
4.	Software	Rheocompass
5.	Maximum RPM	3000
6.	Actuating System	Pneumatic
7.	Company	Antonpar

The rheometer uses rheocompass software which explains the relation between the rheological property of the sample in the graphical form. The rheocompass gives the variation of the shear stress with respect to shear rate and the variation of viscosity with respect to the shear rate. The TACAFM process consists of movement of media due to the pressure difference and also the rotation of the electrode causes the disturbance in the media which causes variation in the media property. The viscosity variation in the media is the key parameter for the TACAFM process. The software gives the variation of the shear stress and shear rate on the logarithmic scale. For the TACAFM process the media should have an increasing viscosity trends which compensates the increasing temperature of the media due to the spark formation. Also the another point of consideration is that the variation of shear stress should remain constant with the change in the shear rate. As it affects the machining capability of the TACAFM process.

4.6. Constituent of the Media

The media used in the TACAFM process is the combination of the gel and the polymer material along with the abrasive material. The constituents are responsible for the media property. The variation of the constituent materials results in the variation of its property. The function of the gel material is to provide the suitable binding capacity to the media which holds the abrasive particles and the polymer particle to maintain the machining property of the media even at the high temperature. The polymer provides flow property to the media. The material of the polymer is so selected that it provides a crosslinking polymer chain structure which provides rigidity to the media and ensure its integrity during the extrusion process. The next main component of the media is the abrasives. Abrasives act as the cutting tools and provide base for the abrasion process in the abrasive flow machining. The different combinations of

the gels were used in the present investigation to attain the requisite property of the media, which are discussed in the subsequent sections.

Since the TACAFM process involve addition of the thermal energy in the media, as a result the temperature of the media increases which results in the decrease in the viscosity of the media. Due to this decrease in the viscosity the abrasive holding capacity of the media gets decreases which in turn decreases the machining capacity of the media. In order to make gel possessing optimum viscosity which could hold the abrasive particles along with the temperature rise, different gels material was used which are discussed. viscosity of different gels is studied and then the suitable material is selected after observing the trends.

4.7. Preparation of gel

The gel is the prominent constituent of the media which provides viscoelastic properties to the media **Yadav et al, (2019)**. The viscosity of the gel holds the abrasive particles present in the media which further accelerates in the abrasion process in the TACAFM process (**Zhang et al. (2020)**). The property of the viscosity of gel is obtained from the base oil used in the preparation of the gel (**Srinivas et al (2019)**). Thus in order to strengthen this property of the media 3 different base oil were chosen for the computation of the media. The base oil used in the computation of the were mainly hydrocarbon as the bond between the hydrogen and carbon provides enough sufficient energy which strengthen the cohesive force of the gel particles (**Dixit et al. 2021**), also the crosslinking polymer of the gel material also helps in the enticement of the polymer particles present in the media. The three different types of the base oil were engine oil, transformer oil and the hydrocarbon oil.

4.8. Engine oil

The engine oil is generally used for the lubrication in the automobile, aerospace and in the heavy machinery sectors. The engine oil basically performs two functions. Firstly, it overcomes the frictional force between the rubbing parts and also it minimise the heat produces due to the rubbing action in the machinery. The second point of consideration is the composition of the engine oil. The engine oil is mainly composed of two main constituents which includes natural gas or crude oil and the other components are additives which makes the engine oil suitable for its application for the media of the TACAFM process. The engine oil used in the investigation is of SAE 40. The 40 present in the grade shows the temperature of the ambient with which the engine oil can withstand. Although its viscosity remains intact during the very high working temperature which is very effective for the TACAFM process. Table 3 shows the value

corresponding to data points for the prediction of the viscosity trends. Figure 16 shows the sample of prepared engine oil gel sample.

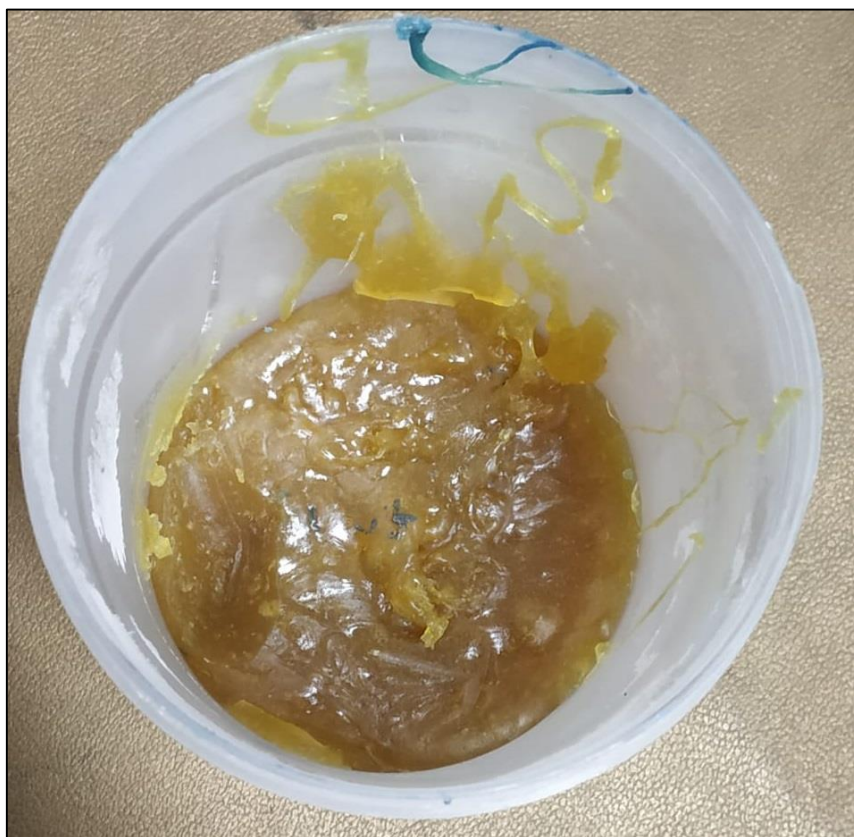


Figure 16 Engine oil based gel sample

Table 3 Engine oil viscosity trends

Point No.	Shear Rate	Shear Stress	Viscosity	Temperature	Torque
	[1/s]	[Pa]	[mPa·s]	[°C]	[mN·m]
1	0.0999	718.62	7.19E+06	26.02	13.546
2	0.121	762.26	6.29E+06	26.03	14.368
3	0.147	838.54	5.71E+06	26.03	15.806
4	0.178	927.1	5.21E+06	26.03	17.476
5	0.216	995.11	4.62E+06	26.03	18.757
6	0.261	1038.1	3.97E+06	26.03	19.568
7	0.316	1068.8	3.38E+06	26.03	20.146
8	0.383	1137.3	2.97E+06	26.03	21.437
9	0.464	1160.9	2.50E+06	26.04	21.882
10	0.562	1132.5	2.01E+06	26.04	21.347
11	0.681	1076.1	1.58E+06	26.04	20.284
12	0.825	982.26	1.19E+06	26.04	18.515
13	1	907.8	9.08E+05	26.04	17.112
14	1.21	847.63	7.00E+05	26.05	15.977

15	1.47	813.44	5.54E+05	26.05	15.333
16	1.78	753.62	4.24E+05	26.05	14.205
17	2.15	792.06	3.68E+05	26.05	14.93
18	2.61	688.49	2.64E+05	26.05	12.978
19	3.16	664.65	2.10E+05	26.05	12.528
20	3.83	719.94	1.88E+05	26.06	13.571
21	4.64	632.72	1.36E+05	26.06	11.927
22	5.63	665.67	1.18E+05	26.06	12.548
23	6.81	656.21	96334	26.06	12.369
24	8.25	631.08	76460	26.06	11.896
25	10	637.51	63760	26.07	12.017
26	12.1	637.96	52667	26.07	12.025
27	14.7	621.1	42310	26.07	11.707
28	17.8	608.35	34210	26.07	11.467
29	21.5	646.97	30030	26.08	12.195
30	26.1	675.46	25879	26.08	12.732
31	31.6	694.46	21963	26.08	13.09
32	38.3	705.35	18411	26.08	13.296
33	46.4	786.06	16931	26.09	14.817
34	56.2	786.39	13984	26.09	14.823
35	68.1	826.28	12128	26.09	15.575
36	82.5	819.19	9924.6	26.1	15.441
37	100	993.73	9936.5	26.11	18.731

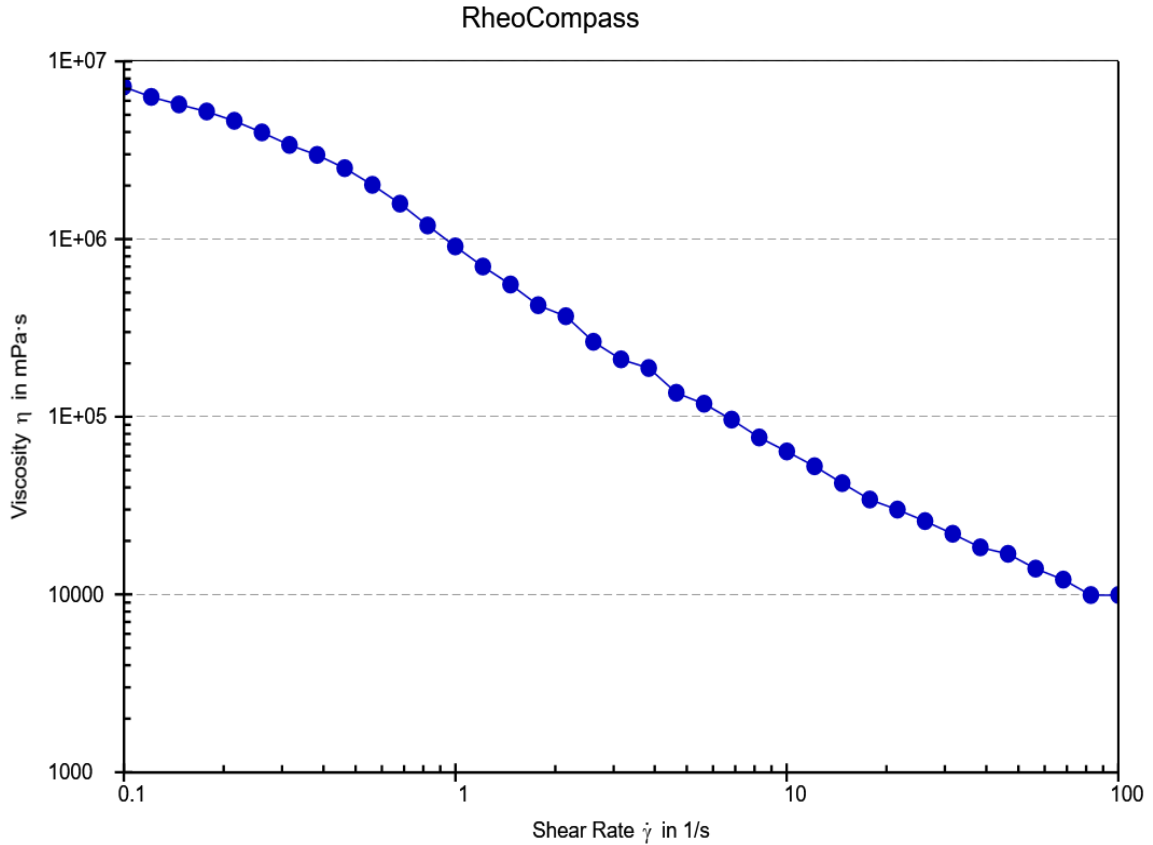


Figure 17 Viscosity Vs Shear rate for engine oil

The figure 17 shows the variation of viscosity with respect to the shear rate. The viscosity decreases with the shear rate which is not the desirable condition for the application of the media in the TACAFM process as it may not compensate the increase in temperature due to the addition of the heat in the media which tends to decrease the viscosity. This decrease in the viscosity affects the abrasive holding capacity resulting in the decrease in the material removal. Figure 18 shows the variation of the shear stress with respect to the shear rate which actually gives the trends of viscosity. The figure shows that the trend almost remains constant which highlights the fact that shear stress does not vary much with shear rate, which is a required characteristic for the TACAFM process. This is because in TACAFM process, there is a continuous movement of media due to the pressure difference also the rotation of the electrode causes a subsequent movement of the media particles that cause a variation in the shear stress of the media. Due to this variation in the shear stress the viscosity of the media changes which results in the abrasive holding capacity of the media. Thus a little variation in the shear stress with respect to shear rate is desirable for the TACAFM process. Thus from the observation the usage of engine oil for the media gel in TACAFM process is not consider due to decreasing viscosity trend with respect to the shear stress.

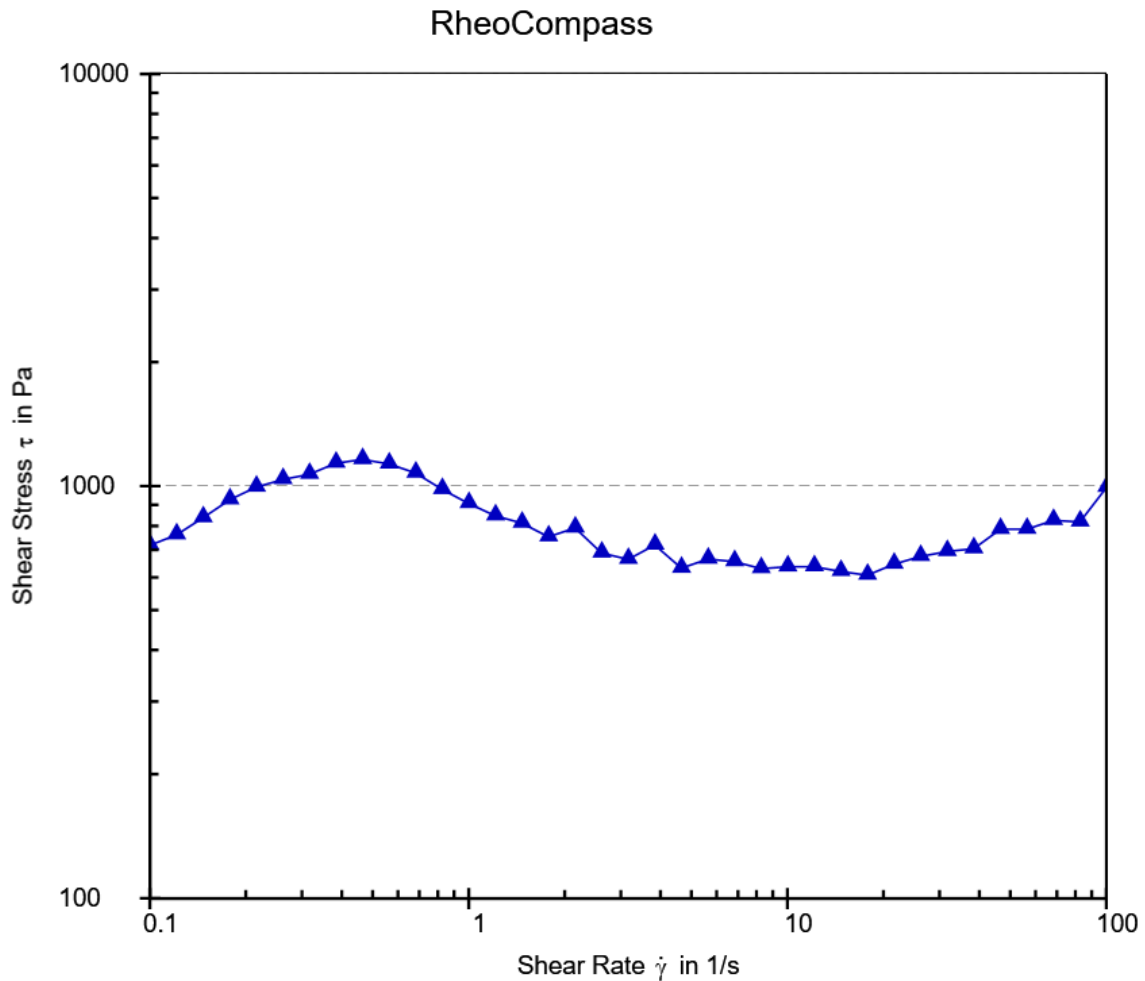


Figure 18 Shear stress vs Shear rate for engine oil

4.9. Transformer oil

Transformer oil is one of the prominently used in the lubrication and insulation of the heavy electric equipment working on the high voltages. The transformer oil finds its application in insulating high voltage infrastructure prominently transformer, switches, circuit breaker and the capacitors. The transformer oil are mainly organic compounds and shows the characteristic of paraffin and aromatic nature. They predominately constitute of naphthalene with the nepthalic structure containing 45 to 50 percent naphthelinic, 5 percent paraffin and the remaining constituting the aromatics. The transformer oil is selected as the possible gel material as it clear both the basic requirement for the media that is the hydrocarbon mineral oil with the crosslinking polymer structure and also its ability to withstand high temperature. These transformer oil are designed to operate on high temperature for lubricating, cooling, insulating and stopping arching and corona discharge and curb the electric field effect. Thus the proposed oil shows he suitability in holding the viscosity as it offers good abrasive holding capacity for

the machining purpose in TACAFM process. Figure 19 shows the gel sample of transformer oil and table 4 shows the rheological property of transformer oil.



Figure 19 Transformer oil based gel

Table 4 Viscosity trend for transformer oil

Point No.	Shear Rate	Shear Stress	Viscosity	Temperature	Torque
	[1/s]	[Pa]	[mPa·s]	[°C]	[mN·m]
1	0.0992	703.83	7.10E+06	25.59	13.267
2	0.121	678.46	5.61E+06	25.59	12.789
3	0.147	677.59	4.62E+06	25.59	12.772
4	0.178	678.45	3.82E+06	25.59	12.789
5	0.215	694.24	3.22E+06	25.58	13.086
6	0.261	709.87	2.72E+06	25.59	13.381
7	0.316	723.05	2.29E+06	25.58	13.629
8	0.383	734.47	1.92E+06	25.58	13.845
9	0.464	758.61	1.63E+06	25.59	14.299
10	0.562	787.28	1.40E+06	25.59	14.84
11	0.682	833.13	1.22E+06	25.58	15.704
12	0.827	892.58	1.08E+06	25.58	16.825
13	1	948.58	9.49E+05	25.58	17.88

14	1.21	1051.2	8.68E+05	25.58	19.815
15	1.47	1122.9	7.66E+05	25.58	21.167
16	1.78	1180.2	6.63E+05	25.58	22.246
17	2.16	1254	5.80E+05	25.59	23.637
18	2.62	1431	5.46E+05	25.58	26.973
19	3.18	1535.3	4.83E+05	25.58	28.939
20	3.83	1360.1	3.55E+05	25.58	25.638
21	4.64	1398.1	3.01E+05	25.58	26.353
22	5.62	1411.1	2.51E+05	25.58	26.599
23	6.81	1321.7	1.94E+05	25.58	24.913
24	8.26	1179.4	1.43E+05	25.59	22.231
25	10	1140.6	1.14E+05	25.59	21.499
26	12.1	1005.7	83002	25.59	18.957
27	14.7	1007.9	68668	25.59	18.998
28	17.8	987.31	55532	25.59	18.61
29	21.5	853.38	39609	25.59	16.086
30	26.1	744.59	28526	25.59	14.035
31	31.6	652.34	20628	25.59	12.296
32	38.3	626.03	16342	25.59	11.8
33	46.4	624.37	13453	25.59	11.769
34	56.2	630.97	11221	25.59	11.894
35	68.1	580.83	8525	25.59	10.948
36	82.5	492.97	5972.2	25.6	9.2922
37	100	443.87	4438.4	25.6	8.3667

RheoCompass

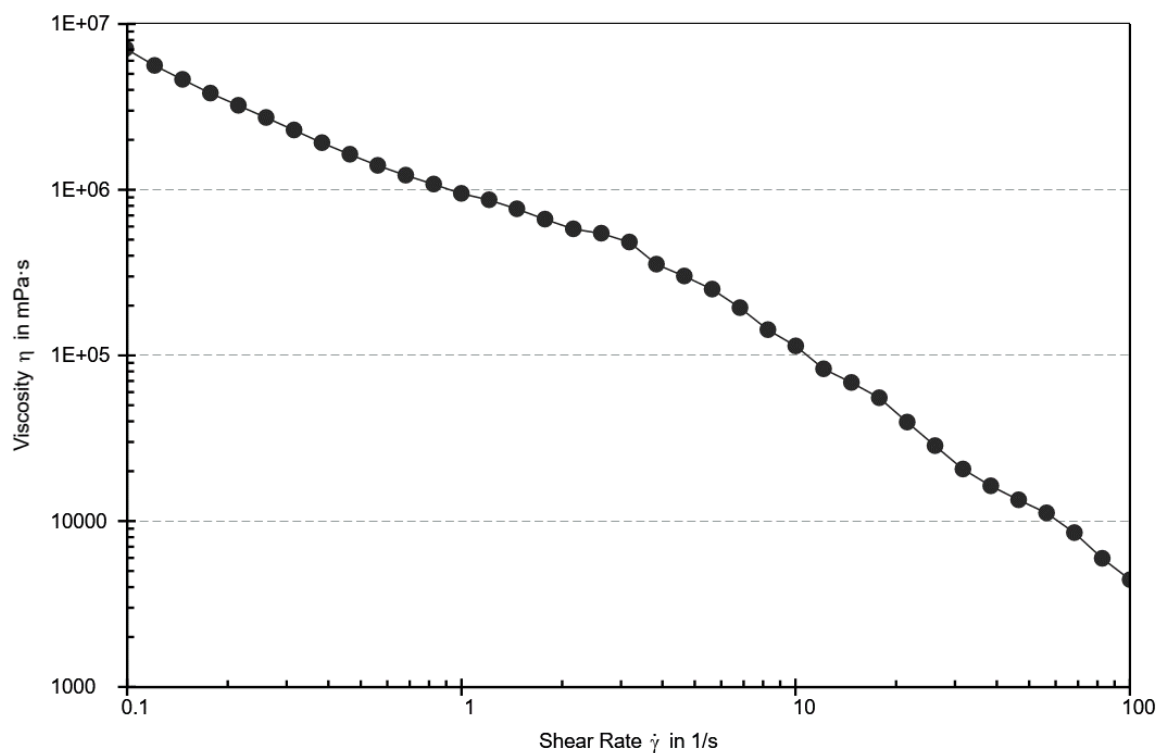


Figure 20 Viscosity vs Shear rate for transformer oil

The figure 20 shows the variation of the viscosity with respect to the shear rate for transformer oil. The figure shows that the viscosity decreases with respect to the shear rate. The decrease is at constant trend which is not desirable and makes transformer oil not fit for the application in the TACAFM process. Figure 21 shows the variation of the shear stress with shear rate. The figure shows that the variation of the shear stress slightly increases with the shear rate and then decreases with the shear rate. The increase in the shear stress with shear rate is desirable as it indicates the increase in viscosity which indicates the high abrasive holding capacity but the shear stress eventually decreases with the shear rate which reduces the machining characteristic of the media as the viscosity decreases. Thus the combine effect of the rheological results for the transformer oil shows the unsuitability of the transformer oil for the TACAFM process. The main reason is the decreasing viscosity trend with respect to the shear rate. In the TACAFM process the rotation of centrifugal force generating electrode increases the centrifugal force on the media particle. Also the media particle undergoes the axial force due to the extrusion process which increases the resultant cutting force on the abrasive particles. This process increases the resultant shear rate of the media. Thus the resultant viscosity and the shear stress increases must decrease with the shear rate as it increases in actual process and affects the machining process with the present combination.

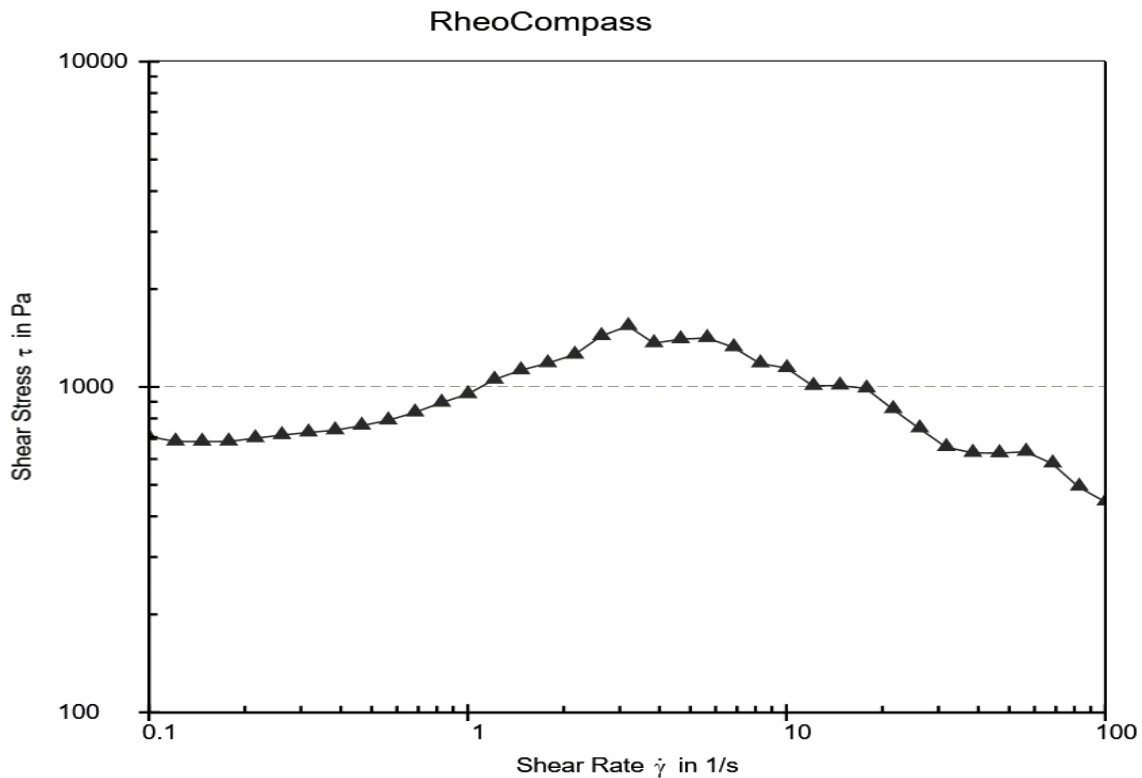


Figure 21 Shear stress vs shear rate for transformer oil

4.10. Hydrocarbon oil

The next base oil for the gel material is the hydrocarbon oil. The hydrocarbon oil mainly consists of crude oil, natural gas and the coal gas. The hydrocarbon oil is generally petroleum based oil with crosslinking polymer structure with propane, kerosene, diesel, gasoline and the jet fuel. The hydrocarbon oil finds its application in the lubrication of the heavy industry and preparation of refined petroleum products. The hydrocarbon oil is selected for the TACAFM process because it consists of rich polymeric linkage chain which binds the abrasive and the polymer present in the media. Due to this property the hydrocarbon oil does not lose the abrasive particle with the increase in the shear rate. The another advantage of the hydrocarbon oil is that its dielectric property. The hydrocarbon consists of kerosene and the diesel and kerosene environment which support and stabilize the spark. The combination of EDM and CFAAFM results in machining process and thus hydrocarbon oil is considered for arc stabilization process. Table 5 shows the rheological data related to hydrocarbon oil. Figure 22 shows the hydrocarbon oil based gel samples. Figure 23 shows the trends of viscosity with respect to the shear rate and figure 24 shows the shear stress vs shear rate.



Figure 22 hydrocarbon oil based gel

Table 5 Viscosity trends for hydrocarbon oil

Point No.	Shear Rate	Shear Stress	Viscosity	Temperature	Torque
	[1/s]	[Pa]	[mPa·s]	[°C]	[mN·m]
1	0.1	0.18084	1808.7	25.02	0.003409
2	0.121	0.20263	1672.9	25.02	0.00382
3	0.147	0.23328	1589.5	25.02	0.004397
4	0.178	0.264	1484.6	25.02	0.004976
5	0.215	0.30217	1402.7	25.02	0.005696
6	0.261	0.35422	1357.1	25.02	0.006677
7	0.316	0.41053	1298.2	25.01	0.007738
8	0.383	0.48955	1277.8	25.01	0.009228
9	0.464	0.57058	1229.3	25.01	0.010755
10	0.562	0.6941	1234.4	25.01	0.013084
11	0.681	0.89541	1314.3	25.01	0.016878
12	0.825	1.1155	1351.5	25.01	0.021026
13	1	1.1241	1124.1	25.01	0.021189
14	1.21	1.0994	907.51	25.01	0.020724
15	1.47	1.2657	862.31	25.01	0.023858
16	1.78	1.5417	866.99	25.01	0.029061
17	2.15	1.6684	774.42	25.01	0.031449
18	2.61	1.9788	758.1	25.01	0.0373
19	3.16	2.1609	683.33	25	0.040732
20	3.83	2.7093	707.17	25	0.051069
21	4.64	2.9482	635.18	25	0.055573
22	5.62	3.5036	623.04	25	0.066041
23	6.81	4.303	631.59	25	0.08111
24	8.25	5.0154	607.62	25	0.094537
25	10	5.8477	584.77	25	0.11023
26	12.1	6.9954	577.41	25	0.13186
27	14.7	8.4109	573.03	25	0.15854
28	17.8	10.017	563.28	25	0.18881
29	21.5	12.021	557.97	25	0.22659
30	26.1	14.326	548.87	25	0.27005
31	31.6	17.063	539.6	25	0.32164
32	38.3	20.433	533.34	25	0.38516
33	46.4	24.526	528.39	25	0.4623
34	56.2	29.51	524.78	25	0.55626
35	68.1	35.424	519.96	25	0.66772
36	82.5	42.651	516.73	25	0.80395
37	100	51.381	513.82	25	0.96851

The figure 23 shows the variation of viscosity with respect to the shear rate. The variation shows that the viscosity is in decreasing trend but this decrease is very less compare to the

decrease viscosity trend for the transformer oil and engine oil. Thus this viscosity is in increasing trend compared to other samples.

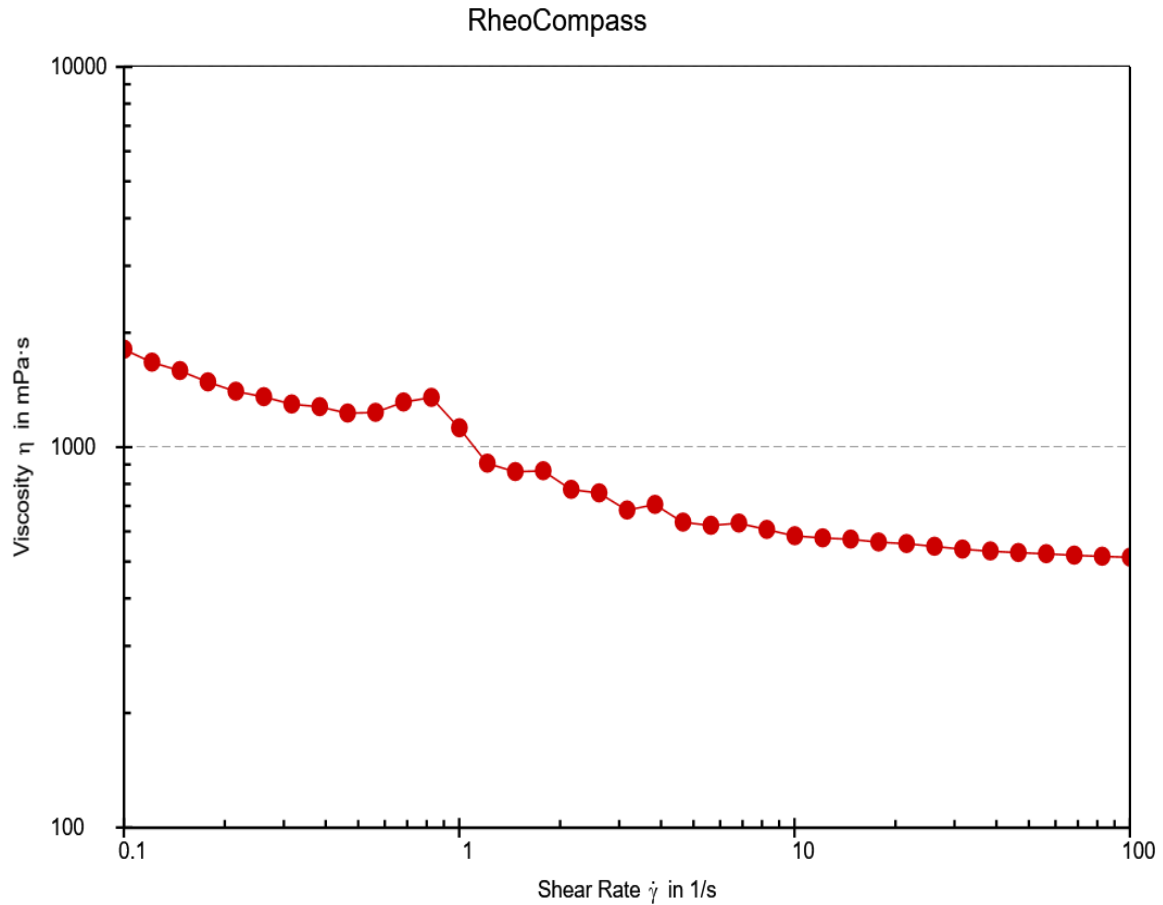


Figure 23 Viscosity Vs shear rate for hydrocarbon oil

Figure 24 shows the variation of shear stress with shear rate. The graph clearly shows that the shear stress is in increasing trends. It indicates the increasing trends of the viscosity. The increase in the viscosity increases the abrasive holding capacity of the media which tend to increase the machining process.

Thus hydrocarbon oil is selected for the gel preparation as it shows the requisite rheological property with increasing viscosity and increasing shear stress with respect to shear rate. Also the hydrocarbon oil shows the adequate dielectric property for the spark generation and stabilization of spark inside the media.

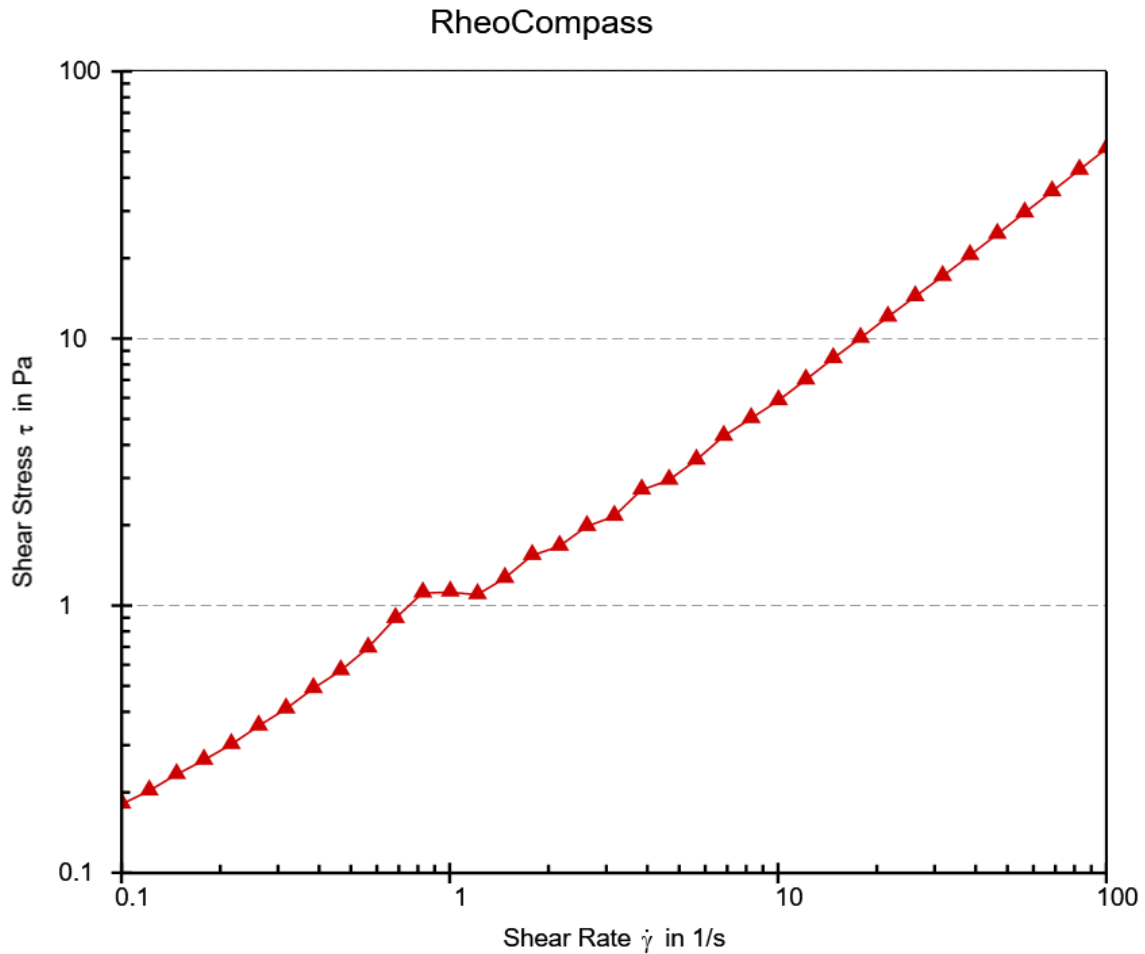


Figure 24 Shear stress Vs Shear rate for hydrocarbon oil

4.11. Selection of Gel material and preparation

On the basis of the viscosity trend of the gel from the engine oil, hydrocarbon oil and transformer oil, the hydrocarbon oil is selected as it shows the increasing viscosity trends compared to that of the engine oil and the transformer oil. As due to the thermal energy in the process, the temperature of the media would increase that will result in the decrease in the viscosity of the media. Hence to compensate this effect a media of high viscosity is required to overcome the effect of the temperature rise in the TACAFM process. The gel is prepared by taking ½ L of hydrocarbon oil and mixing 30 gm of aluminium stearate to it. It is stirred continuously until the proper mixing is achieved. Once it gets white colour, heating is done along with the stirring. The mixture is stirred until we get thick viscous gel.

The aluminium stearate used in the preparation process acts as a binder which thickens the gels also it ensures a very less quantity of the oil to be used in the preparation process. The continuous stirring of the gel along with the heating process strengthens the polymeric linkage for the gel preparation.

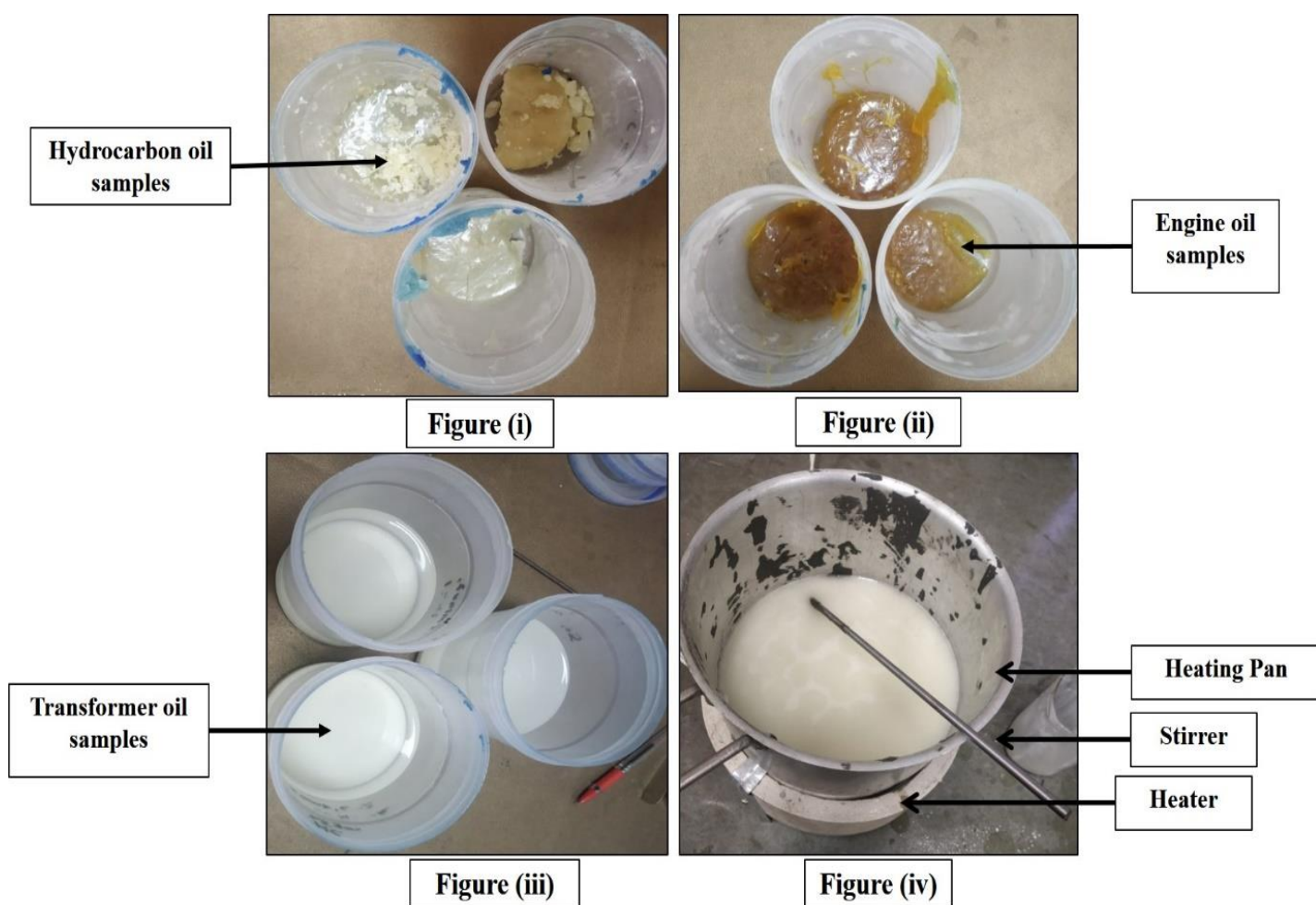


Figure 25 Different samples of Gel (i) Hydrocarbon oil sample gel (ii) Engine oil sample Gel (iii) Transformer oil sample gel (iv) Setup for gel preparation

Figure 25 shows the different gel samples and the equipment used for the preparation of gel. Figure 25 (i) shows the gel made up of hydrocarbon oil while the Figure 25 (ii) shows the gel samples made up of Engine oil. Figure 25 (iii) shows the gel sample made of transformer oil and figure 25 (iv) shows the arrangement of the equipment for the preparation of the gel. For all the samples, the gel is prepared by same methodology considering the same amount of aluminium stearate as the binder material and heating with continuous stirring until the material gets viscous in nature.

The continuous stirring is done with the help of hand along with the constant heating at initial stage. Once the aluminium stearate is added to the mixture, the polymeric chain begins to develop which increases the cohesive force within the particle resulting in the thickening of the gel. The viscosity of the sample is tested when the gels are finally prepared.

4.12. Preparation of polymer

Polymer are the key constituent of the media used in the abrasive flow machining process. The constituent constituting the media plays different role in the media process. The gel used in the media holds the abrasive and polymer particles whereas the abrasive particle used in the media results in the machining process through the abrasion process. The polymer used in the media plays a vital role in the functioning of media. The polymer provides fluidity to the media which enables the axial movement of media on the basis of pressure difference. The polymer used in the process is silicon oil based.

The polymer is prepared using by mixing 60 gm of boric acid with the silicon oil. The mixture is stirred until its colour become green. Then 10 gm of Lewis acid is added and the solution is stirred with heating. As the heat is continuously supplied to the mixture, the solution becomes rubber like structure. Finally, 10 gm of NH_4CO_3 was added for the and stirred continuously till it become viscous. It is then kept undisturbed until it gets cool.

The boric acid used in the process acts as a binding agent which tends to increase the cohesive property of the polymer and the Lewis acid acts as a polymerizing agent in the process of polymerization. The ammonium carbonate used in the process enhances the rheological property of the polymer which in turn strengthen the machining property of the media.

The silicon oil used in the polymer preparation is viscoelastic hydrocarbon oil which provides the polymeric linkage for binding the media and also provides dielectric effect to the media for the arc stabilization. The silicon oil also possessed excellent fluidity which helps in the movement of media and enhancement of machining process.

The polymer prepared from the above method is tested using the rheometer and the results were analyse for the rheological property. The desired rheological property of the polymer is similar to that of gel which includes viscosity computation. Table 6 shows the rheological data for the polymer. Figure 26 shows the variation of viscosity with respect to the shear rate and figure 13 shows the variation of shear stress vs shear rate.

Table 6 Viscosity data for Polymer

Point No.	Shear Rate	Shear Stress	Viscosity	Temperature	Torque
	[1/s]	[Pa]	[mPa·s]	[°C]	[mN·m]
1	0.0995	793.46	7.97E+06	25.01	14.956
2	0.121	756.3	6.24E+06	25.01	14.256
3	0.147	736.01	5.02E+06	25.01	13.873
4	0.178	732.82	4.12E+06	25.01	13.813
5	0.215	738.24	3.43E+06	25.01	13.916
6	0.261	749.67	2.87E+06	25.01	14.131
7	0.316	774.59	2.45E+06	25.01	14.601
8	0.383	811.79	2.12E+06	25.01	15.302
9	0.464	853.27	1.84E+06	25.01	16.084
10	0.563	883.37	1.57E+06	25.01	16.651
11	0.682	934	1.37E+06	25.01	17.606
12	0.825	992.01	1.20E+06	25.01	18.699
13	1	1018.8	1.02E+06	25.01	19.204
14	1.21	1106.2	9.13E+05	25.01	20.852
15	1.47	1117.6	7.61E+05	25.01	21.067
16	1.79	1140.2	6.38E+05	25.01	21.493
17	2.16	1203.6	5.58E+05	25.01	22.687
18	2.61	1238.3	4.74E+05	25.01	23.342
19	3.16	1047.8	3.31E+05	25.01	19.751
20	3.83	1045.7	2.73E+05	25.01	19.71
21	4.64	910.66	1.96E+05	25.01	17.165
22	5.63	788.18	1.40E+05	25.01	14.857
23	6.81	705.43	1.04E+05	25.01	13.297
24	8.26	666.82	80777	25.01	12.569
25	10	655.62	65546	25.01	12.358
26	12.1	612.35	50556	25.01	11.542
27	14.7	580.58	39555	25.01	10.944
28	17.8	549.5	30910	25.01	10.358
29	21.5	551.66	25604	25.01	10.399
30	26.1	539.25	20663	25.01	10.165
31	31.6	477.49	15102	25.02	9.0004
32	38.3	527.49	13768	25.02	9.943
33	46.4	479.47	10329	25.02	9.0378
34	56.2	494.82	8800.6	25.02	9.3271
35	68.1	419.63	6159.6	25.02	7.9099
36	82.5	407.67	4939.2	25.02	7.6845
37	100	383.73	3837.8	25.02	7.2332

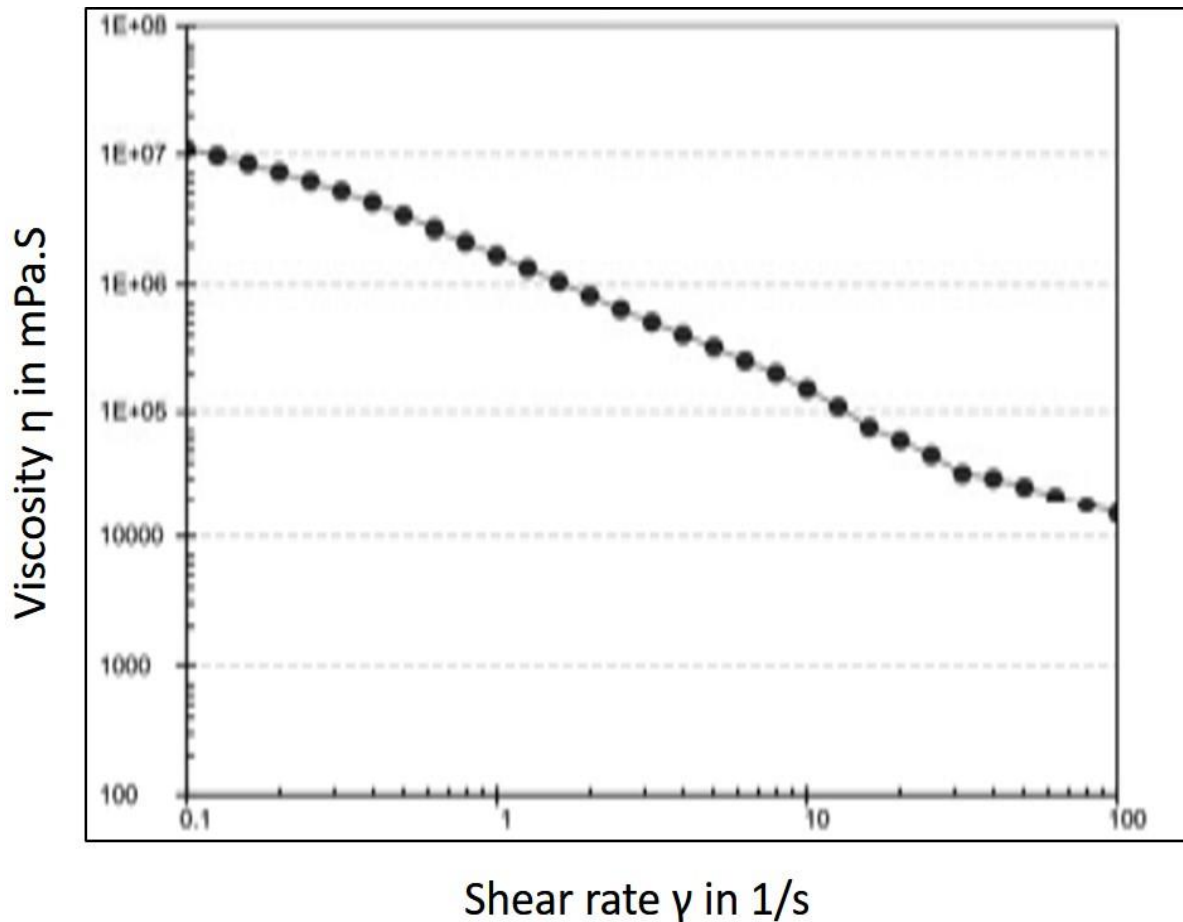


Figure 26 Viscosity vs shear rate for polymer

Figure 26 shows the variation of viscosity with respect to the shear rate. There is a viscosity drop with respect to the shear rate but this viscosity drop is not very rapid and may be considered for the TACAFM process. The viscosity drop is not very rapid which means the polymer particle can compensate the viscosity drop due to the temperature rise in the TACAFM process. The shear rate continuously increases during the TACAFM process as there is continuous movement of the media and also there is a centrifugal action due to the rotation of the CFG electrode.

Figure 27 shows the variation of the shear stress with respect to the shear rate. The shear stress variation seems to be constant with initial increase and then remains constant. The variation of shear stress supports the application of the silicon based polymer for the TACAFM process as the continuous increase in the shear stress would result in the strong polymeric linkage with the strong viscoelastic property that binds the abrasive and polymer particles. Also in actual process there would be loss of viscosity as the developed shear rate would be high along with the significant temperature increase. Thus the obtained rheological results are desirable.

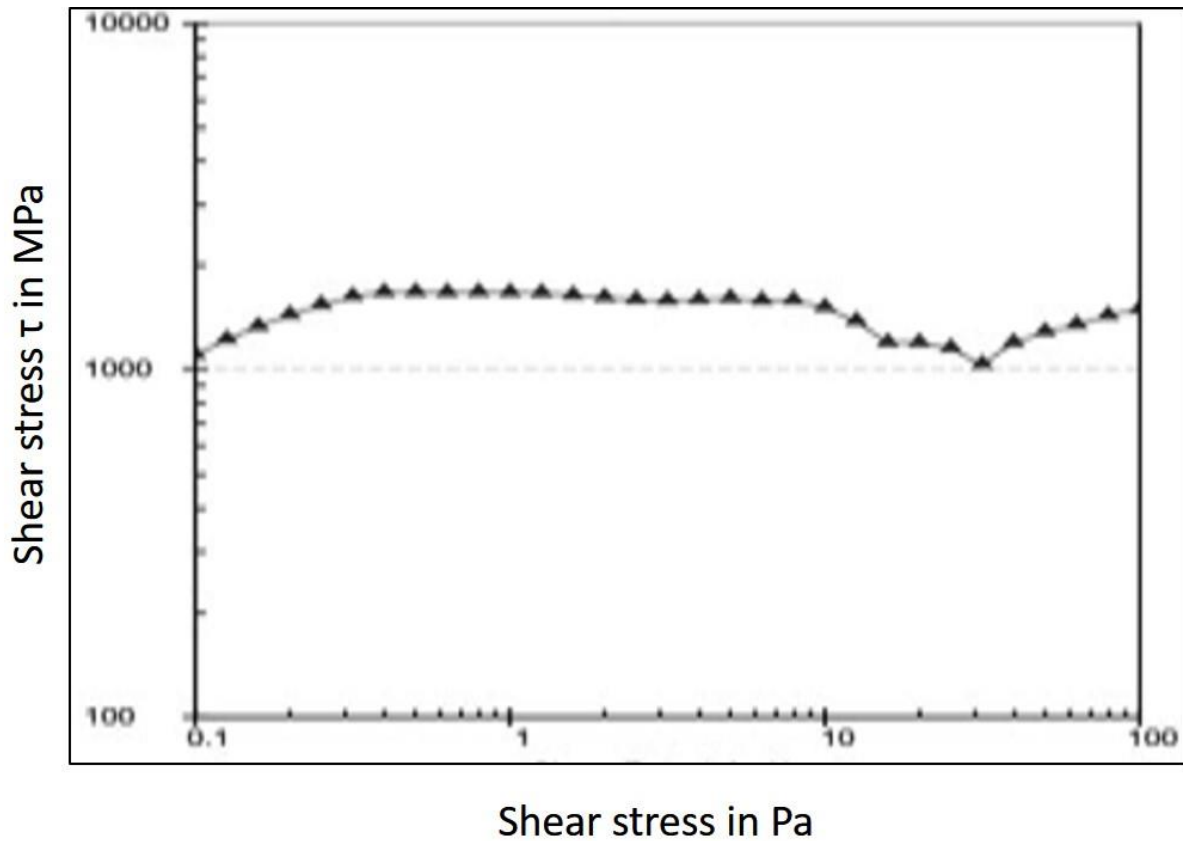


Figure 27 Shear Stress vs Shear rate for polymer

4.13. Preparation of Media

The media used in the investigation is prepared by mixing of polymer, gel and the abrasive in the requisite ratio so that a fine machining is obtained. The abrasive used in the investigation is silicon carbide with 400 mesh size. The initial solution is prepared by mixing the gel and polymer by hand and then mixing the abrasive to the final solution. For preparation of media the polymer to gel ratio is taken as 1:1. The mixing of polymer and the media is done with the hands when the mixture is mixed properly then silicon carbide (SiC) abrasive particles are mixed in the mixture with the ratio of 2:1 by weight.

Figure 28 shows the stepwise preparation of media. Figure 28 (i) shows the initial setup showing the heater, stirrer and the utensil. Figure 28 (ii) shows the preparation of the polymer, initial heating with continuous stirring is done until the polymer is prepared. Figure 28 (iii) shows the preparation of the gel which is separately prepared from the polymer. Figure 28 (iv) shows the mixing of polymer and gel, which is done by hand. Figure 28 (v) shows the mixing of abrasive particles in the media which is done by hand and figure 28 (vi) shows the freshly prepared media which is put into the media cylinder for the machining process. Table 7 shows the rheological data for the polymer given by the rheometer. Figure 29 shows the variation of

the viscosity with respect to the shear rate and the figure 30 shows the variation of shear stress with respect to the shear rate for the prepared media.



Figure (i)



Figure (ii)



Figure (iii)



Figure (iv)



Figure (v)



Figure (vi)

Figure 28 Preparation of Media (i) Equipment used for the preparation (ii) preparation of polymer (iii) preparation of gel (iv) mixing of polymer and gel by hand (v) mixing of abrasive particle (vi) Freshly prepared media for TACAFM process.

Table 7 Viscosity data corresponding to rheometer

Point No.	Shear Rate	Shear Stress	Viscosity	Temperature	Torque
	[1/s]	[Pa]	[mPa·s]	[°C]	[mN·m]
1	0.1	679.23	6.79E+06	27.74	12.803
2	0.126	822.49	6.53E+06	27.73	15.504
3	0.159	783.51	4.94E+06	27.73	14.769
4	0.2	779.39	3.91E+06	27.73	14.691
5	0.251	846.33	3.37E+06	27.73	15.953
6	0.316	863.81	2.73E+06	27.73	16.282
7	0.398	616.97	1.55E+06	27.73	11.63
8	0.501	489.57	9.77E+05	27.72	9.2281
9	0.631	608.26	9.64E+05	27.72	11.465
10	0.794	343.89	4.33E+05	27.72	6.4821
11	1	375.37	3.75E+05	27.72	7.0755
12	1.26	425.57	3.38E+05	27.72	8.0217
13	1.58	362.18	2.29E+05	27.72	6.827
14	2	300.47	1.51E+05	27.72	5.6637
15	2.51	345.11	1.37E+05	27.71	6.5051
16	3.16	370.76	1.17E+05	27.71	6.9886
17	3.98	353.29	88759	27.71	6.6593
18	5.01	405.17	80826	27.71	7.6372
19	6.31	433.52	68722	27.71	8.1716
20	7.94	461.18	58067	27.71	8.693
21	10	494.37	49447	27.71	9.3187
22	12.6	555.05	44099	27.71	10.463
23	15.8	647.55	40858	27.71	12.206
24	19.9	767.2	38458	27.7	14.461
25	25.1	836.17	33297	27.7	15.761
26	31.6	584.37	18470	27.7	11.015
27	39.8	553.26	13902	27.7	10.429
28	50.1	598.1	11930	27.7	11.274
29	63.1	652.57	10343	27.7	12.301
30	79.5	316.84	3984.6	27.7	5.9723
31	100	143.96	1439.4	27.7	2.7135

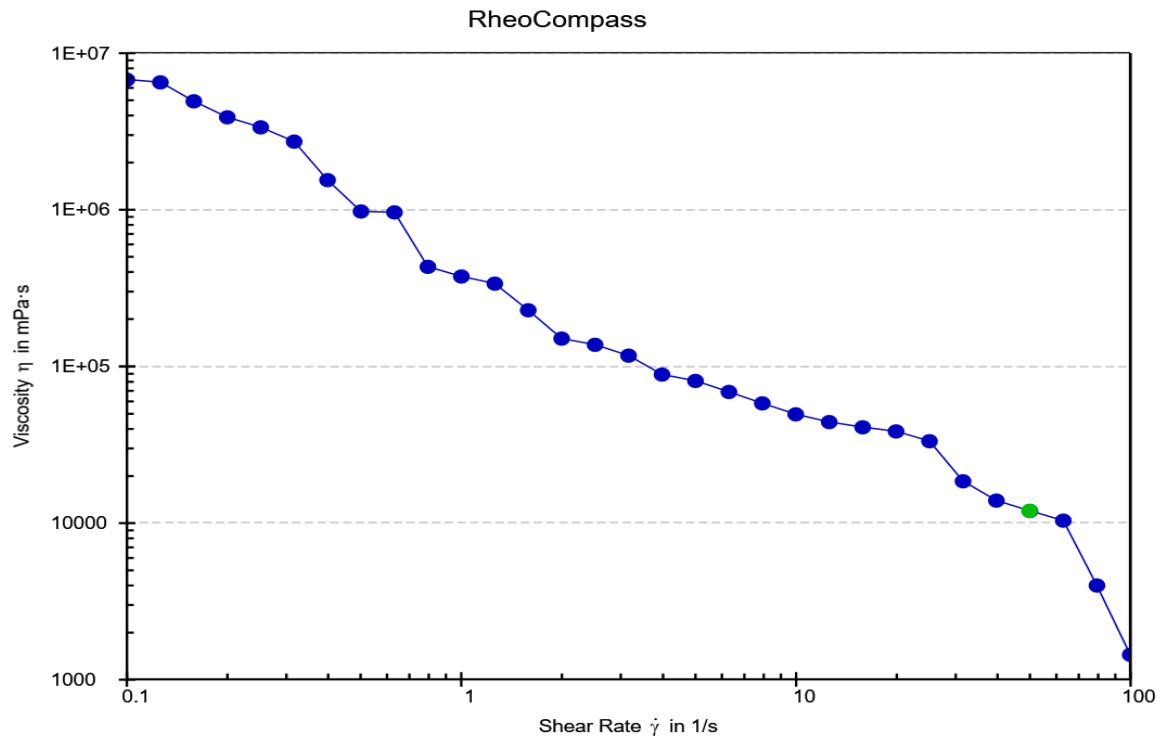


Figure 29 Viscosity vs shear rate for the media

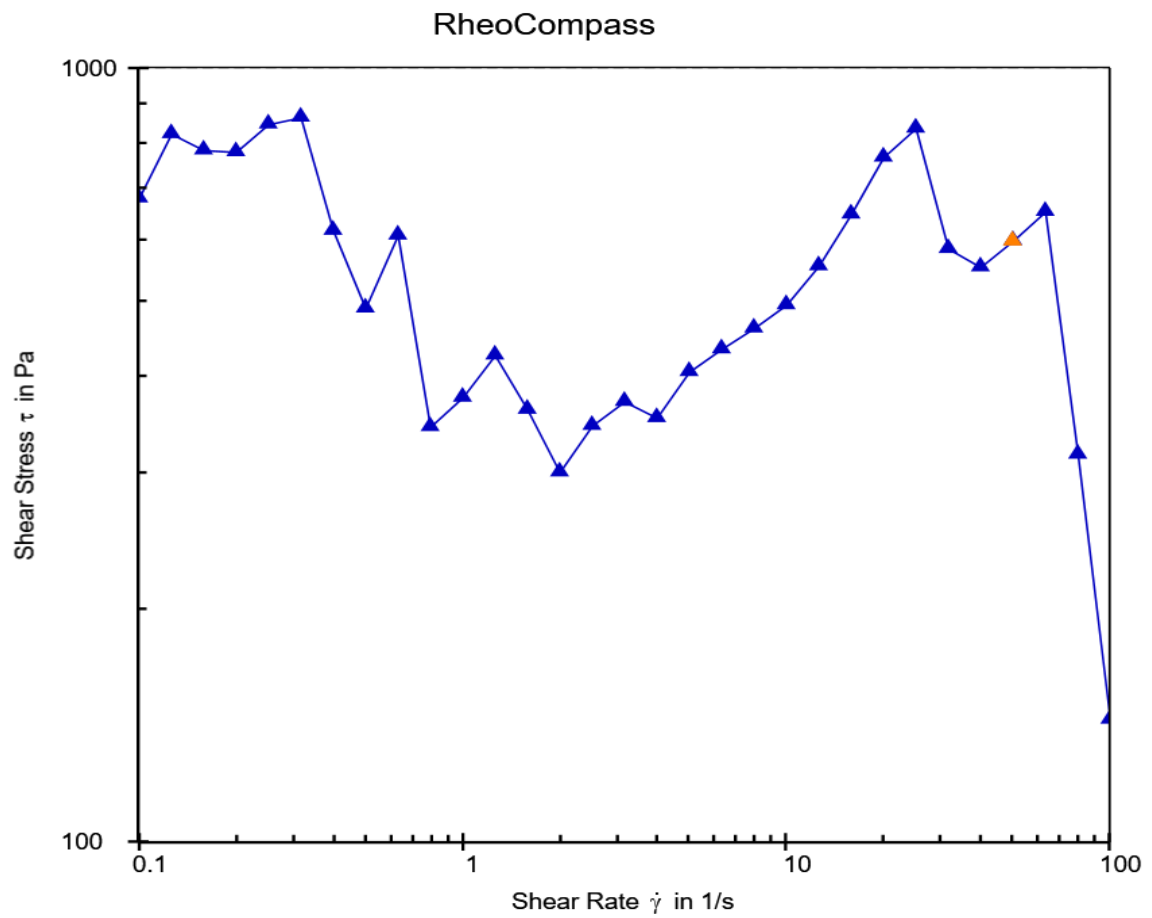


Figure 30 Shear stress with respect to shear rate

The variation of viscosity with the shear rate for the media shows the decrease of viscosity with respect to the shear rate which is obvious trend for the viscoelastic media. The shear rate increases due to the increase in the movement of media which results in the viscosity decrease. The variation of the shear stress with respect to the shear rate shows the unobvious trend. The main reasons for this is that the media is prepared by the mixing of gel and polymer in the same ratio by volume and also the another point of consideration is that there is various lump formation in the mixture which tends to vary the shear stress trends of the media as a results the value shows the sudden increase or decrease with absurd rheological data. But the overall trend of viscosity is not decreasing which validates the application of the proposed media for the TACAFM process. The increasing viscosity trend is required for the compensation of the temperature rise in the media. And this viscosity rise also holds the abrasive particles as they possess strong polymeric linkage which accelerates the machining process of the TACAFM proposed TACAFM process.

4.14. FTIR of Media

Fourier transfer infrared spectroscopy is done to check the constituent of the media and also to get the idea of the polymeric linkage of the proposed media. The sample of the prepared media is analysed and the peaks were analysed. The basic principal of FTIR is that the when infrared falls on the object, some energy or the radiation absorbed. These radiations are absorbed and the structure of the structure of the sample is analysed.

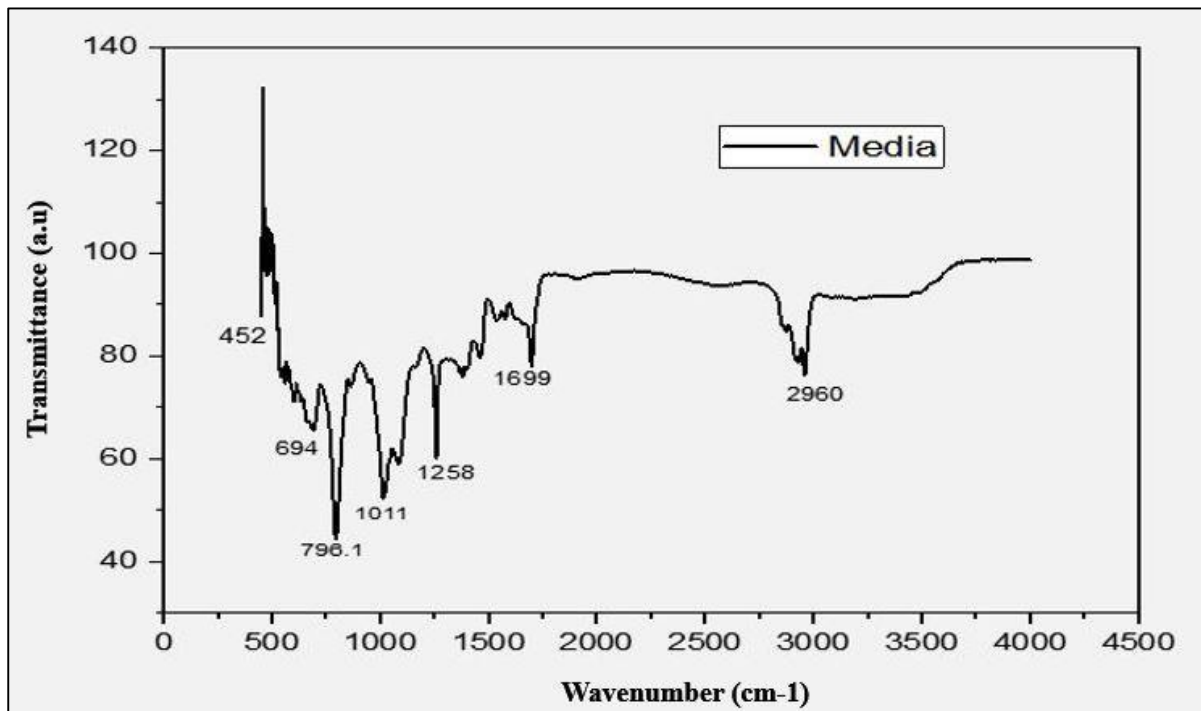


Figure 31 FTIR analysis of the Prepared Media

Figure 31 shows the FTIR plots which highlights the viscoelastic dielectric trend containing hydrocarbon structure. It can be observed that the wavenumber corresponding to 2960 highlights the presence of alkanes with carbon, carbon single bond and carbon hydrogen single bond. Whereas the wave number corresponding to 1699 represents the presence of alkenes which corresponds to carbon, carbon double bond or C=C (Al-Akhras et al. 2018). The wavenumber corresponding to 1258, 1011, 769.1, 694 and 452 corresponds to dielectric medium (liu et al. 2022). The pattern is similar to hydrocarbon based viscoelastic dielectric medium, which is a requisite for the TACAFM process as the of C=C and C-C provides sufficient polymeric linkage to hold the abrasive particle and makes it suitable for the machining process (chen et al. 2020). Thus the proposed media is suitable for carrying the machining process for the machining process and stabilization of the arc.

Summary

- 1. Viscosity is the prominent property for the media for TACAFM process**
- 2. Gel provides adequate viscosity to the media, polymer provides fluidity to the media and the abrasives provides the machining action to the media.**
- 3. Hydrocarbon oil based gel is used for the preparation of the gel**
- 4. Silicon based oil is used for the preparation of polymer.**
- 5. The media used for TACAFM process should resembles a viscoelastic dielectric hydrocarbon based media.**

Chapter 5. Computational Modelling of TACAFM Process

The present chapter involves the modeling and simulation to check the feasibility of different shape of electrode for the TACAFM process. The TACAFM process with different electrode geometry is analyzed on ANSYS Fluent to justify the spark formation and to analyze the flow parameters. The variation of pressure and temperature on the brass workpiece is analyzed which gave the idea of material removal for the TACAFM process and the temperature distribution validates the spark formation.

5.1. Background

Abrasive flow machining is used for the finishing of the internal surfaces of the hard to reach material. The process finds its application where the conventional finishing surfaces like buffing tool, honing tool and other are unable to use. The finishing of material takes place due to abrasion process by the abrasive present in the media. The media binds the abrasive particles and strikes over the wall of the surface whose finishing is to be achieved. In the TACAFM process a CFG electrode is brought into the scenario along with the EDM effect which increases the material removal of the conventional AFM process. The CFG electrode present in the TACAFM process plays a vital role in the computation of MR as it increases the centrifugal force in the media and increases the dynamic number of abrasive particles hitting the wall of the workpiece. The different shapes of the electrode show different throwing ability of the media (abrasive particles) over the wall of the workpiece. It has been reported in the literature that the throwing ability of spline shape electrode is better as compare to the square and triangular shape electrode which provides a significant difference in the computation of MR. Thus the study of the effect of the shape is an important process in this regard which need to be taken into care. The present investigation uses different shapes of the CFG electrode to check their application in the TACAFM process. The prominent shapes include square shape electrode, triangular shape electrode and the spline shape electrode. The spline shape electrode is the electrode which consist of blades around a circular electrode. These blade are at the minimum distance from the wall of the workpiece so that the EDM effect comes into the picture. Also the advantage of the spline shape electrode is that it they contain sufficient space for the flow of media which encourages the abrasive and the wall interaction resulting in the higher material removal. The present work also proposes a novel spline shape electrode containing a curved blade which increases the centrifugal force on the media which accelerates the material removal process which is one on the major limitation of conventional AFM

process. Also different shapes produce different temperature distribution over the workpiece resulting in the variation in spark pattern which affects the machining of the workpiece.

5.2. Effect of flow parameter

As discussed in the earlier section, media plays a vital role in the machining of TACAFM process. The prominent parameters that affect the media flow inside the cylinder are significantly affect the material removal. The prominent parameters are the extrusion pressure, media flow rate, abrasive concentration and the rotational speed of the electrode.

5.3. Extrusion Pressure

The increase in the extrusion pressure ensures the rapid movement of media due to the reciprocation from upper cylinder to lower and from lower to upper cylinder. The maximum working pressure on which the AFM works is 20 MPa and the simulation the were performed for 20 MPa. It has been reported that the increasing extrusion pressure increases the pressure distribution over the workpiece. This increase in the pressure difference results in the increase in the material removal (Shankar et al. 2009).

5.4. Media Flow Rate

The media flow rate controls the abrasive interaction with the wall of the workpiece. Increasing media flow rate results in the increase in the abrasion process (walia et al 2006). The media flow rate is generally kept constant for the flow simulation.

5.5. Abrasive Concentration

The abrasive concentration plays a vital role in the machining process. The increase in the abrasive concentration present in the media results in the increase in the dynamic number of abrasive particle for the abrasion process which results in the machining process (**Brar et al, 2013**).

5.6. CFG electrode rotation

The next important parameter consider in the simulation of the AFM is the rotation of the CFG electrode. The increase in the rotation of the CFG electrode results in the increase in the centrifugal force in the media directly increasing the material removal of the proposed TACAFM process. It has been reported that the increasing rotational speed increases MR in the AFM process but decreases the surface roughness of the machined workpiece (**walia et al. 2006**).

In the present investigation different electrode geometry mainly spline shape electrode with straight blade, curved blade, triangular shaped electrode and the square shaped electrode are

separately modelled to analyzed their effect and the effect of other flow parameter on the material removal and on the percentage improvement in surface finish.

5.7. Solid Modelling of TACAFM Process

The electrode used for the TACAFM process are separately modelled along with the workpiece, abrasive and the solid media and then assembled for the analysis. The CREO 3.0 is used for the initial modelling and then the entire assembly is transfer to the ANSYS Fluent for the analysis of flow parameters through IGES files. The subsequent sections deal with the different component of the geometry.

5.7.1. Workpiece

The workpiece used in the investigation is separately modelled on the CREO Parametric 3.0. The dimensions of the workpiece is kept similar to that used in the experimental process. The workpiece is made hollow cylindrical with the outer diameter of 10 mm, inner diameter of 8 mm and the height of 16 mm as per the Kohut recommendations (**Kohut 1988**). The material used for the workpiece is brass on the basis of its application in modern finishing processes (**Gaurav et al. 2022**). Figure 32 shows the solid model of the workpiece used in the simulations.

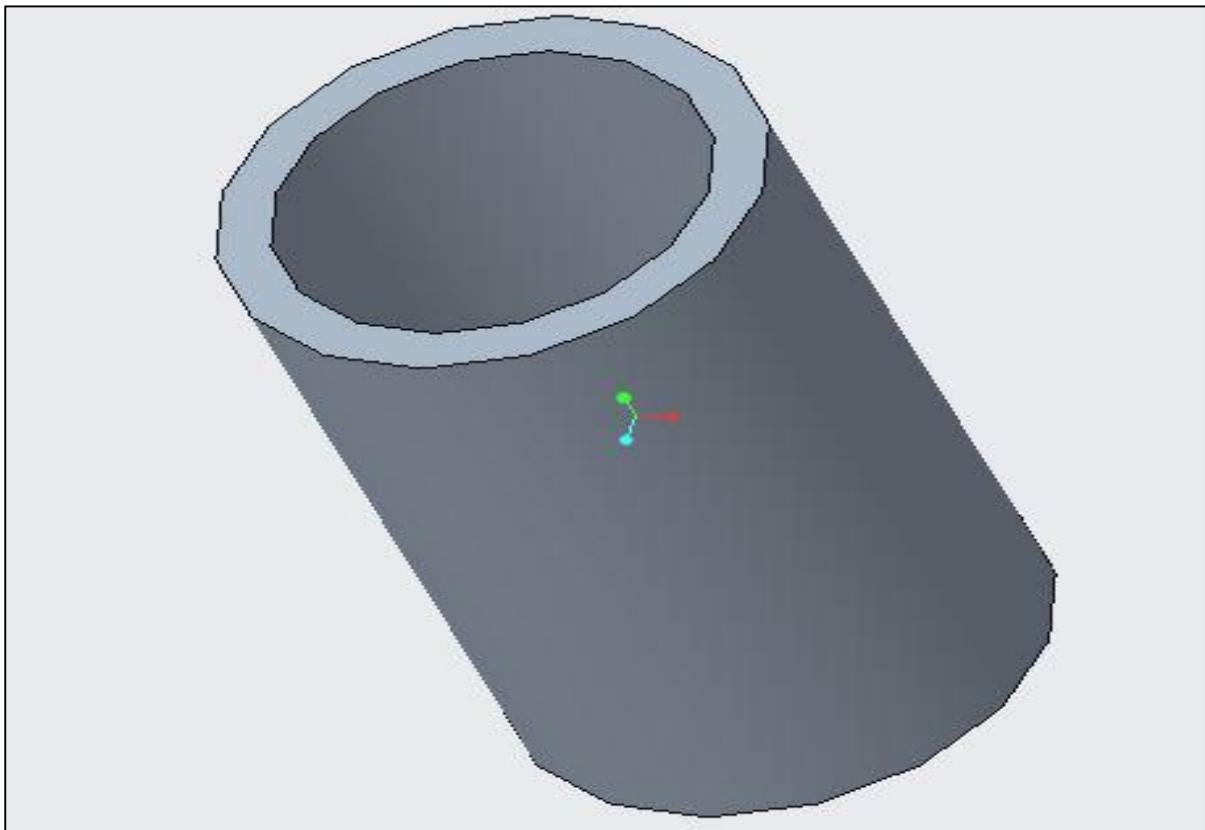


Figure 32 Solid Model of Workpiece on CREO Parametric

5.7.2. Media

The media is made as the solid wall covering the workpiece. It is made solid as the stationary property is to be provided to the media so that the boundary condition of the wall is provided to the media. The media represents the shape of the flow pattern of the upper and lower media cylinder and the internal surface of the workpiece. Figure 33 shows the solid model of the media used in the investigation.

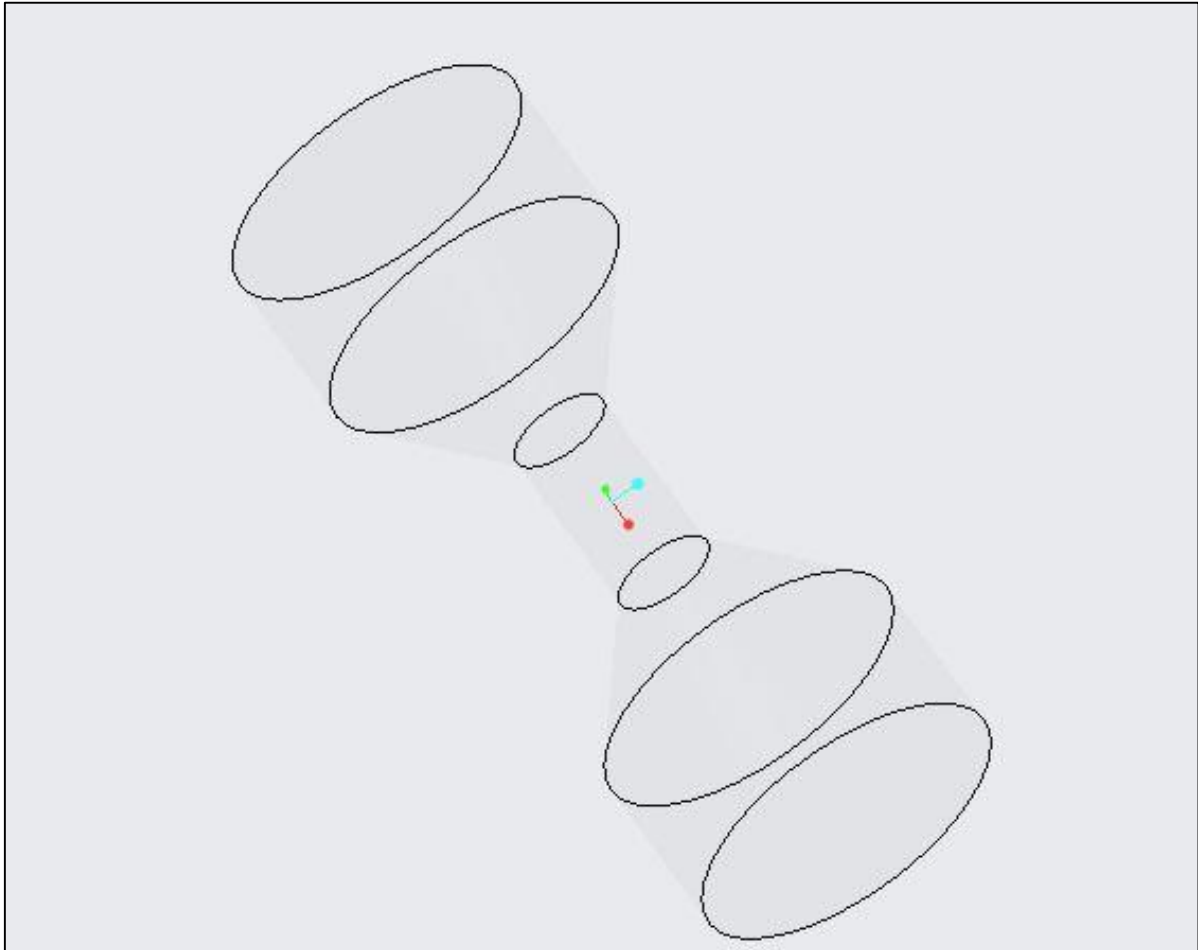


Figure 33 Solid Model of Media used in investigation

5.7.3. Centrifugal Force Generating Electrode

The centrifugal force generating electrode is the key component in the TACAFM process as it caters the centrifugal action and also support the spark by acting as anode. The four type of electrode were modelled for the analysis and their assemblies were separately analyzed in the simulation. The dimensions of the CFG electrodes was decided on the minimum area of flow for the media and the minimum gap between the electrode and the workpiece for the spark generation. This is because a minimum gap is required for the spark formation in the EDM process also the minimum area of flow of media increases the dynamic number of abrasive

particles near the wall of the workpiece resulting in the higher rate of abrasion. The different types of electrode used in the investigation are square shape electrode, triangular shape electrode and the spline shape electrode. Further the spline shape electrode is again taken of 2 type, firstly the spline electrode with straight blade and the other the spline electrode with the curved blade. The details of geometry are discussed in the further sections.

5.7.3.1. Square electrode

The square shape rod shows suitable performance in material removal when compare to conventional shape rod when used in Centrifugal force assisted abrasive flow machining process (CFAAFM) when used without the spark. On that basis the square shape electrode is analyzed for the TACAFM process in the present investigation. The square shape electrode is modelled on CREO parametric with dimensions of side as 5.62 mm. Figure 34 shows the solid model of the square electrode used in the investigation.

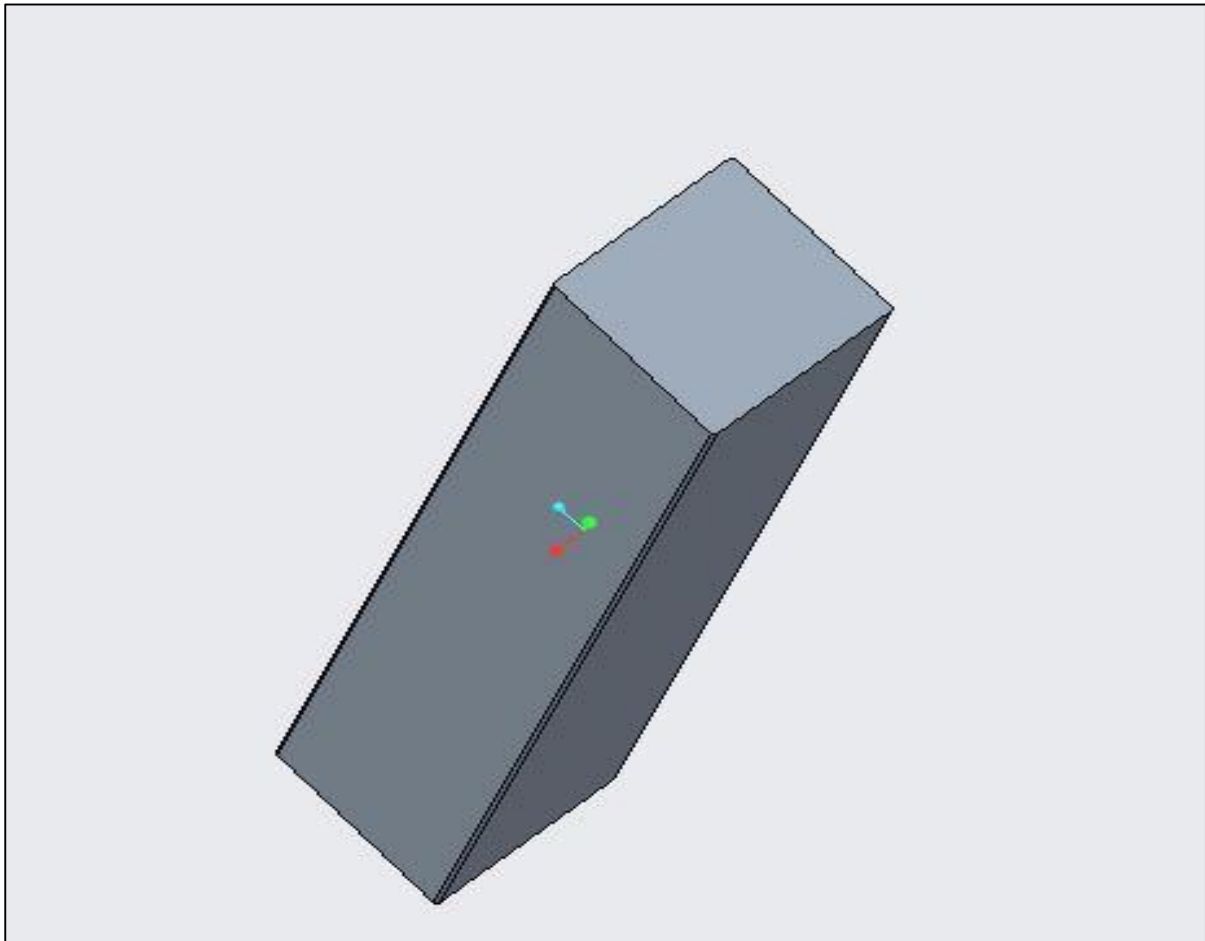


Figure 34 Solid Model of square electrode used in investigation

5.7.3.2. Triangular electrode

Triangular shape electrode is one of the prominent centrifugal force generating electrode used in the Centrifugal force assisted abrasive flow machining process. It shows significant improvement in surface finish when consider in use. Considering this point, it is analyzed in TACAFM process. The type of the triangular taken is equilateral triangle with each side measuring 6.2 mm. Figure 35 shows the solid model of the triangular shape electrode used in the investigation which is made on CREO Parametric 3.0.

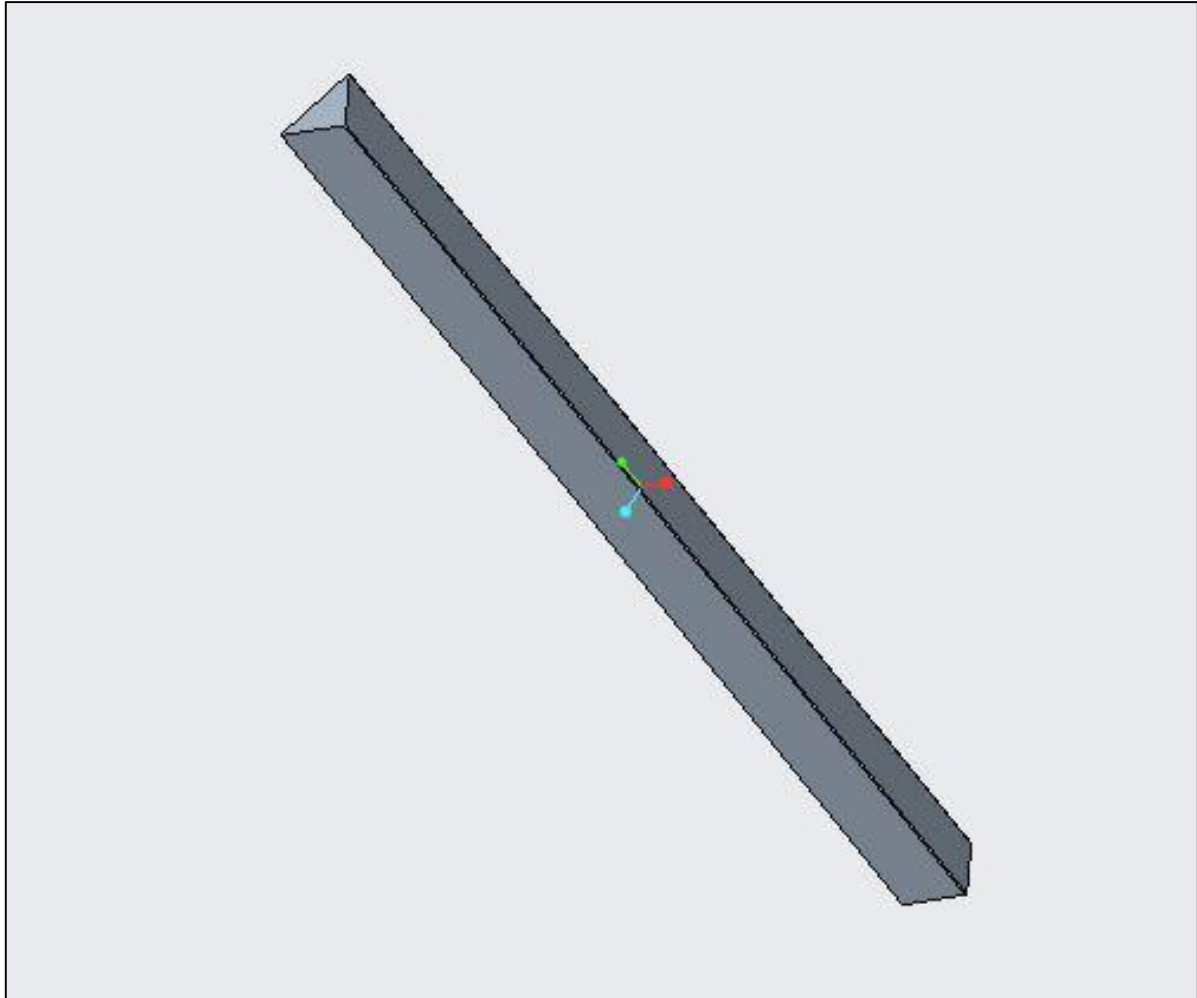


Figure 35 Solid Model of Triangular electrode used in investigation

5.7.3.3. Spline shape electrode with straight blade

Spline shape electrode provides the sufficient space for the media to flow which increases the dynamic number of active particles towards the wall of the workpiece. The blade present on the spline shape electrode provides significant centrifugal force inside the cylinder which tends to initiates the material removal process. The spline shape electrode used in the TACAFM process consist of straight blade with the blade of 7.95 mm flange and the diameter of circular

base is 4 mm. Figure 36 shows the spline electrode with straight blade. Ali et al (Ali et al, 2020) reported that the proposed TACAFM process with the straight spline shape electrode showed a significant improvement in the material removal and the surface finish. The literature reported that the increase in the material removal is 44.34 percent, compare to the conventional abrasive flow machining process and also it is reported that the percentage improvement in surface finish is 39.74 percent higher as compare to the conventional AFM process. The dimensions of the blade are so designed that it can be placed inside the internal surface of the workpiece.

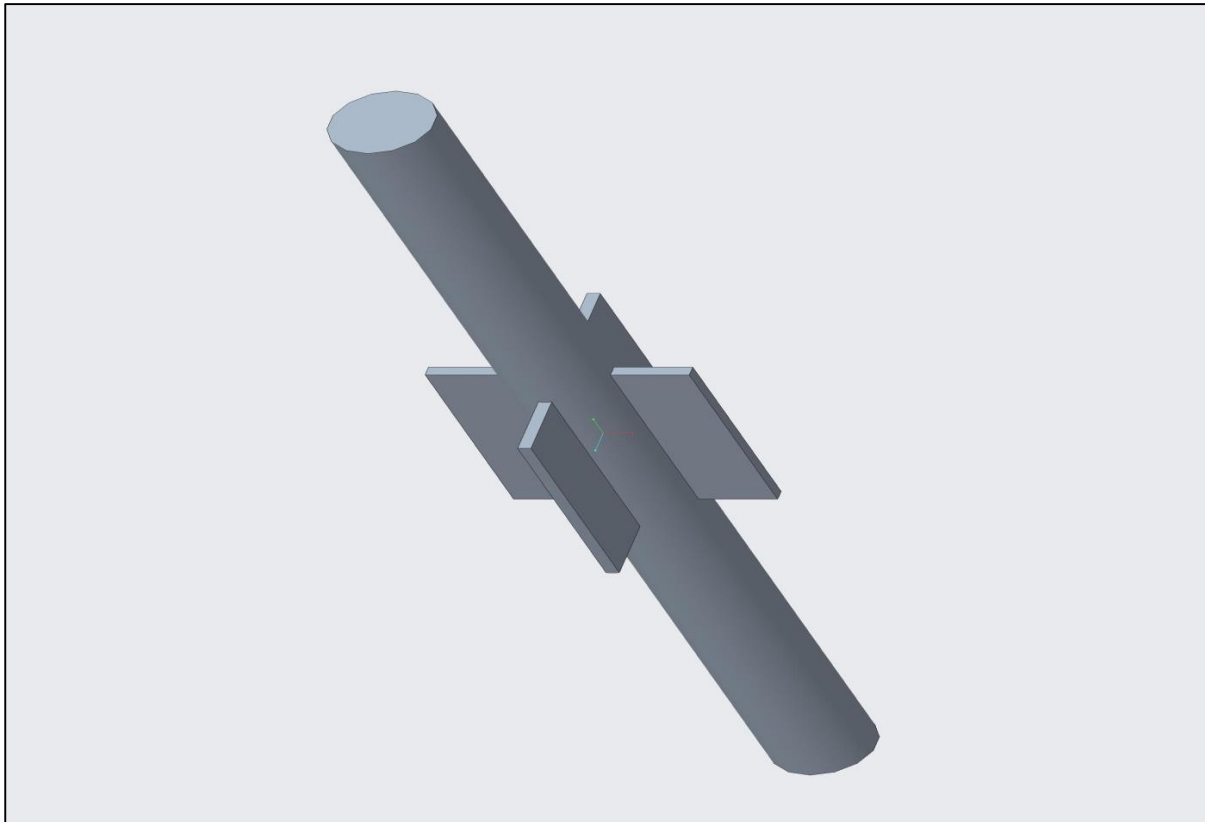


Figure 36 Solid Model of Spline Shape Electrode with straight blade used in investigation

5.7.3.4 Spline shape electrode with curved blade

The spline shape electrode with the curved blade provides an increase centrifugal force on the abrasive particles which increase the abrasion process to cater the low MR of the TACAFM process. The concept of the curved blade is taken from the centrifugal fan which reveals that the curving the blade would results in the increase in the abrasion process. The dimension of the spline shape used in the process consists of circular shaft with 4 mm diameter and the curved blade with the span of 7.95 mm diameter. The inner curve radius is 1.35 mm and the outer curve radius is 1.5 mm. The dimensions are decided on the basis of minimum area of flow of the media so that the dynamic number of particles increases with the abrasion process.

Thus the dimensions of the curved shape electrode are so made that it fits inside the internal surface of the workpiece ensuring the minimum gap (0.01 to 0.9 mm) for the spark formation for the EDM process. Figure 37 shows the solid model of the spline shape electrode with the curved blade.

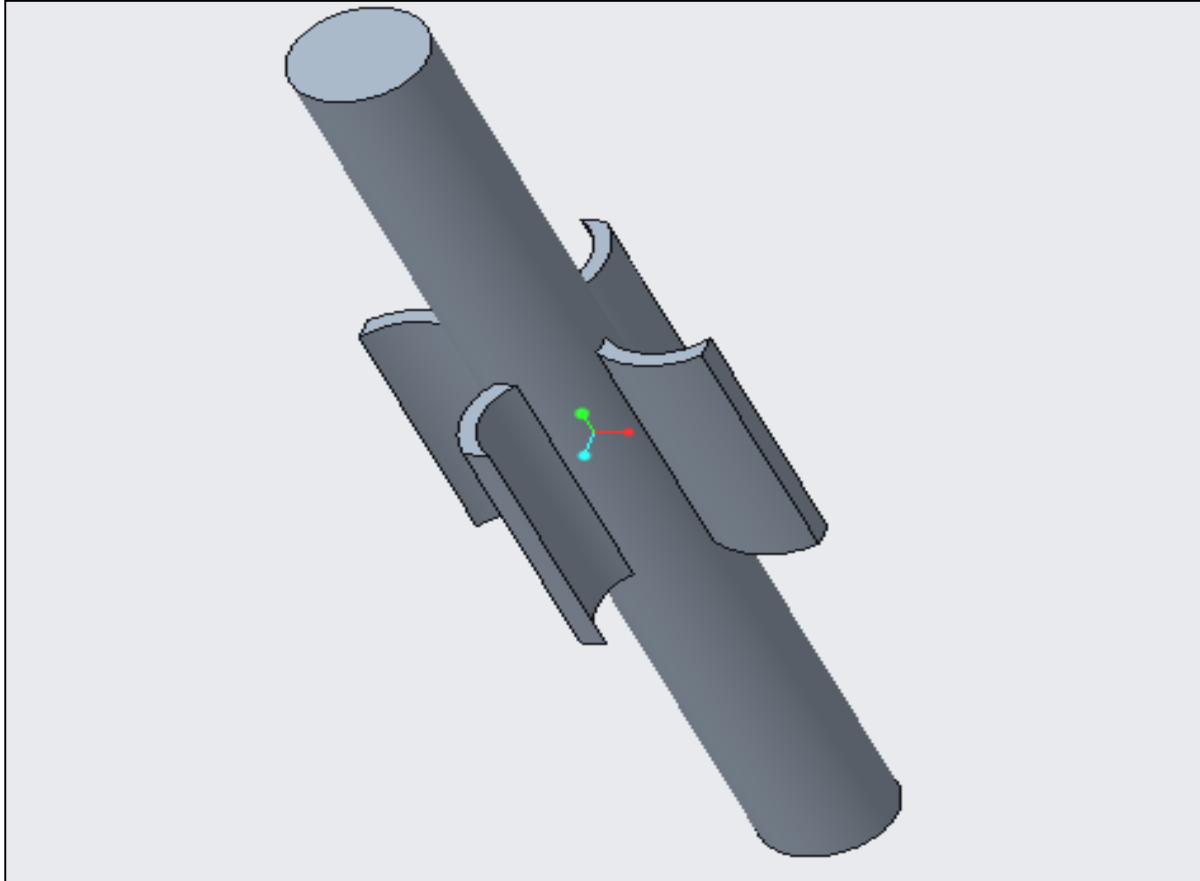


Figure 37 Solid Model of spline shape electrode with curved blade used in investigation

5.8. Assembly of the CFG different shaped CFG electrode

The next step in the to assemble the various solid modelled components into the assembly. For this purpose, the assembly module of the CREO parametric is used. Separate assemblies were made for the different shape of the electrode. Figure 38 shows the assembly of the TACAFM process containing the square shape centrifugal force generating electrode along with the workpiece and the media. The size of the workpiece and the length of media cylinder and that of the electrode is kept constant. Figure 8 shows the assembly of the triangular shape electrode. It contains the workpiece, media and electrode. Similarly figure 39 shows the assembly of the spline shape electrode with straight blade. Figure 40 shows the assembly of the spline shape electrode with the curved blade. The requisite parts are labelled on the figure and also contain abrasive particle. In actual process the media is a combination of abrasive, gel and polymer. In Ansys fluent, combine property of the mixture is applied to the media component which does

same effect as done by the actual media. Thus the media is made as a solid component and its property are given in the fluent. The Boolean operation is used in fluent which provides a media flow path.

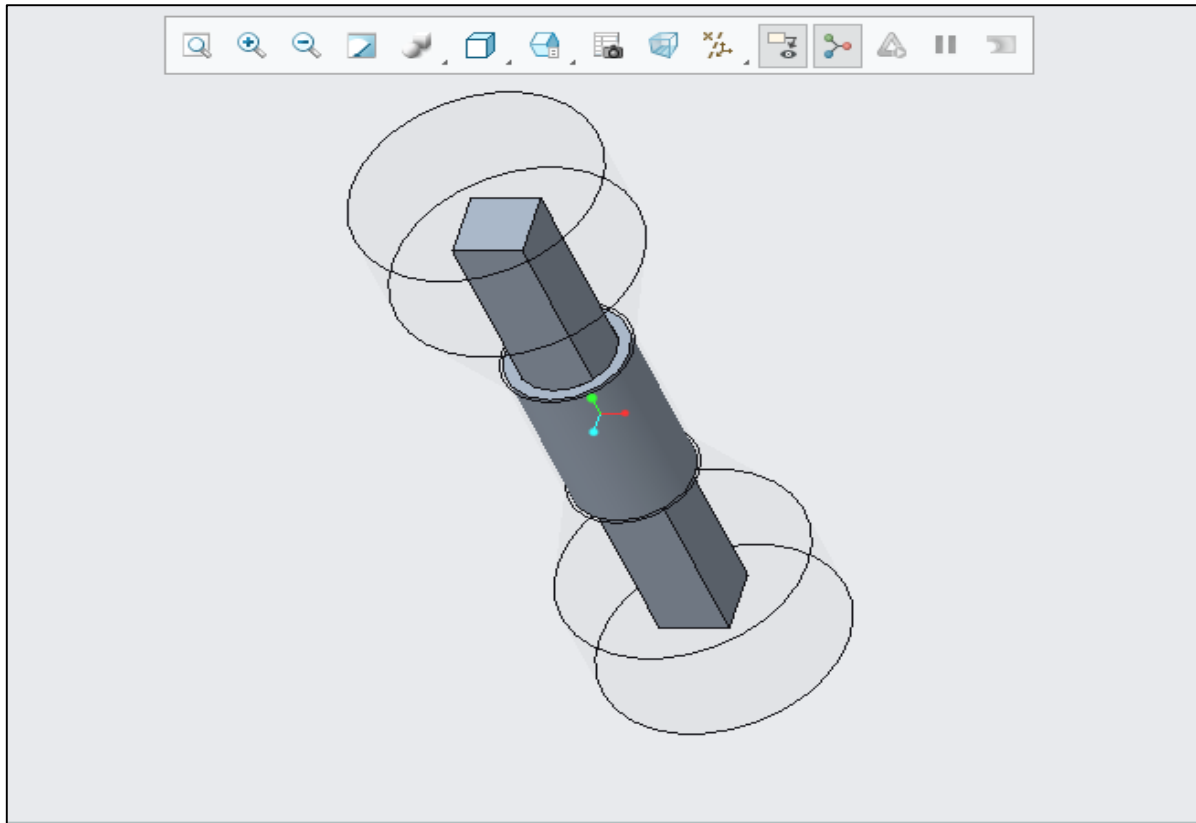


Figure 38 Square shape CFG electrode assembly

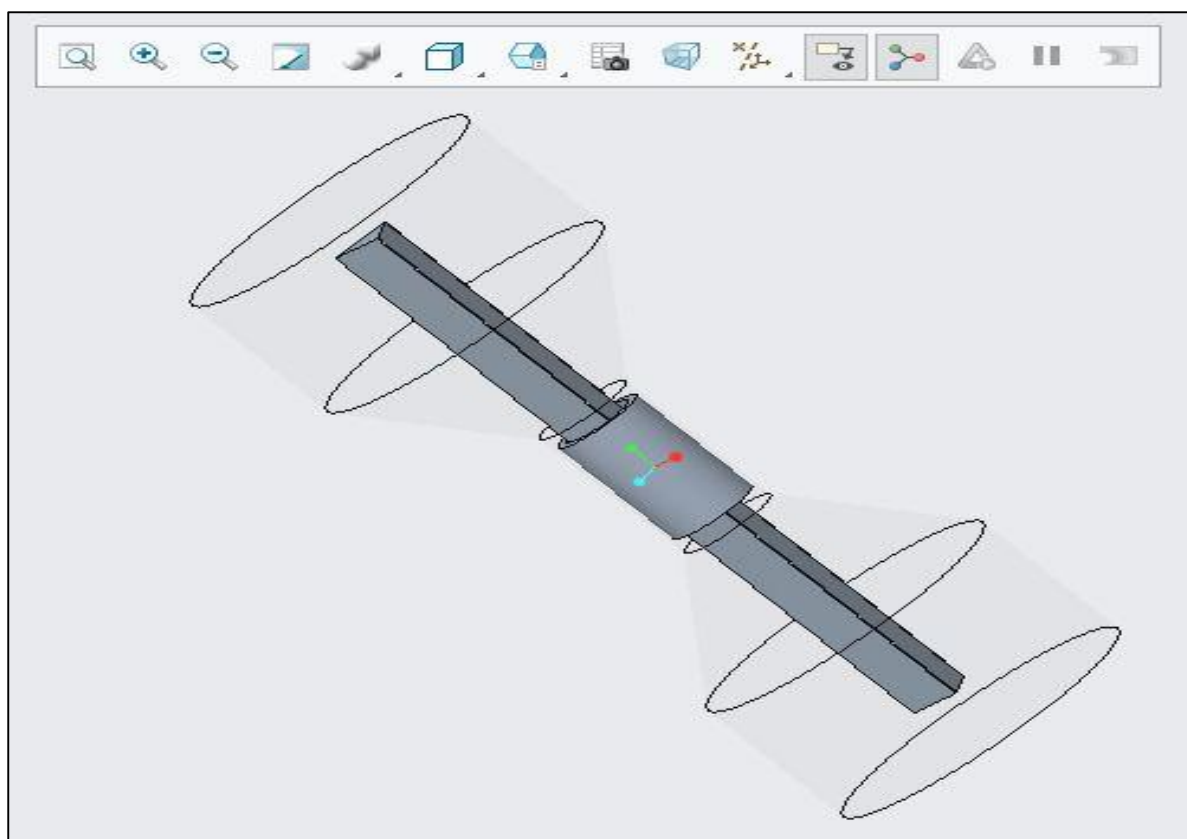


Figure 39 Triangular shape CFG electrode Assembly

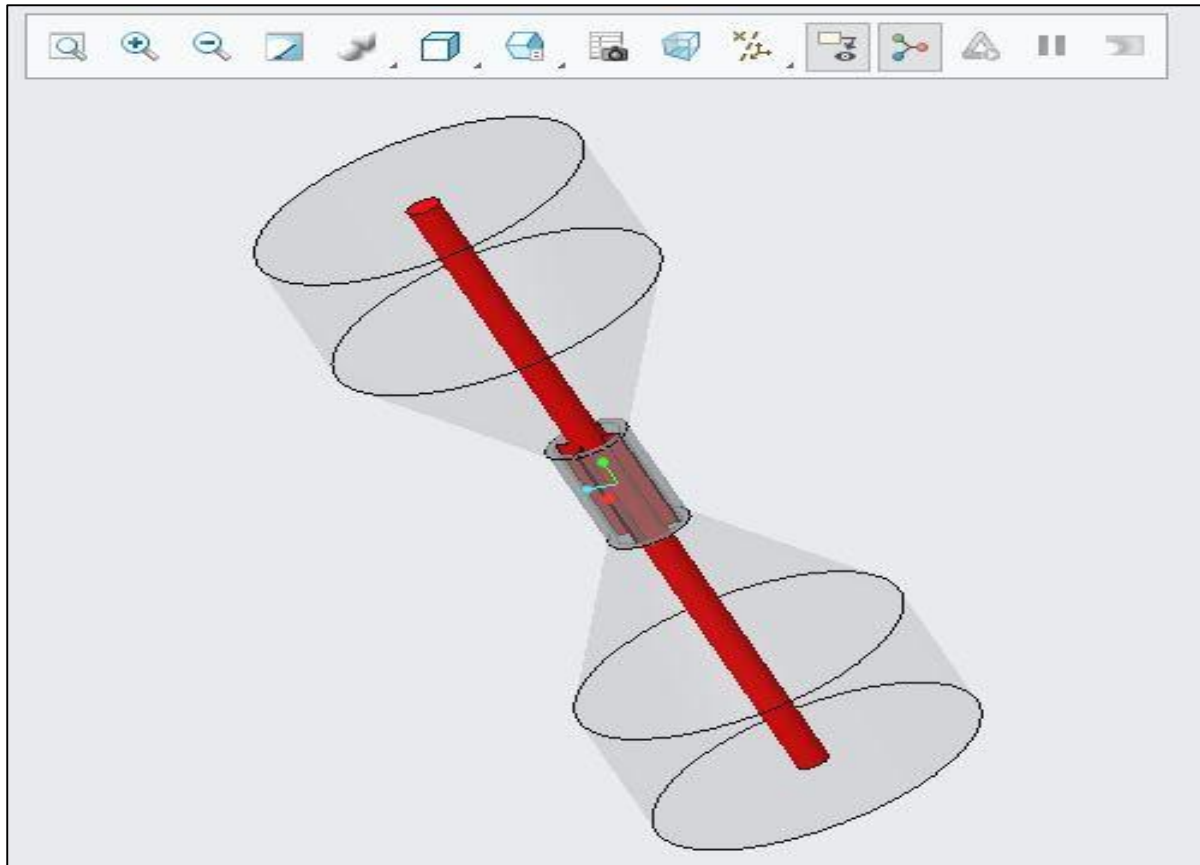


Figure 40 Triangular shape CFG electrode assembly

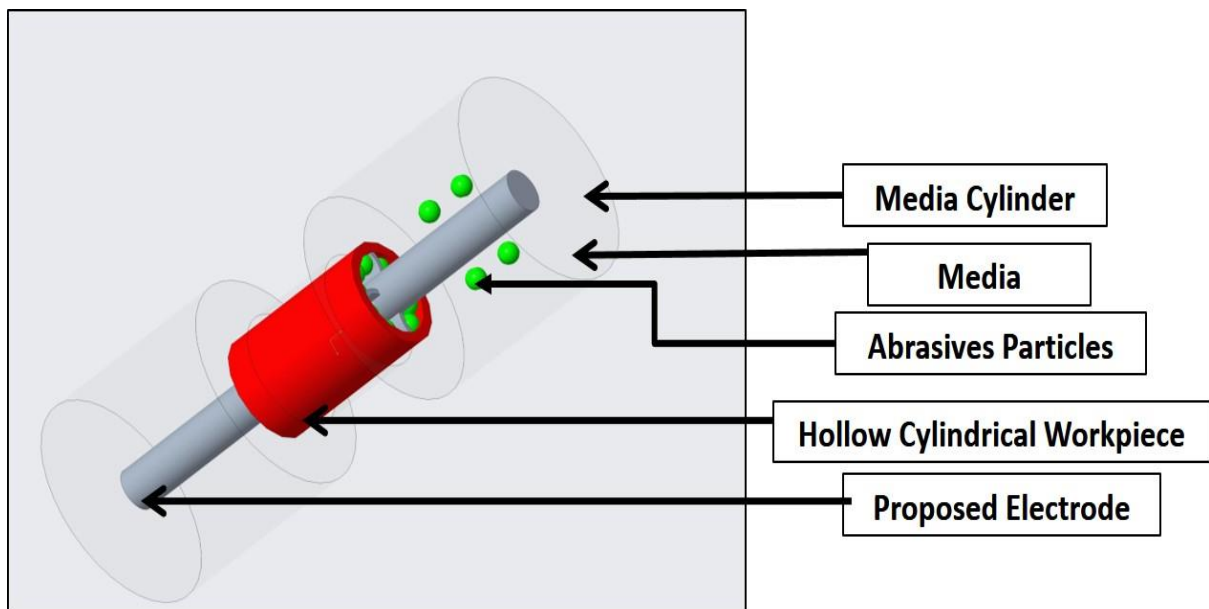


Figure 41 Spline shape CFG electrode Assembly

The actual process which would happen in the TACAFM Process is shown by the schematic diagram in figure 42, 43 and 44 where detailed labelled part is shown. Figure 42 highlights the spline shape electrode, 43 square electrode and figure 44 as triangular shape electrode.

The figure shows the extrusion of media particle from upper cylinder to lower cylinder and from lower cylinder to the upper cylinder by virtue of pressure difference. This extrusion pressure generally varies with size and in present case 20 MPa is taken as the extrusion pressure. The centrifugal force generating electrode is co-axially placed along the workpiece whose rotation results in the increase in the centrifugal force in the media which increases the abrasion process. The assembly also shows the positive and the negative terminals which will be used for the supply of pulsed DC for the spark generation. Hence the machining would occur as the result combination of abrasion and melting and evaporation effect. Figure 43 shows similar effect for the triangular shape electrode.

The process consists of a Centrifugal force generating a negatively charged electrode which pulsed DC Supply Electrode charges. The material removal is done on the anodic workpiece, which should be conductive. As the current is supplied to the electrode, it emits electrons, which tend toward the positively charged workpiece. In between, these electrons collide with the media particle, which is non-conductive. As a result of these collisions and also due to the media's repulsive action, the spark generated between the workpiece and the electrode surface, which makes the process capability of more material removal and continuous extrusion of media with abrasive, provides a smoother and improved surface finish.

Figure 44 shows the mechanism of spark formation, and figure 44 (i) shows the top view of the electrode and the workpiece with the gap between the electrode and the workpiece. Figure 44 (ii) shows the enlarged view of the gap between the electrode and the workpiece. When the pulsed DC is supplied to the workpiece and electrode, the electrons move towards the workpiece from the electrode surface, where they strike with media particles and ionize them. As the concentration of electrons increases, the ionization increases, resulting in the formation of the plasma layer. This plasma layer forms the required spark and removes the material by melting and erosion.

The similar effect can be observed for the square and triangular shape electrode which is shown in figure 45 and 46 respectively. Thus the crucial parameters involve in the design of the electrode is the gap between the electrode and the workpiece which is basis of the spark generation inside the media. The design of electrode is done in same basis which is the minimum gap between the electrode and workpiece and the minimum area of flow between the electrode and the workpiece.

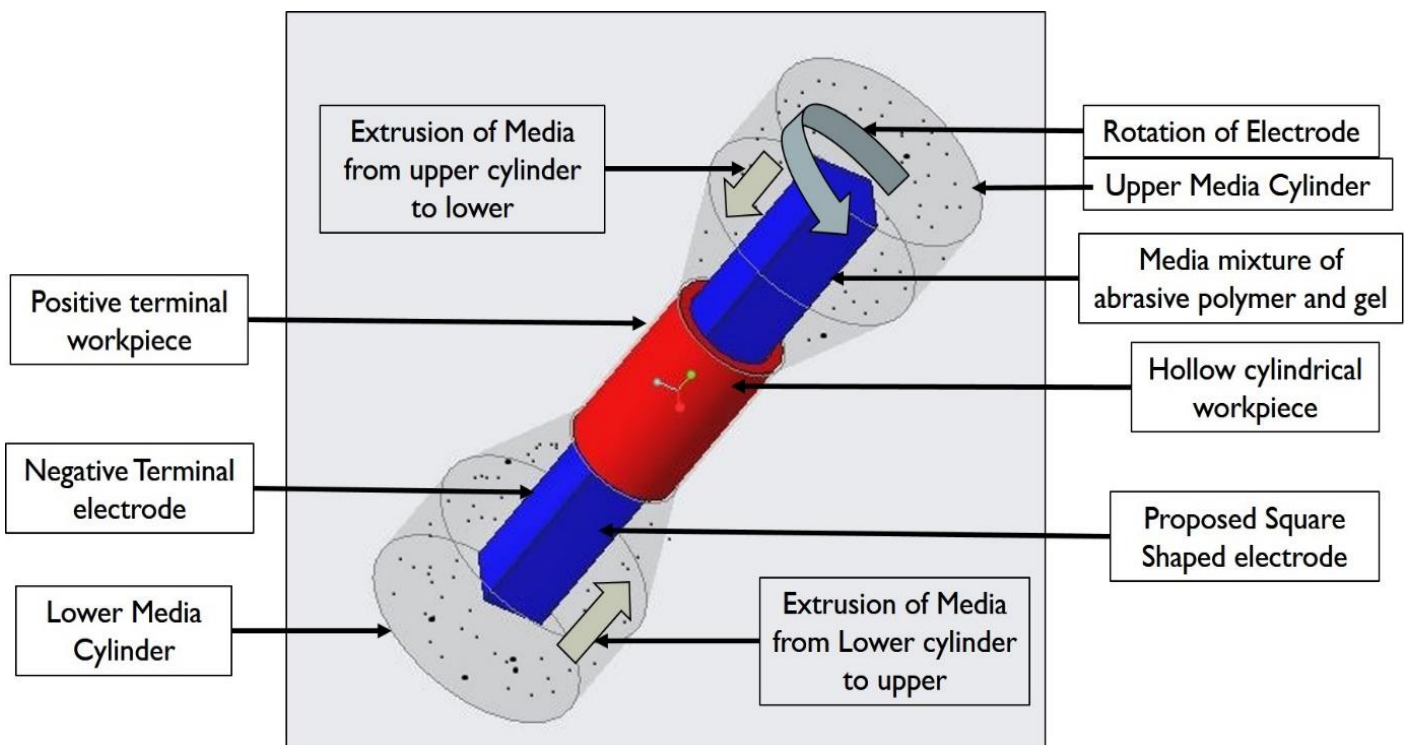


Figure 42 Schematic diagram of square shape electrode

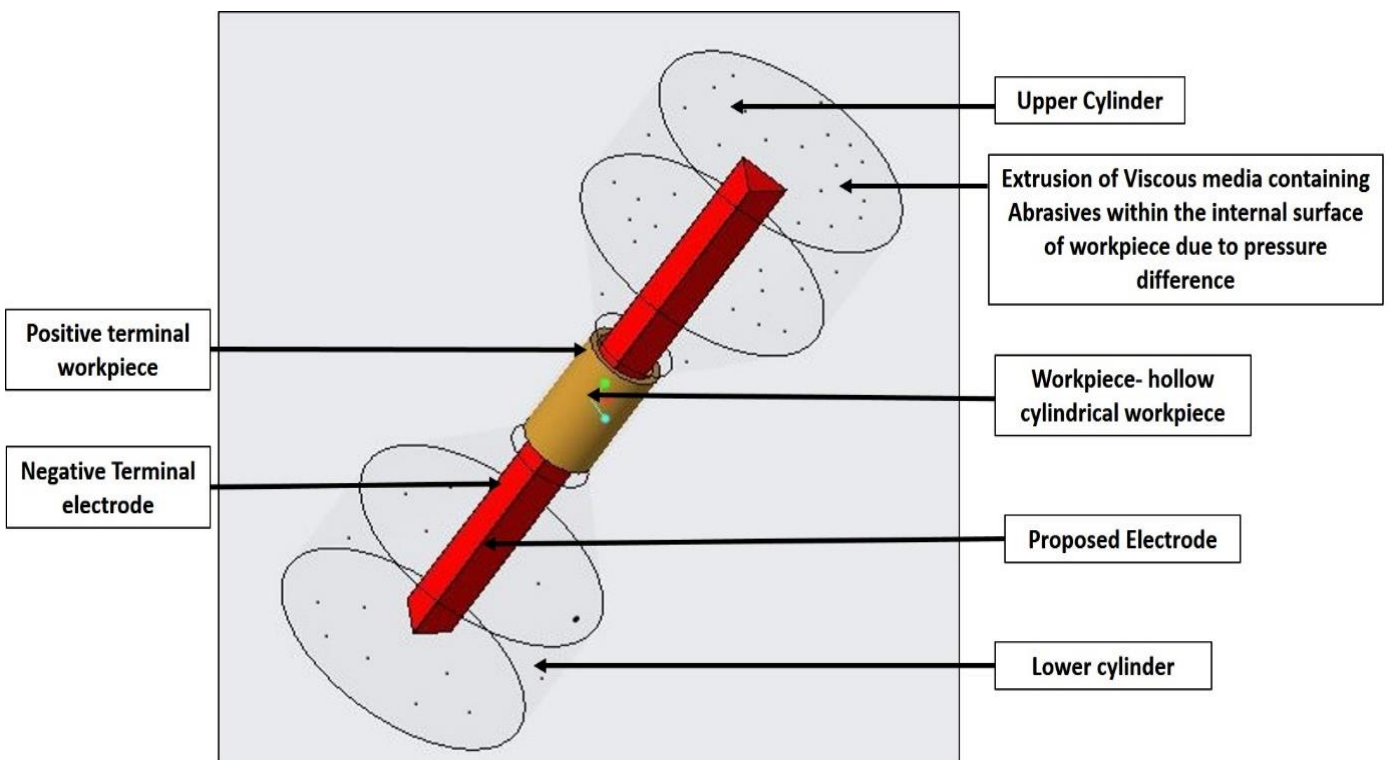


Figure 43 Schematic diagram for triangular shape electrode

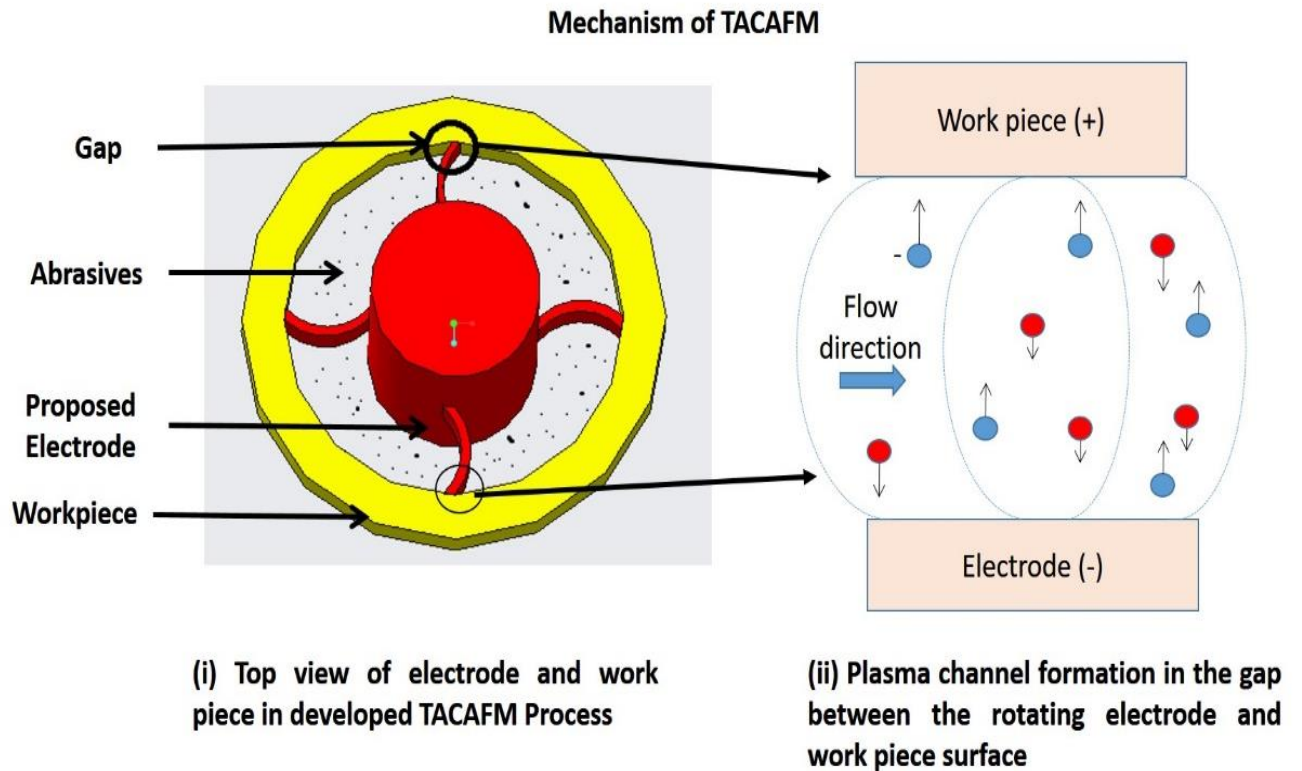


Figure 44 Mechanism of spark formation for spline shape electrode with curved blade

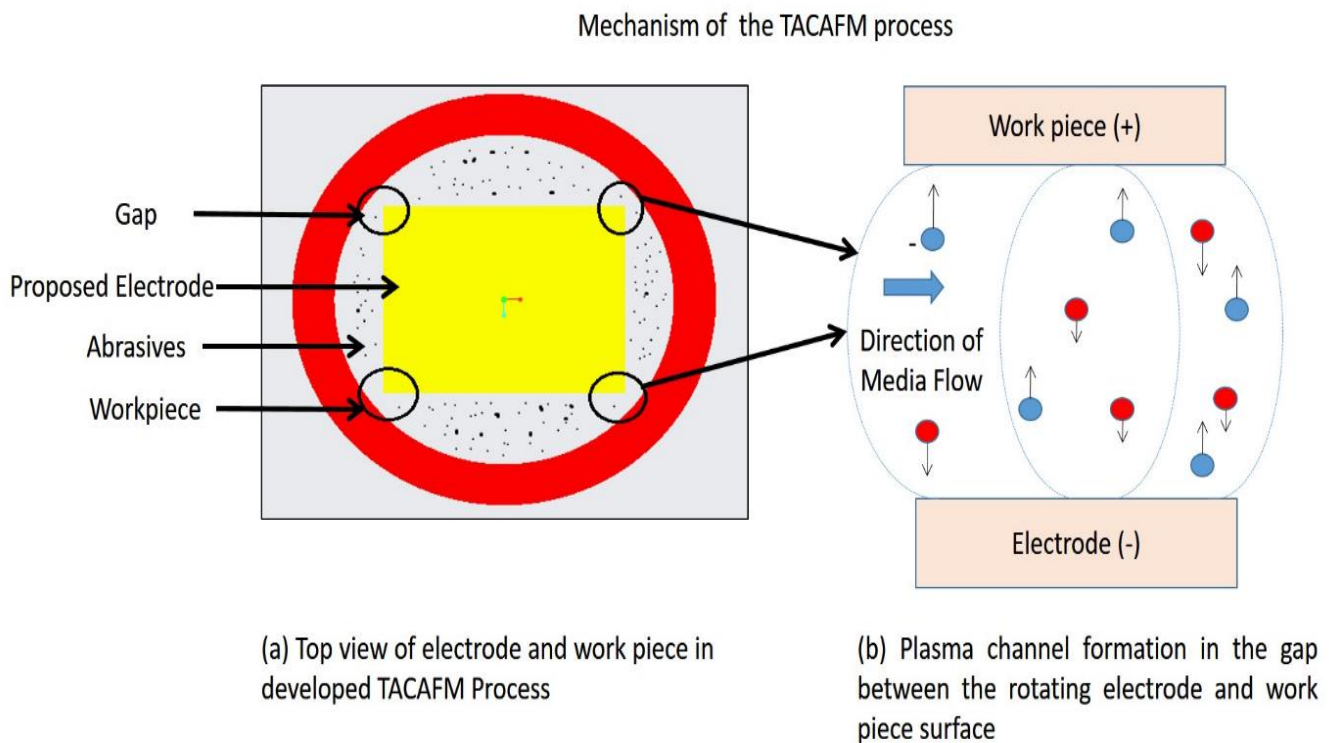


Figure 45 Mechanism of TACAFM process with square electrode

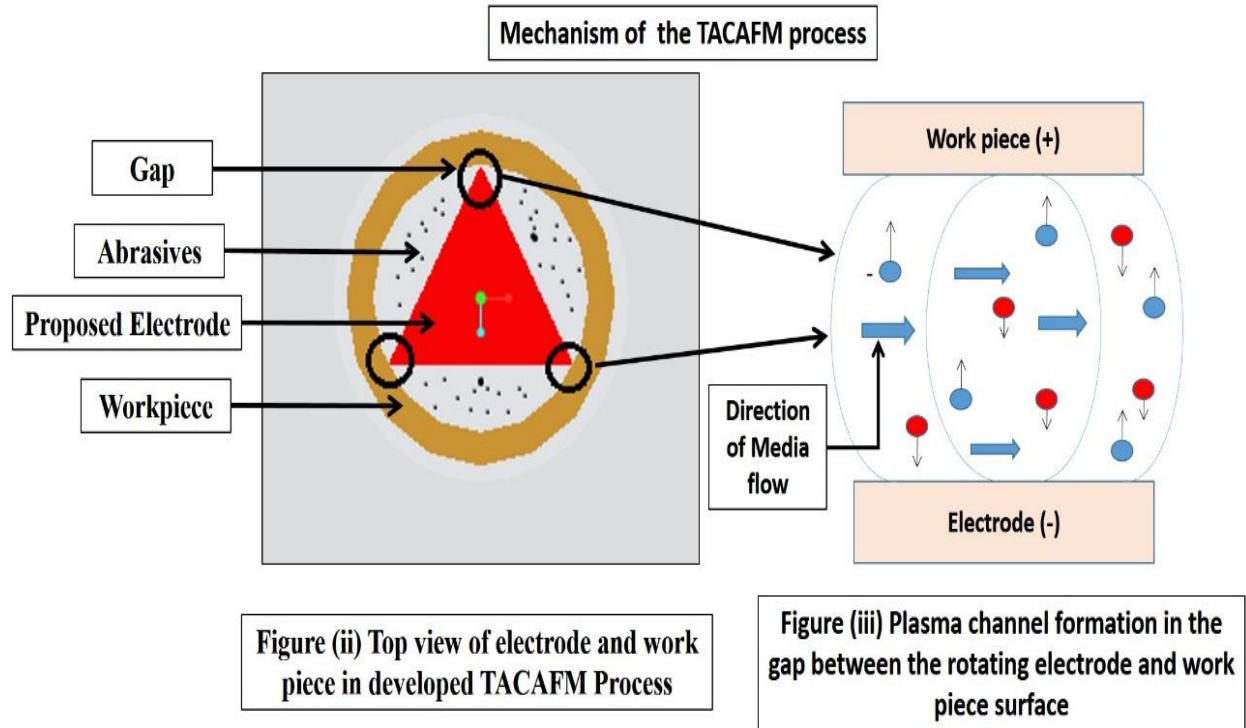


Figure 46 Mechanism of TACAFM Process with triangular electrode

5.9. Analysis of TACAFM process

In the next step the solid model of the assembly is transfer to the ANSYS Fluent for the simulation. This is done by converting the assembly file of the solid model into the IGES file which stand for initial graphics exchange information file. IGES files can be open easily on any platform without any issue. Once the file is received, the name selection to the assembly is done on the components on which the effect of the flow parameters is to be analyzed. After the name selection the path for the flow of media is made using the subtraction operation of the Boolean function of the ANSYS geometry module. The various names selections are inlet, outlet, media and the workpiece. In total 2 Boolean operations were performed for the geometry preparation. One was done for the adjustment of workpiece inside the media and the other was done for the adjustment of CFG electrode inside the media and the workpiece. The similar process is repeated for each electrode assembly as the separate simulations were performed for the different electrode geometry. Figure 47 shows the Geometry of the square shape electrode in design modular in Ansys Fluent, figure 48 shows the Geometry of the triangular shape electrode in design modular in Ansys Fluent and the figure 49 shows the Geometry of the square shape electrode in design modular in Ansys Fluent. After the successful geometry preparation in the design modular, the geometry is transferred to the meshing window where the requisite mesh is prepared.

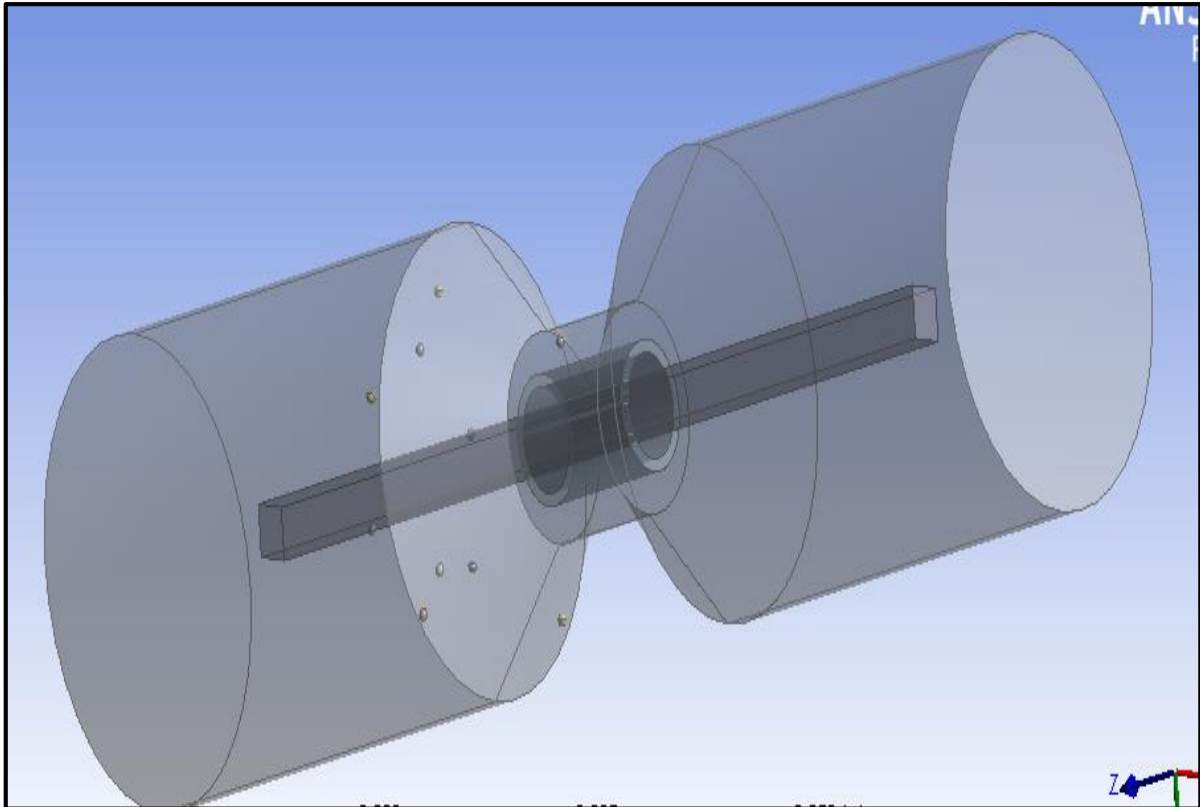


Figure 47 Geometry of the square shape electrode in design modular in Ansys Fluent

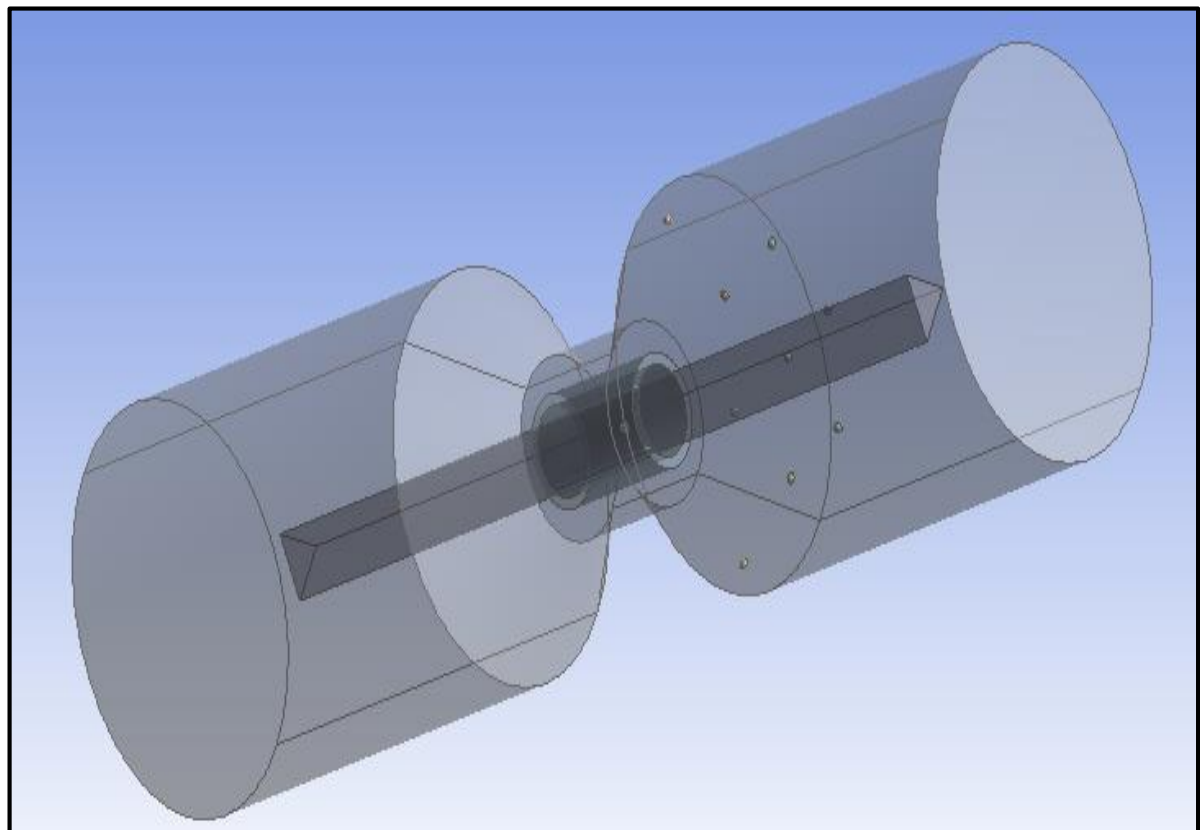


Figure 48 Geometry of the triangular shape electrode in design modular in Ansys Fluent

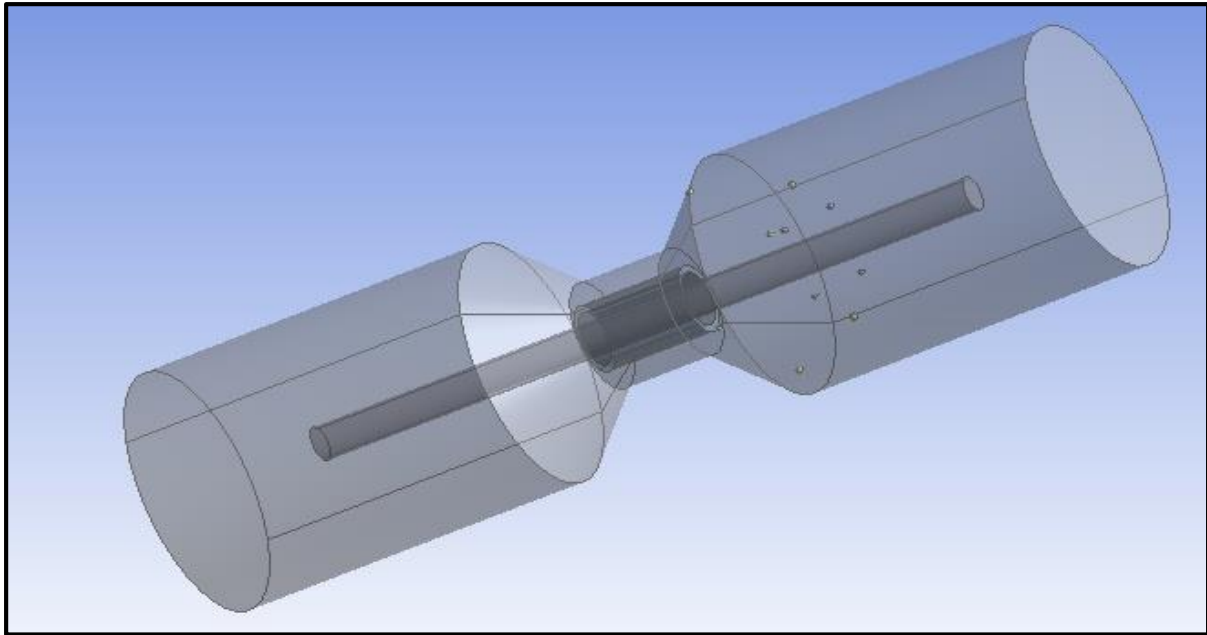


Figure 49 Geometry of the square shape electrode in design modular in Ansys Fluent

5.10. Meshing of TACAFM Process

In order to perform the simulation process, the prepared geometry is transferred to the meshing module where the mesh is prepared. The meshing of each element is separately done. For meshing the total assembly is divided into nodes and elements. Actually a node is a simply a coordination location in space where a degree of freedom is defined. Whereas an element defines a mathematical relation how DOF of nodes are related to each other. The mesh is prepared by taking the size of element as 0.001 mm. For meshing the total number of nodes for CFG electrode were 701430, 5742 for the workpiece, 10599 for the media and the total number of the nodes for the assembly were 2180493. For the elements, the total number of elements for CFG electrodes were 613811, for workpiece it was 3936, for the media it was 2522 and for the entire assembly, the total number of elements were 2159633. The mesh is properly prepared with appropriate edge preparation and skewness. The maximum number of mesh type were tetragonal. Figure 50 shows the meshing of the entire assembly, figure 51 shows the meshing of the workpiece, figure 52 shows the meshing of the square electrode and figure 53 shows the meshing of the square electrode with the workpiece. Figure 54 shows the meshing of novel spline shape electrode with the curved blade. It is to be noticed that the edge precreation near the curved is done to cater the smooth analysis of the spark. Figure 55 shows the arrangement of the spline shape electrode with curved blade and the workpiece. Figure 56 shows the triangular shape electrode while the figure 57 shows the meshing arrangement of triangular

shape electrode and the workpiece. After meshing file is transfer to the Fluent module. Table 1 shows the detail of number of elements and nodes for the mesh.

Table 8 Meshing details

Sr. No	Components	Elements	Nodes
1.	CFG Electrode	613811	701430
2.	Workpiece	3936	5742
3.	Media	2522	10599
4	Assembly	2159633	2180493
Elemental Size – 0.001 mm			
Maximum shape of element - Tetragonal			

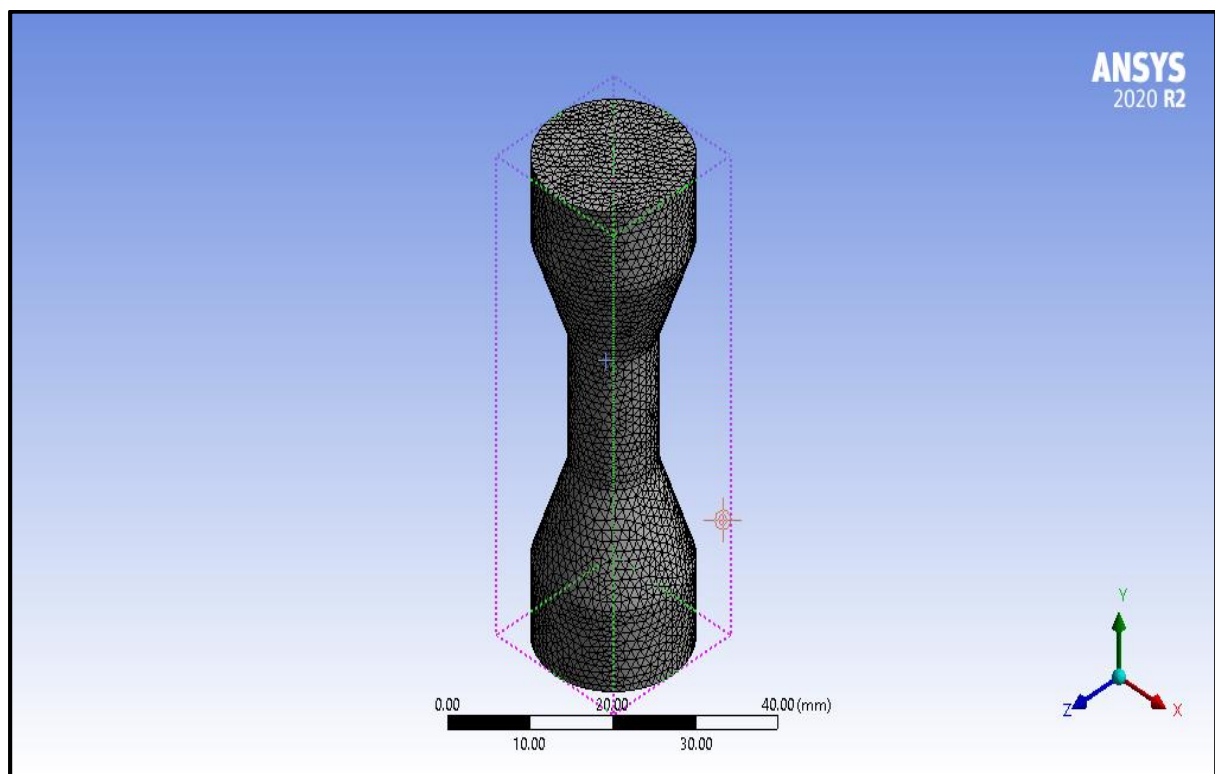


Figure 50 Meshing of electrode assembly

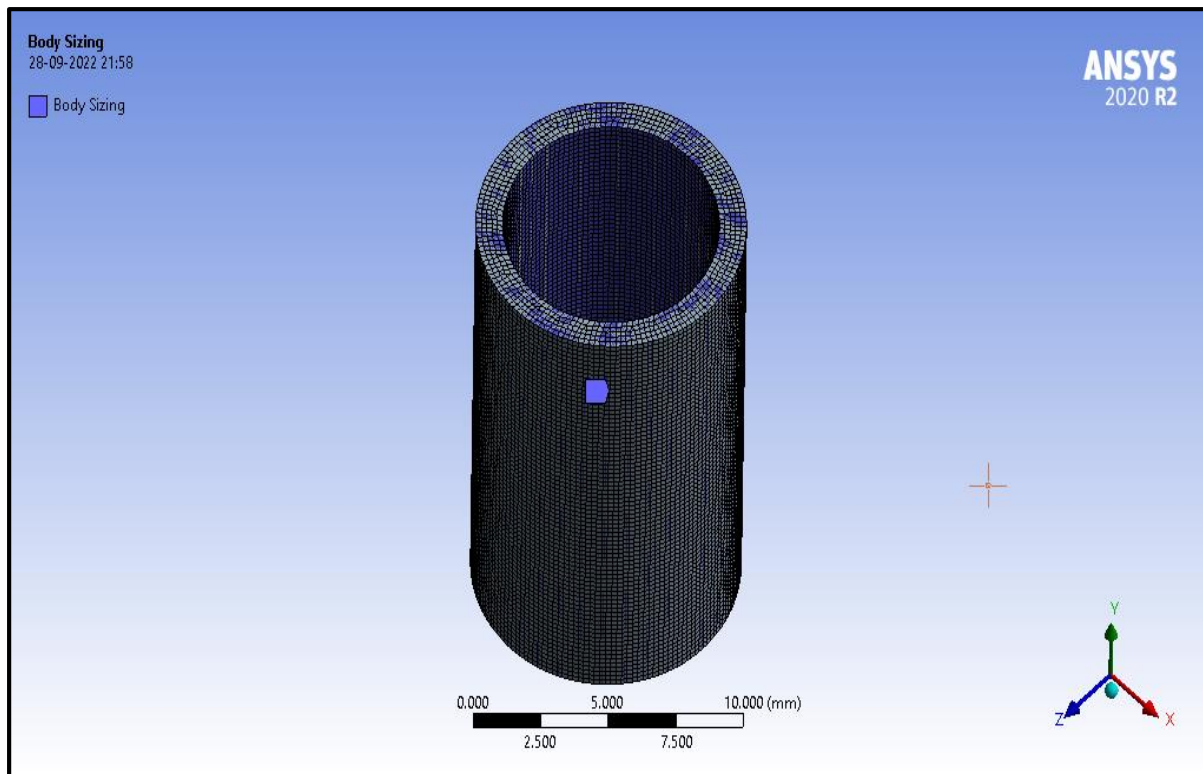


Figure 51 Meshing of workpiece

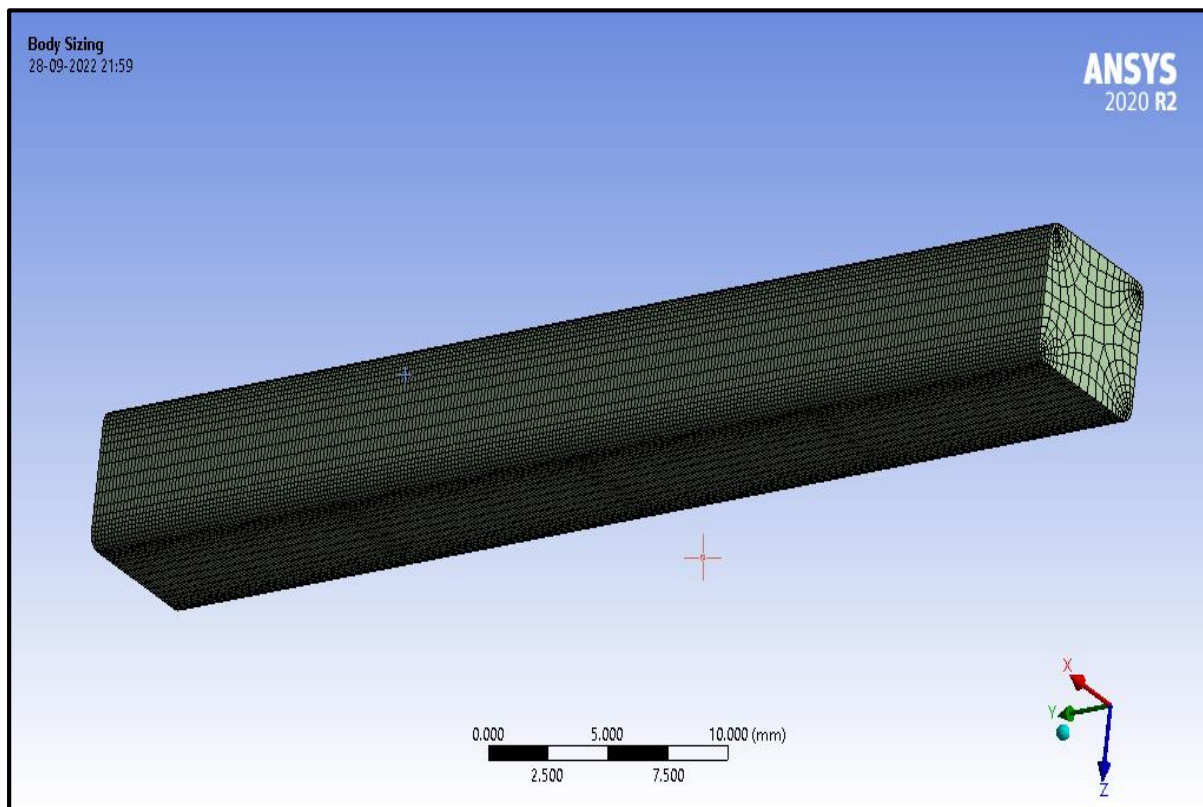


Figure 52 Meshing of square shape electrode

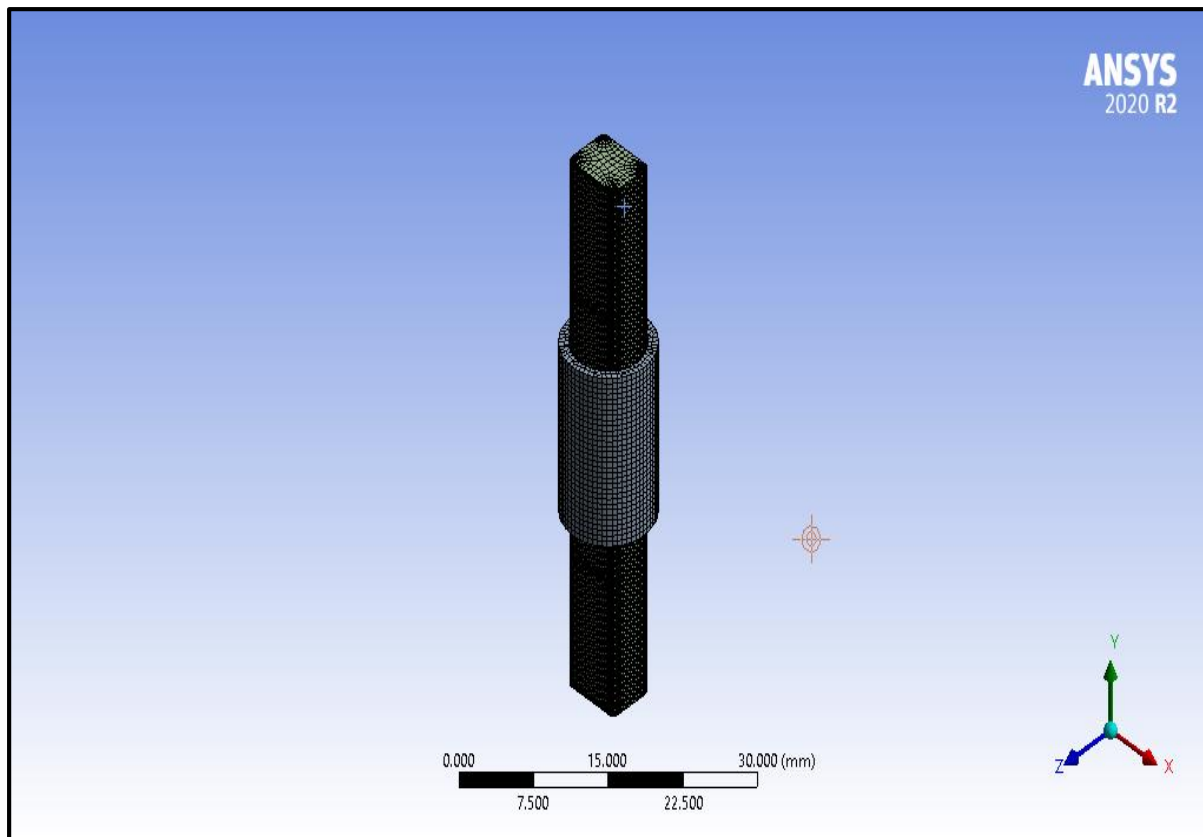


Figure 53 Meshing of square shape electrode with the workpiece

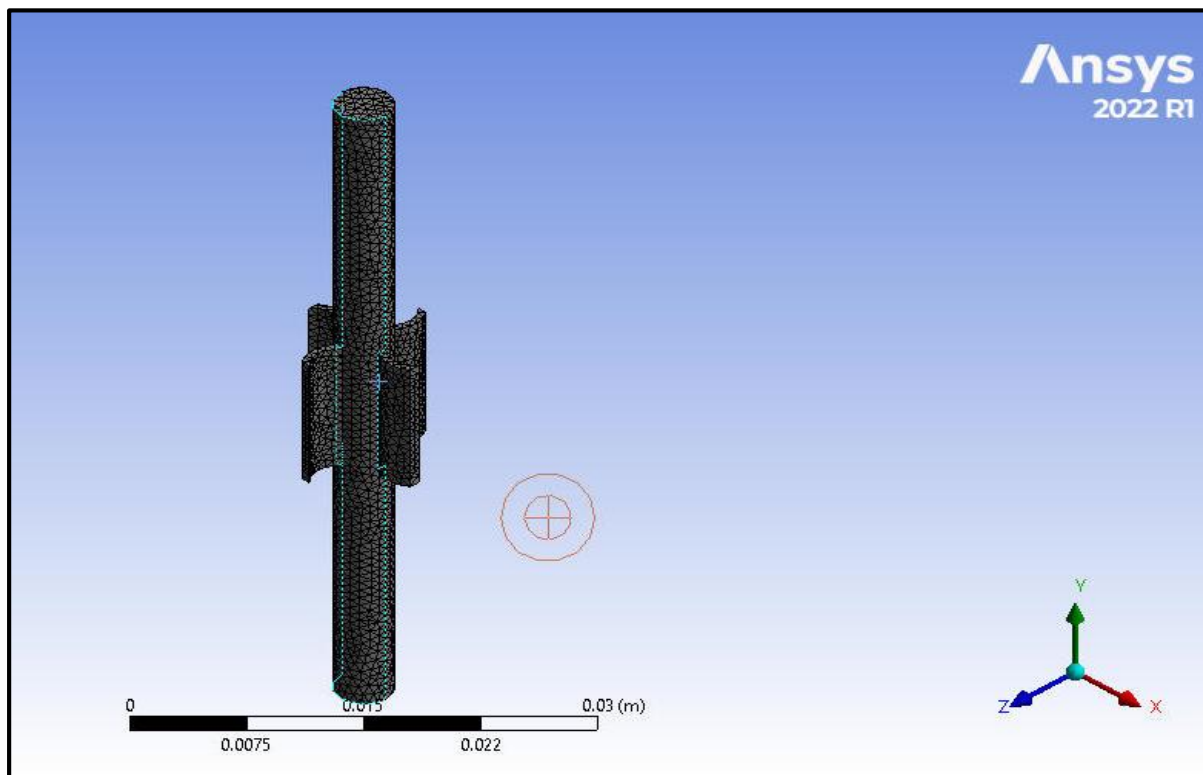


Figure 54 Meshing of spline shape electrode

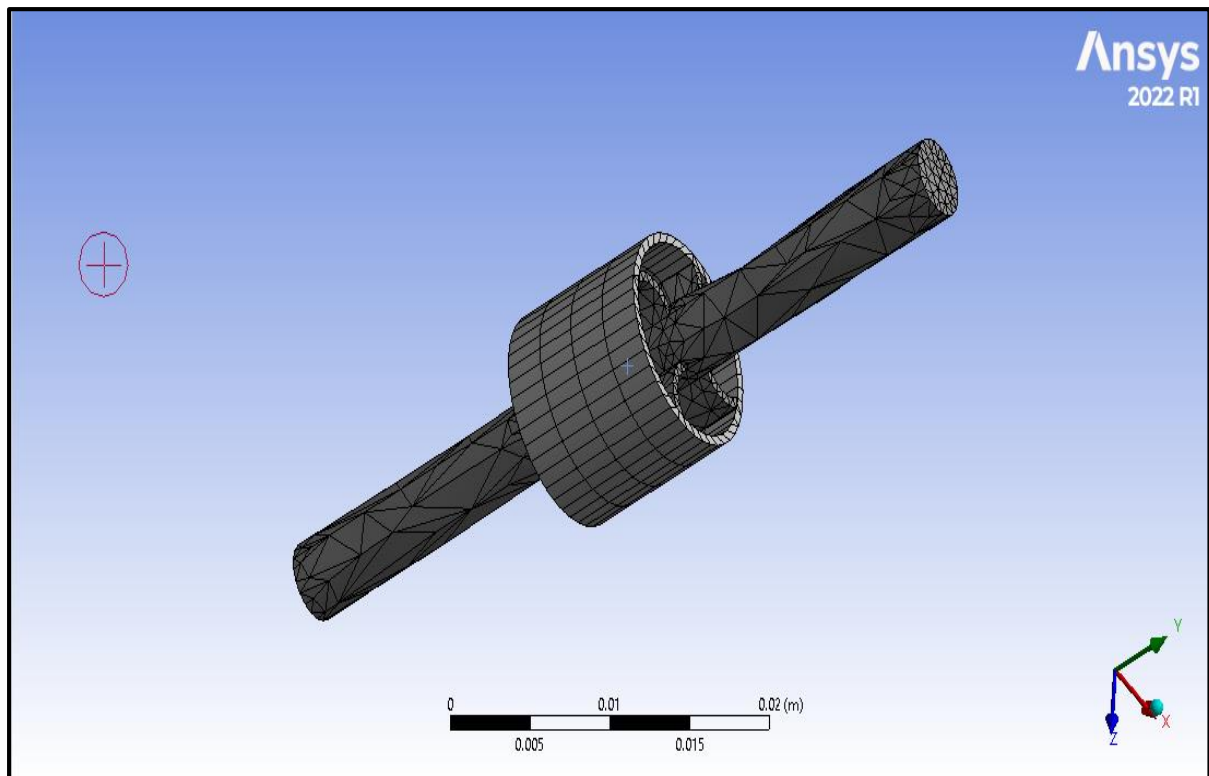


Figure 55 Meshing of spline shape electrode with the workpiece

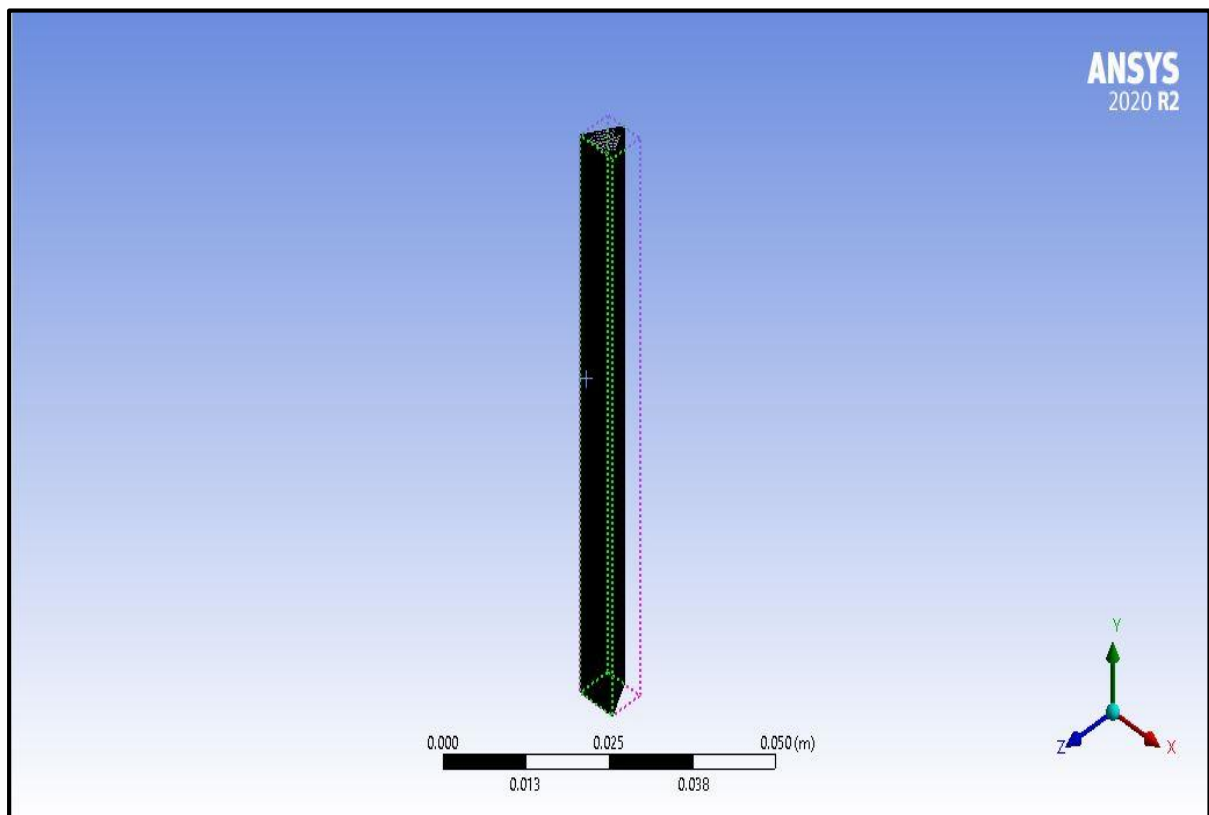


Figure 56 Meshing of triangular shape electrode

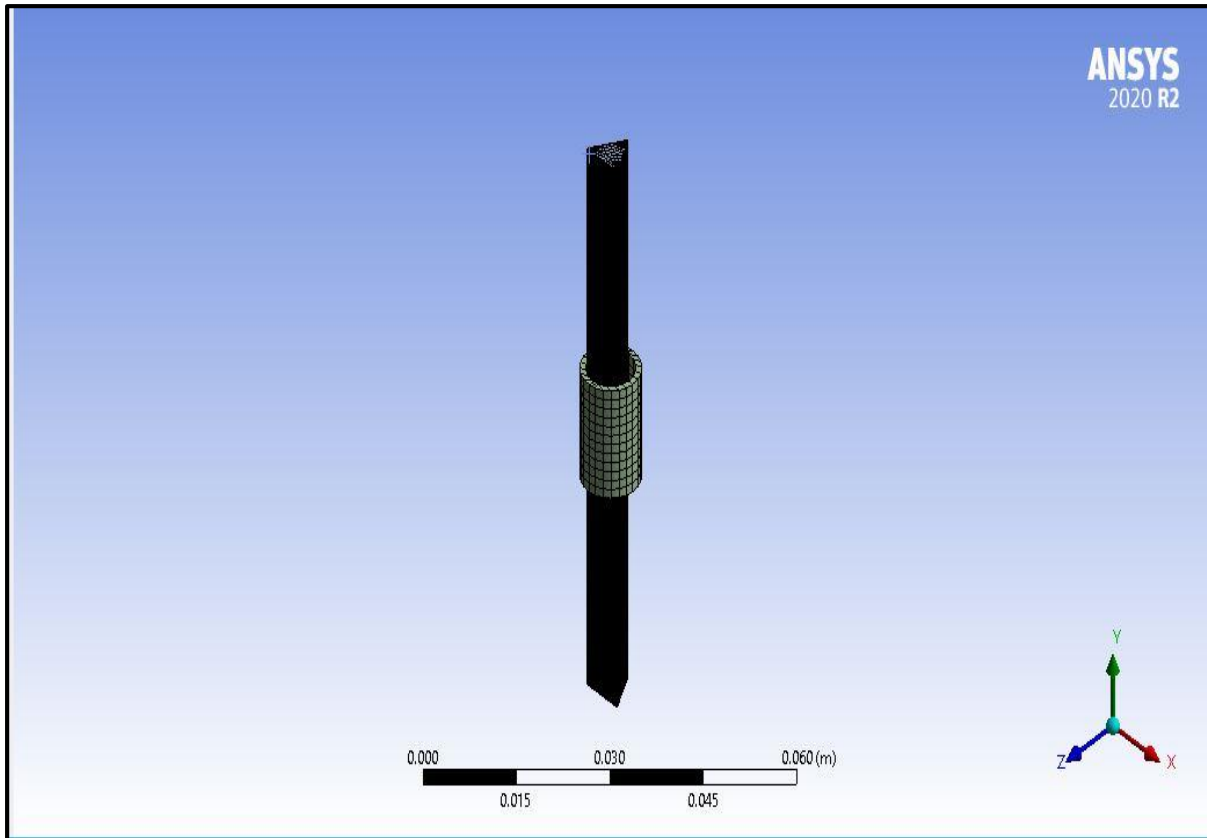


Figure 57 Meshing of triangular shape electrode with workpiece

5.11. ANSYS Fluent setup

The next step is to set the ANSYS fluent and load the requisite mesh file to the setup. Figure 58 shows the Fluent set up with the requisite with the setting and graphical window intact. The initial setting was done on the model by putting pressure based model with velocity formulation as absolute and implicit and steady flow of the media. The effect of gravity is considered along with the energy equation put on to analyse the effect of temperature during the simulation. In the next step the materials are defined which were taken as copper for electrode, the polyborosiloxine with alumina abrasives is consider as the media material for the simulation point of view, brass is consider as the workpiece material. Table 9 shows the material property used in the simulation. The prominent property of the material which are used in the Ansys fluent simulation are the density, viscosity, thermal conductivity and the specific heat. Here the viscosity is a property related to the flow which is not seen in solid material like brass, alumina and copper while it is prominently there for the media. The next step after defining the material and their property is the boundary condition, which is discussed in the subsequent section.

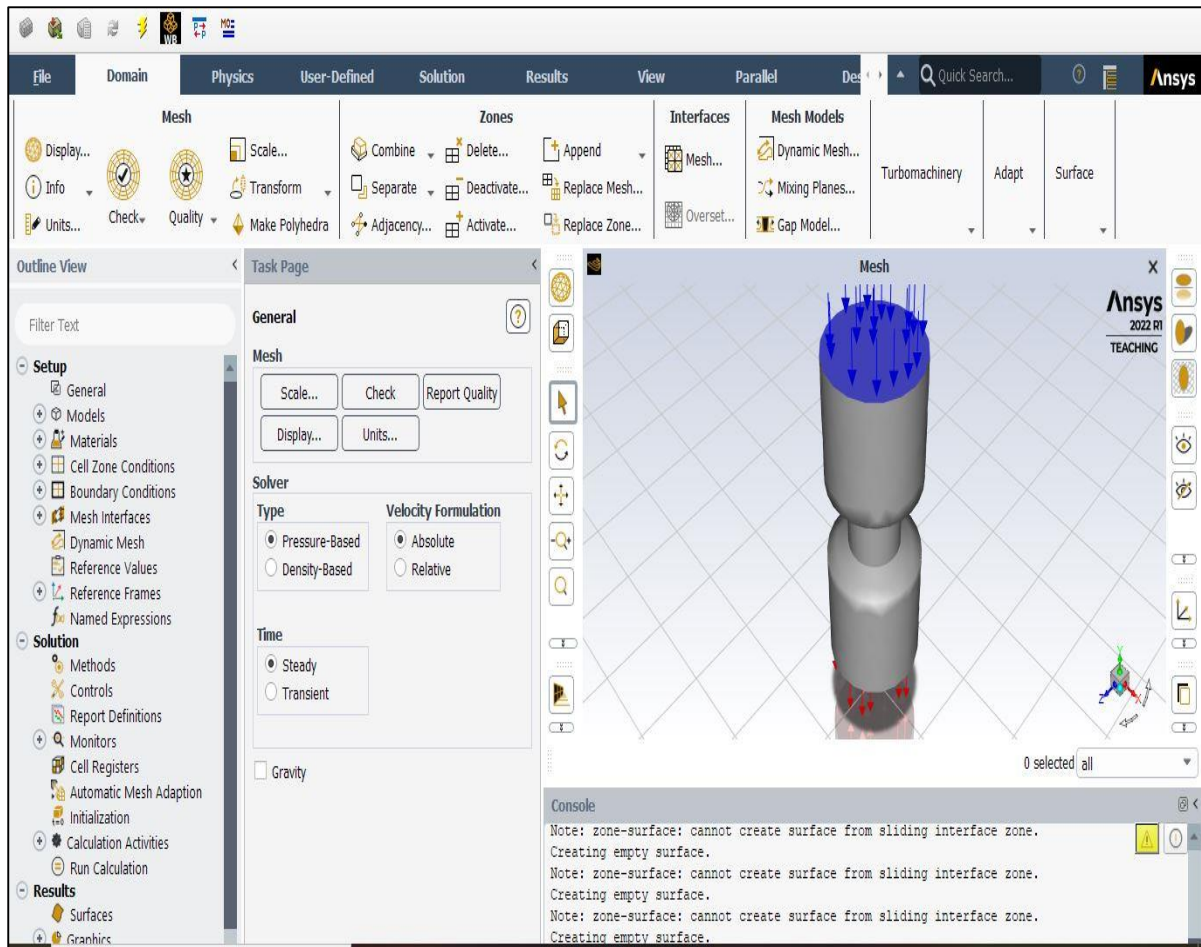


Figure 58 ANSYS Fluent Setup

Table 9 Materials and their Property

Material	Media	Brass Work piece	Alumina abrasives	Copper Electrode
Type	Fluid	Solid	Solid	Solid
Density (kg/m ³)	1218	8300	3950	8830
Viscosity (kg/m-s)	0.789	-	-	-
Thermal conductivity (w/m-k)	0.22	401	451	387.6
Specific Heat(J/kg-k)	20.25	109	12	381

5.12. Boundary conditions

The analysis was done with the assumption that the model is pressure based with absolute velocity and implicit function. The media flow is considering homogeneous and isotropic and the flow is considering as laminar and steady. Thus the pressure inlet and outlet is provided

with the working pressure of 20 MPa. As a result, the pressure inlet was kept for 40 MPa and the pressure outlet was kept for 20 MPa. The media is made stationary wall without any physical motion and temperature. The workpiece was kept as a stationary wall. 2 separate simulations were performed by keeping the CFG electrode as stationary and next by keeping the CFG electrode in rotation of 100 rpm with other parameters as constant. Figure 59 shows the boundary conditions of pressure inlet, pressure outlet, workpiece and the electrode. Note that 2 separate simulations were done for each electrode. One for the stationary condition and other for the rotation of the electrode at 100 rpm. The CFG electrode was given temperature of 2300 degree Celsius as EDM effect is to be provided. The tool used in TACAFM generally gets heated to 2300 to 3500 degree Celsius (**Patil et al. 2023**) and also there is no provision to provide pulsed DC in the fluent, hence to analyse the effect of spark, the temperature is provided to the electrode. Figure 60 highlights the boundary condition of the media which is consider as a stationary fluid. The media is a mixture of polymer, gel and abrasives. Table 10 highlights the boundary condition along with the model assumption and the numerical values.

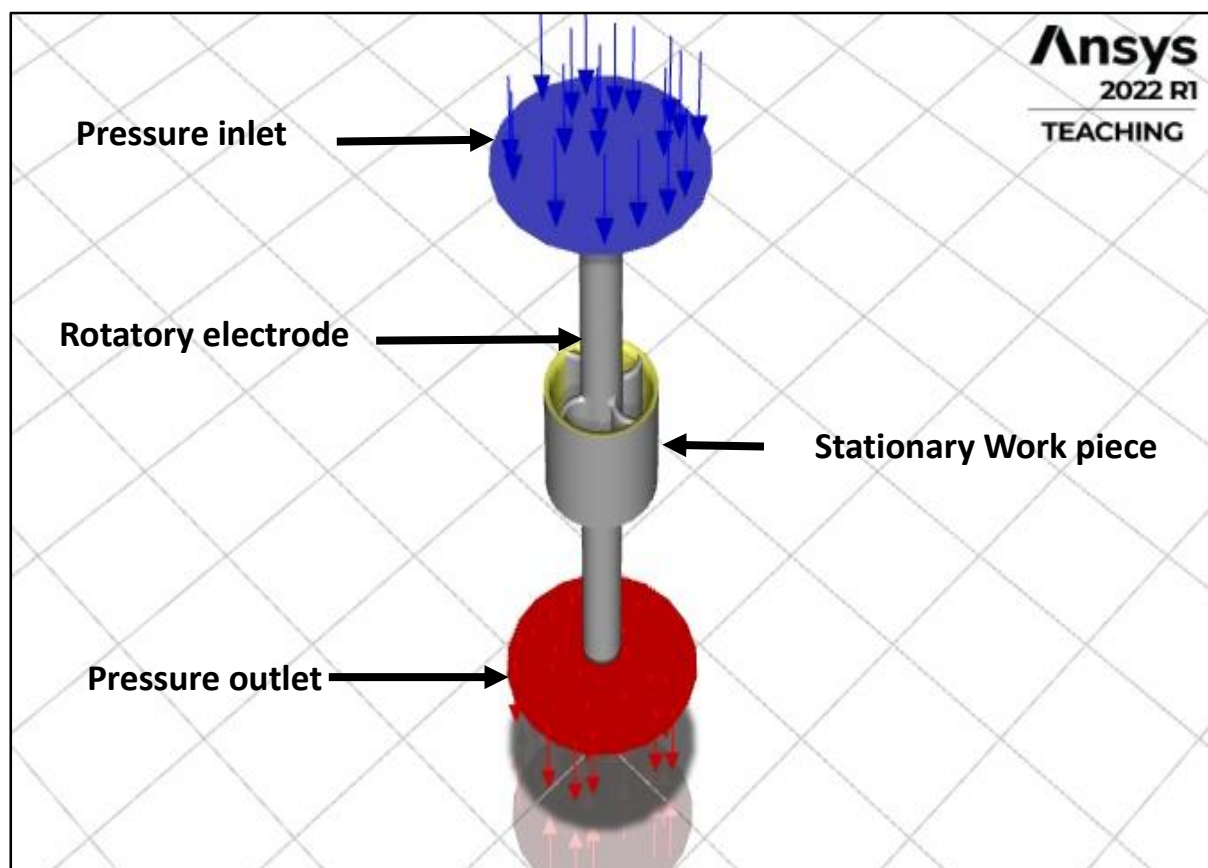


Figure 59 Boundary condition highlighting inlet, outlet, workpiece and the CFG electrode

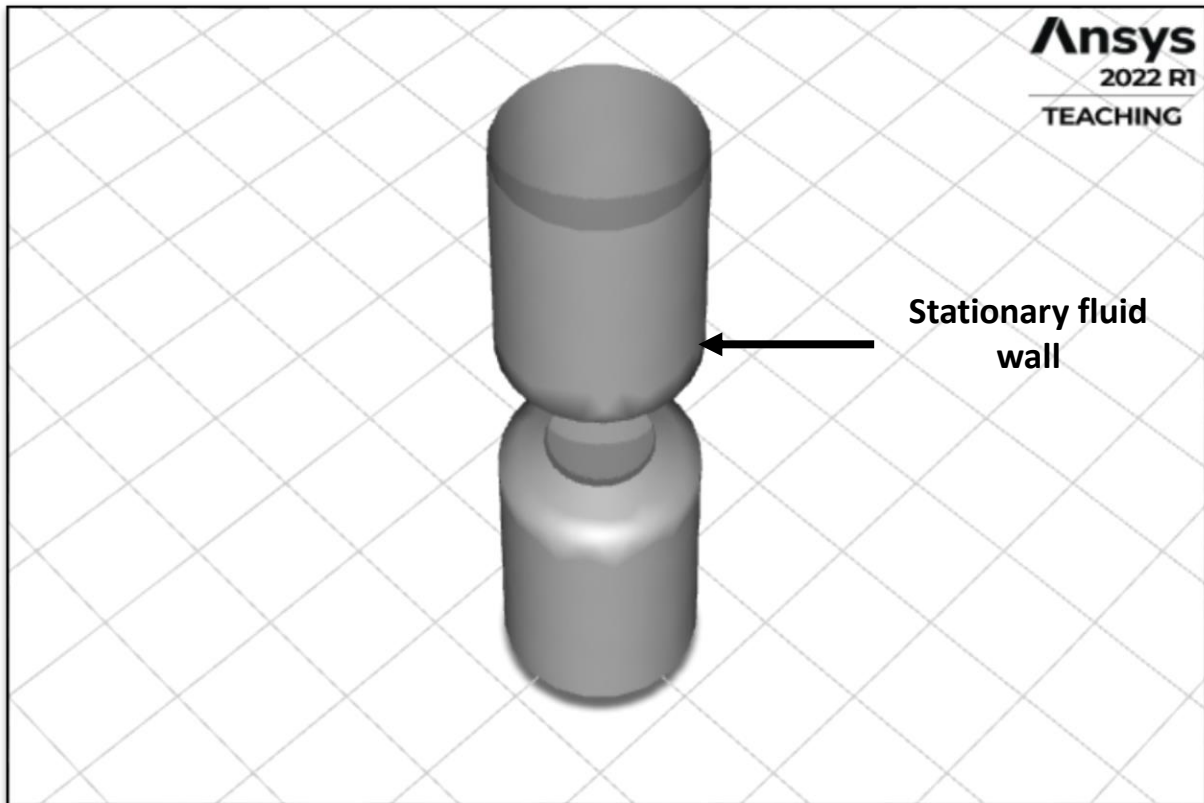


Figure 60 Boundary condition for the Stationary wall

Table 10 Boundary conditions

Sr. No	Components	Boundary condition
1	Inlet	<ul style="list-style-type: none"> Pressure inlet 40MPa
2	Fluid (media)	<ul style="list-style-type: none"> Stationary fluid
3	CFG Electrode	<ul style="list-style-type: none"> Stationary/100 rpm rotation 2300 degree Celsius
4	Workpiece	<ul style="list-style-type: none"> Stationary
5	Outlet	<ul style="list-style-type: none"> Pressure outlet 20 MPa
Assumptions for the model <ul style="list-style-type: none"> Pressure based model Absolute velocity and implicit formulation Media homogeneous and isotropic Flow is laminar and steady The Energy equation on. 		

5.13. Simulation Results

After the boundary conditions the data is fed to the solver and the simulation is run for 100 iterations. The figure 61 shows the conversion curve which highlights the smooth conversion process upto 10^{-6} . The curve shows the total energy line below the continuity, X, Y and Z velocity line which is a desirable factor in the conversion process. Once the solution is achieved the post CFD window is opened for the analysis of the results. The key observation in the post CFD windows were pressure distribution over the workpiece during stationary and rotational motion of the electrode. Similarly the distribution of temperature over the workpiece during the stationary and in the rotational condition of the CFG electrode is observed. The path of the flow of media is observed by the streamline pattern of the media and also the distribution of pressure and temperature inside the media is also analyzed in the subsequent result section for each type of electrode. The similar procedure is observed for all the assembly having different CFG electrodes.

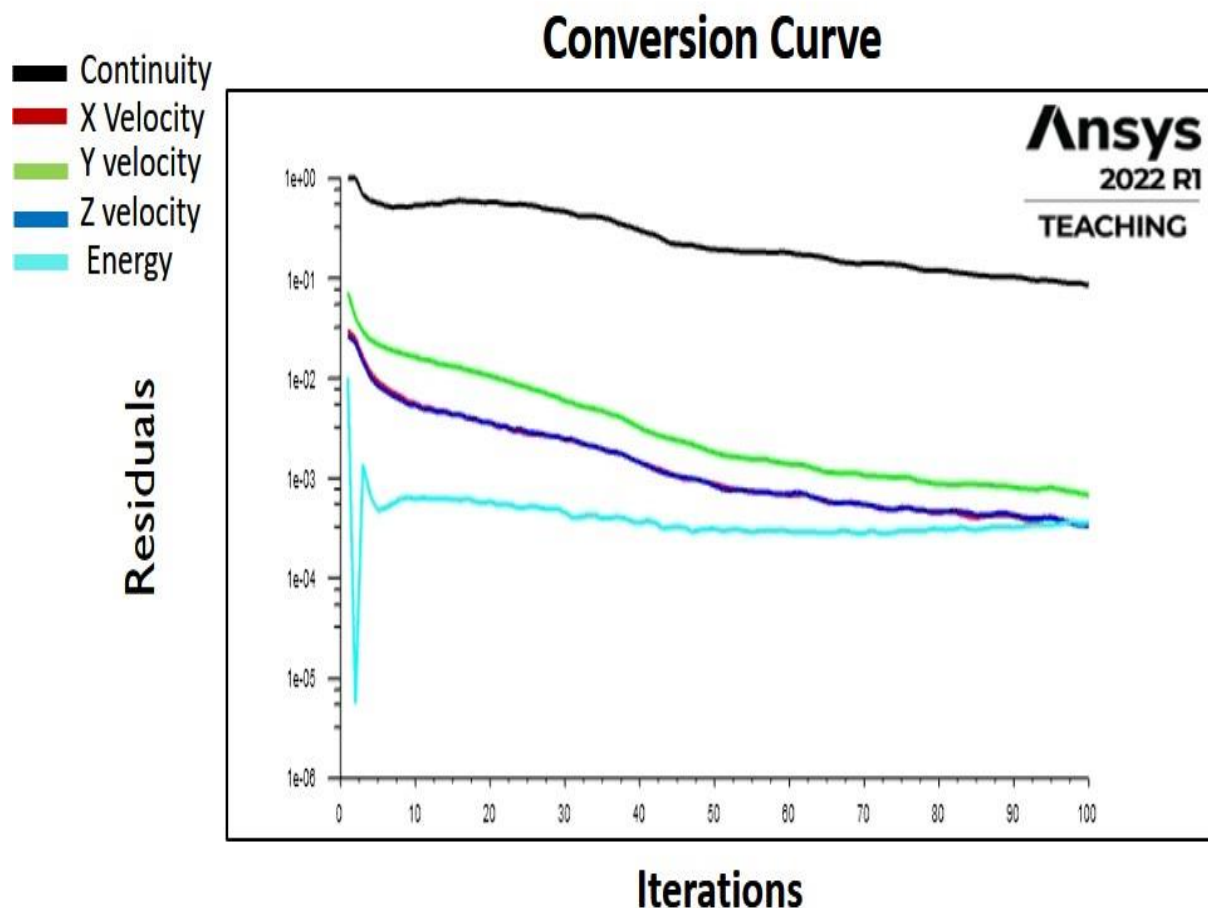


Figure 61 Conversion curve showing Energy, continuity, X,Y and Z velocity trends on residual Vs iterations curves

5.13.1. Spline Shape electrode with straight blade

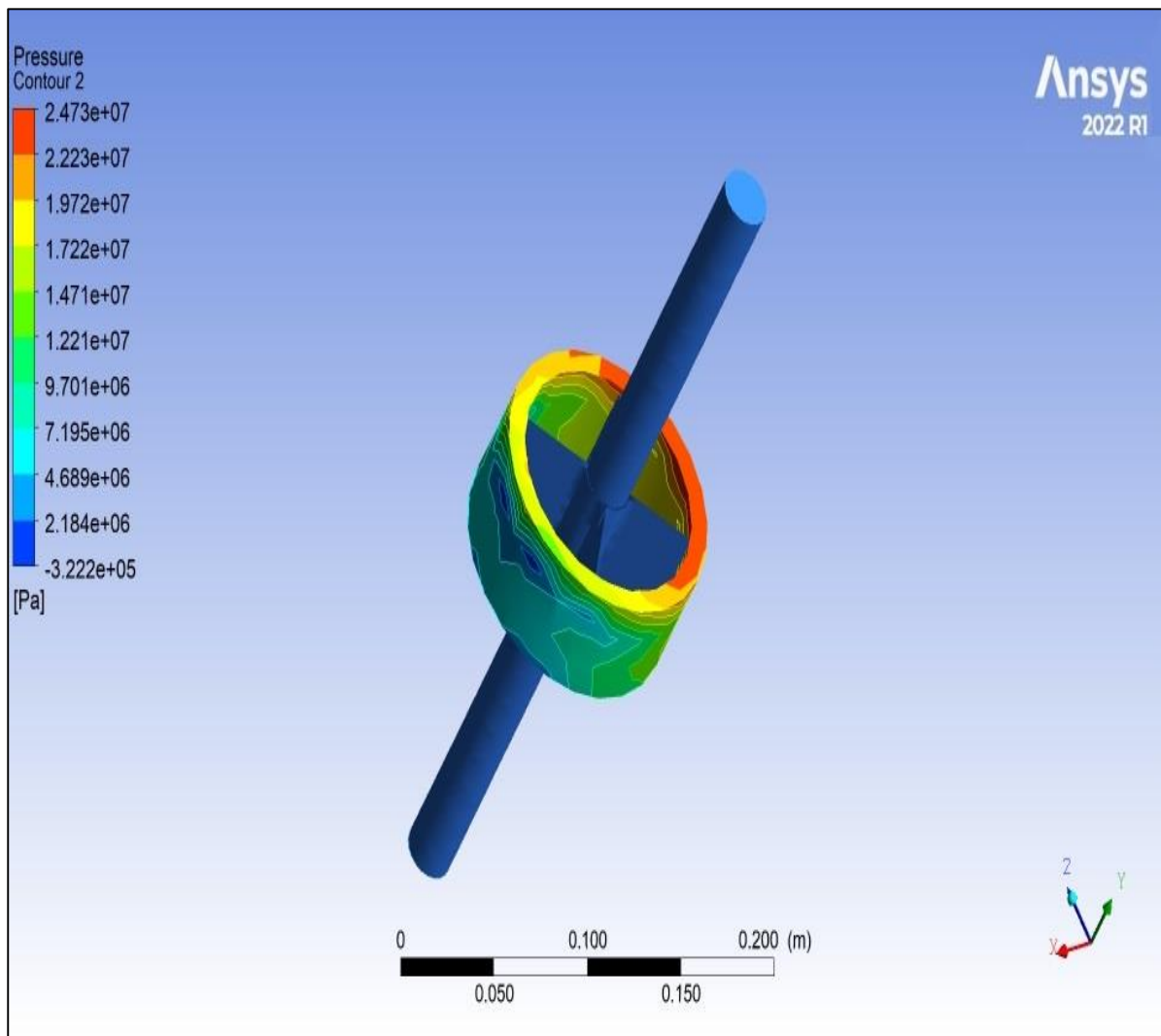


Figure 62 Pressure distribution for the straight spline electrode at stationary condition

Spline shape electrode was the first centrifugal force generating electrode used in the TACAFM process when it was introduced. So in order to compare the performance of different CFG electrode geometry, pressure and temperature distribution for the spline shape electrode with straight blade was observed. Figure 62 shows the pressure distribution over the workpiece when the spline electrode with straight blade is used. The spline shape electrode is in stationary condition. The results show that the maximum value of the pressure is 24.73 MPa when the working pressure is of 20 MPa. This range is higher than the pressure range over the workpiece when centrifugal force assisted AFM is consider and when the conventional AFM is consider [Srinivas and Bhardwaj 2018]. The pressure distribution over the workpiece highlights the abrasive action over the workpiece which results in the increase in the abrasion process. The increase in the abrasion process is the key parameters for the enhancement of material removal.

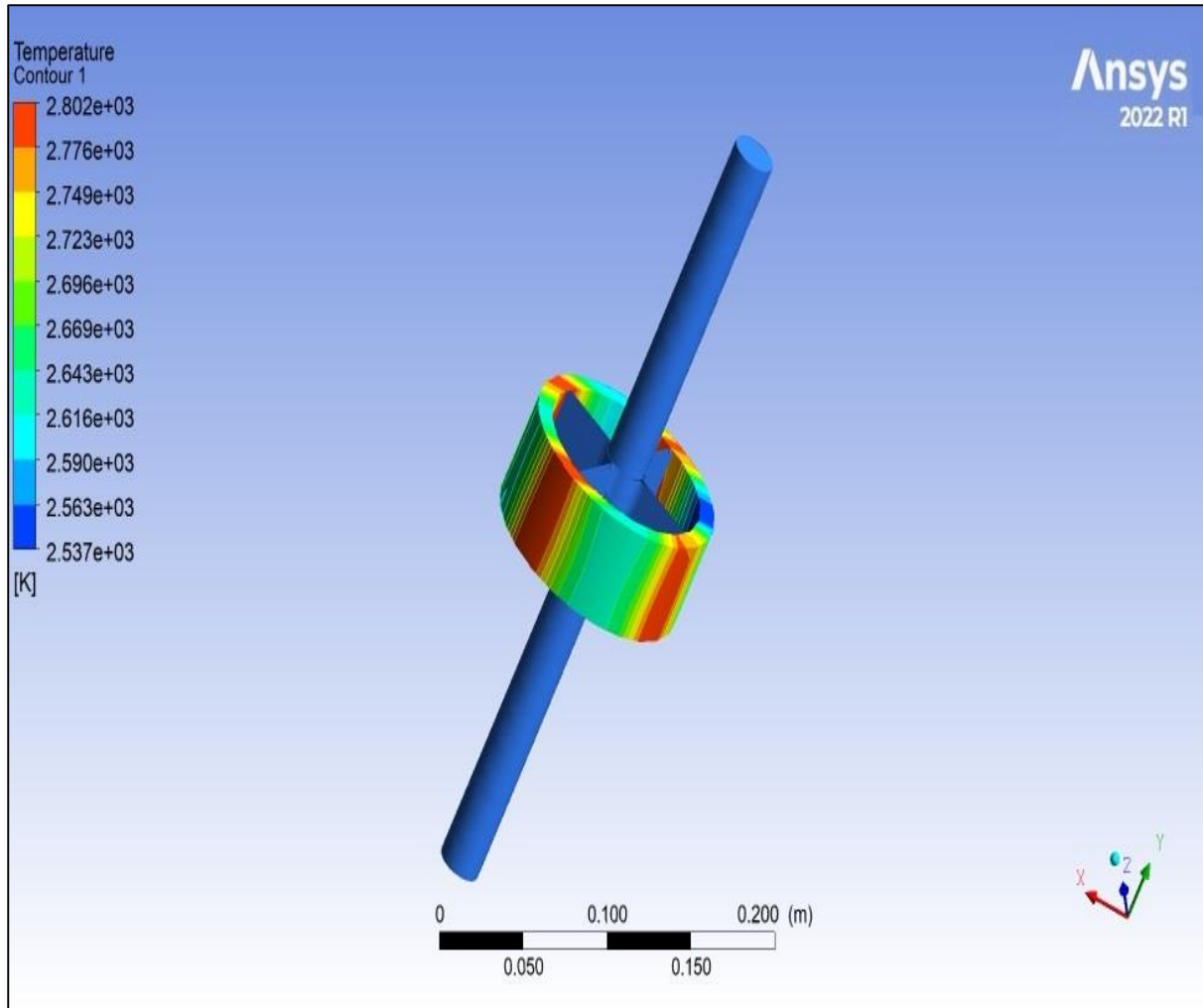


Figure 63 Temperature distribution over the workpiece with straight spline electrode at stationary conditions

The figure 63 shows the temperature distribution over the workpiece when the extrusion pressure of 20 MPa (40 MPa from inlet and 20 MPa from outlet) is applied at the media along with the temperature of 2300-degree Celsius temperature of the CFG electrode. The results highlight the high temperature marks around the edges of the blades of the workpiece which highlights the spark generation during the TACAFM process. This spark generation results in the softening of the material and also results in the material removal through melting and erosion process as don in EDM process. The maximum temperature is of 2802 K which is more than the electrode temperature which is possible due to the spark generation which raises the temperature at the periphery of the blade.

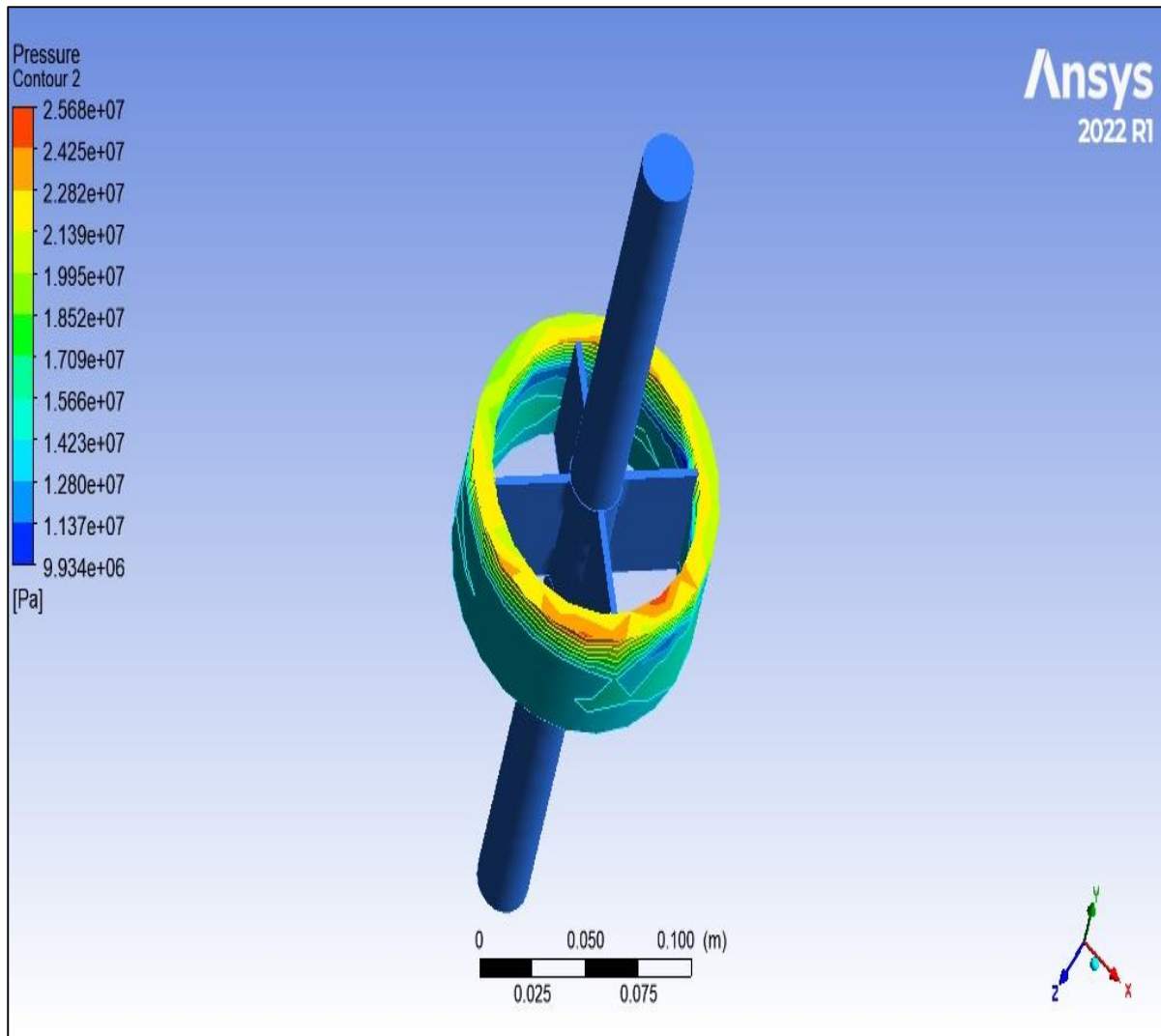


Figure 64 Pressure distribution over the workpiece with Spline shape electrode with straight blade at rotation of the electrode

Figure 64 shows the pressure distribution over the workpiece due to the rotation of the spline shape electrode with the straight blade. The rotational speed of the CFG electrode is kept constant at 100 rpm. The value of maximum pressure is 25.68 MPa under the inlet pressure of 40 MPa and the outlet pressure of 20 MPa (working pressure of 20 MPa). It can be observed that the maximum pressure is more in case of rotation as compare to the stationary condition of the electrode which was around 24 MPa. This is due to the fact that the rotation of the electrode provides an extra centrifugal force which directs the abrasive particles towards the wall of workpiece resulting in higher abrasion process. Also the rotation of the CFG electrode results in the uniform distribution of media over the wall of the workpiece which results in the uniform material removal from the workpiece.

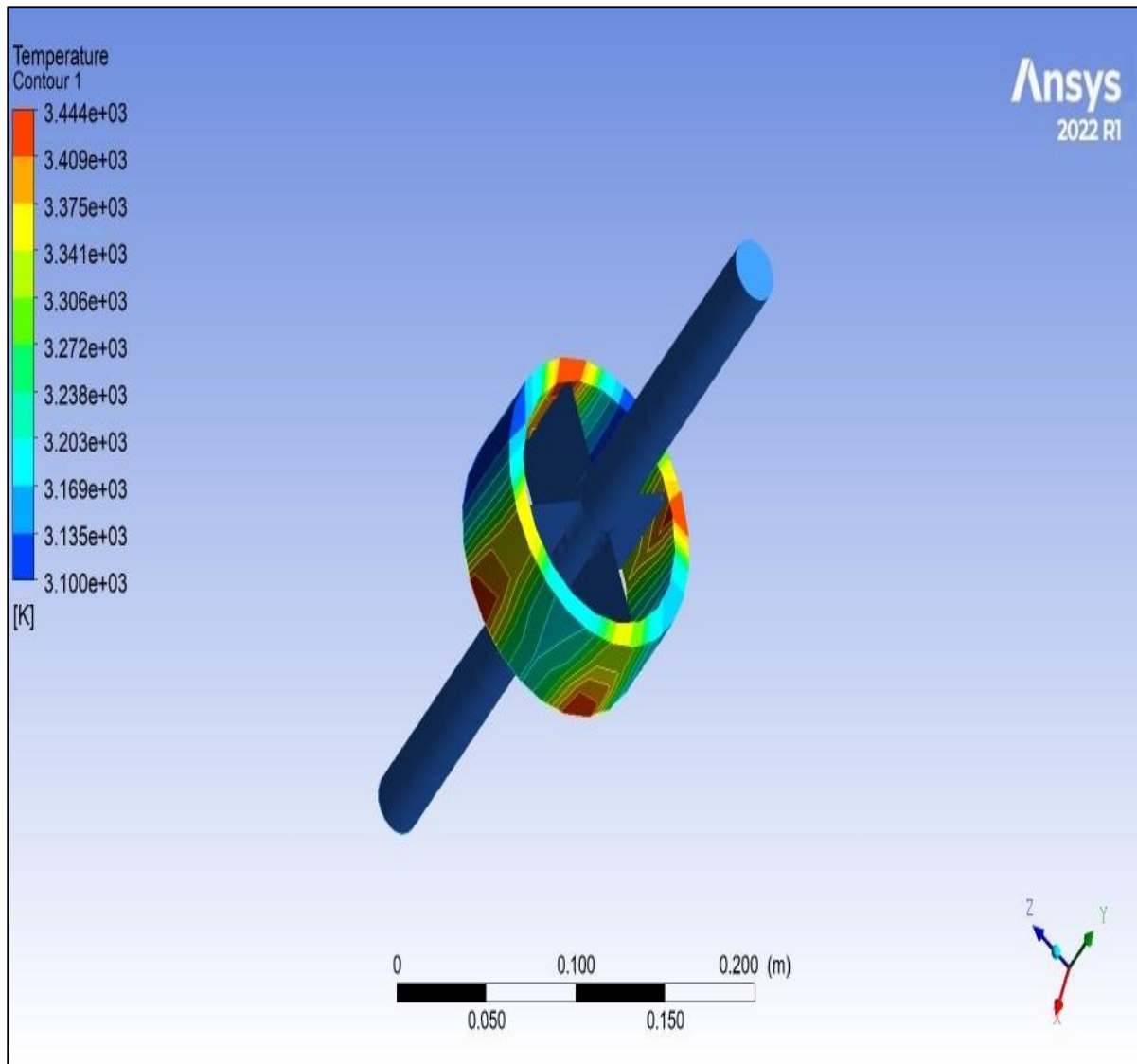


Figure 65 Temperature distribution over the workpiece by spline electrode with straight blade during the rotation of CFG electrode at 100 rpm

Figure 65 shows the temperature distribution over the workpiece when the spline shape electrode with the straight blade is given rotation of 100 rpm. The results show the maximum temperature on the edges of the blades which highlights the spark generation during the process. Also the value of the maximum temperature is around 3444 K which is higher as compare to the electrode temperature at the stationary conditions. This is because the rotation of electrode provides the kinetic energy in the media particle which raises their temperature also it results in the increase in the intensity of the spark formation. Also the another point of consideration is that the rotation of the electrode results in the uniform spark travel as a result uniform melting of the workpiece is achieved unlike in the case of stationary CFG electrode. Thus rotation of the CFG electrode gives the improve results in terms of material removal.

5.13.2. Spline shape electrode with curved blade

In order to improve the material removal of the TACAFM process, the spline shape electrode is improved such that its ability to increase the centrifugal force generating electrode is increases. For this purpose, a small curvature is provided to the blade instead of the straight spline blade. Figure 66 shows the conversion curve highlighting the smooth conversion value of 10^{-6} . The graph shows the pattern of X, Y, Z velocity line along with the continuity and energy line. The energy line lies below the continuity and X, Y and Z velocity line which highlights the smooth conversion process. The initial disturbance in the velocity trends highlights the increase in the centrifugal force which in turns results in the improvement in the material removal process.

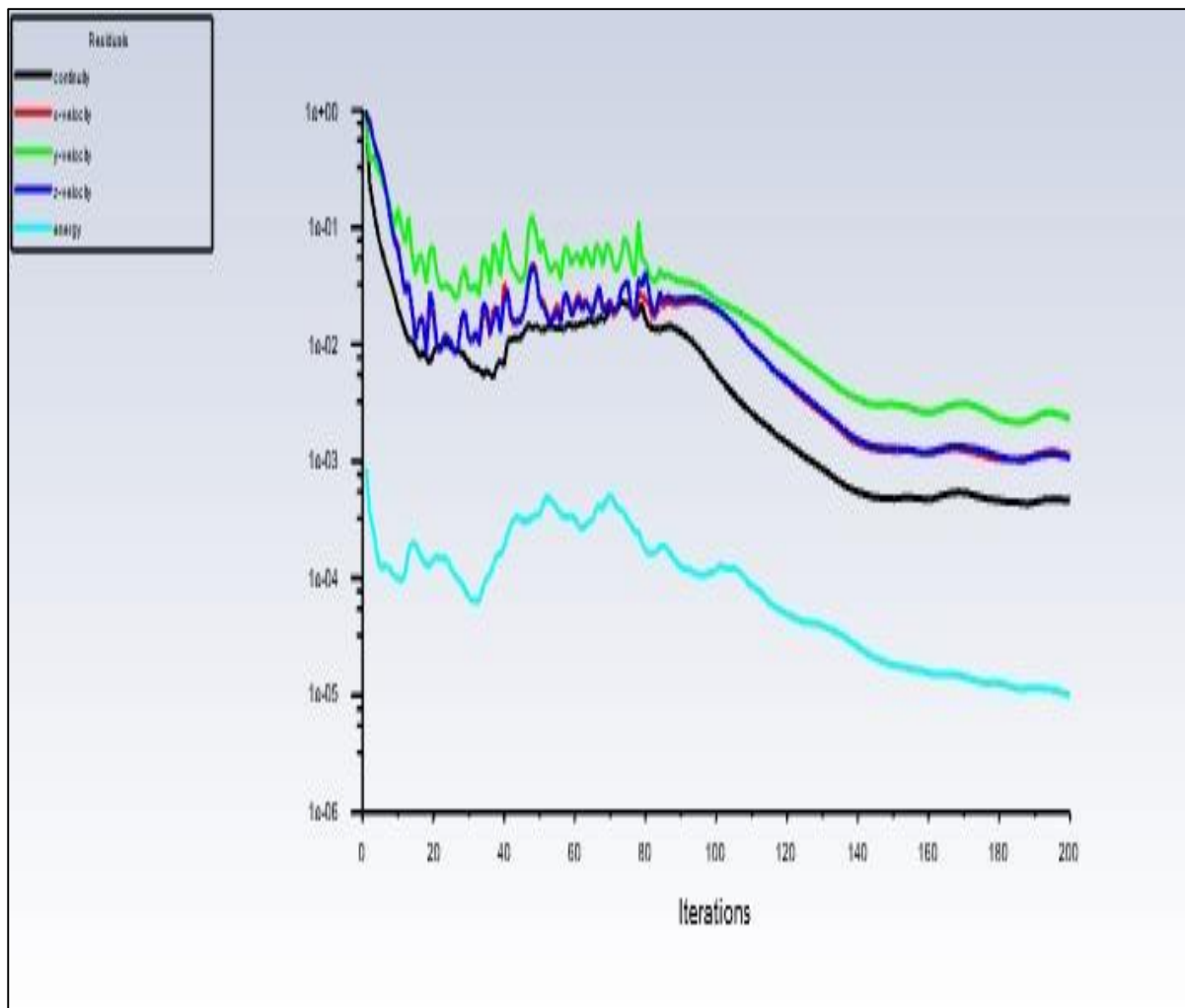


Figure 66 Conversion curve of spline electrode with curved blade

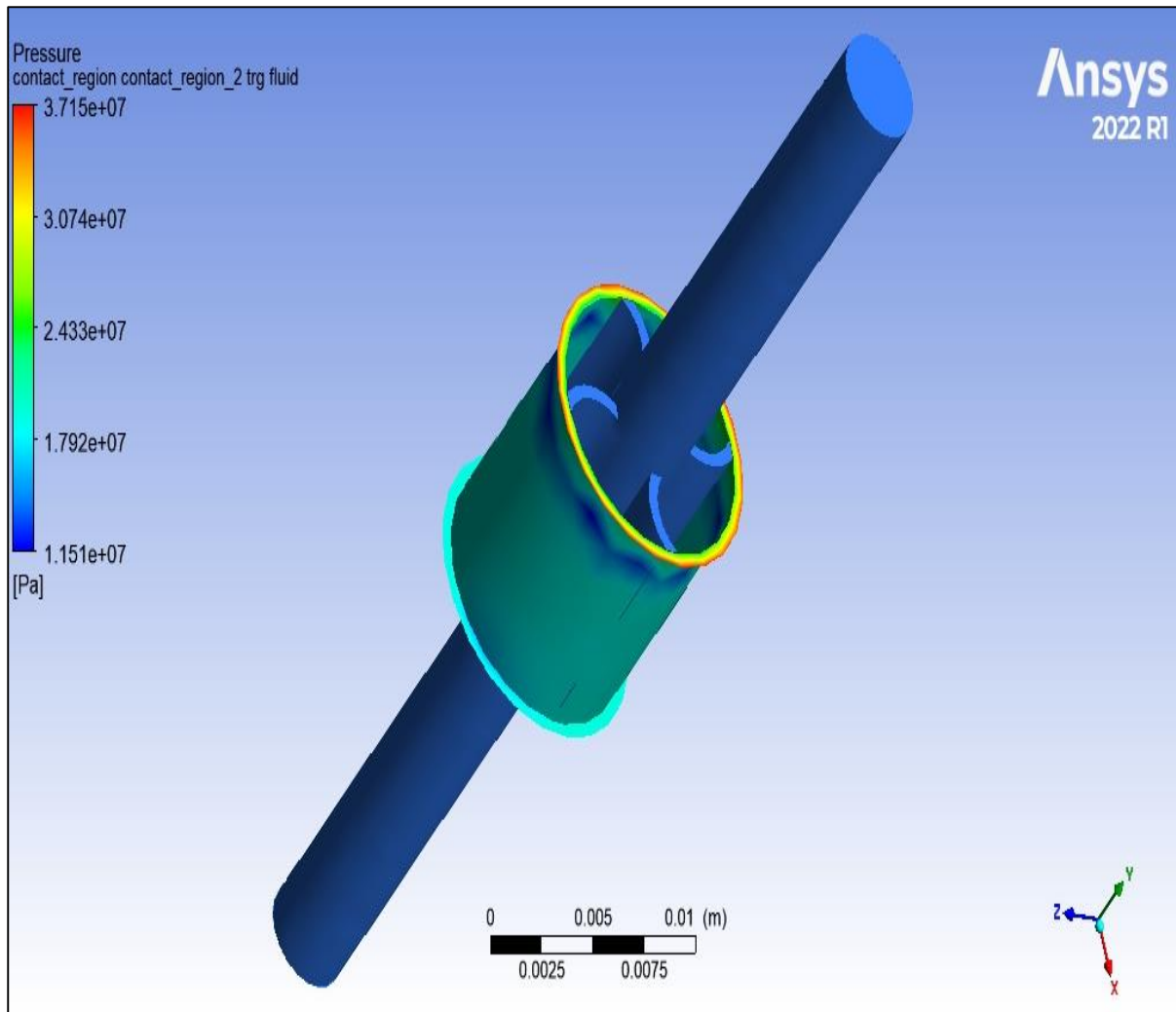


Figure 67 Pressure distribution over the workpiece by spline shape electrode with curved blade at stationary condition.

Figure 67 shows the pressure distribution over the workpiece when a spline shape electrode with curved blade is used at the stationary condition. The figure shows that the value of maximum pressure is 37.15 MPa at the extrusion pressure of 20 MPa which is far more than that of the pressure distribution of the straight spline electrode with 20 MPa working pressure range as the maximum value of pressure at that condition is 24.73 MPa. This increase in the pressure value is due to the increase in the centrifugal force inside the media and due to the pressure distribution over the workpiece. The results also highlight the increase in the increase in the material removal process when the proposed electrode would be in use.

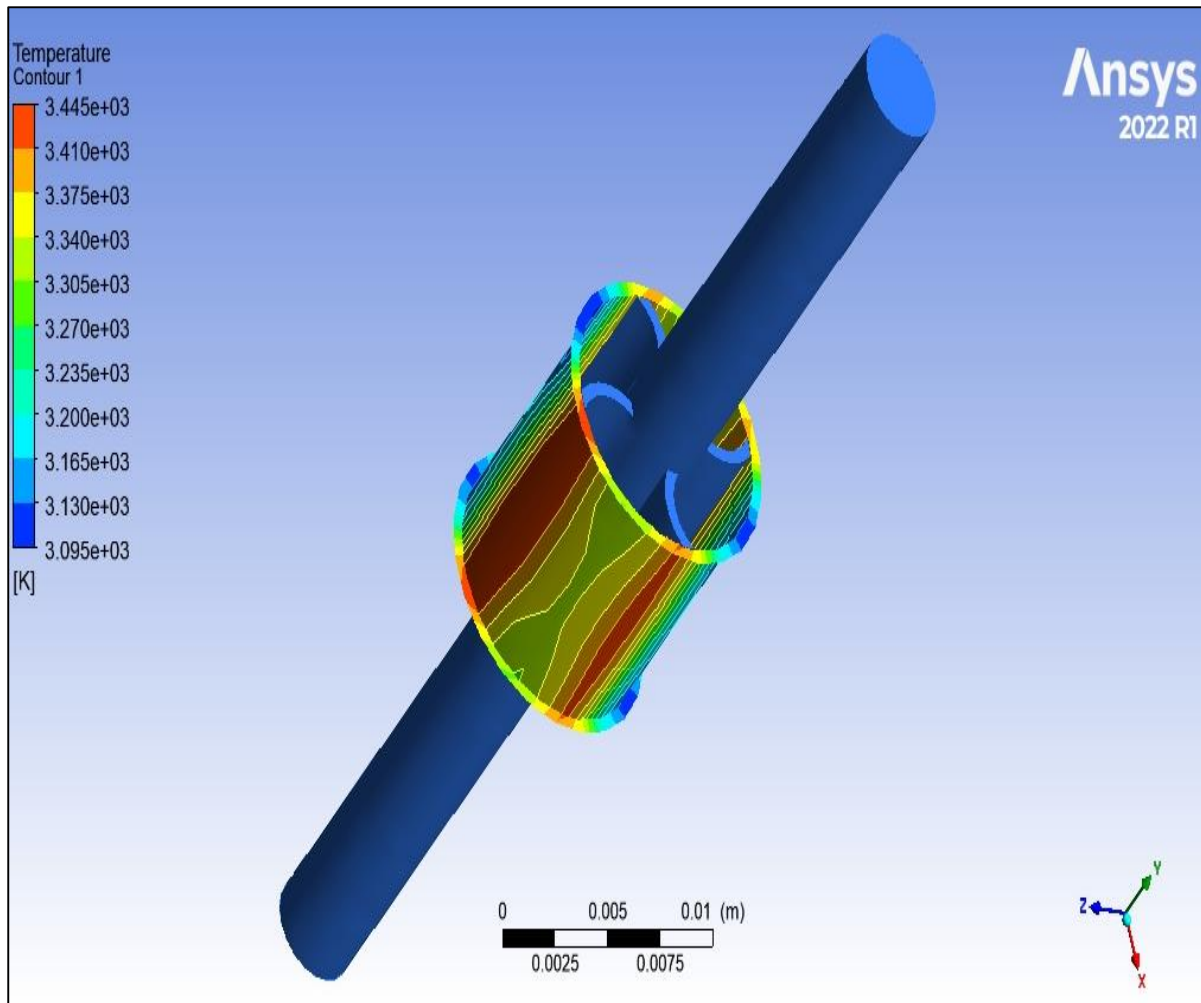


Figure 68 Temperature distribution over the workpiece by the Spline shape electrode with curved blade during the stationary condition of the electrode

Figure 68 shows the temperature distribution of the spline electrode with curved blade over the workpiece. The results highlight the maximum temperature spot at the edges of the curved blade which justify the spark formation at that point. Also the important point of consideration is that the maximum value of temperature is around 3445 K which is higher than the supply temperature of the CFG electrode and also the value is higher than that of the CFG electrode with the straight blade which shows its improvement in the melting and abrasion process. The higher value of the temperature results in an increase in the melting and evaporation of the workpiece which results in an increase in the material removal process.

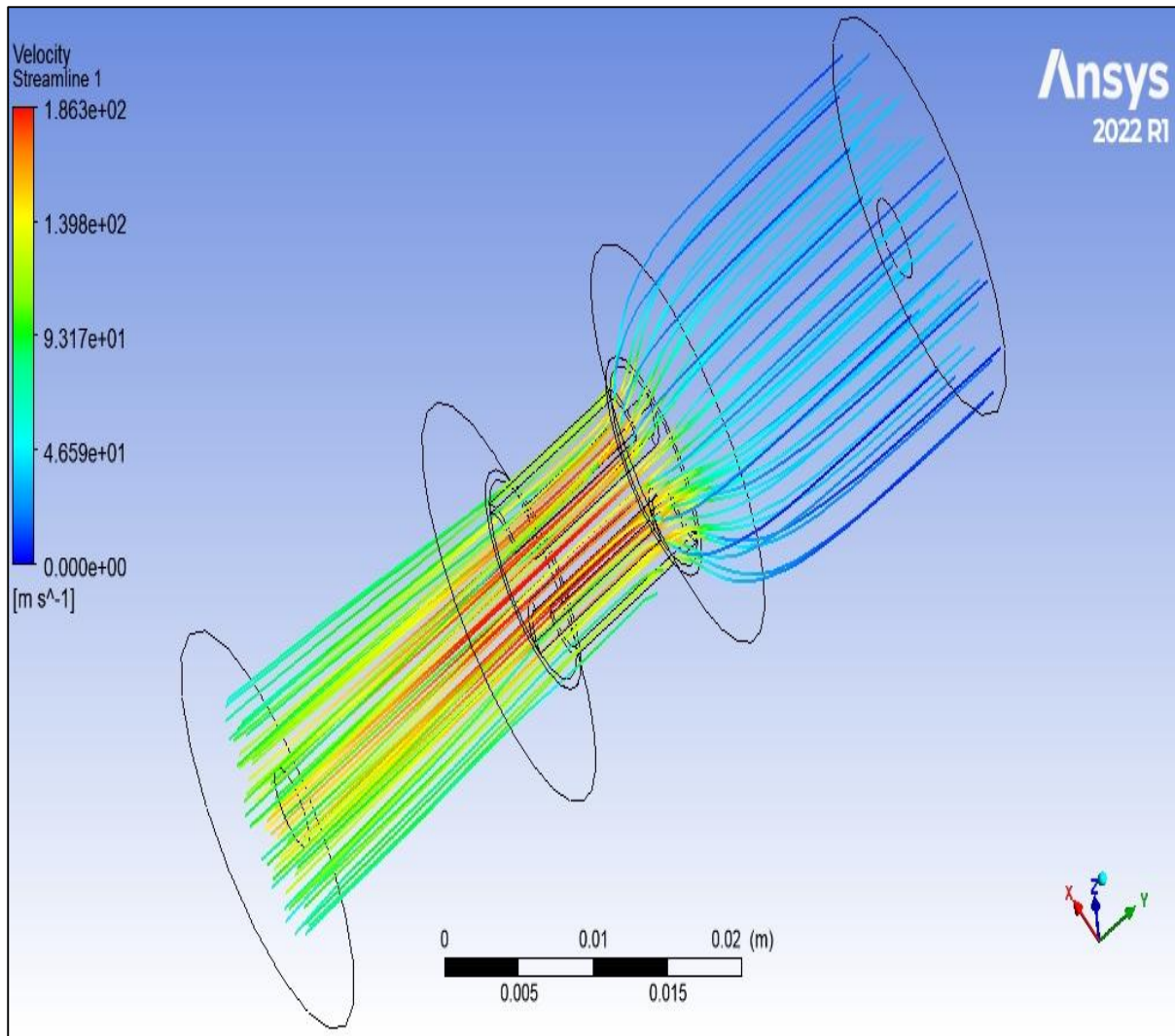


Figure 69 Streamline pattern of the media for spline shape electrode

Figure 69 shows the streamline pattern representing the media flow when the electrode is at stationary condition. The media flow is due to the pressure difference between the upper and lower cylinder with a working pressure of 20 MPa. The streamline shows the smooth movement of media particle. The streamline converges inside the workpiece which highlights the dynamic increase in the number of abrasive particles present between the workpiece and the electrode. Due to this the abrasion process significantly increases which results in an increase in the material removal rate.

Figure 70 shows the pressure distribution inside the media during the TACAFM process for the extrusion cycle. The figure shows the cyclic pressure difference during the extrusion which results in the axial movement of media inside the workpiece. This axial movement along with centrifugal force results in abrasion process desired for machining.

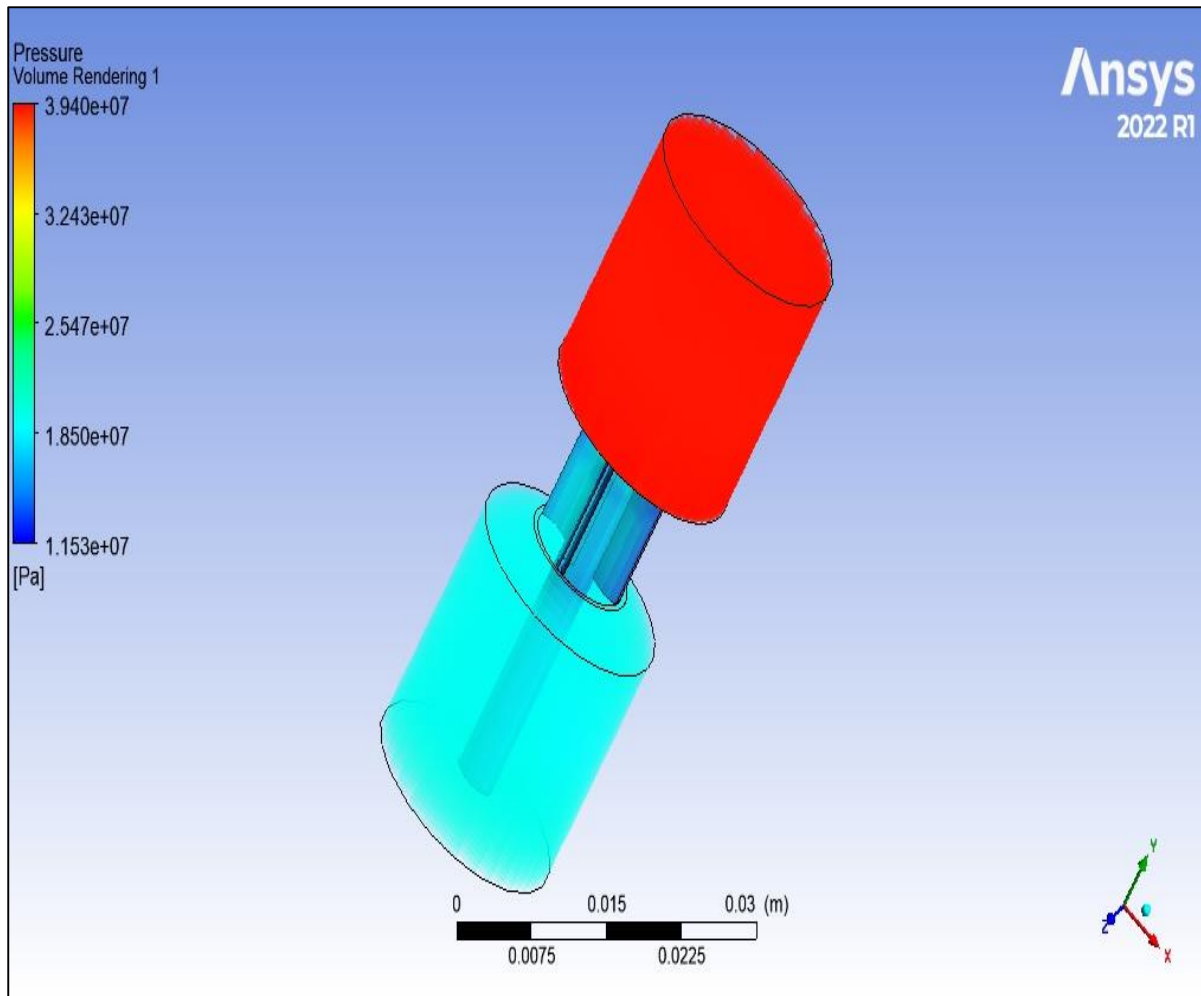


Figure 70 Pressure distribution inside the media with spline shape electrode

Figure 71 shows the temperature distribution inside the media during the TACAFM process. It can be observed that the reason of the maximum temperature is the electrode and the workpiece area. This is desirable as the higher temperature reason near the workpiece results in the increase in the melting of the workpiece. Also the higher temperature results in the softening of the workpiece which supports the material removal as the abrasive can easily dig inside the surface of the workpiece compare to the hard surface of the workpiece.

The another point of consideration is that the temperature inside the media remains the same. This is a desirable condition as the viscosity of the media remains unaffected as the temperature does not vary inside the media. The viscosity of the liquid generally decreases with the increase in the temperature and this decrease in the viscosity results in the decrease in the abrasive holding capacity of the media. This results in the decreases in the material removal of the media as the abrasion process decreases. But since the temperature variation of the media does not occur hence the material removal process of the media does not decrease.

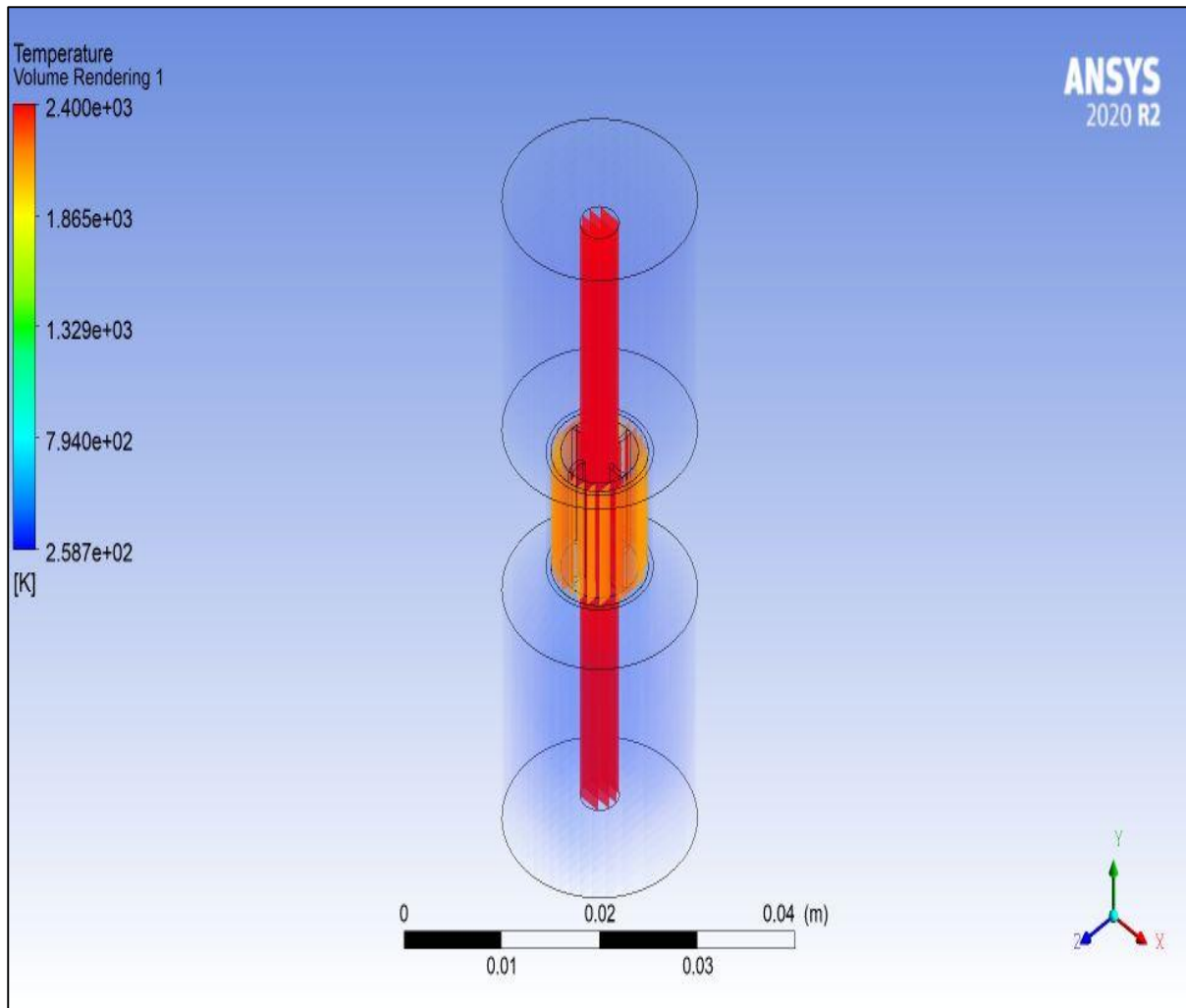


Figure 71 Temperature distribution inside the media with the spline shape electrode

Figure 72 shows the pressure distribution over the workpiece when the spline shape electrode with the curved blade is rotated at 100 rpm. The figure shows that the maximum pressure is of the 39.40 MPa which is higher than the pressure at the stationary condition which is about 37 MPa. This is because of the fact that the rotation of the electrode provides extra centrifugal force to the media which directs the abrasive particle towards the wall of the workpiece.

Figure 73 shows the temperature distribution over the workpiece when the spline shape electrode with the curved blade is rotated at 100 rpm. The figure shows that the maximum temperature of 3445 K at the edges of the blade. The important point of consideration is that the value of maximum temperature in case of rotation is more than that of the value of maximum temperature at stationary condition which was 3440 K. This increase in the value of the temperature is due to the increase in the kinetic energy of the media particle which increases the abrasion process for the material removal of the workpiece also the temperature increase

promotes the softening of the work surface resulting in the easy impact of abrasive on the work surface.

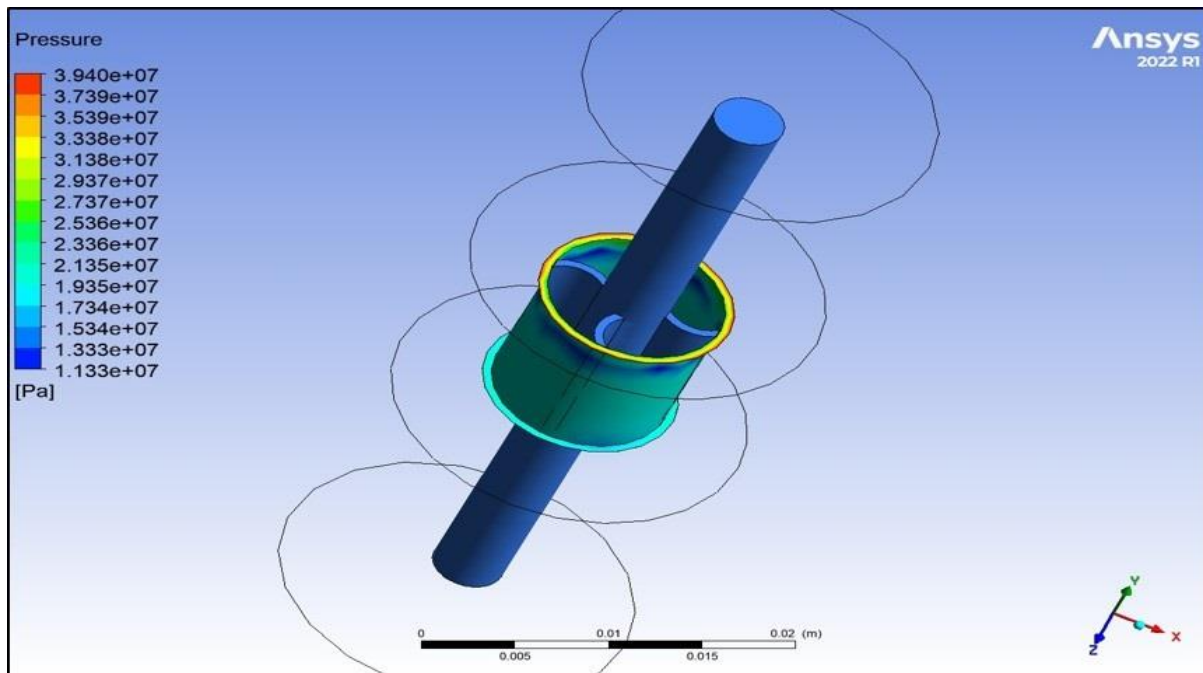


Figure 72 Pressure distribution over the workpiece due to spline electrode with curved blade at 100 rpm rotation

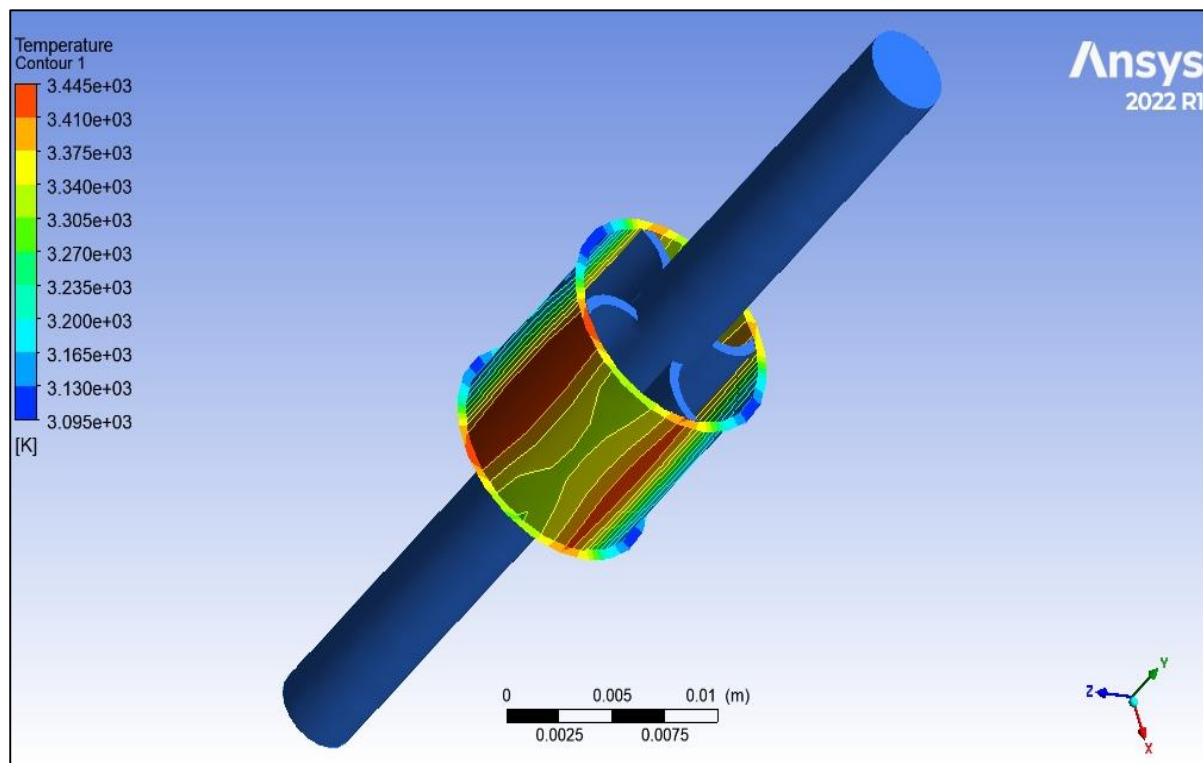


Figure 73 Temperature distribution over the workpiece by the spline shape electrode with the curved blade at 100 rpm rotation of the electrode

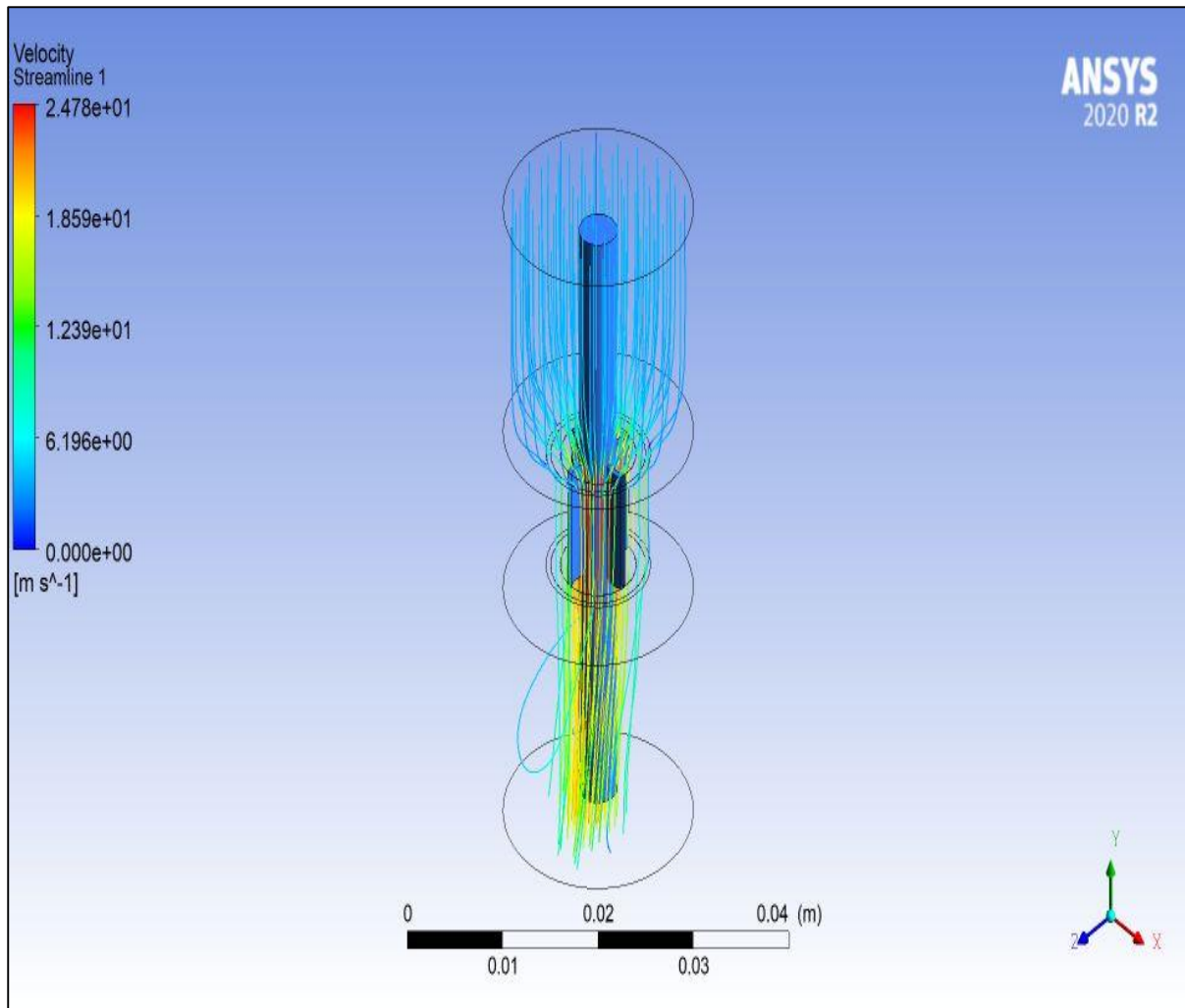


Figure 74 Streamline pattern of the spline shape electrode with curved blade at 100 rpm rotation

Figure 74 shows the stream line variation of the media when the spline shape electrode with curved blade is rotated at 100 rpm. The figure shows that the stream line converges at the mouth of the workpiece which shows the active number of dynamic abrasive particle are higher near the wall of the workpiece. Due to which the machining of the workpiece is enhanced. Also the rotation of the electrode results in the increases the centrifugal force inside the media which can be observed by the difference in distribution of the streamline pattern. Here the streamline is distributed due to the rotation of the electrode which increase the effective machining of the TACAFM process.

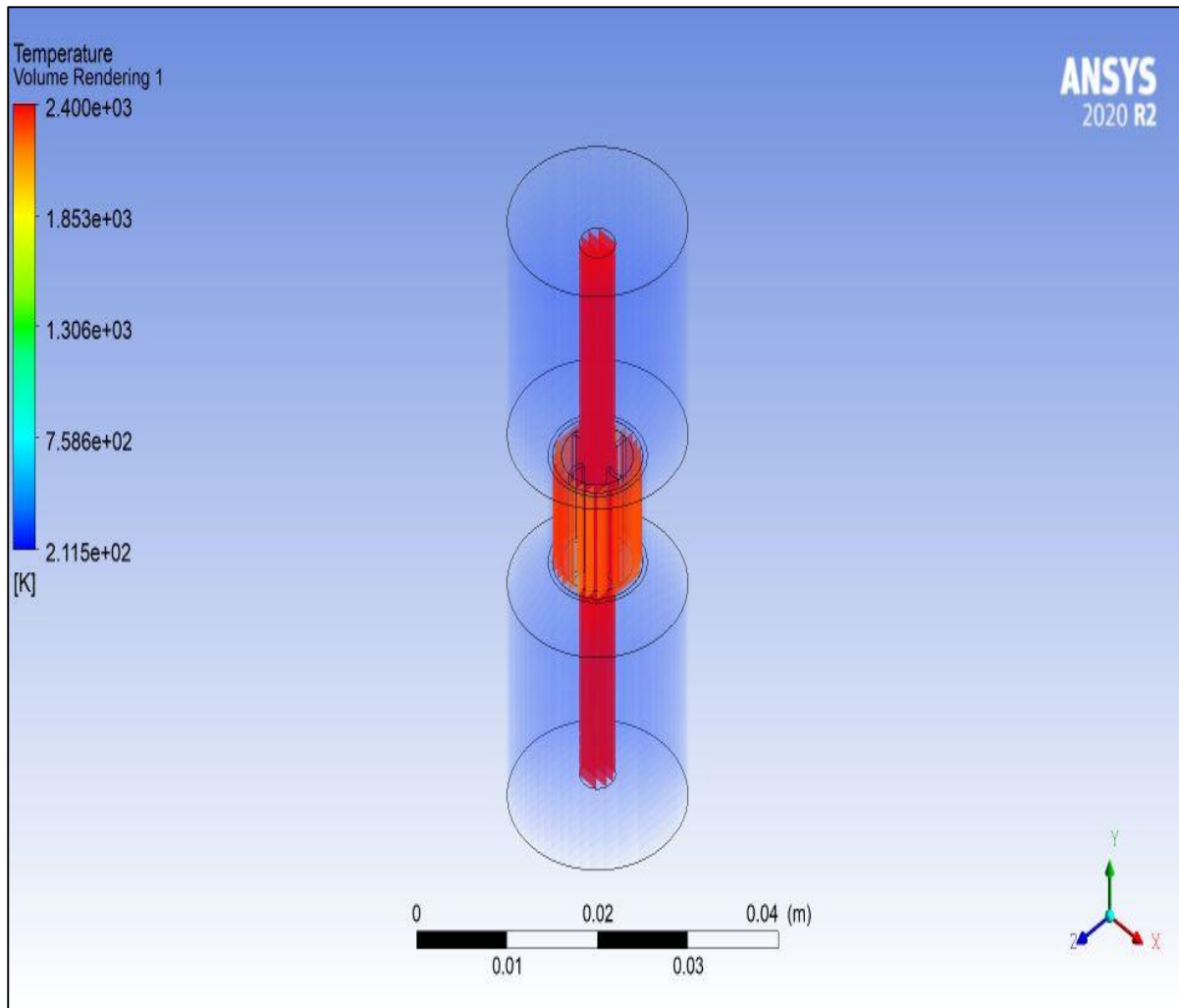


Figure 75 Temperature distribution inside the media during the 100 rpm rotation of the spline shape electrode with the curved blade

Figure 75 shows the temperature distribution inside the media when the spline shape electrode with curved blade is rotated at 100 rpm. The results show the maximum temperature at the electrode and the workpiece which is desirable. The maximum temperature at the workpiece shows that the spark formation which accelerates the material removal process. Also like the temperature distribution in the media during the stationary condition, the temperature of the media is uniform and does not vary resulting in the minimum variation in the viscosity which further results in the increase in the material removal.

Figure 76 show the pressure distribution inside the media by the spline shape electrode with curved blade when the electrode is rotated at the 100 rpm. The results is similar to the pressure difference inside the media during the stationary condition of the electrode. This enhances the material removal of the TACAFM process with the spline shape electrode with the curved blade.

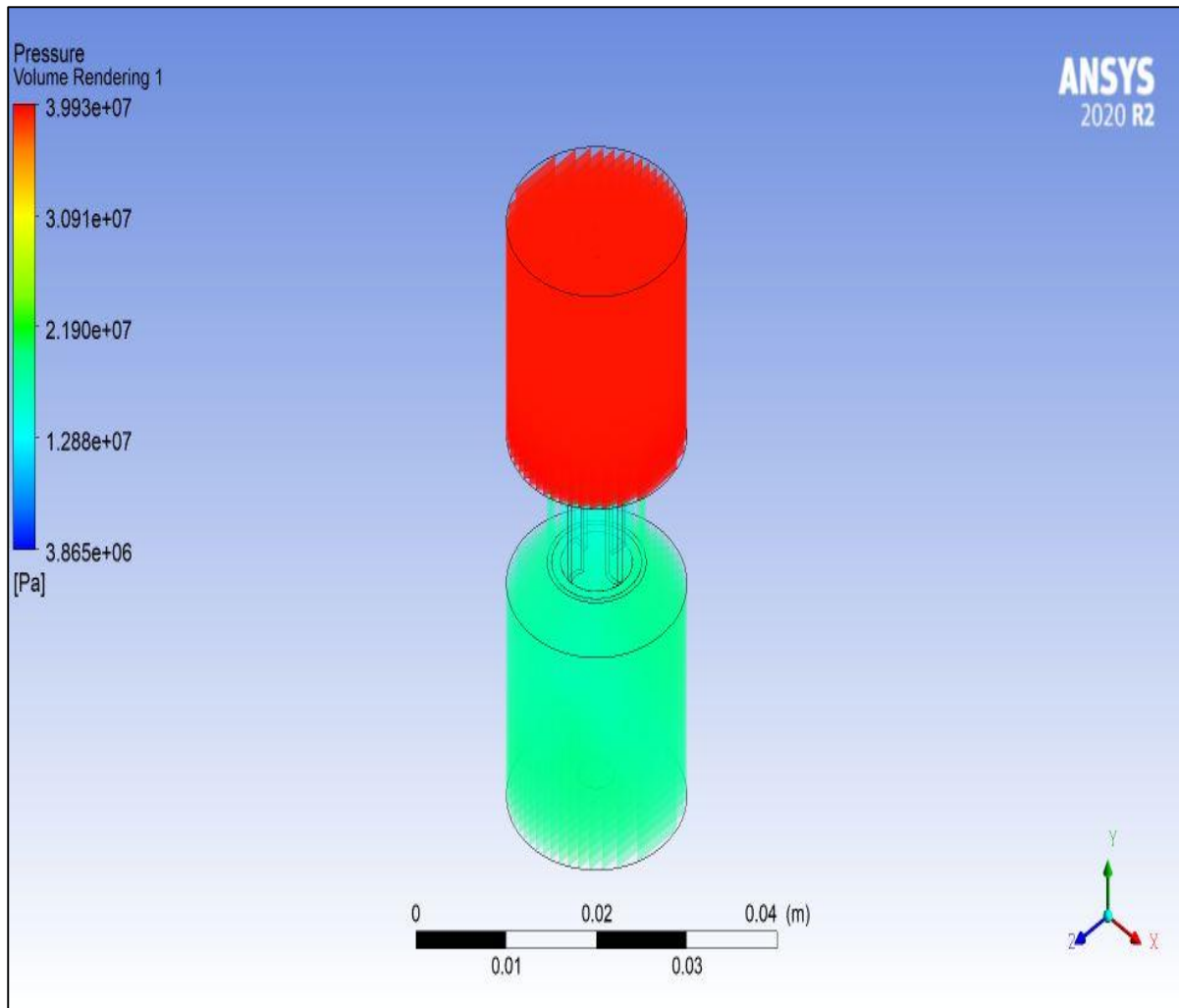


Figure 76 Pressure difference inside the media with spline shape electrode with curved blade at 100 rpm rotation of the electrode

5.14. Square shape CFG electrode

The next type of electrode used in the consideration is the square shape electrode. The square shape electrode has the uniform cross-section which provides an adequate throw ability of the media particles towards the wall of the workpiece. This is a desirable concept as it also promotes the uniform mixing of the abrasive particle with the gel and abrasive particle present in the media. The other advantage with the square shape electrode is that unlike spline shape electrode the media flow path is restrictive, due to this the interaction of media with the wall of the workpiece is increased. Also this interaction occurs with the force as the flow of media is pressurized in the constrictive passage. The greater cutting force results in the higher abrasion process resulting in the increase in the material removal which curbs the limitation of low MR of conventional AFM process. The another factor associated with square electrode is its fabrication which is easy as compare to spline electrode. The analysis of the square shape

electrode is done on the similar basis as done for the spline shape electrode. Two separate simulations were done for this electrode in which one is done at stationary condition and the other is done at the rotation at 100 rpm. The computation of pressure distribution, temperature distribution over the workpiece, over the media and the variation of the stream line is thoroughly analyzed to study the effect of square shape electrode on the material removal and the feasibility spark formation in TACAFM process.

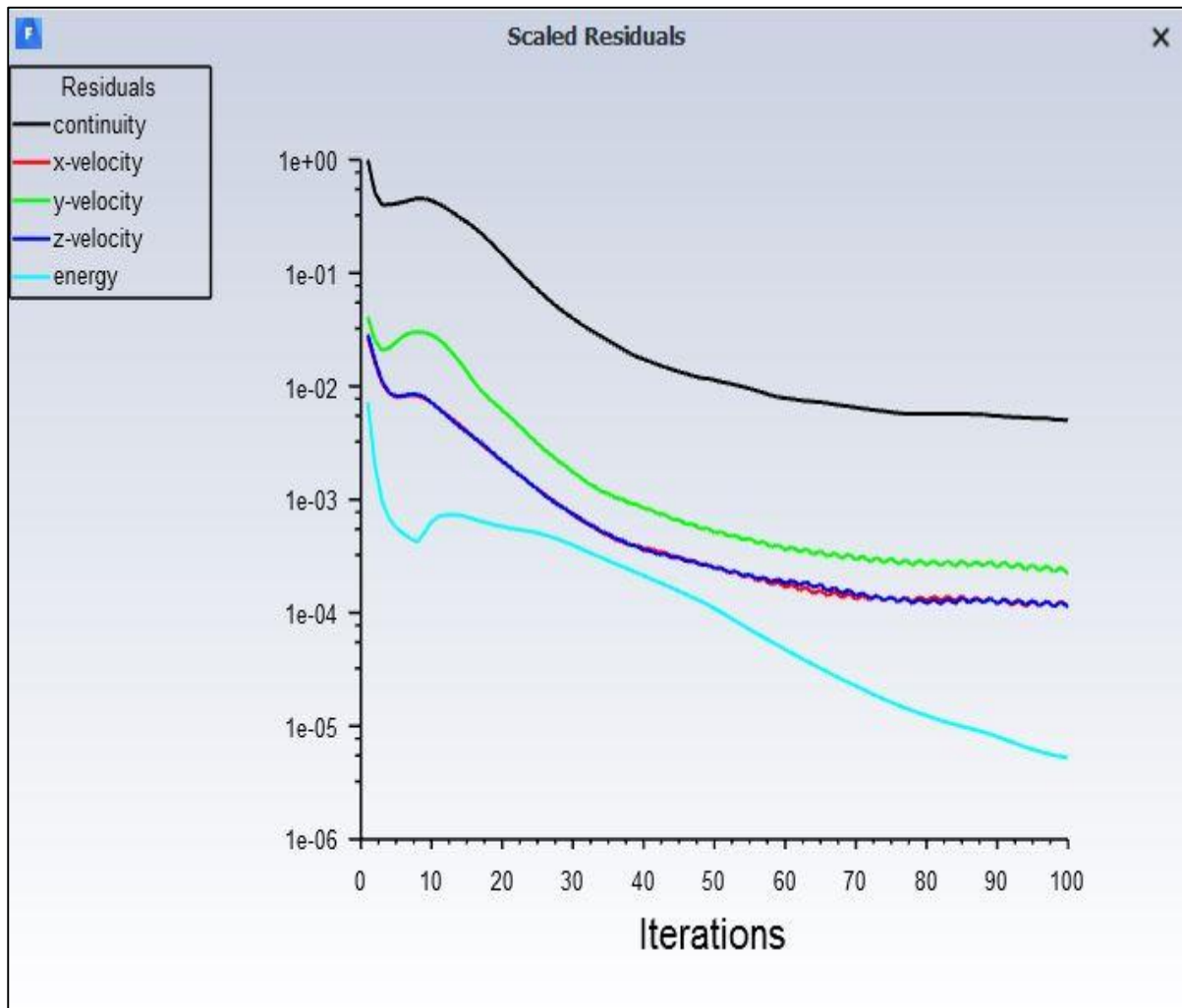


Figure 77 Conversion curve for square shape electrode at stationary condition

Figure 77 shows the conversion curve of the X velocity, Y velocity, Z velocity, continuity and the energy line with the number of iterations. The conversion is smooth up to 10^{-6} . And the energy line lies below the X, Y, Z and continuity line which shows the smooth conversion process. The subsequent figures show the simulation results obtained with square shape electrode at the stationary condition.

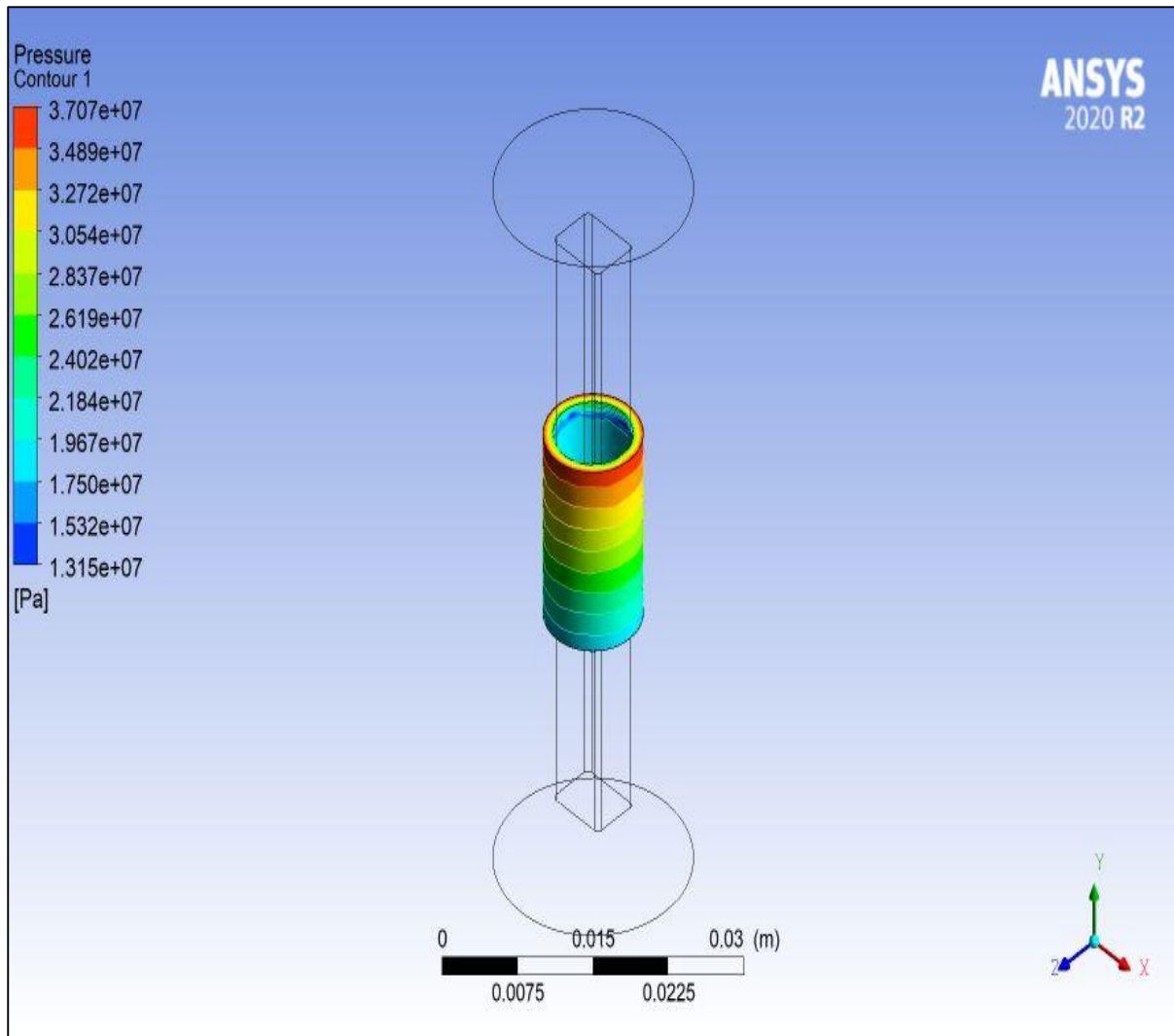


Figure 78 Pressure distribution over the workpiece by square shape CFG electrode at the stationary condition

Figure 78 shows the pressure distribution over the workpiece exerted by the media flow over the workpiece when square shape CFG electrode is used in the TACAAM process. The Figure shows that the maximum value of the pressure is 37.07 MPa, which is higher than the value of maximum pressure in case of centrifugal force assisted abrasive flow machining (CFAAFM) and the conventional abrasive flow machining process. The another point of consideration is that the maximum pressure over the workpiece is less than that of the maximum pressure in case of the spline shape electrode at the stationary condition. This shows that the material removal for the square shape electrode is less compare to the spline shape electrode. The reason behind this is that the generation of the centrifugal force is less than that of the spline shape electrode. The blade present in the spline shape electrode is responsible for this generation of the centrifugal force generating electrode.

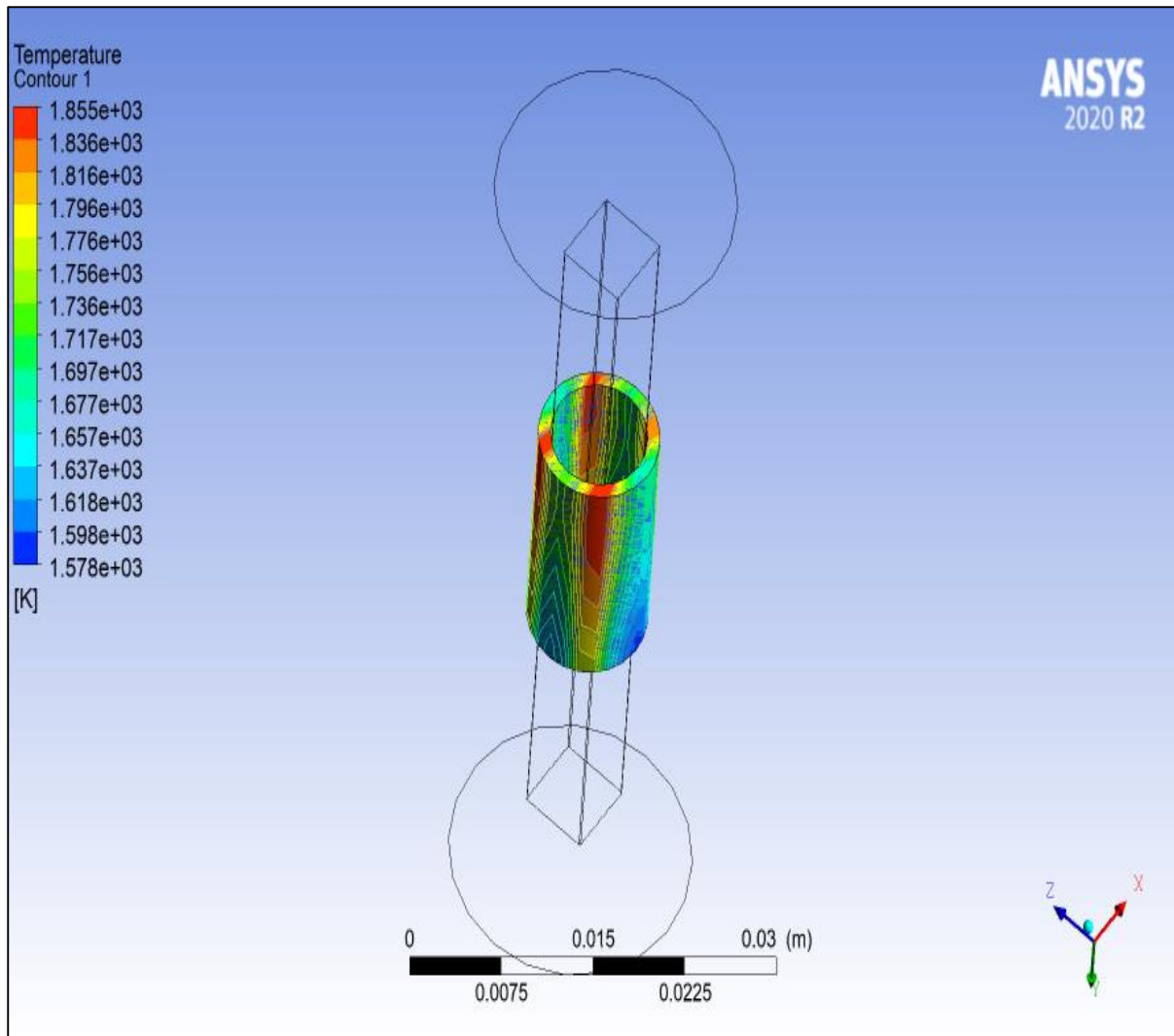


Figure 79 Temperature distribution of the square shape CFG electrode at the stationary condition of the electrode

Figure 80 shows the temperature distribution over the workpiece by the square shape CFG electrode during the stationary condition of the CFG electrode. The figure shows that the maximum temperature is shown at the edges of the square shape electrode. This is because the difference between the workpiece and the CFG electrode is minimum at the edges which results in the spark generation at these reasons. Also the another point of consideration is that the maximum temperature in case of the square shape electrode is less as compare to the spline shape electrode under the same external conditions. This shows that the spark generation of the spline shape electrode is better in comparison to the square shape CFG electrode. The reason for this may be blades provided adequate gap between the workpiece and the electrode which results in the proper generation of the spark.

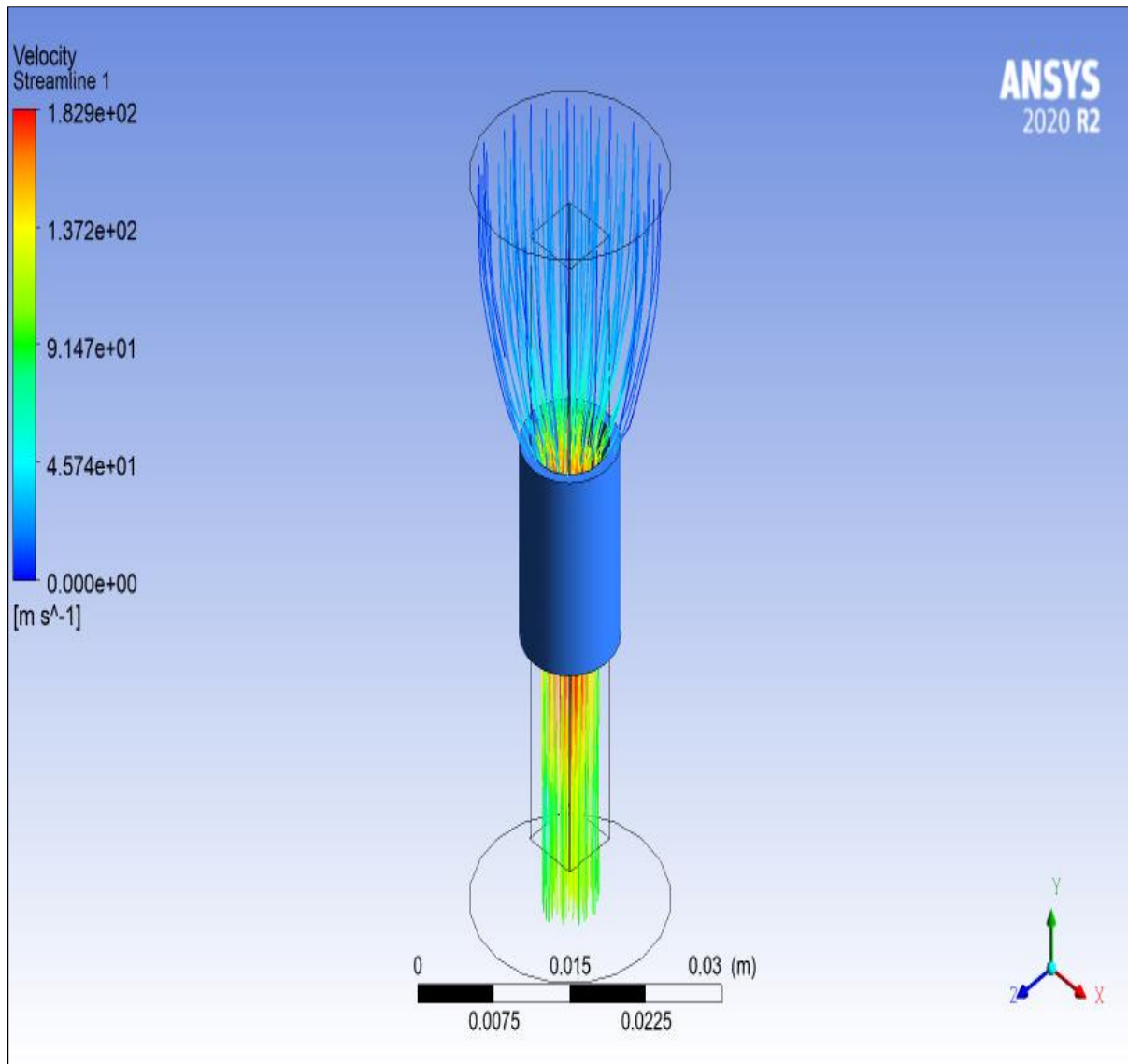


Figure 80 Stream line distribution of the media in TACAFM process with square shape CFG electrode at stationary condition of CFG electrode

Figure 81 shows the distribution of the media during the TACAFM process with the spline shape electrode at stationary condition. The streamline shows the uniform flow of media under the pressure difference. The media converges at the mouth of the workpiece which results in the increase in the media and the wall of the workpiece interaction. This interaction increases the dynamic number of abrasive particle resulting in the increase in the abrasion process which further increases the material removal process. Figure 82 shows the pressure distribution over the media during the TACAFM process with the square shape CFG electrode which shows the effect of extrusion pressure on the media. The figure shows the similar trends with the spline shape electrode and is desirable for the TACAFM process. Figure 83 shows the temperature distribution over the media during the TACAFM process. The trend is similar to the pattern

shown by the spline shape electrode. This can be observed that the temperature of the media does not vary inside the media which is desirable. The temperature variation results in the viscosity changes as the viscosity of the liquid decreases with the increases in the temperature. In case of the media the viscosity does not vary thus the abrasive holding capacity of the media does not decrease which does not affect the material removal process of the TACAFM process.

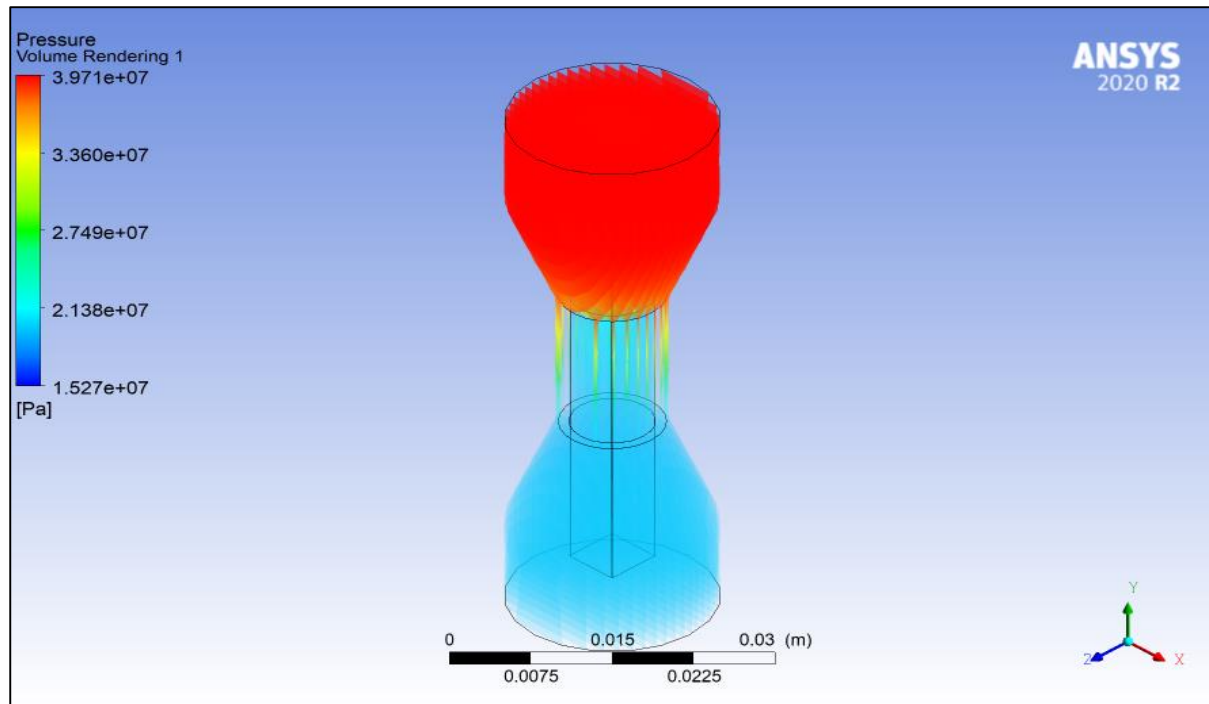


Figure 81 Pressure distribution inside the media with square shape electrode at stationary condition of the electrode during the TACAFM process

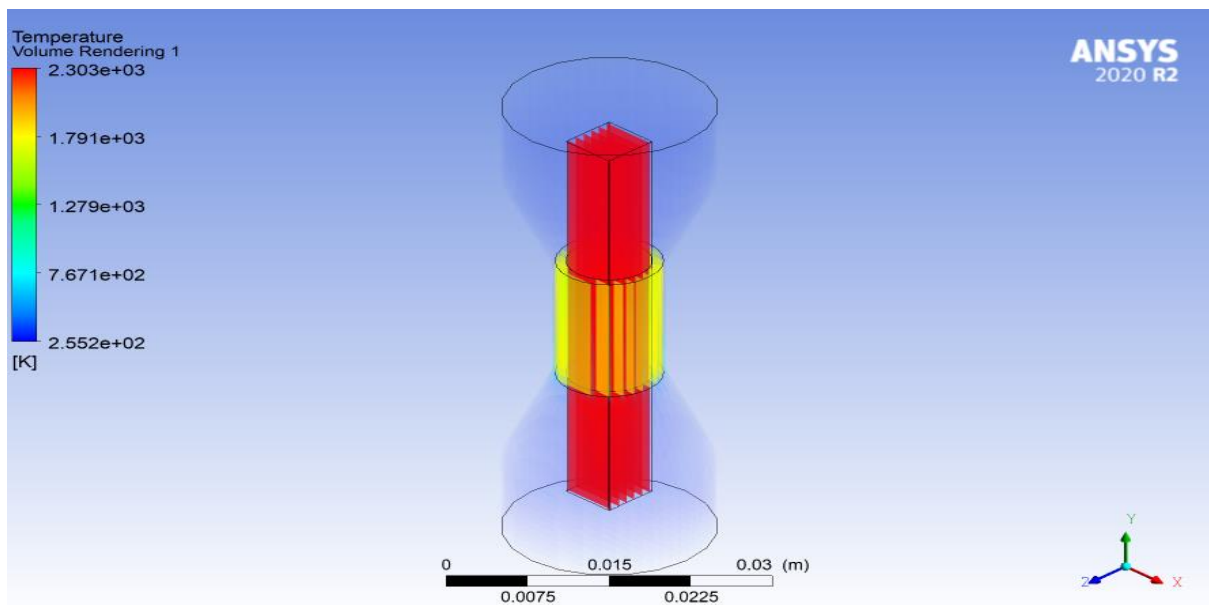


Figure 82 Temperature distribution inside the media with square shape electrode at stationary condition of the electrode during the TACAFM process

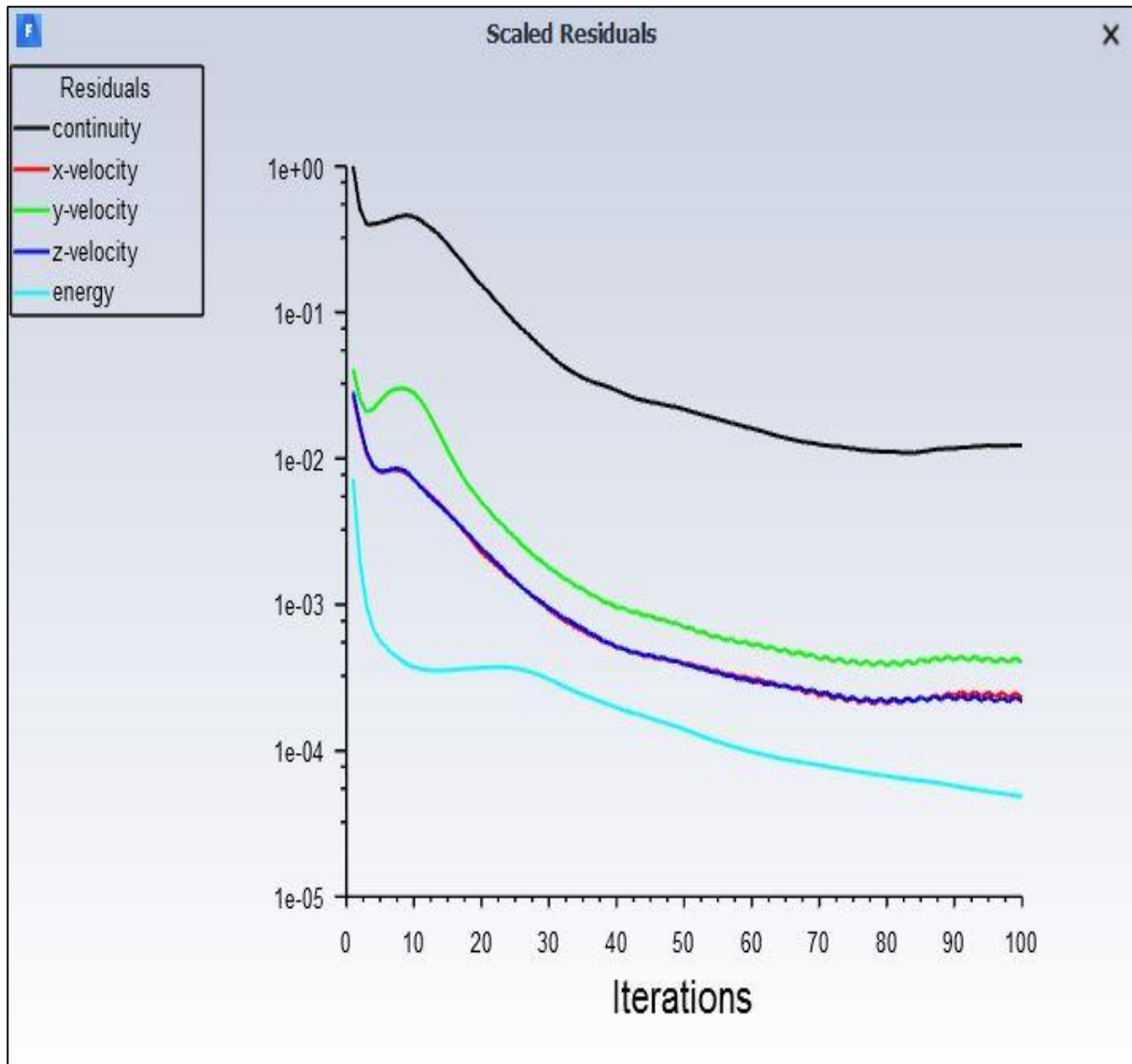


Figure 83 Conversion curve for rotation of the square electrode

Figure 84 shows the conversion curve corresponding to the rotation of the square shape centrifugal force generating electrode at 100 rpm. The curve shows the smooth conversion with the energy line below the continuity, X, Y and Z velocity line. Figure 85 shows the pressure distribution over the workpiece during the TACAFM process with square shape electrode at 100 rpm. The results show the maximum pressure of 38 MPa which is higher than the maximum pressure compare to the stationary condition of the CFG electrode at the stationary condition (37 MPa). The increase in pressure value is due to the increase in the centrifugal force produced due to the rotation of the electrode, which increase the pressure force, which further increases the cutting force resulting in the increase in MR.

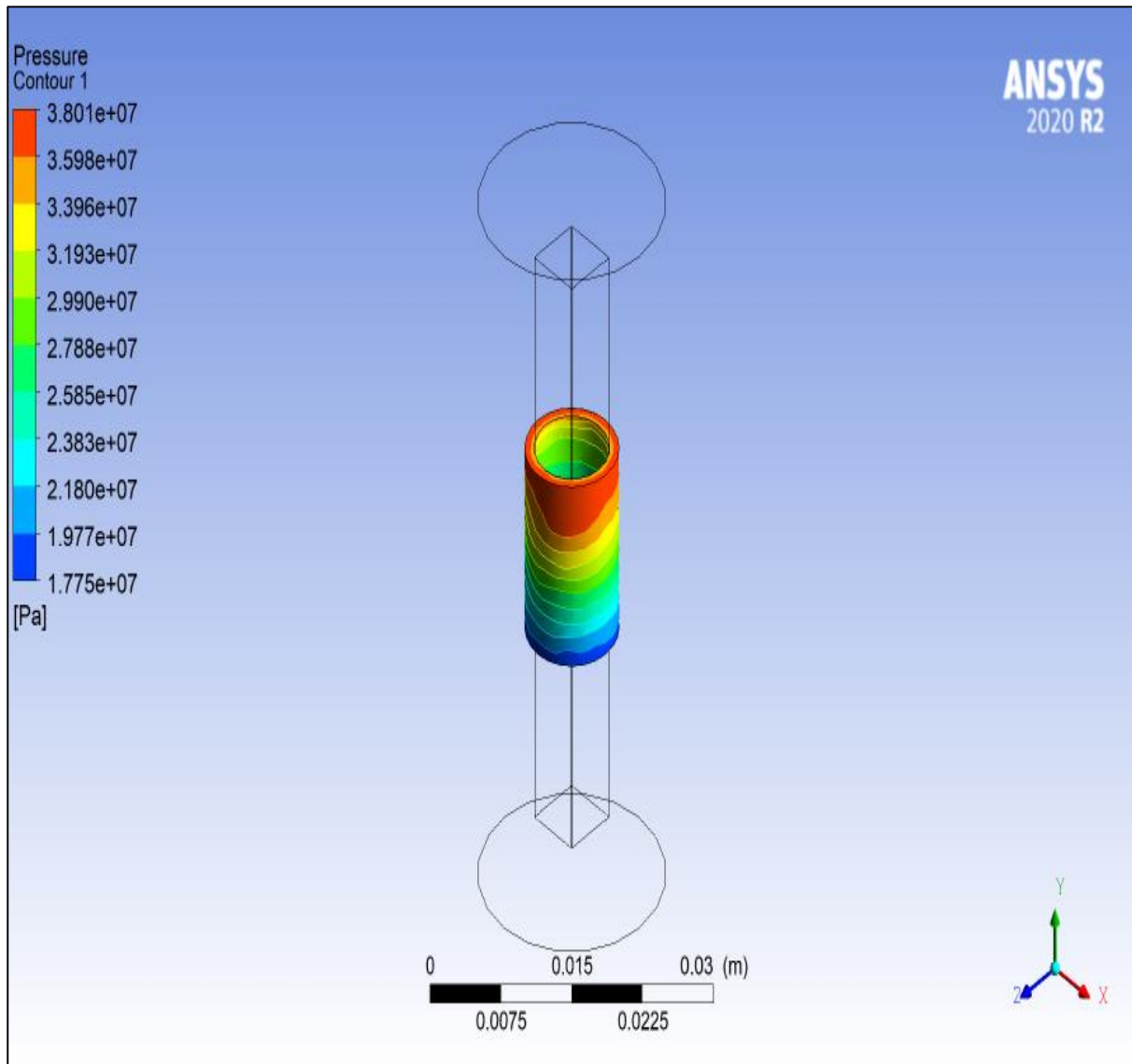


Figure 84 Pressure distribution over the workpiece by TACAFM process by square shape electrode with 100 rpm rotation of the electrode

Figure 85 shows the temperature distribution of the over the workpiece with square shape centrifugal force generating electrode at 100 rpm rotation. The figure shows the maximum temperature of the 2468 K which is much higher than that of the maximum temperature at the stationary conditions. The figure shows the distribution of temperature over the workpiece. The temperature is uniformly distributed over the workpiece due to the uniform distribution of the spark over the workpiece. The rotation of electrode makes the spark travel uniformly around the workpiece. Thus the stationary condition of the electrode results in the spark formation and the rotation of electrode results in the spark travel which accelerate the uniform removal of the material from the workpiece which is a desirable in case of the TACAFM process where high material removal is required.

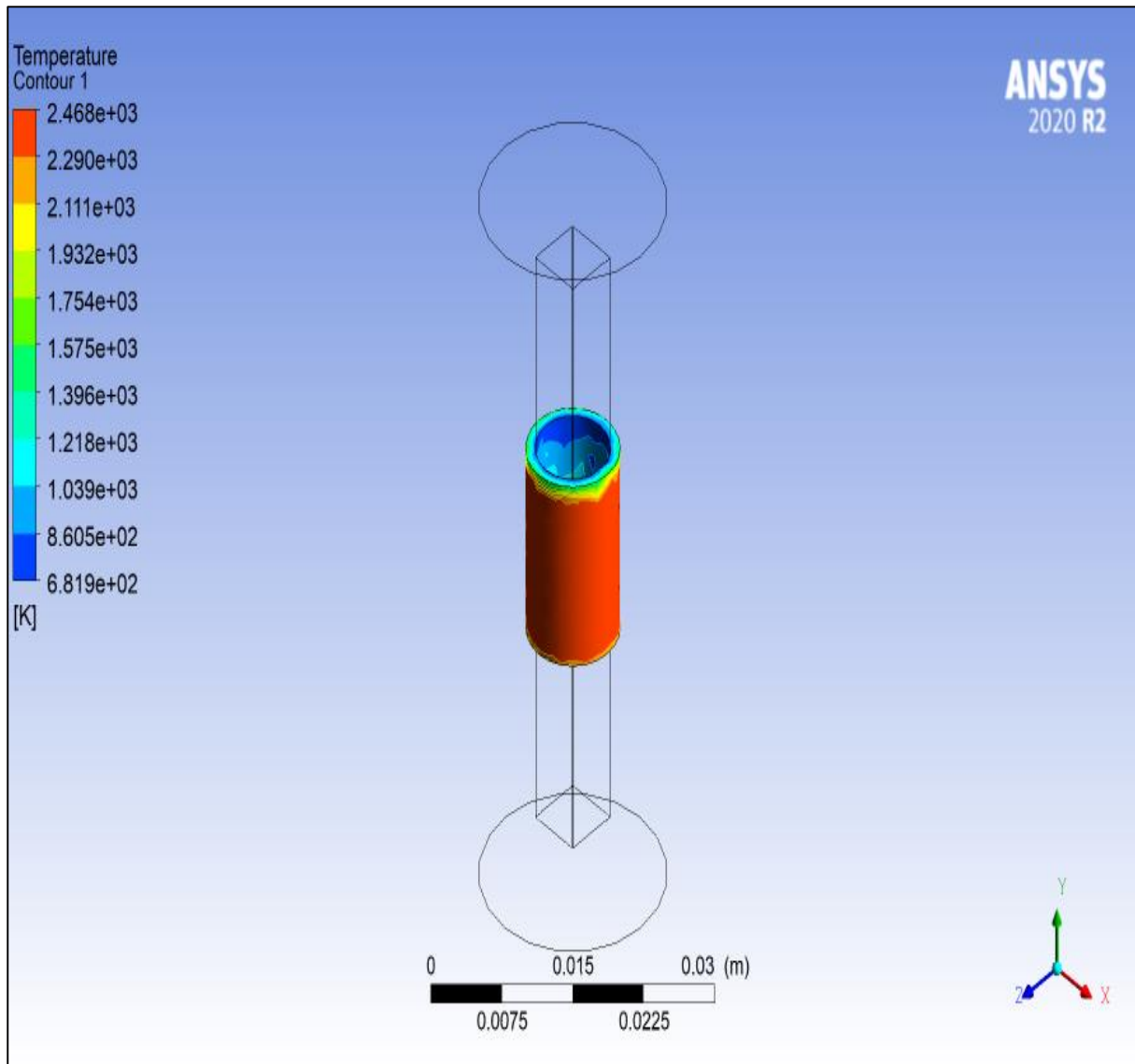


Figure 85 Temperature distribution over the workpiece by TACAFM process by square shape electrode with 100 rpm rotation of the electrode.

Figure 86 shows the streamline distribution of the TACAFM process by the square shape electrode during the rotation of electrode. The figure shows the extrusion of the media due to the pressure difference. The streamline shows the conversion of media inside the workpiece resulting in the increase in the dynamic number of the active abrasive particles which further increase in the value of the material removal. Figure 87 and figure 88 shows the pressure and temperature distribution inside the media with the square shape centrifugal force generating electrode with rotation at 100 rpm. The result is similar to that of the stationary shape electrode as the characteristic of the media does not change during the TACAFM process.

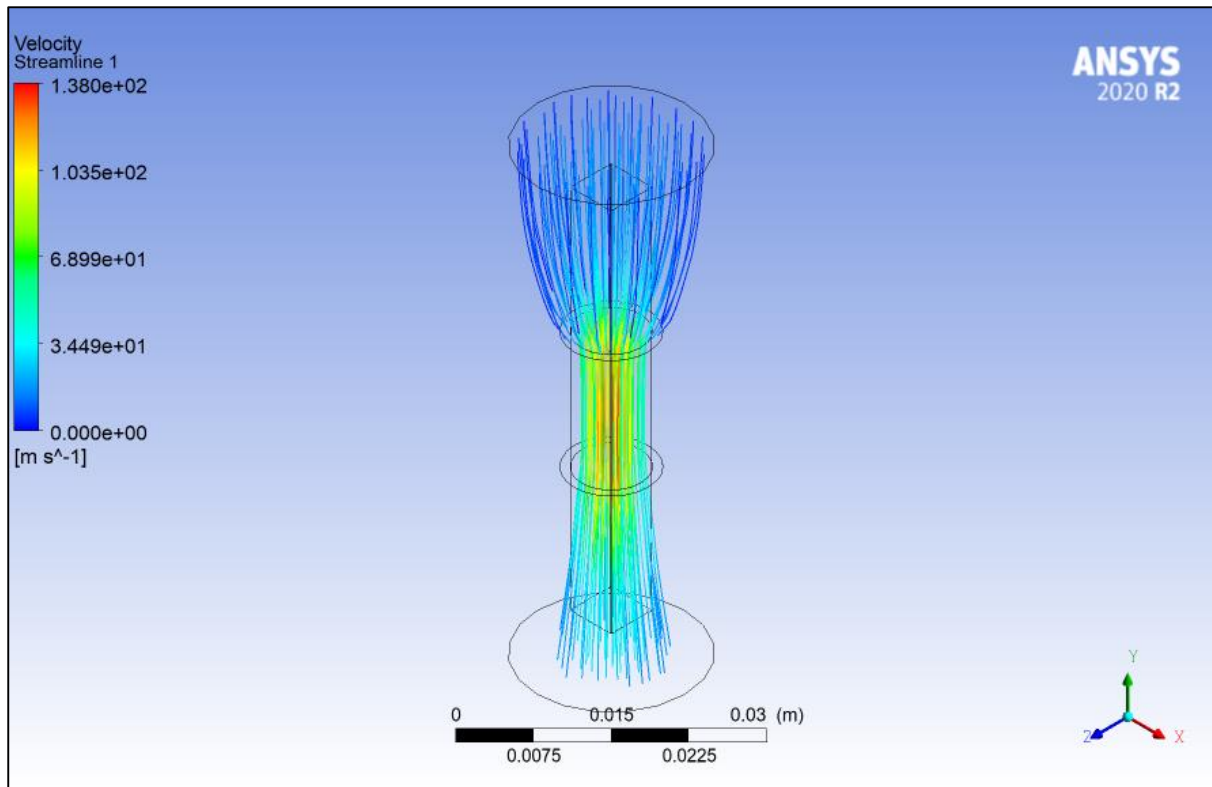


Figure 86 Stream line distribution of the media in TACAFM process with square shape CFG electrode at the rotation of 100 rpm of CFG electrode

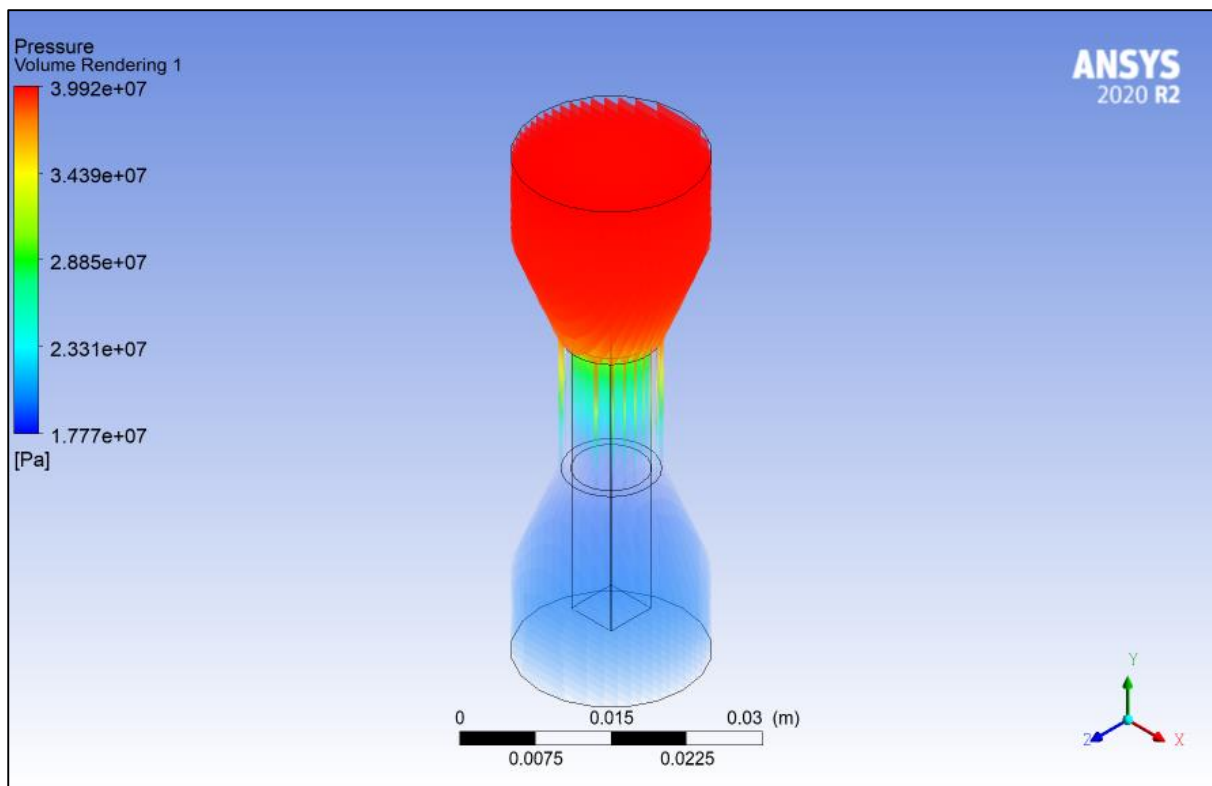


Figure 87 Pressure distribution inside the media with square shape electrode at 100 rpm rotational condition of the electrode during the TACAFM process

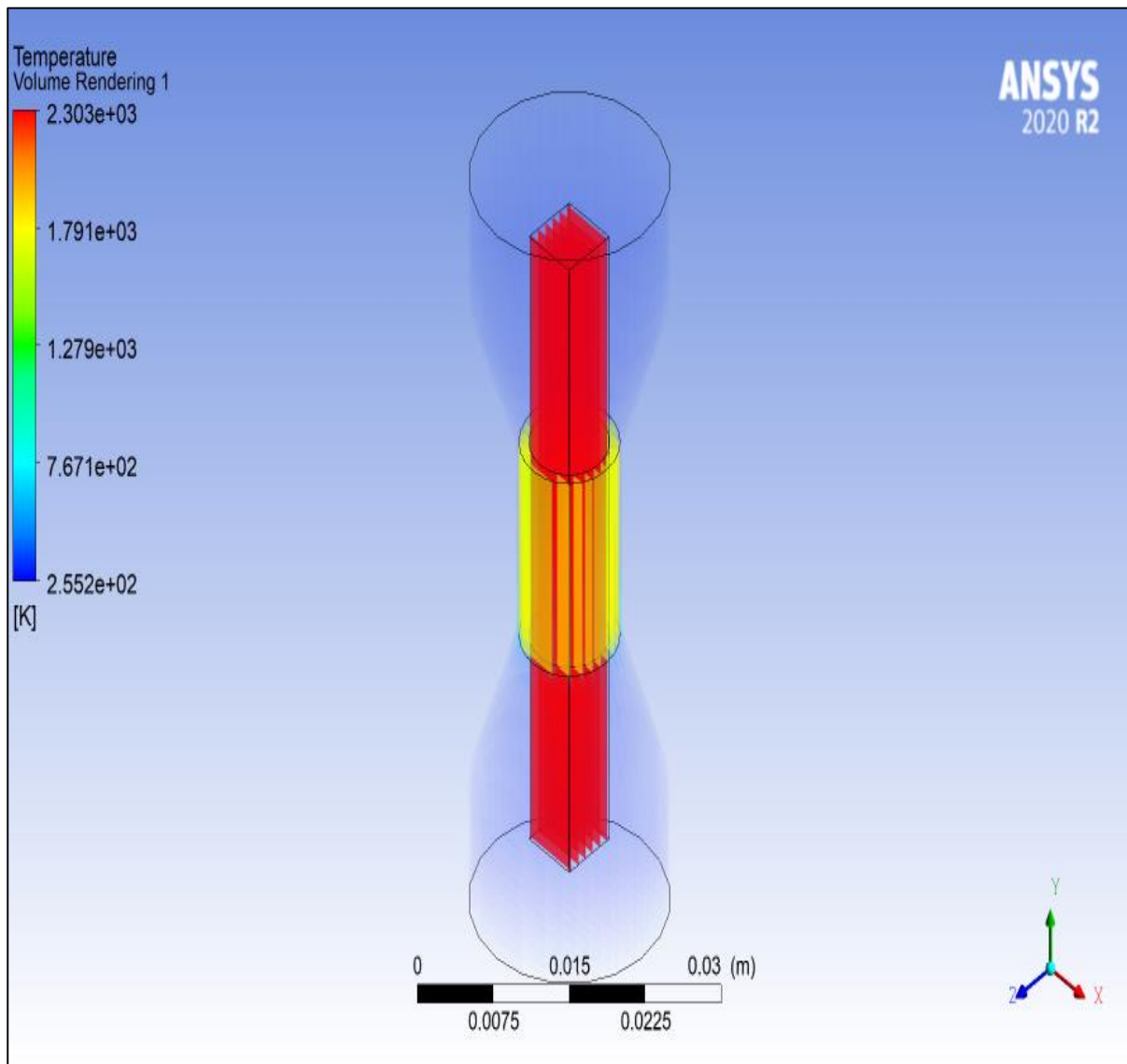


Figure 88 Temperature distribution inside the media with square shape electrode at 100 rpm rotation

5.14. Triangular shape CFG electrode

The next analysis for the TACAFM process is the triangular shape electrode. The model of the triangular shape is taken as the similar to that used in the experimental process. The similar commotion is consider for the triangular electrode which include the working pressure of 20 MPa and the 2300-degree Celsius supply temperature to the electrode. Two separate simulations were conducted one with the stationary condition of the triangular electrode and the other with the rotation of the CFG electrode with 100 rpm.

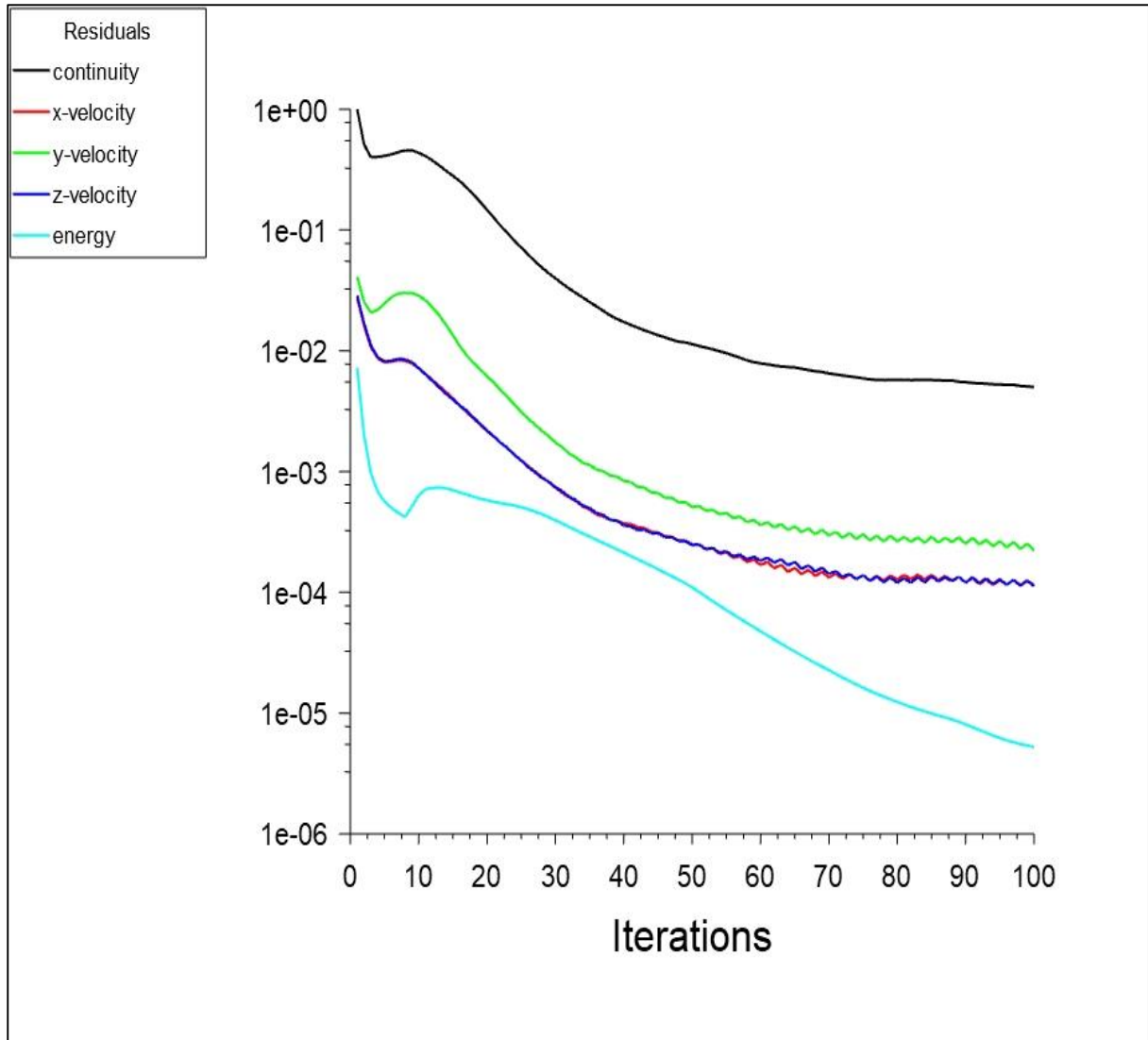


Figure 89 Conversion curve for triangular electrode at stationary conditions

Figure 89 shows the conversion curve when the triangular shape electrode is rotated at 100 rpm. The plot shows the variation of the X, Y, Z velocity and the continuity equation line with respect to the iterations. The figure shows a smooth conversion process with the conversion of 10^{-6} . The energy line lies below the continuity, X velocity, Y velocity and Z velocity line which shows a stable process. The subsequent figure 90 gives the distribution of pressure distribution over the workpiece during the TACAFM process by the triangular shape electrode. The graph shows the maximum pressure of 35.54 MPa which is below the maximum pressure compared to maximum pressure over the workpiece during TACAFM process by the spline shape electrode and by the square shape electrode (about 37 MPa). The decrease in the maximum pressure value for the triangular electrode shows the decrease in the material removal process compare to that of the spline shape and square shape CFG electrode.

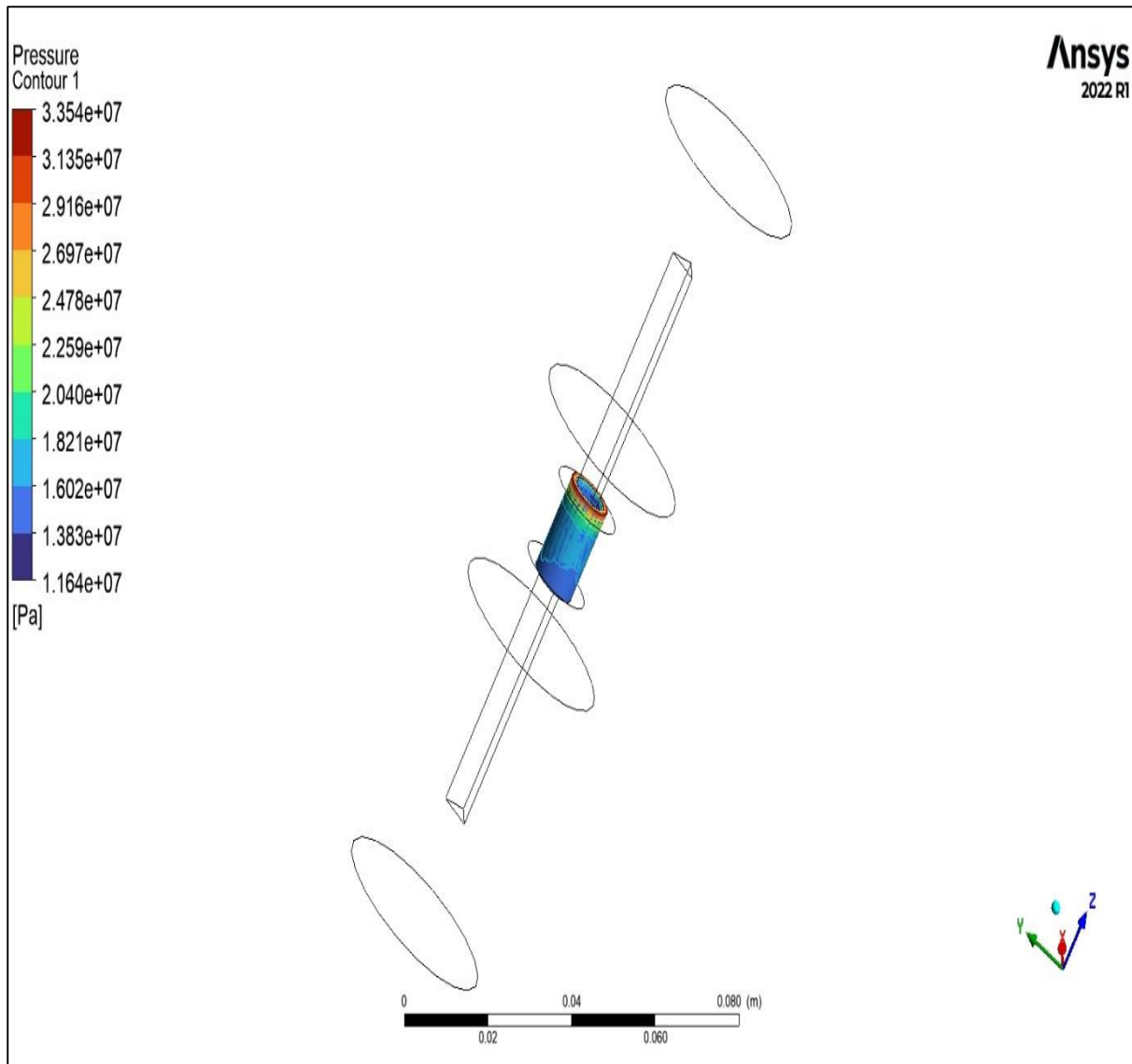


Figure 90 Pressure distribution over the workpiece at TACAFM process by the triangular shape CFG electrode at stationary condition

Figure 91 shows the temperature distribution during the TACAFM process when the triangular electrode at stationary condition is used for the TACAFM process. The figure shows the maximum temperature at the edges of the triangular electrode which justify the generation of spark in the TACAFM process. The another point of consideration is that the value of maximum temperature is around 2009 K which is less compare to the spline shape electrode and the square shape CFG electrode. This shows that the spark formation ability of the triangular shape electrode is less compare to the spark forming ability of the square and spline shape CFG electrode which further show the low material removal of the triangular shape centrifugal force generating electrode.

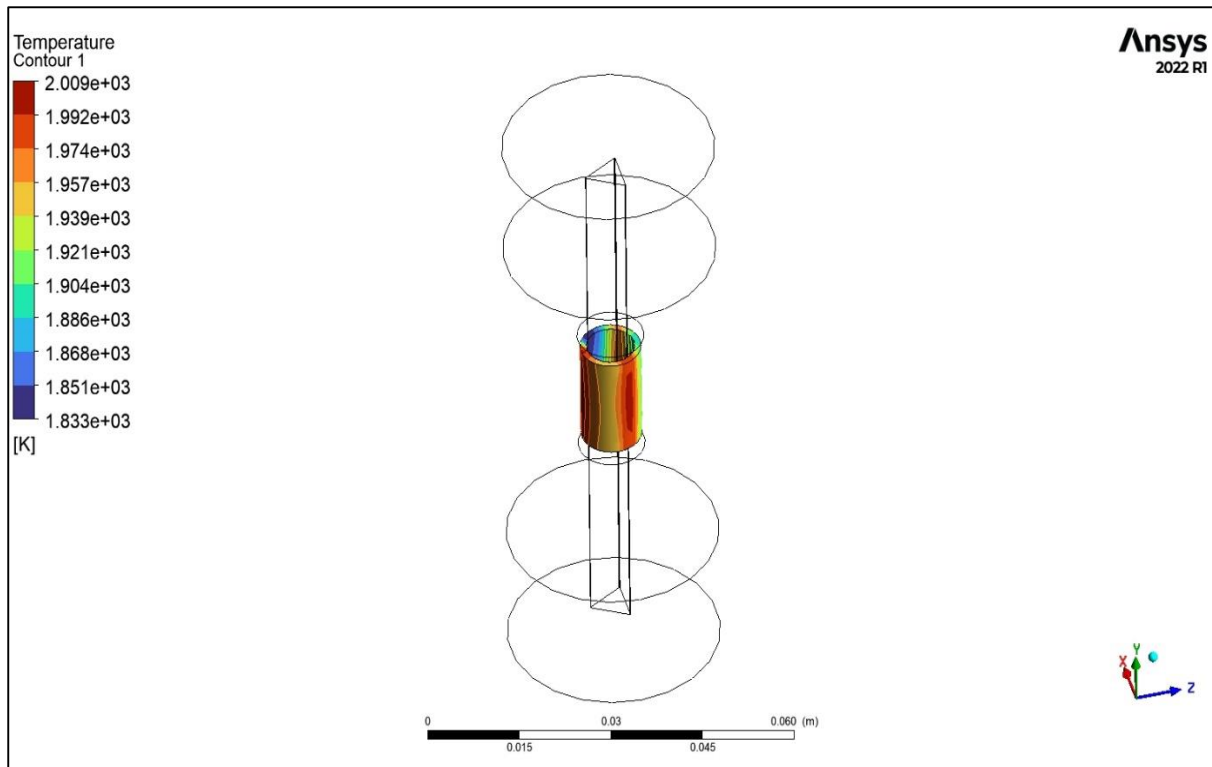


Figure 91 Temperature distribution over the workpiece by triangular shape CFG electrode at stationary condition

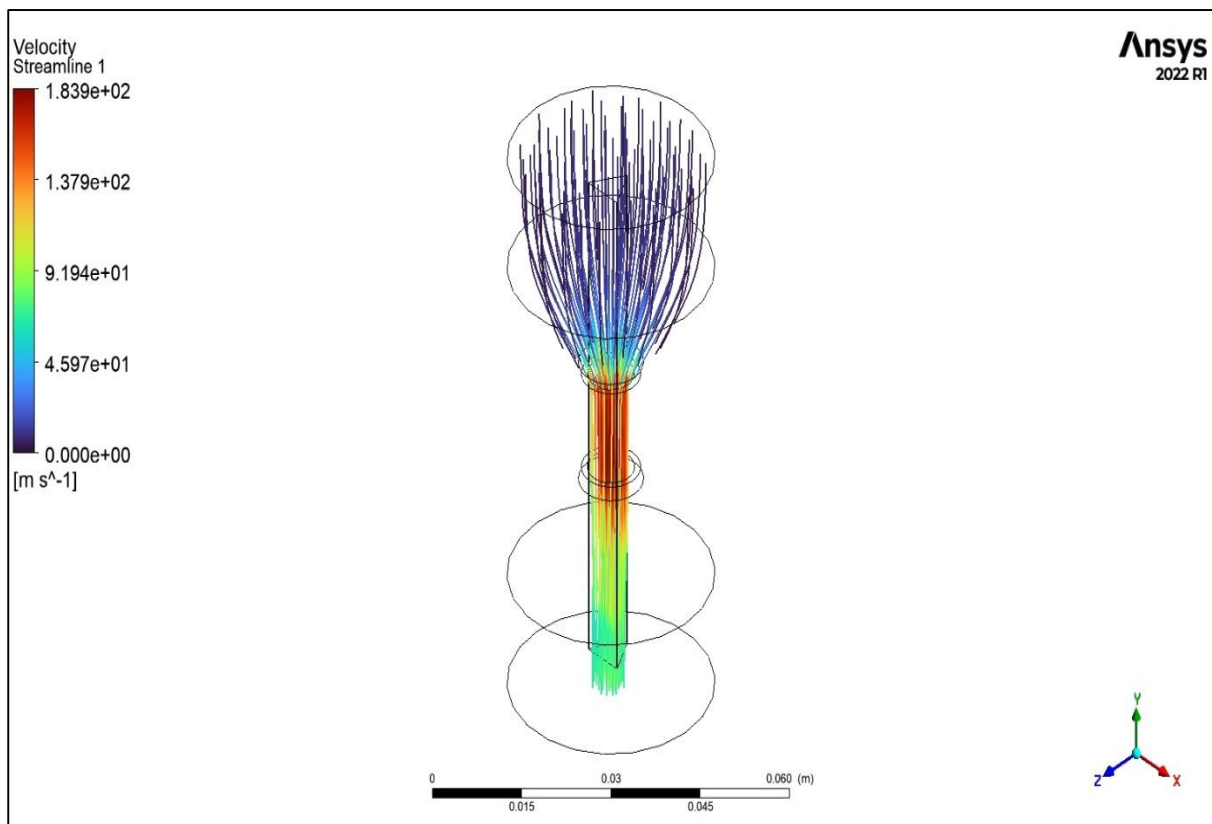


Figure 92 stream line pattern of the media flow in TACAFM Process by triangular shape CFG electrode at stationary condition

Figure 92 shows the streamline pattern of the flow of media during the TACAFM process with the triangular shape electrode at stationary condition. The stream line shows the smooth flow of media and conversion of media at the mouth of the workpiece resulting the material removal process from the internal surface of the workpiece.

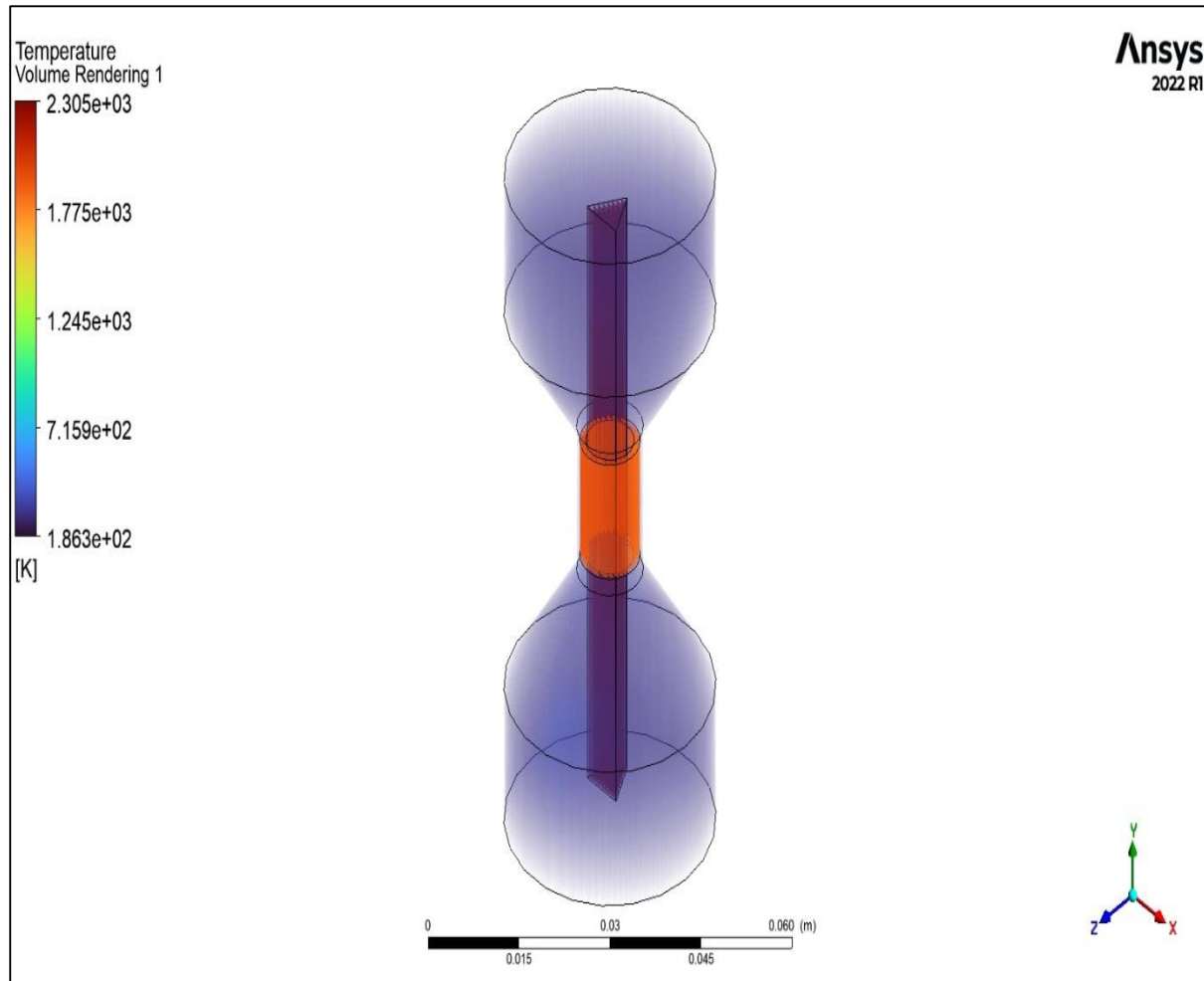


Figure 93 Temperature distribution inside the media during the TACAFM process at stationary condition of the CFG electrode.

Figure 93 shows the temperature distribution inside the media during the TACAFM process by the triangular electrode at the stationary condition. The figure shows that there is no temperature variation inside the media which is a desirable process as there is no viscosity variation due to variation in the temperature. This ceases the abrasive losing capacity of the media which does not decrease the material removal ability of the media. The workpiece is at higher temperature region which is again desirable as the temperature hike results in the softening of material which makes it easy for the abrasive to accelerate the abrasion process which increases the material removal of the TACAFM process.

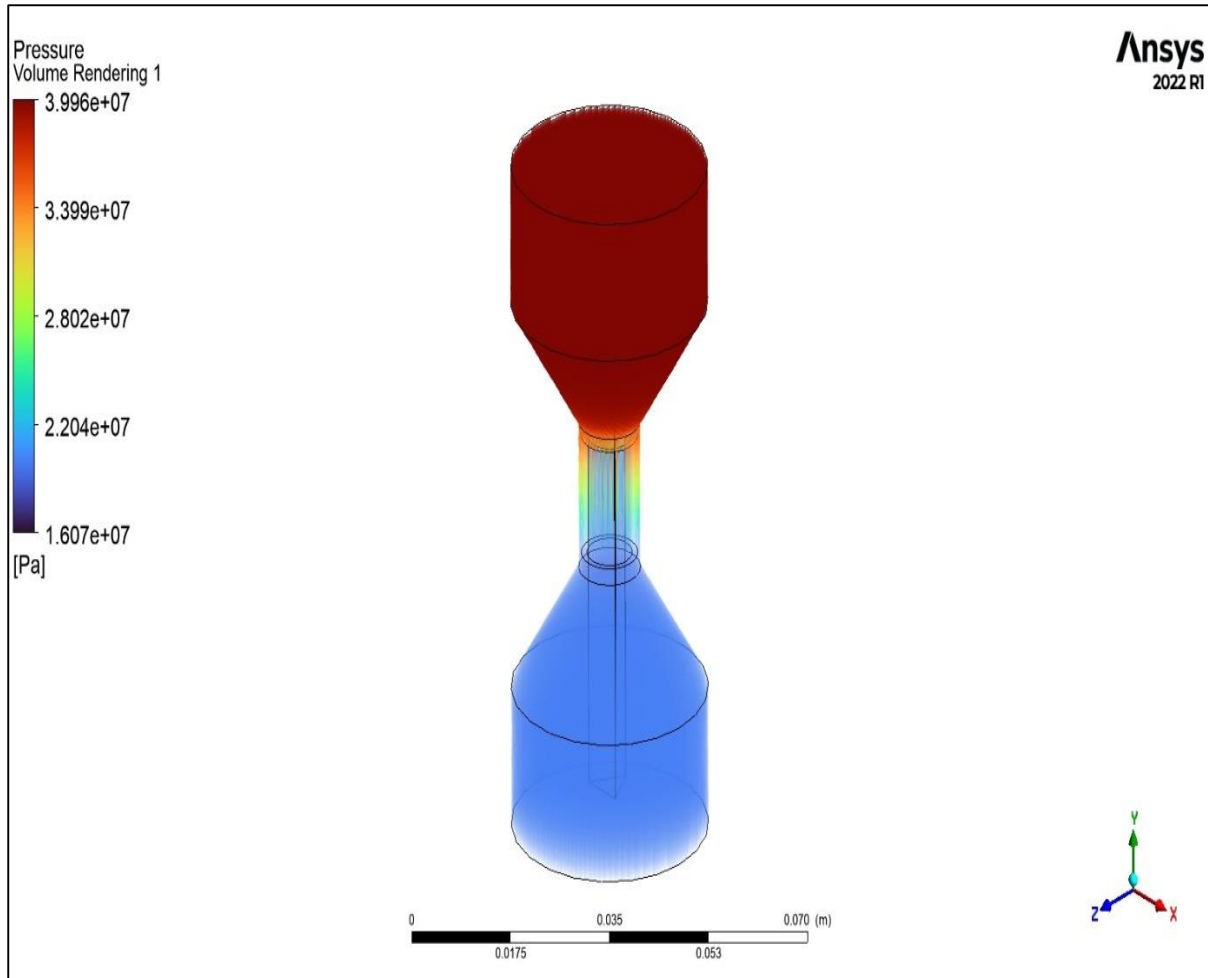


Figure 94 Pressure distribution inside the media during the TACAFM process at stationary condition of the CFG electrode.

Figure 94 shows the pressure distribution over the media during the TACAFM process with the triangular shape electrode. Here the pressure distribution is governed by the extrusion pressure which is clearly observed during the process with the extrusion pressure of 20 MPa. Thus the pressure trend shown by the media during the stationary condition of the triangular shape electrode shows the satisfactory results.

Figure 95 shows the conversion curve when the triangular shape CFG electrode is rotated at 100 rpm during the TACAFM process. The figure shows the trend of Continuity, X velocity, Y velocity and Z velocity and the energy equation line with the iterations and shows the smooth conversion up to 10^{-5} . The solution is run for the 100 iteration and the process show a stable simulation with energy line lie below the X, Y and Z velocity line and the continuity line.

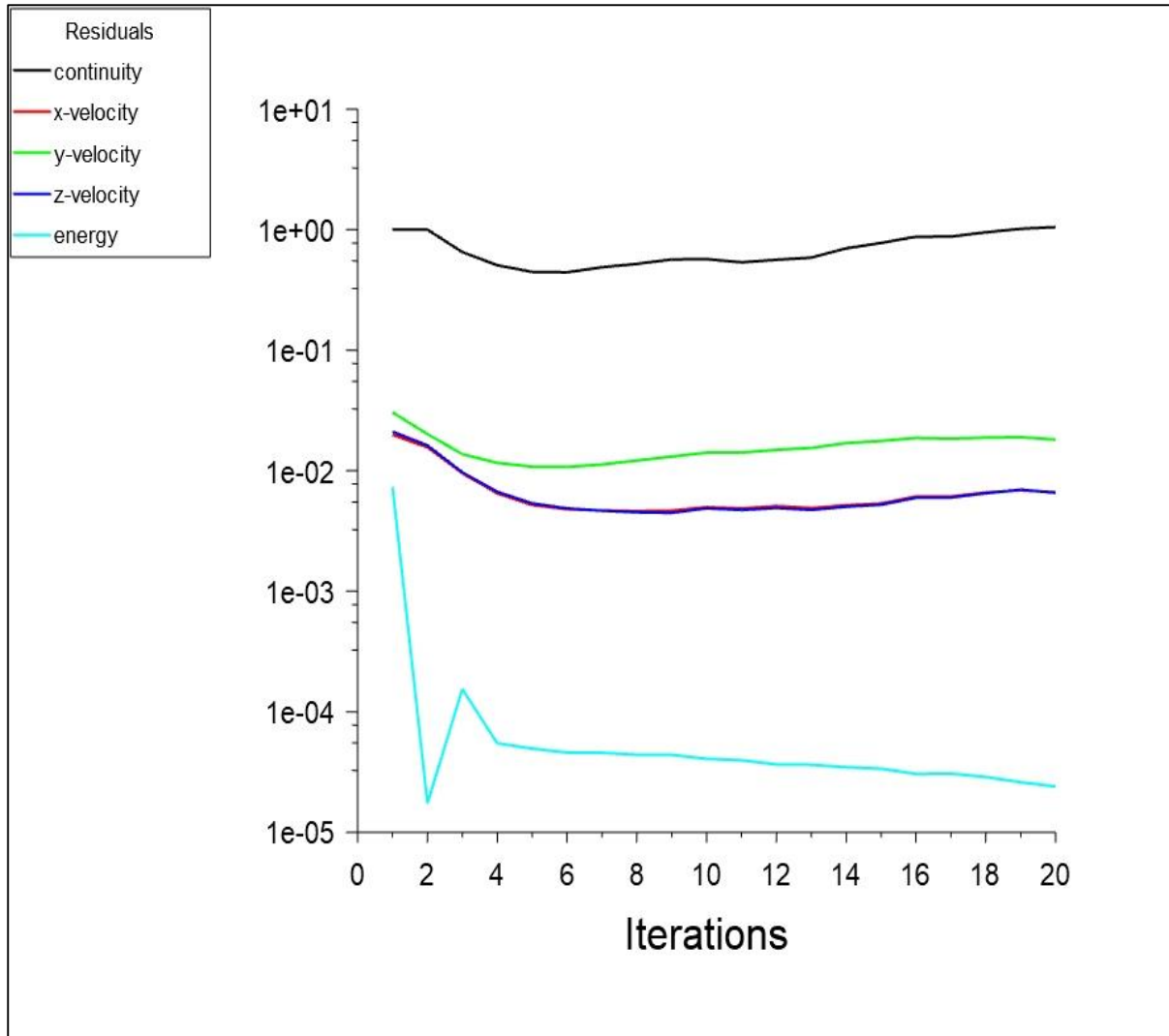


Figure 95 Conversion curve for triangular electrode at rotation of 100 rpm.

Figure 96 shows the pressure distribution over the workpiece when the rotating triangular shape electrode at 100 rpm is used in the TACAFM process. It can be observed that the maximum pressure over the workpiece is 39.98 MPa. The value is higher than that of the square shape CFG electrode and is comparable to the spline shape CFG electrode with the curved blade at 100 rpm rotation and at 20 MPa extrusion pressure. The distribution of pressure highlights the propose electrode is capable of the material removal in the TACAFM process. Figure 97 shows the temperature distribution over the workpiece during the TACAFM process using triangular shape centrifugal force generating electrode at 100 rpm rotation. The distribution is not uniformly distributed over the workpiece but the reason of higher temperature lies near the edges. The figure shows the maximum temperature of 2124 K which is sufficient for the material removal for the TACAFM process.

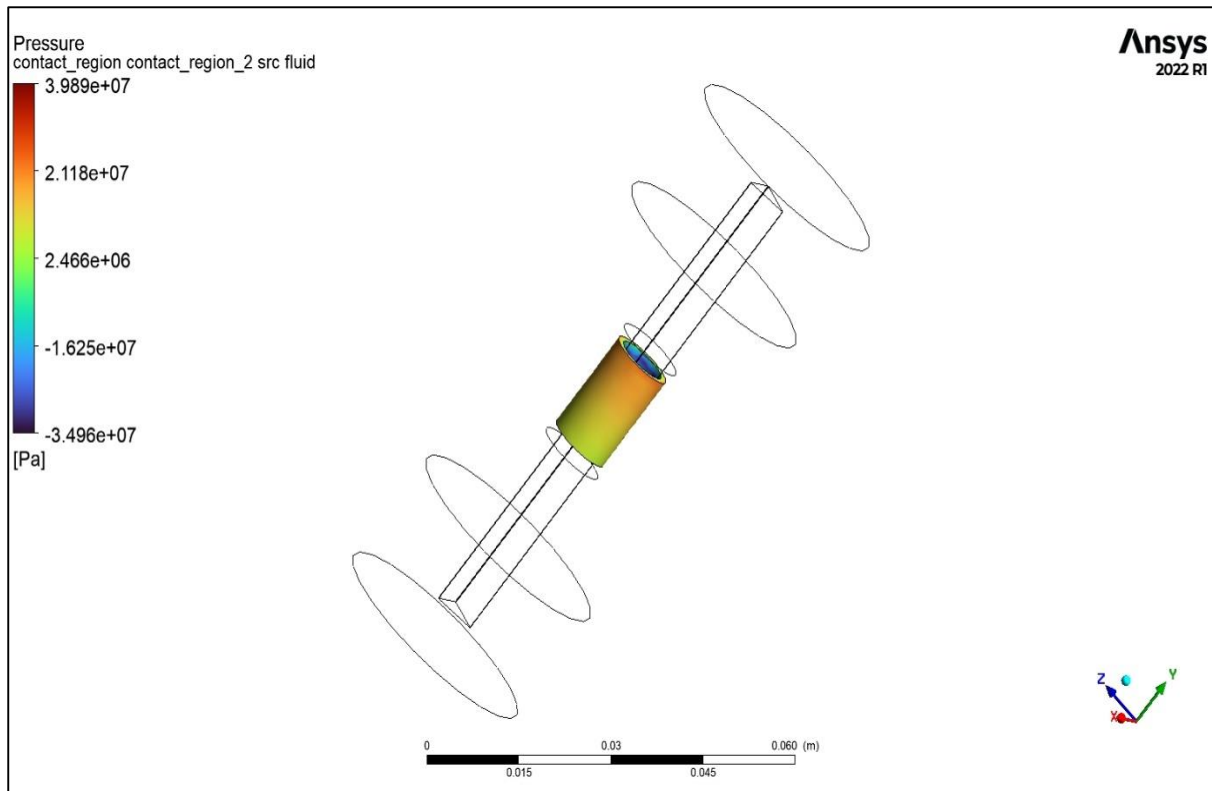


Figure 96 Pressure distribution over the workpiece at TACAFM process by the triangular shape CFG electrode at rotation of CFG electrode at 100 rpm

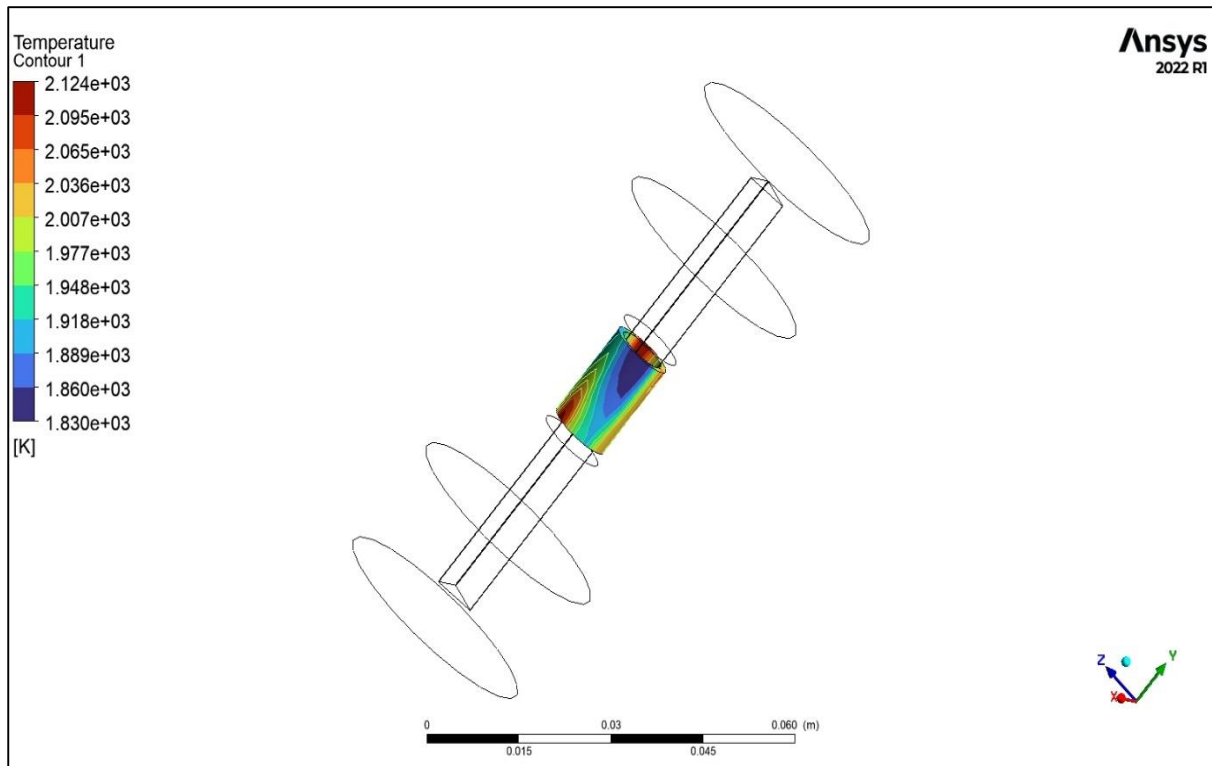


Figure 97 Temperature distribution over the workpiece by triangular shape CFG electrode at rotation of CFG electrode at 100 rpm

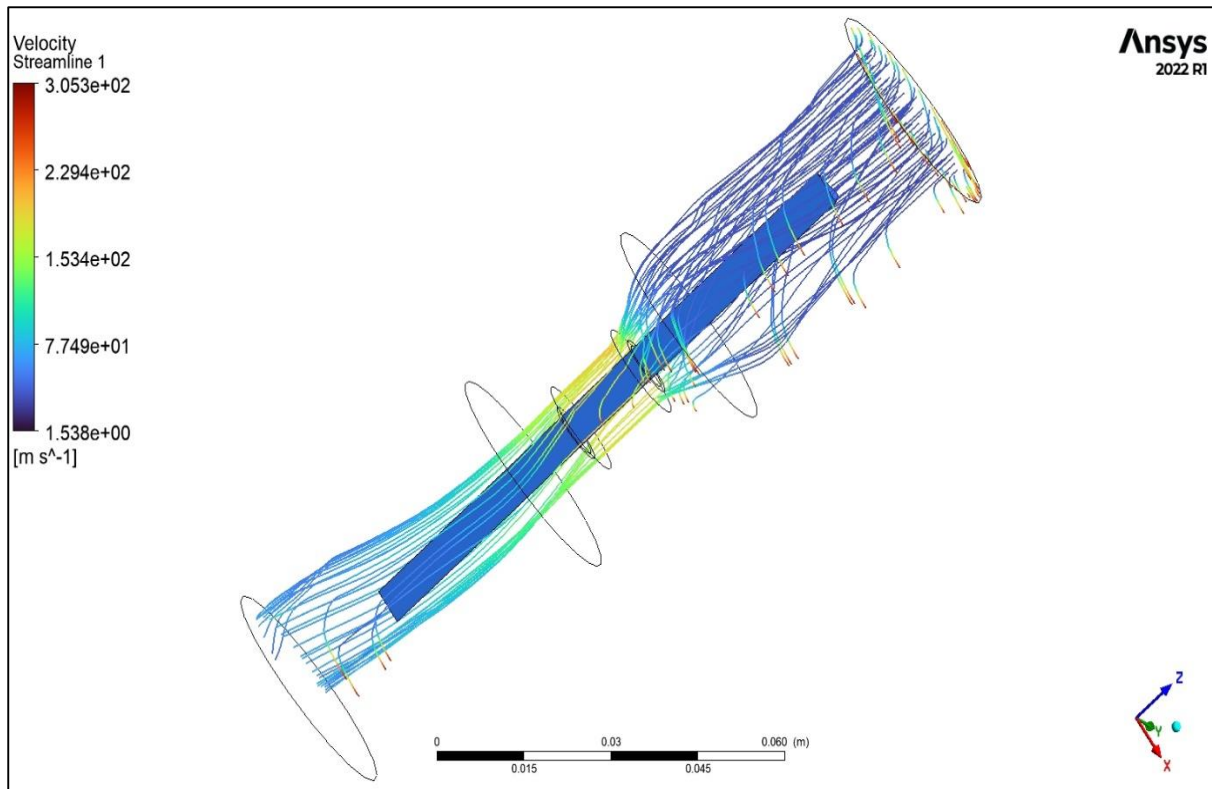


Figure 98 stream line pattern of the media flow in TACAFM Process by triangular shape CFG electrode at 100 rpm of the CFG electrode

Figure 98 shows the streamline distribution of media during TACAFM process by the triangular shape centrifugal force generating electrode with 100 rpm rotation. The figure shows that the rotation of the triangular shape electrode caused disturbance in the media pattern which results in the non-uniform throw of the media towards the wall of the workpiece. The abrasive throw ability of the triangular electrode towards the wall of the workpiece is not uniform because of the non-uniform edges of the triangular CFG electrode. This results in the uneven material removal from the wall of the workpiece which is not desirable as the rotation results in the uniform spark travel but in case of triangular electrode the uniformity of spark and media is not adequate. Figure 99 shows the pressure distribution inside the media during the TACAFM process when the rotating triangular shape electrode is used at 100 rpm. The Pressure distribution is similar in case of the media with the stationary electrode and the rotatory electrode with other shapes. Similarly, the figure 100 shows the temperature distribution over the media with 100 rpm rotation of the which shows that the temperature variation does not vary in the media which shows that the viscosity of the media remains unaffected with the temperature which is desirable for the TACAFM process as the abrasive holding capacity will not be affected in the media.

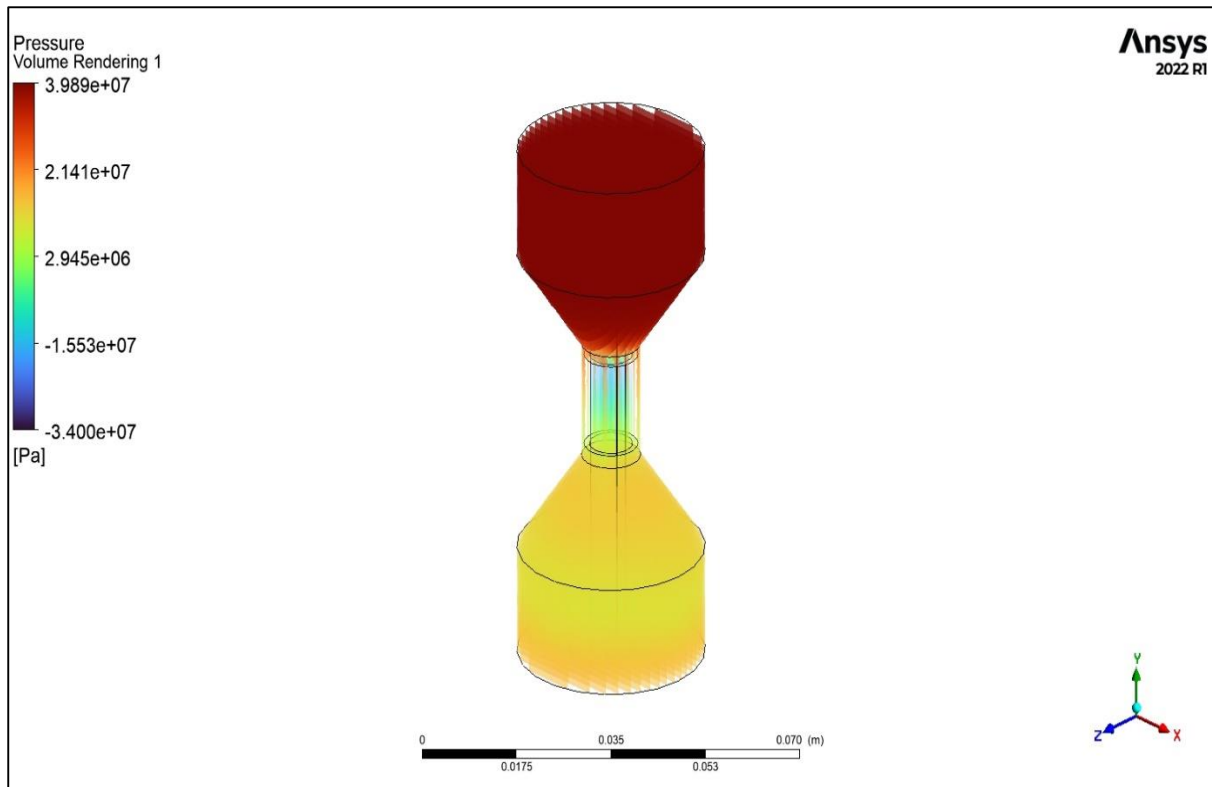


Figure 99 Pressure distribution inside the media during the TACAFM process at stationary condition of the CFG electrode.

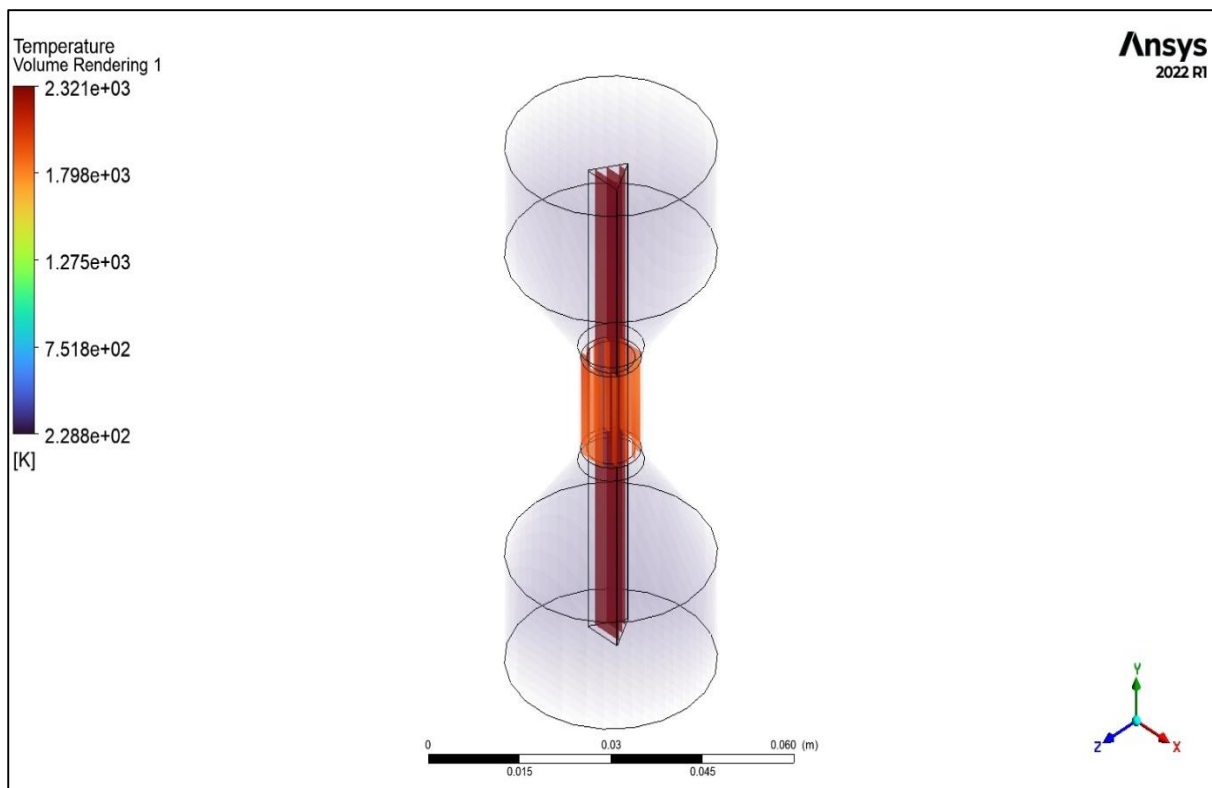


Figure 100 Temperature distribution inside the media during the TACAFM process at stationary condition of the CFG electrode.

Thus it can be concluded that the geometrical shape of the electrode improves the material removal process of the TACAFM process and can cater the limitation of the conventional AFM process. The analysis shows that the spline shape electrode with the curved blade shows an edge compared to other electrode in terms of material removal and the feasibility of the spark formation

Summary

- 1. Spline shape electrode with curved blade shows the improved performance compared to the other CFG electrode geometry in terms of material removal.**
- 2. The pressure distribution over the workpiece gives the idea of the material removal over the workpiece.**
- 3. The temperature distribution over the workpiece shows the feasibility of the spark for the TACAFM process.**
- 4. The streamline distribution shows the flow of media within the TACAFM process and highlights the increase in the number of dynamic number of active particles.**
- 5. The Pressure and temperature distribution over the media highlights the improvement in the TACAFM process.**

Chapter 6. Experimentation

The present chapter involves the experimentation to analyse the effect of the different electrode geometry on the material removal and on the surface finish of the workpiece during the TACAFM process. The experiments are designed on the basis DOE based on RSM Methodology. The chapter discussed RSM methodology and process parameters used in the TACAFM process. The Discussion about parameters affecting the material removal and percentage improvement in surface finish is also discussed in this chapter.

6.1. Background

The TACAFM process is the combination of spark EDM process along with the centrifugal force assisted abrasive flow machining process. The process aims to remove the limitation of low MR of the conventional AFM process. The present study involves the application of different shape of centrifugal force generating electrode to improve the process improvement of the TACAFM process. Three type of CFG electrode are used in the process which includes spline shape electrode with curved blade, spline shape electrode with the straight blade, and the square shape electrode is taken for the analysis. The DOE is prepared on the basis of CCD RSM methodology which is discussed in the later section of the chapter

6.2. Response Surface Methodology

A statistical technique called response surface approach is used to analyse the relationship between input independent elements and output responses in order to simplify complex systems. There are several different experiment design strategies used in the response surface methodology. The two that are most commonly utilized are Central Composite Design (CCD) and Box-Behnken Design (BBD). There is one primary distinction between the two: the quantity of levels for every input variable. Figure 101 shows the process of working of the RSM methodology which includes the selection of input variables and the response parameters which are to be analysed. Once the parameters are decided their levels are selected and experiments were designed on the DOE. The experimentation is done on the basis of DOE and the regression analysis and the analysis of variance is done for each response parameter. The result of ANNOVA and the regression were studied and if they are satisfactory, then the optimal parameters are computed and then the confirmation test are done to analyse the error. The experiments were performed to analyse the effect of proposed electrode on the geometry of the working of TACAFM process. The RSM with CCD is used with type of electrode, supply current, duty cycle and rotational speed of electrode as the process parameter and their effect on the material removal (MR) and percentage improvement in surface finish ($\% \Delta R_a$) is studied.

The reason for choosing RSM is that as it readily gives the interactions between the parameters which provides major aid in analysing there effect on the process.

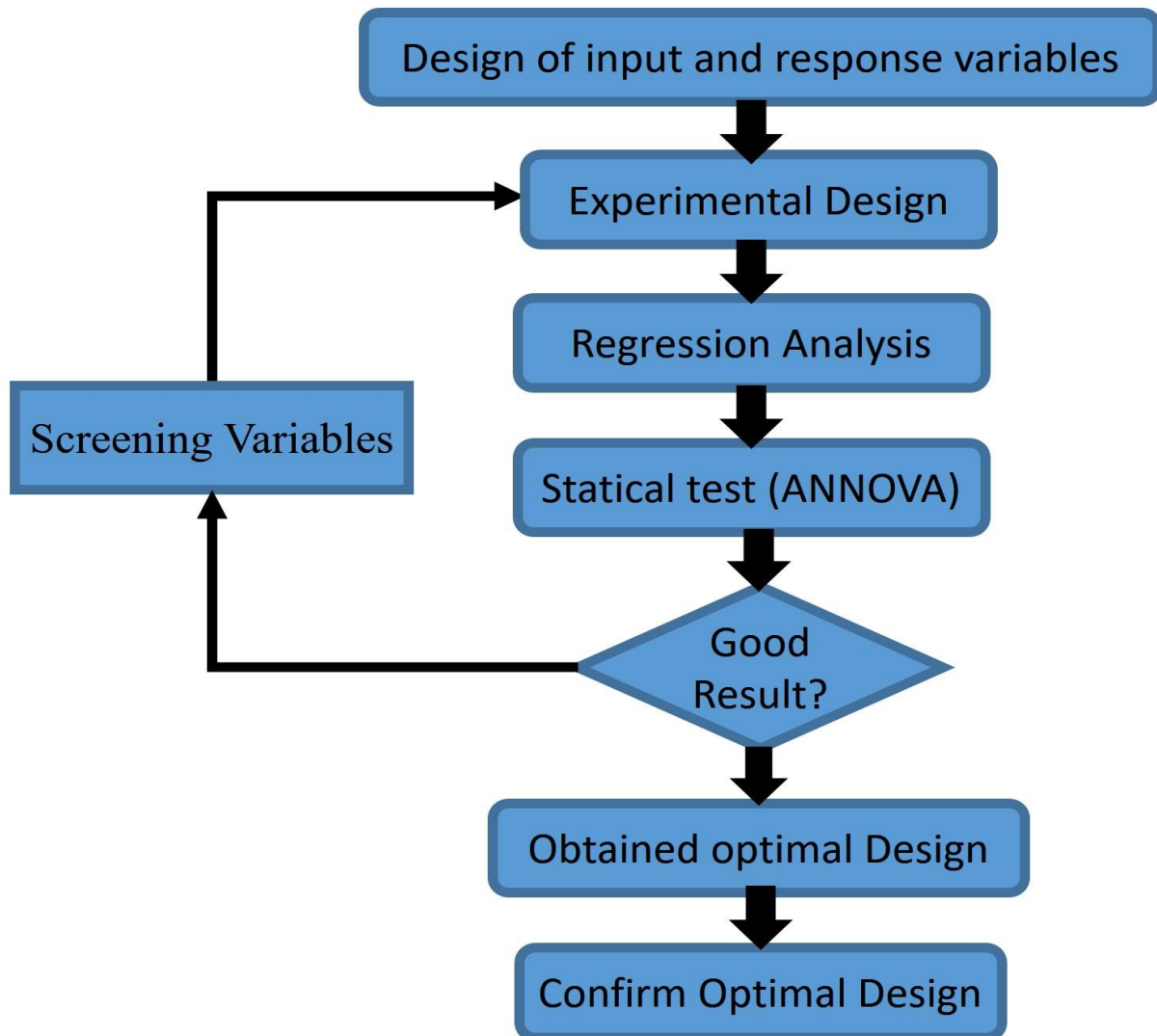


Figure 101 Response surface Methodology flow chart

Table 11 shows the 4 factors which are consider for the analysis of the TACAFM process. The various factors which are consider for the analysis are type of electrode, current, duty cycle and the rotational speed. The electrode used were taken for 3 level which are electrode 1 is spline shape electrode with straight blade, level 2 is spline shape electrode with the curved blade and the third type of electrode is the square shape electrode. The next factor consider into the analysis is the supply current whose values are consider as 4 Ampere, 10 Ampere and the 16 Ampere. The next step is the duty cycle whose values are 0.68, 0.72 and 0.76. The rotational speed is the next factor which includes CFG rotation at 100, 120 and 140 rpm.

Table 11 Factor levels of CCD

Factors	Coded Level		
	-1	0	1
Type of Electrodes	1	2	3
Current (A)	4	10	16
Duty Cycle	0.68	0.72	0.76
Rotational speed (rpm)	100	120	140
<ul style="list-style-type: none"> • Electrode 1 –Spline shape electrode with straight blade • Electrode 2 –Spline shape electrode with curved blade • Electrode 3 –Square shape electrode 			

Table 12 shows the information about the model analysis and the computation mechanism of the RSM. For the analysis the response surface computation with the central composite design. The analysis is based on the quadratic model with total of 30 runs. Table 13 shows the analysis of the response obtained in RSM CCD process. Table 14 shows the scheme and result of CCD.

Table 12 Model Analysis

File Version	13.0.5.0		
Study Type	Response Surface	Subtype	Randomized
Design Type	Central Composite	Runs	30.00
Design Model	Quadratic	Blocks	No Blocks
Build Time (ms)	3.00		

Table 13 Analysis of Response in RSM CCD methodology

Response	Name	Units	Observations	Minimum	Maximum	Mean	Std. Dev	Ratio
R1	Material Removal	mg	30.00	48.14	51.67	50.32	1.13	1.07
R2	Percentage Improvement in Surface Finish	%	30.00	39.38	44.32	42.10	1.08	1.13

Table 14 Scheme and results of Central Composite Design

		Factor 1	Factor 2	Factor 3	Factor 4	Response 1	Response 2
Std	Run	A: Electrode	B:Supply Current	C:Duty Cycle	D:Rotational Speed	Material Removal	Percentage Improvement in Surface Finish
		Ampere		-	rpm	mg	%
14	1	3	4	0.76	140	48.91	41.32
24	2	2	10	0.72	120	51.39	42.78
6	3	3	4	0.76	100	48.62	39.38
5	4	1	4	0.76	100	49.91	40.27
8	5	3	16	0.76	100	49.14	40.78
13	6	1	4	0.76	140	50.37	42.73
30	7	2	10	0.72	120	51.3	42.69
28	8	2	10	0.72	120	51.32	42.73
7	9	1	16	0.76	100	50.42	41.1
23	10	2	10	0.72	80	51.02	42.79
1	11	1	4	0.68	100	49.14	42.55
27	12	2	10	0.72	120	51.34	42.75
21	13	2	10	0.64	120	51.67	41.13
4	14	3	16	0.68	100	49.01	42.71
3	15	1	16	0.68	100	50.13	42.97
29	16	2	10	0.72	120	51.35	42.74
17	17	3	10	0.72	120	49.07	41.8
9	18	1	4	0.68	140	49.4	44.32
19	19	2	16	0.72	120	51.38	42.8
26	20	2	10	0.72	120	51.38	42.77
20	21	2	16	0.72	120	51.45	42.7
10	22	3	4	0.68	140	48.26	43.07
12	23	3	16	0.68	140	49.56	41.09
16	24	3	16	0.76	140	49.72	40.13
18	25	2	10	0.72	120	51.39	42.67
15	26	1	16	0.76	140	51.27	40.97
2	27	3	4	0.68	100	48.14	41.83
22	28	2	10	0.68	120	51.29	42.71
11	29	1	16	0.68	140	50.81	41.85
25	30	2	10	0.72	120	51.34	42.75
Total						1509.5	1262.88
Average						50.31667	42.096

6.3. Effect of Process parameters on Material Removal

The analysis on the material removal is done on the basis of the value obtained in table 14. For the material removal the quadratic model is suggested by the RSM and thus computation was done on that criterion. Table 15 shows the analysis of variance data corresponding to the material removal for the TACAFM process, which shows that the model is significant with p value less than 0.05 and the lack of fit is non-significant having p value 0.6455 which is a desirable situation. The parameters are denoted by A, B, C and D denotes the electrode, supply current, duty cycle and the rotational speed. The terms AB, AC, AD, BC, BD, CD, A², B², C² and D² represents the interaction among the parameters. This is the advantage of the RSM methodology that the contribution due to the interaction of parameters is also highlighted which is not possible in other optimization technique like Taguchi and ANN. The table shows the percentage contribution also which highlights that the type of electrode is the major contributing factors in the evaluation with the percentage contribution of 17.71 percent followed by the supply current which is about 9.23 percent, the contribution of duty cycle is 2.63 percent and that of the rotational speed is 2.43 percent. For the material removal the analysis shows the standard deviation of 0.0334 with the mean value of 50.32. The coefficient of variation (C.V %) for the data is 0.064. The value of coefficient of determination (R²) for the data is 0.9996 while the adjusted value of the coefficient of determination (adjusted R²) is 0.9991. The value of predicted coefficient of determination is 0.9979 and the value of the adequate value of precision for the model is 149.79 which is consider as the adequate value. The second order polynomial equation was used to analyse the relation between the process parameters and the response which is given by equation

Material Removal = +103.38431 +7.45831 Electrode +0.546839 Supply Current -172.67484 Duty Cycle -0.045494 Rotational Speed -0.003229 Electrode * Supply Current -1.67187 Electrode * Duty Cycle -0.002219 Electrode * Rotational Speed -0.476562 Supply Current * Duty Cycle +0.000797 Supply Current * Rotational Speed +0.044531 Duty Cycle * Rotational Speed -1.64669 Electrode² -0.010838 Supply Current²+126.08610 Duty Cycle² +0.000091 Rotational Speed².

Figure 102 shows the plot of the predicted and experimental value on the regression curve. The figure shows a little deviation from the actual value which validates the experimentation. Figure 103 shows the perturbation curve which highlights the individual effect of parameters on the material removal.

Table 15 ANOVA for Quadratic model for MR

Source	Sum of Squares	df	Mean Square	F-value	p-value	Significance	% Contributions
Model	37.23	14	2.66	2384.10	< 0.0001	significant	99.95
A-Electrode	6.56	1	6.56	5879.82	< 0.0001		17.61
B-Supply Current	3.44	1	3.44	3083.33	< 0.0001		9.23
C-Duty Cycle	0.9794	1	0.9794	877.94	< 0.0001		2.63
D-Rotational Speed	0.9049	1	0.9049	811.18	< 0.0001		2.43
AB	0.0060	1	0.0060	5.38	0.0348		0.02
AC	0.0716	1	0.0716	64.15	< 0.0001		0.19
AD	0.0315	1	0.0315	28.24	< 0.0001		0.08
BC	0.2093	1	0.2093	187.63	< 0.0001		0.56
BD	0.1463	1	0.1463	131.16	< 0.0001		0.39
CD	0.0203	1	0.0203	18.20	0.0007		0.05
A ²	6.01	1	6.01	5390.93	< 0.0001		16.13
B ²	0.3628	1	0.3628	325.23	< 0.0001		0.97
C ²	0.5228	1	0.5228	468.63	< 0.0001		1.40
D ²	0.0168	1	0.0168	15.04	0.0015		0.05
Residual	0.0167	15	0.0011				0.04
Lack of Fit	0.0066	7	0.0009	0.7435	0.6455	not significant	0.02
Pure Error	0.0101	8	0.0013				0.03
Cor Total	37.25	29					100.00

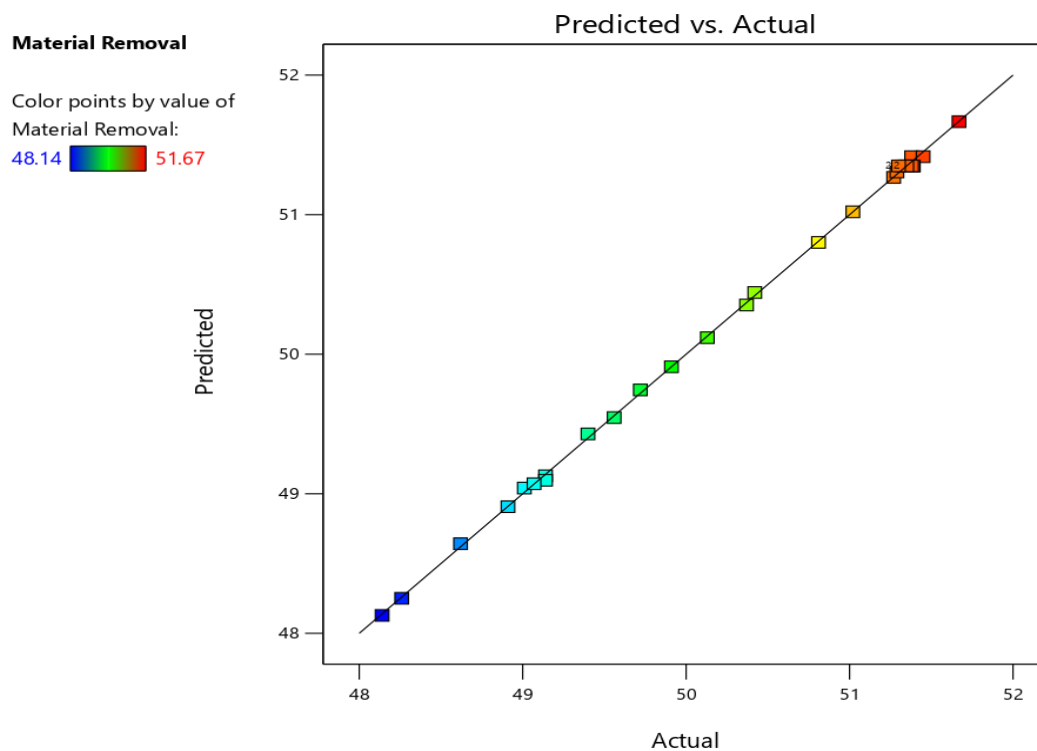


Figure 102 Actual Vs Predicted Value for MR

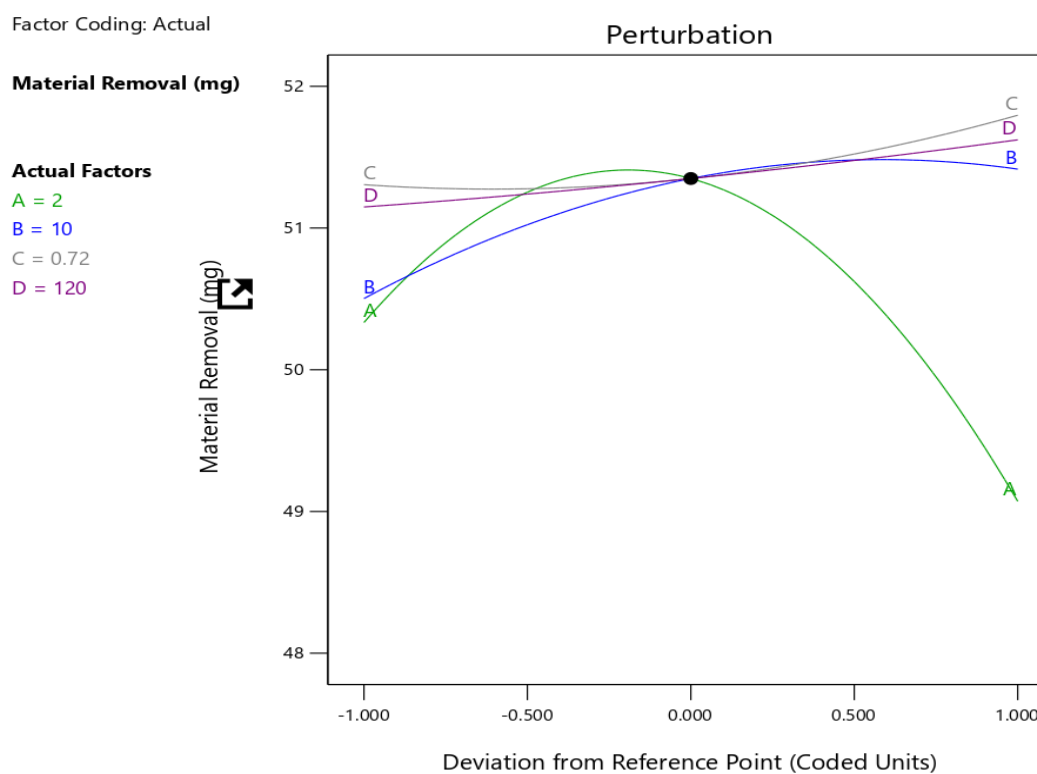


Figure 103 Perturbation curve for MR

Factor Coding: Actual

Material Removal (mg)

● Design Points

--- 95% CI Bands

X1 = A

Actual Factors

B = 10

C = 0.72

D = 120

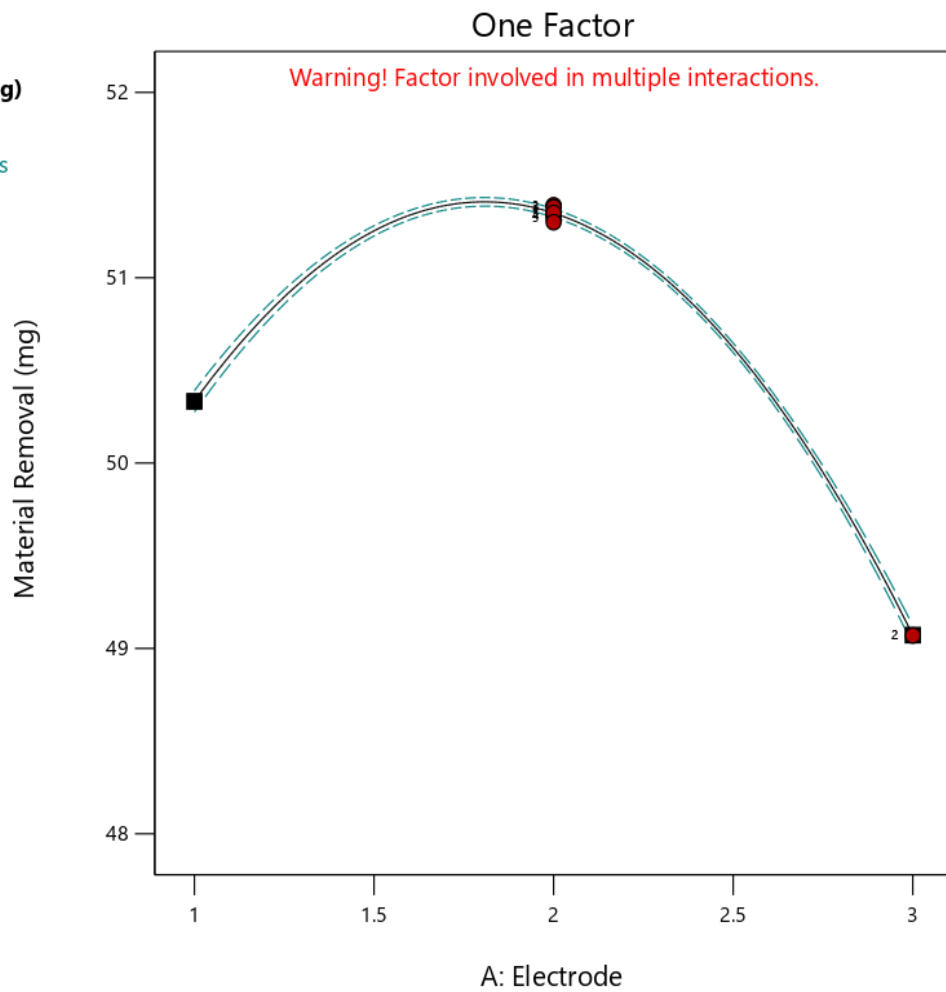


Figure 104 Effect of shape of electrode on material removal

It is observed from the analysis that the process parameters (type of electrode, supply current duty cycle, rotational speed) plays a vital role in the MR prediction. Figure 103 shows the effect of process parameters on the MR. Figure 104 shows the relation between MR and the types of electrode which shows the increasing values with the spline shape electrode and the decreasing value of the square electrode. The reason behind this is that the spline shape electrode provides path for the media flow which is not there in case of the square shape electrode (Walia et al 2006). The spline electrode with the curved blade provides the more centrifugal force in the media which directs the abrasive particles towards the wall of the workpiece which results in the increase in the MR for electrode 2 (Ali et al. 2020).

Factor Coding: Actual

Material Removal (mg)

● Design Points

--- 95% CI Bands

X1 = B

Actual Factors

A = 2

C = 0.72

D = 120

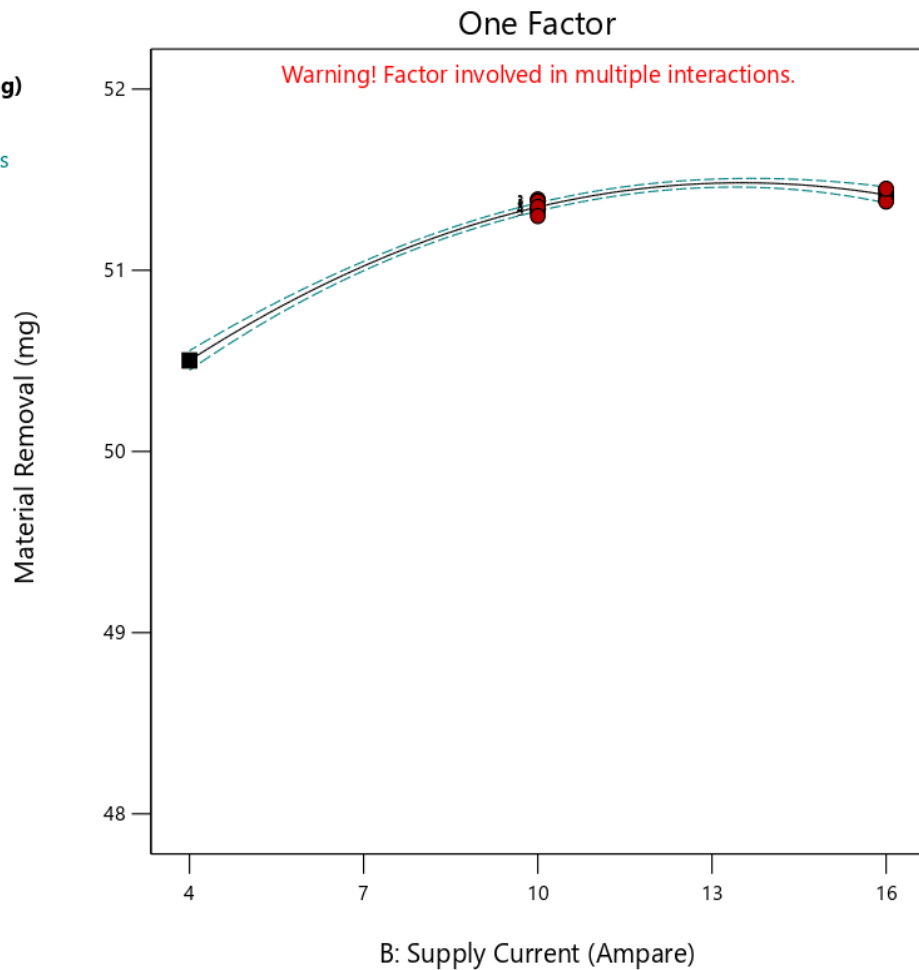


Figure 105 Effect of Supply current on the material removal

Figure 105 shows the variation of MR with current, the curve shows an increasing trend because as the current increase the ionization of media particle will be more as a result there will be formation of plasma and spark inside the media, which accelerates the MR mechanism (Ali et al 2020).

Figure 106 shows the increasing trends of the material removal with the duty cycle, the reason for this is that the duty cycle directly affects the spark formation. As the duty cycle increases, the spark time would increase which results in the enhancement of melting and erosion mechanism near the wall of the workpiece (Ali et al 2020).

Figure 107 shows MR Vs the rotational speed. With the increase in the rotational speed the dynamic number of abrasive particle increases near the wall of the workpiece resulting in the increase in the centrifugal force which enhances the abrasion mechanism of the abrasive near the wall of workpiece which enhances MR (Walia et al 2006).

Factor Coding: Actual

Material Removal (mg)

● Design Points

--- 95% CI Bands

X1 = C

Actual Factors

A = 2

B = 10

D = 120

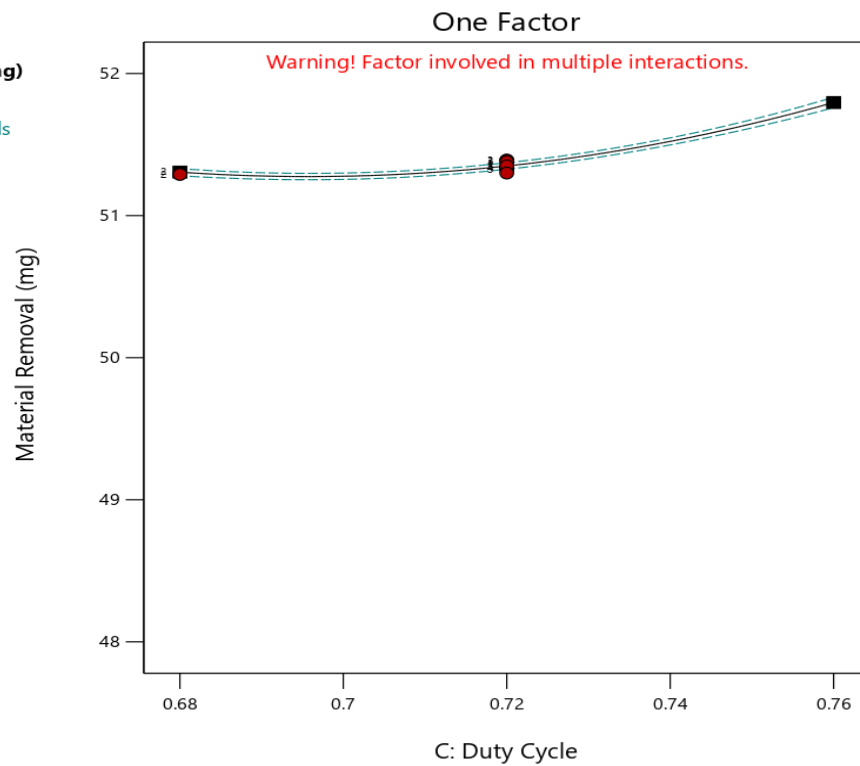


Figure 106 Effect of Duty Cycle on material removal

Factor Coding: Actual

Material Removal (mg)

● Design Points

--- 95% CI Bands

X1 = D

Actual Factors

A = 2

B = 10

C = 0.72

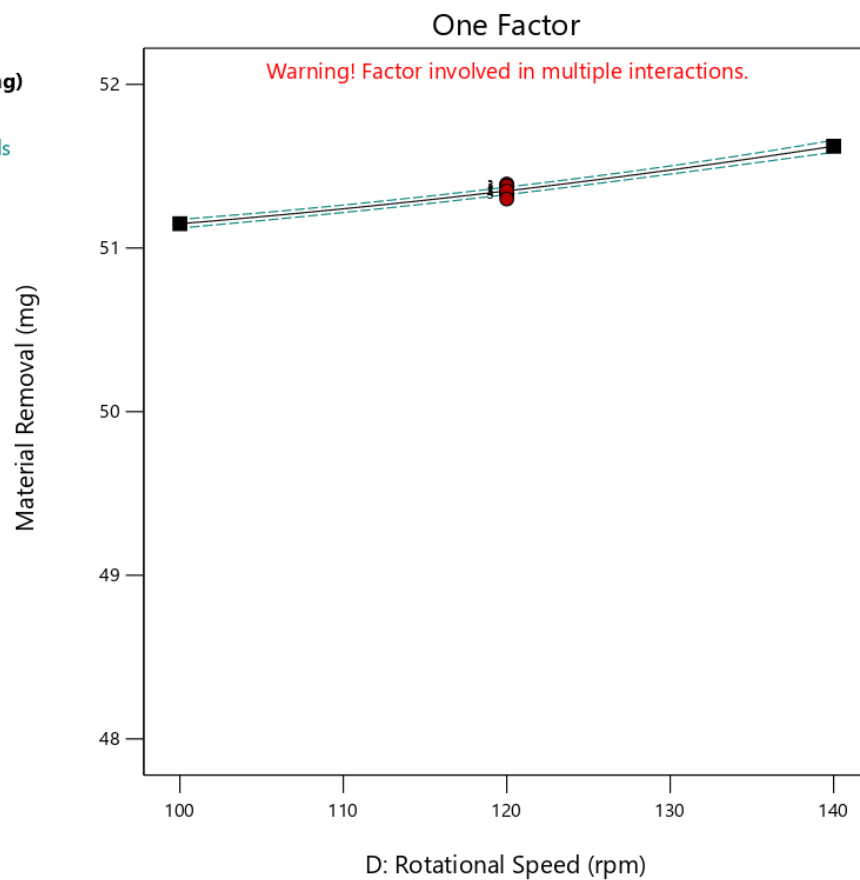


Figure 107 Effect of rotational speed on material removal

Factor Coding: Actual

3D Surface

Material Removal (mg)

Design Points:

● Above Surface

○ Below Surface

48.14 51.67

X1 = A

X2 = B

Actual Factors

C = 0.72

D = 120

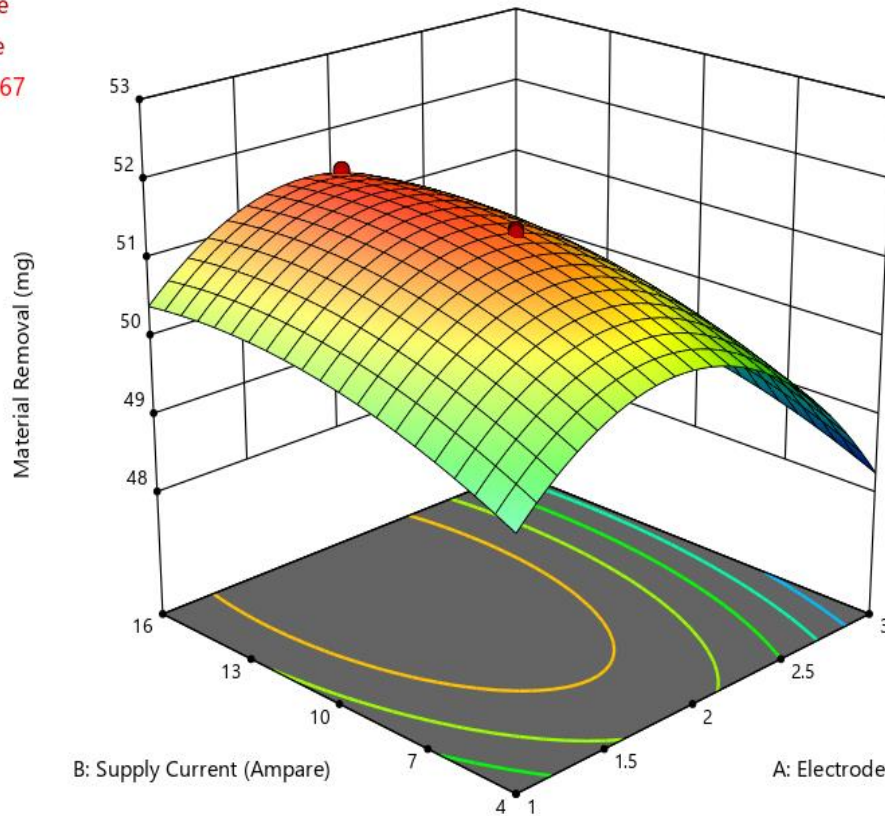


Figure 108 Effect of supply current and electrode type on material removal

Figure 108 onwards shows the 3D surface graph of MR. Figure 108 shows the effect of electrode and supply current on MR. The graph shows that the combination results in an overall increase in the value because of the effect of spline shape electrode and EDM effect of the supply current (Ali et al 2020). Figure 109 shows the combined effect of supply current and duty cycle on the MR. the graph shows an overall increase in the value of the MR. This is because the two parameter are responsible for the spark generation, Once the spark is generated the material removal take place through melting and erosion process (Patil et al 2023).

Factor Coding: Actual


3D Surface

Material Removal (mg)

Design Points:

● Above Surface

○ Below Surface

48.14  51.67

X1 = A

X2 = C

Actual Factors

B = 10

D = 120

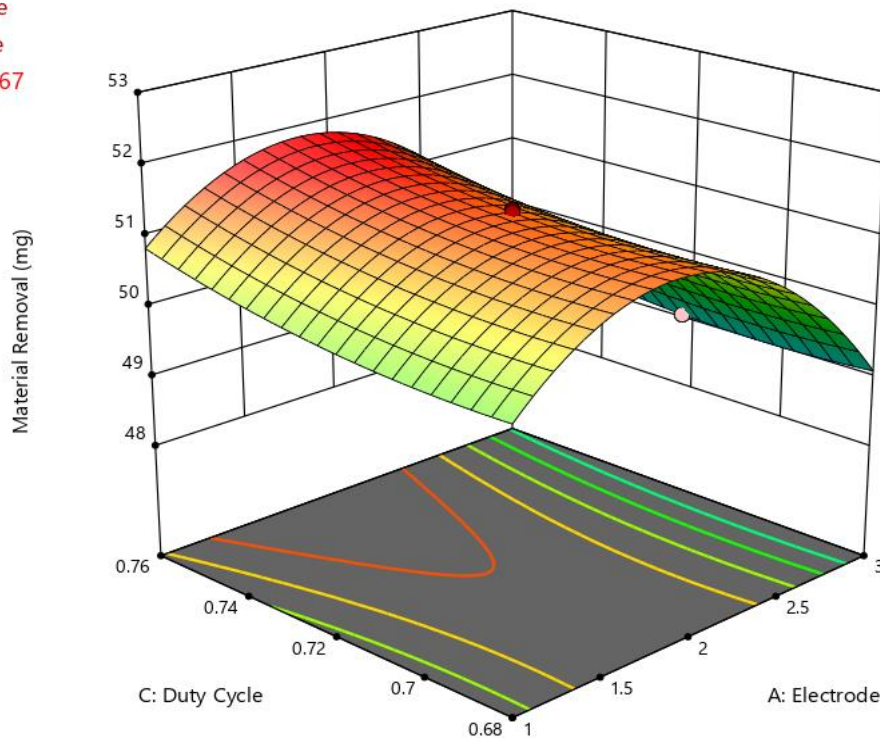


Figure 109 Effect of Duty cycle and electrode on material removal

Figure 110 shows the combine effect of rotational speed and the supply current on material removal. The graph shows an overall increase in the MR due to the combination because both factor individually results in an increase in MR which shows their influence in the combined effect also (Ali et al 2020, Shankar et al. 2010).

Figure 111 shows the effect of duty cycle and rotational speed on the MR. It is evident from the graph that overall value of MR increases. The increase in duty cycle results in the arc stabilization as the application of current increases which results in arc generation, accelerating the MR by melting and erosion process. Also with the increase in rotational speed, the centrifugal force on the media increases resulting in the increase in the abrasion process and material removal process

Factor Coding: Actual

3D Surface

Material Removal (mg)

Design Points:

● Above Surface

○ Below Surface

48.14 51.67

X1 = A

X2 = D

Actual Factors

B = 10

C = 0.72

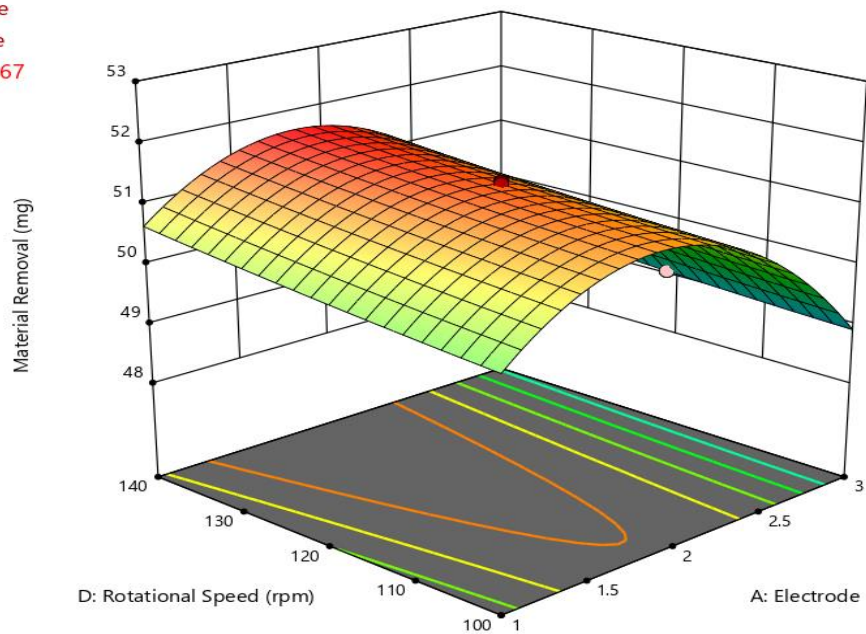


Figure 110 Effect of rotational speed and electrode on material removal

Factor Coding: Actual

3D Surface

Material Removal (mg)

Design Points:

● Above Surface

○ Below Surface

48.14 51.67

X1 = B

X2 = C

Actual Factors

A = 2

D = 120

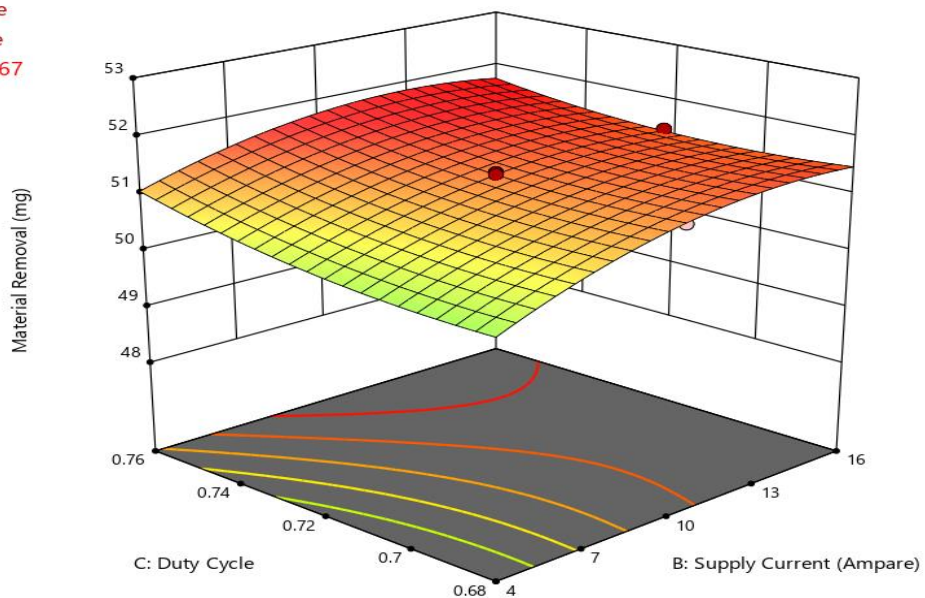


Figure 111 Effect of duty cycle and supply current on material removal

Factor Coding: Actual

3D Surface

Material Removal (mg)

Design Points:

● Above Surface

○ Below Surface

48.14  51.67

X1 = B

X2 = D

Actual Factors

A = 2

C = 0.72

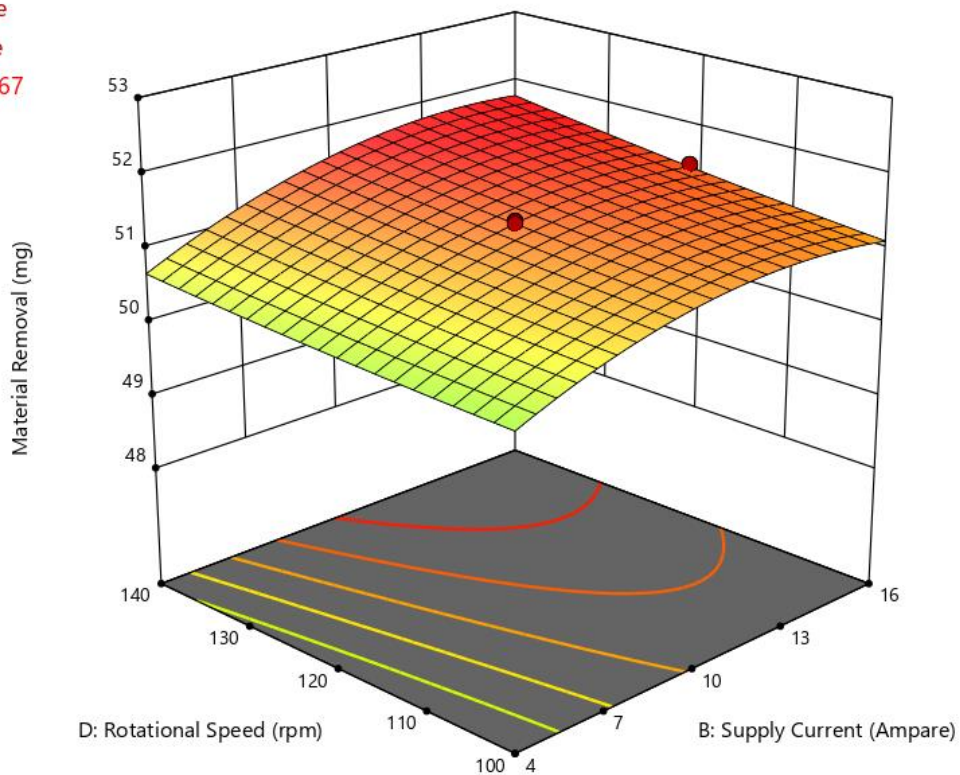


Figure 112 Effect of Rotational speed and supply current on Material removal

Figure 112 shows the graph of combined effect of electrode and duty cycle. It is evident that the value of MR increases with the increase in the duty-cycle but the individual electrode shows its effect (Ali et al 2020). The MR value increases with the spline shape electrode compare to the square shape electrode and the value of MR is maximum with the spline shape electrode with the curved blade as it increases the centrifugal force on the abrasive particle (Ali et al 2020, walia et al 2006).

Figure 113 shows the combined effect of electrode and the duty cycle. The figure shows an increase in the MR with the spline shape electrode with curved blade due to its centrifugal action along with the EDM effect produced by duty cycle. Thus the material removal takes place with the combination of melting and abrasion process (Ali et al 2020).

Factor Coding: Actual

3D Surface

Material Removal (mg)

Design Points:

● Above Surface

○ Below Surface

48.14  51.67

X1 = C

X2 = D

Actual Factors

A = 2

B = 10

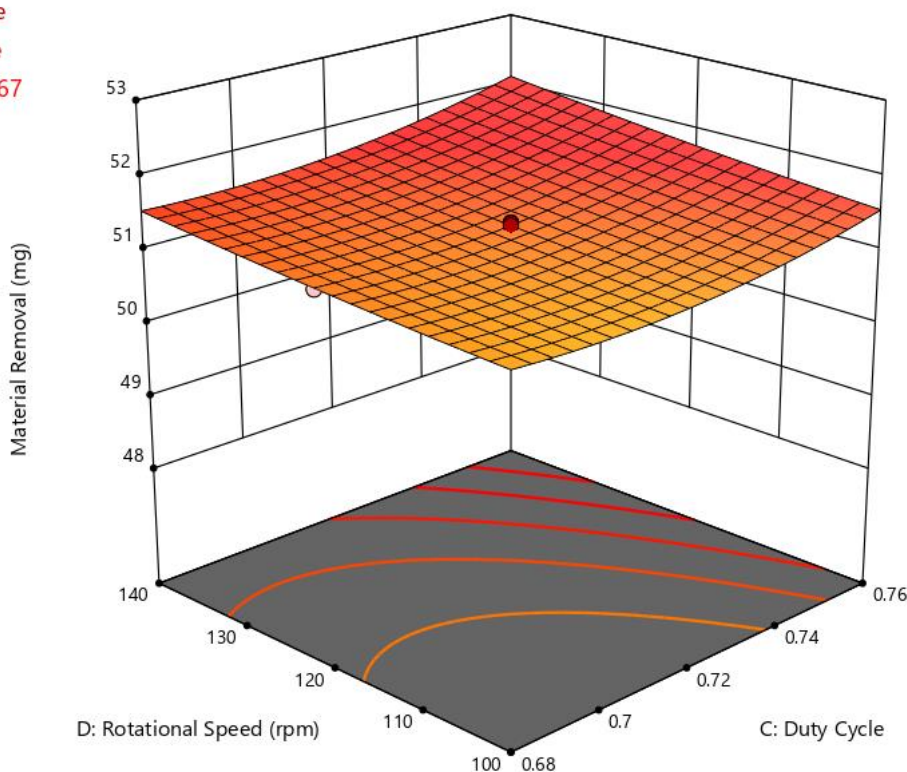


Figure 113 effect of rotational speed and duty cycle on material removal

6.4. Effect of Process Parameters on percentage improvement in Surface finish

It is observed from the analysis that the process parameters (type of electrode, supply current duty cycle, rotational speed) plays a vital role in the percentage improvement in surface finish ($\% \Delta R_a$). The analysis of the percentage improvement in surface finish is done on the basis of the value obtained in table 16. For the percentage improvement in surface finish the quadratic model is suggested by the RSM and thus computation was done on that criterion. Table 6 shows the analysis of variance data corresponding to the material removal for the TACAFM process, which shows that the model is significant with p value less than 0.05 and the lack of fit is non-significant having p value 0.1559 which is a desirable situation. The parameters are denoted by A, B, C and D denotes the electrode, supply current, duty cycle and the rotational speed. The terms AB, AC, AD, BC, BD, CD, A^2 , B^2 , C^2 and D^2 represents the interaction among the parameters. The analysis shows that the given model is based on the quadratic model.

Table 16 ANNOVA table for the percentage improvement in surface finish

Source	Sum of Squares	df	Mean Square	F-value	p-value	Significant	% contribution
Model	33.93	14	2.42	846.89	< 0.0001	significant	99.88
A-Electrode	2.65	1	2.65	925.55	< 0.0001		7.80
B-Supply Current	0.9462	1	0.9462	330.65	< 0.0001		2.79
C-Duty Cycle	11.98	1	11.98	4184.53	< 0.0001		35.27
D-Rotational Speed	0.9438	1	0.9438	329.79	< 0.0001		2.78
AB	0.2730	1	0.2730	95.40	< 0.0001		0.80
AC	0.0138	1	0.0138	4.82	0.0442		0.04
AD	0.2678	1	0.2678	93.58	< 0.0001		0.79
BC	0.3691	1	0.3691	128.96	< 0.0001		1.09
BD	7.47	1	7.47	2609.05	< 0.0001		21.99
CD	0.7014	1	0.7014	245.09	< 0.0001		2.06
A ²	0.7291	1	0.7291	254.78	< 0.0001		2.15
B ²	0.1303	1	0.1303	45.52	< 0.0001		0.38
C ²	8.96	1	8.96	3132.64	< 0.0001		26.38
D ²	0.2220	1	0.2220	77.57	< 0.0001		0.65
Residual	0.0429	15	0.0029				0.13
Lack of Fit	0.0279	7	0.0040	2.13	0.1559	not significant	0.08
Pure Error	0.0150	8	0.0019				0.04
Cor Total	33.97	29					100.00

The standard deviation for the data corresponding to value of the surface roughness is 0.035 with the mean value of 42.10 and the percentage C.V of 0.1271. The value of coefficient of determination is 0.9987. The adjusted value of coefficient of determination is 0.9976 and the predicted value the coefficient of determination is 0.9877 and the value of adequate precision for the data is 130.3260. Figure 114 shows the predicted vs actual curve for the percentage improvement in the surface finish while figure 115 shows the perturbation curve for the which highlights the effect of individual parameters on the percentage improvement in surface finish. The second order polynomial equation corresponding to the percentage improvement in surface finish is given below.

Percentage Improvement in Surface Finish = - 191.51004 + 2.98002 Electrode + 0.014149 Electrode + 0.014149 Supply Current + 694.20718 Duty Cycle - 0.185580 Rotational Speed + 0.021771 Electrode * Supply Current - 0.734375 Electrode * Duty Cycle - 0.006469 Electrode * Rotational Speed + 0.632812 Supply Current * Duty Cycle - 0.005693 Supply Current * Rotational Speed + 0.261719 Duty Cycle * Rotational Speed - 0.573387 Electrode² + 0.006494 Supply Current² - 522.14279 Duty Cycle² + 0.000330 Rotational Speed².

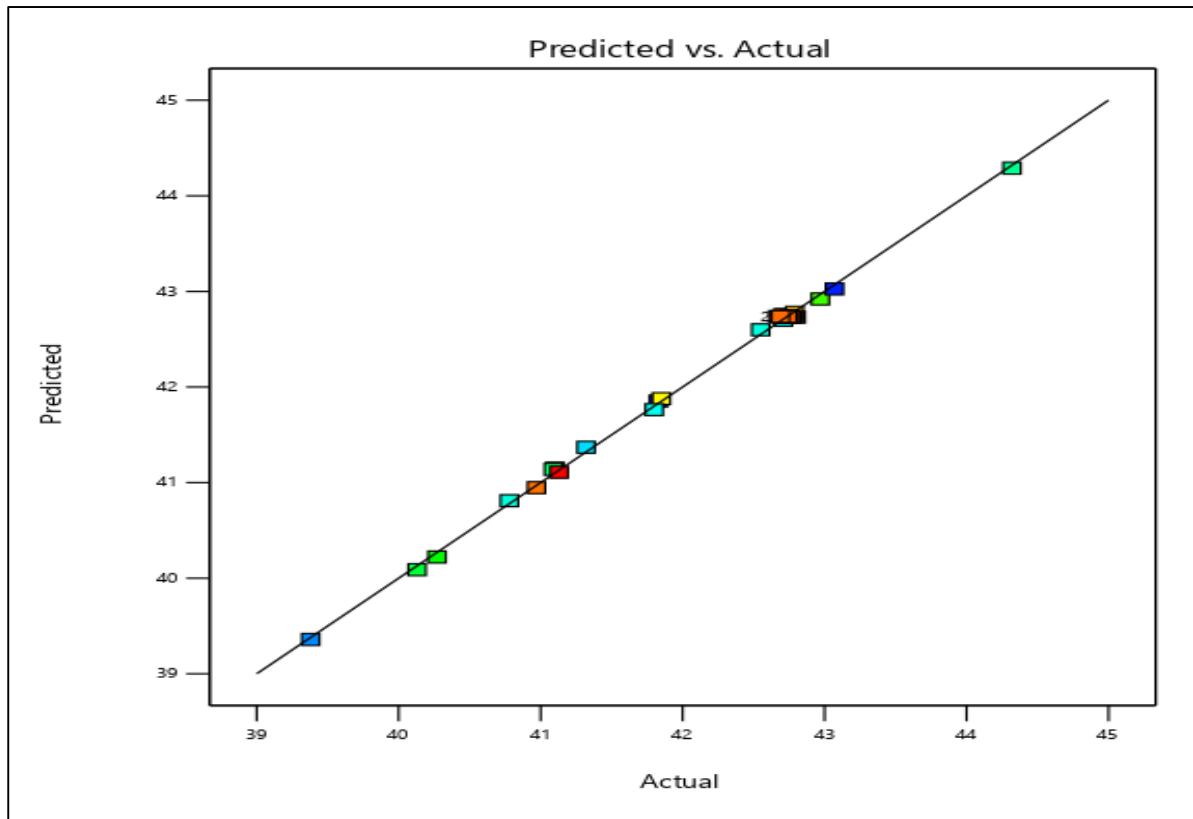


Figure 114 Predicted and experimental value for the percentage improvement in surface finish

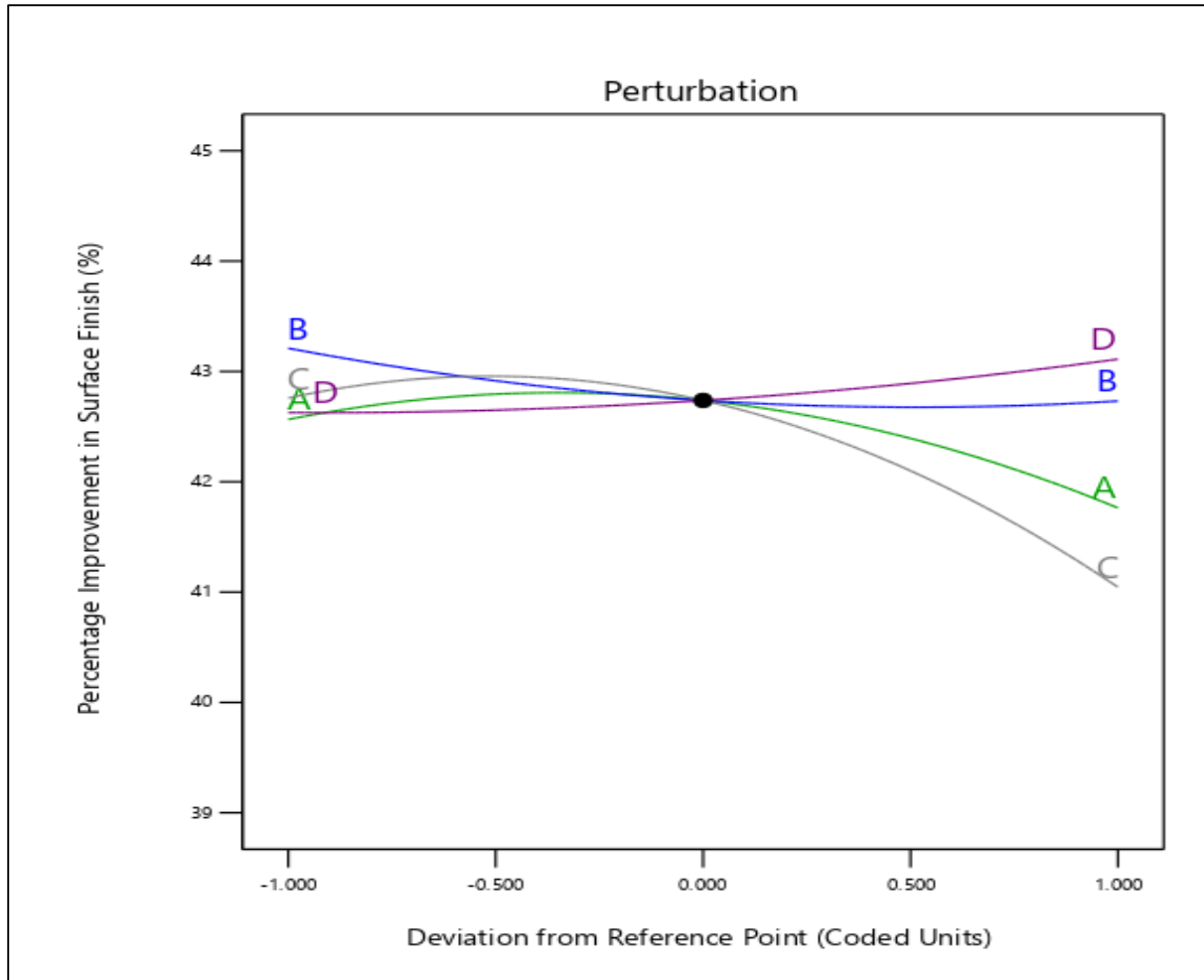


Figure 115 Perturbation curve for the percentage improvement in surface finish

Figure 116 onwards shows the effect of individual parameters on the $\% \Delta R_a$. Figure 117 shows the effect of electrode type on the $\% \Delta R_a$. It can be observed that the value of $\% \Delta R_a$ increases with the use of spline shape electrode. The reason behind this is that the spline shape provides more path for the media flow which increases the interaction of the abrasive particles with the wall of the workpiece (Ali et al 2020).

However, for square electrode the path is restricted due to which the interaction is less but due to high media pressure MR is more which results in decrease in the $\% \Delta R_a$. Figure 118 shows the effect of supply current on $\% \Delta R_a$. The value of $\% \Delta R_a$ decreases with the increase in supply current because of the fact that supply current increases the MR which results in the degradation of the surface quality (Patil et al. 2023).

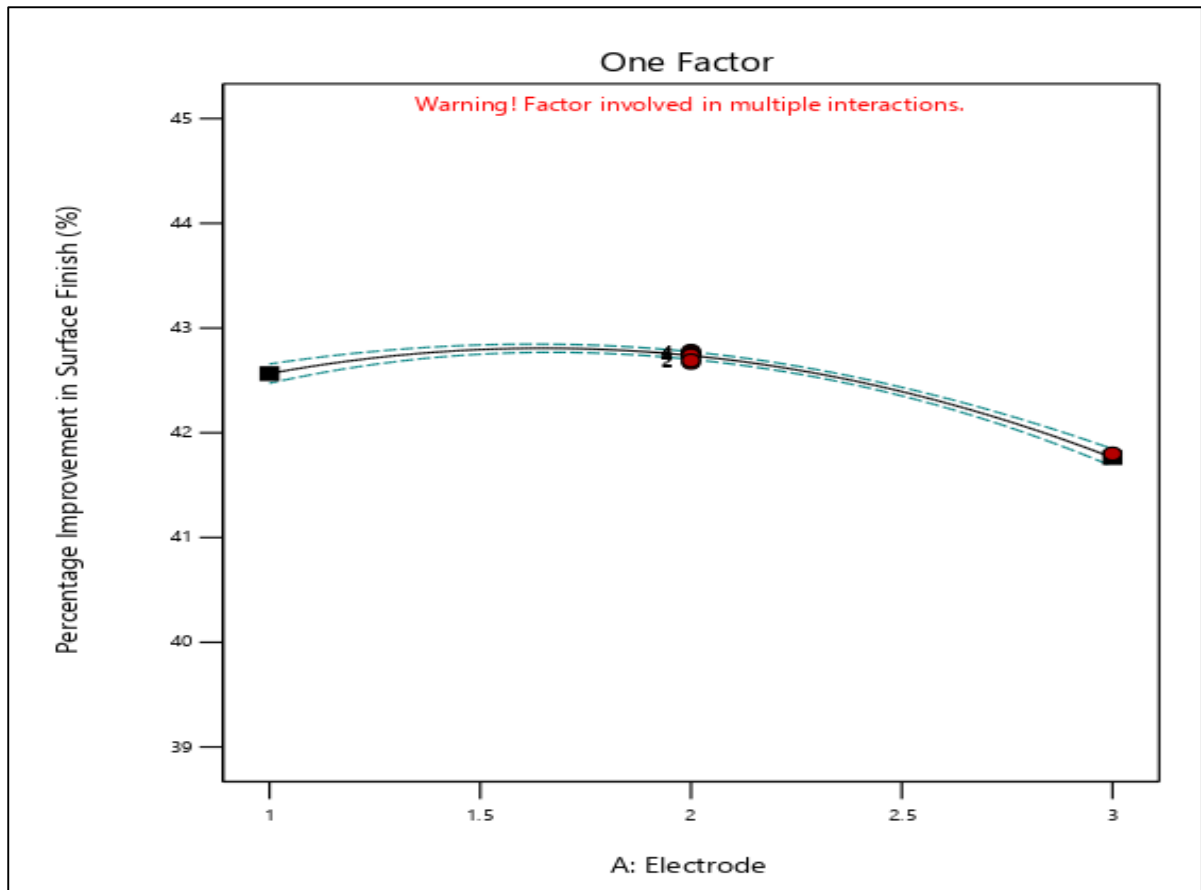


Figure 116 Effect of type of electrode on percentage improvement in surface finish

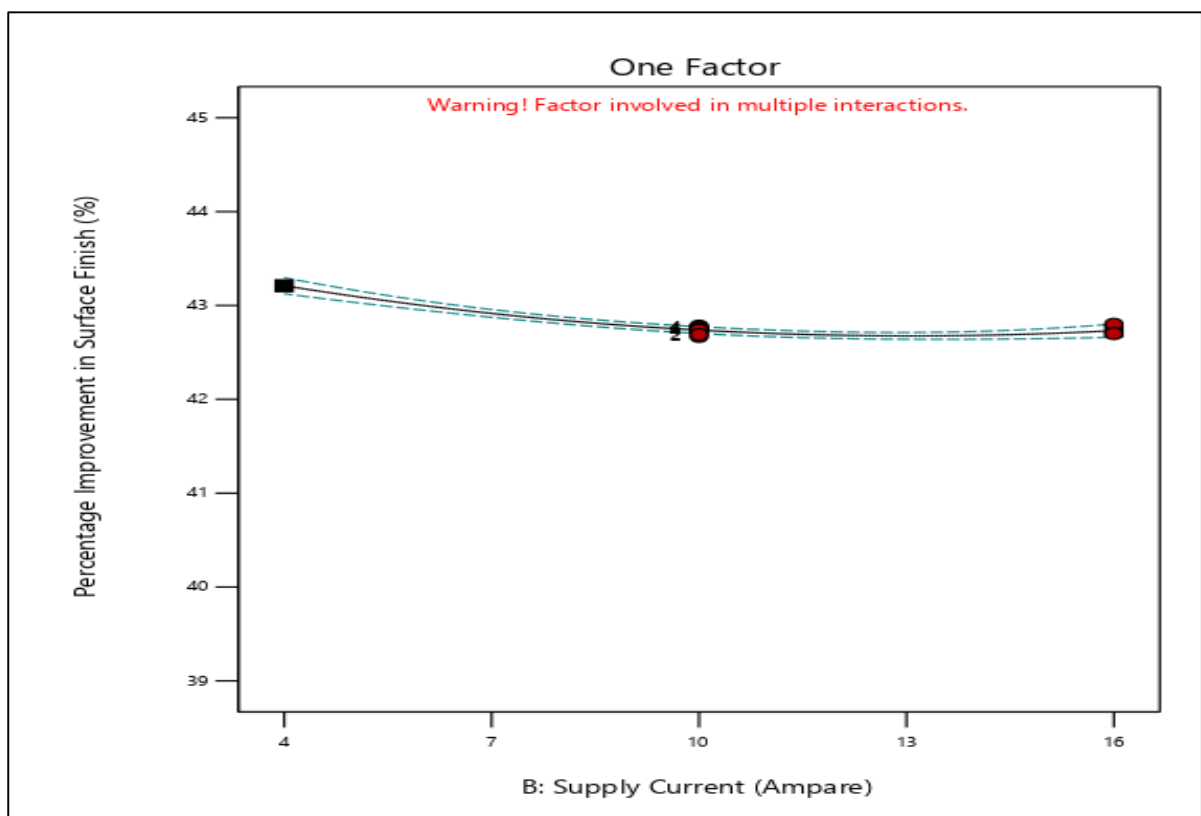


Figure 117 Effect of supply current on the percent improvement in surface finish

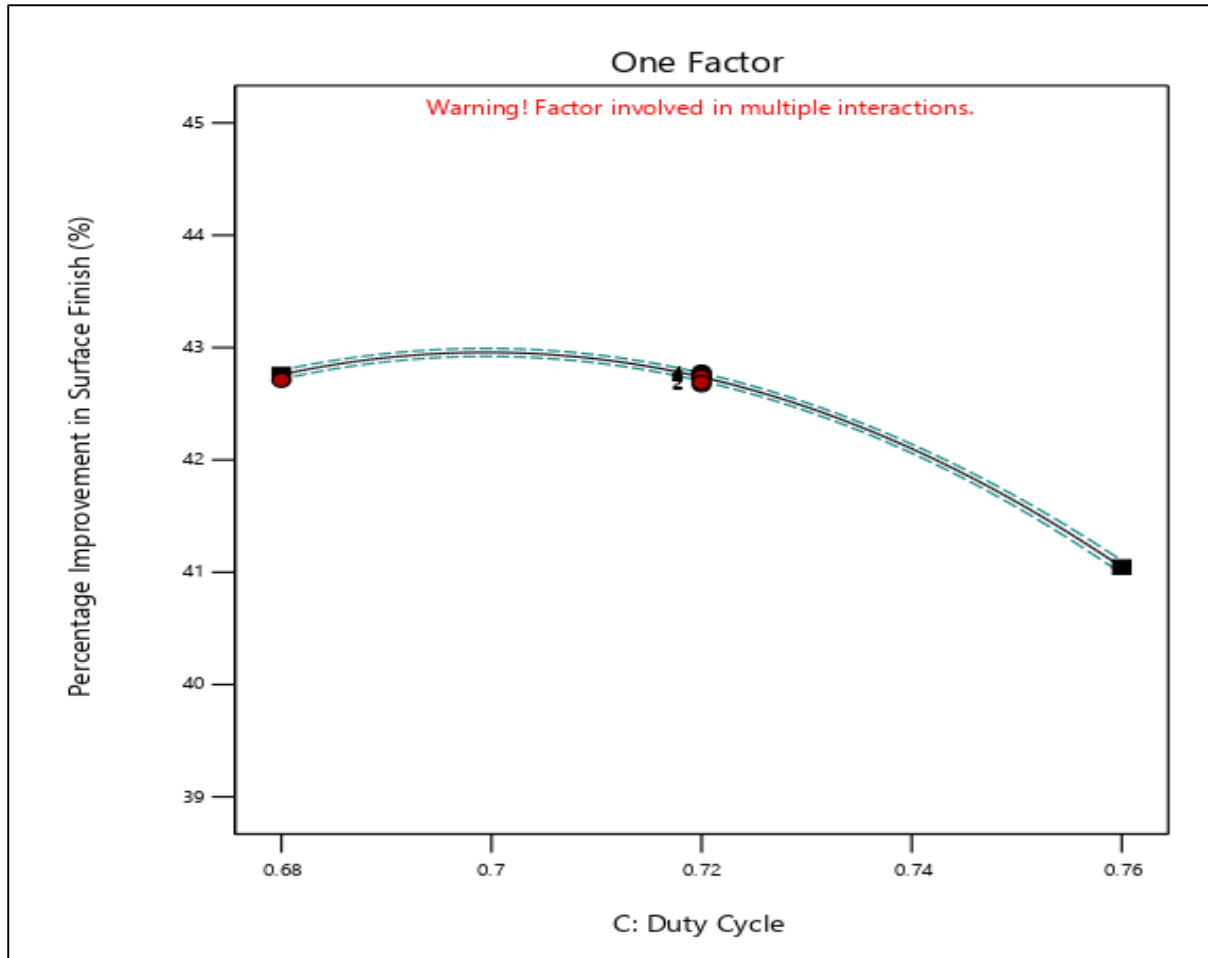


Figure 118 Effect of Duty cycle on the percentage improvement in the surface finish

Figure 119 shows the effect of duty cycle on $\% \Delta R_a$ which shows a slight increase initially and then decreasing value, the reason is that when the spark is initially formed than initial material removal along with finishing operation take place but as the arc stabilizes, the value of MR increases resulting in the degradation of surface integrity (Ali et al 2020).

Figure 120 shows an increase of $\% \Delta R_a$ value with the increase in rotational speed. This is because as the rotational speed increases, the centrifugal force acting on the media increases resulting in an increase in the abrasive and workpiece wall interaction, resulting in an increase in $\% \Delta R_a$ (walia et al. 2006, Shankar et al 2009).

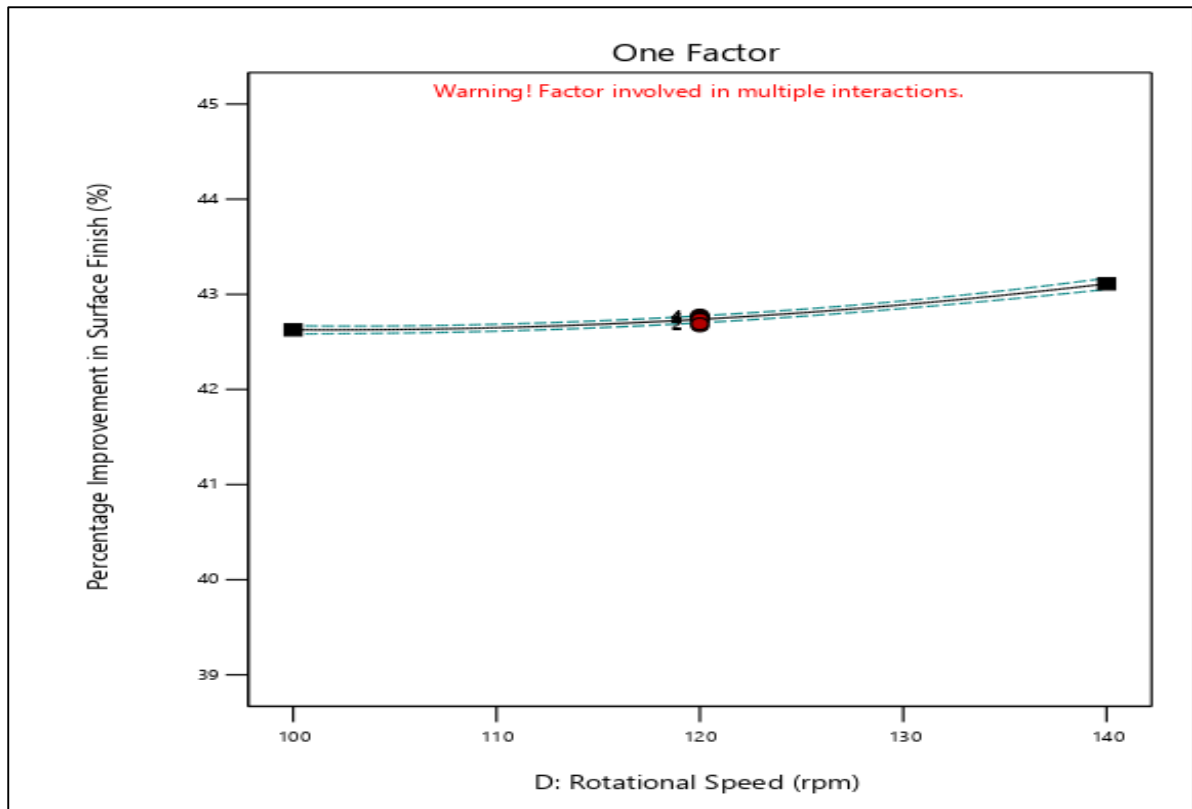


Figure 119 Effect of rotational speed on the percentage improvement in surface finish

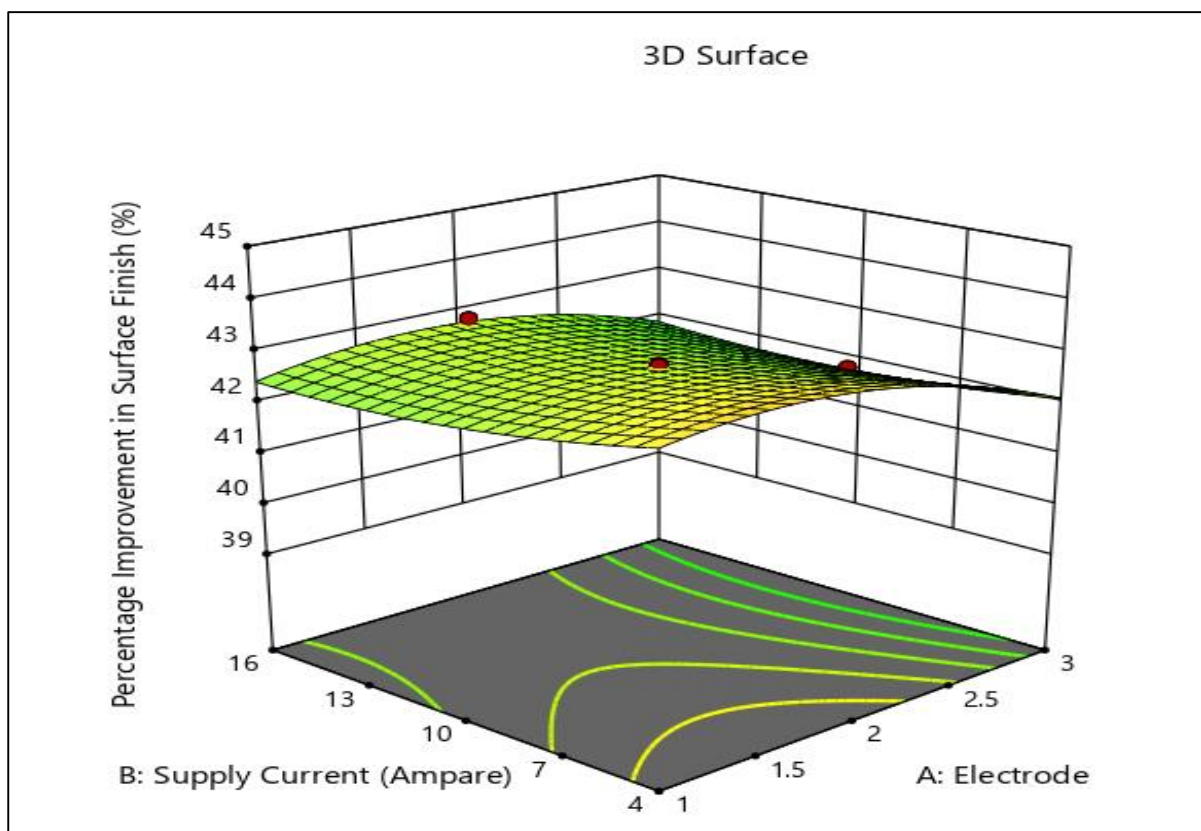


Figure 120 Effect of type of electrode and supply current on the percentage improvement in surface finish

Figure 121 onwards shows the 3D graph of percentage improvement in surface finish with the combination of two factors. Figure 121 shows the combine effect of electrode and supply current on the $\% \Delta R_a$. The graph shows an initial increase in the value of $\% \Delta R_a$ and then slight decrease. This is due to the fact that the value of MR and $\% \Delta R_a$ increases when initially sparks generate but with the increase in current, the MR increases which degrades the surface quality. The spline shape electrode provides better media flow path which contributes in increase in $\% \Delta R_a$ [Ali et al 2020].

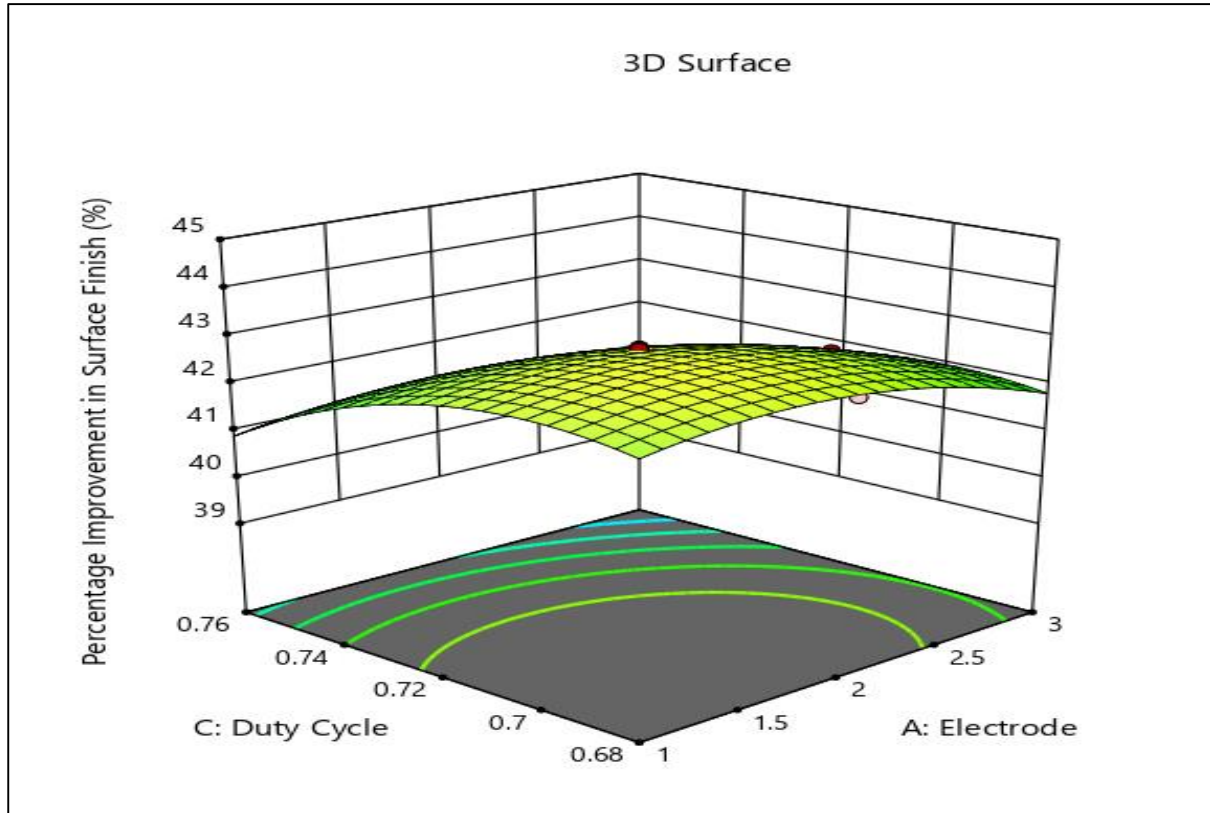


Figure 121 Effect of duty cycle and electrode on the percentage improvement in surface finish

Figure 122 shows the effect of electrode type and the duty cycle. The graph shows the influence of spline electrode with curved blade on $\% \Delta R_a$ value due to its centrifugal effect. But the overall value of $\% \Delta R_a$ decreases due as duty cycle results in improvement in MR due to arc stabilization which degrades the surface quality [Ali et al 2020]. Figure 123 shows the combined effect of electrode and rotational speed on the $\% \Delta R_a$. The graph shows an increase in the MR with the combination of spline shape electrode with curved blade and higher rotational speed as the combination results in effective machining process. Figure 124 shows the combined effect of the duty-cycle and the supply current. The combination results in the

decrease in the $\% \Delta R_a$ value as the individual factors results in the increase in MR which degrades the surface quality of finished workpiece [Patil et al 2023].

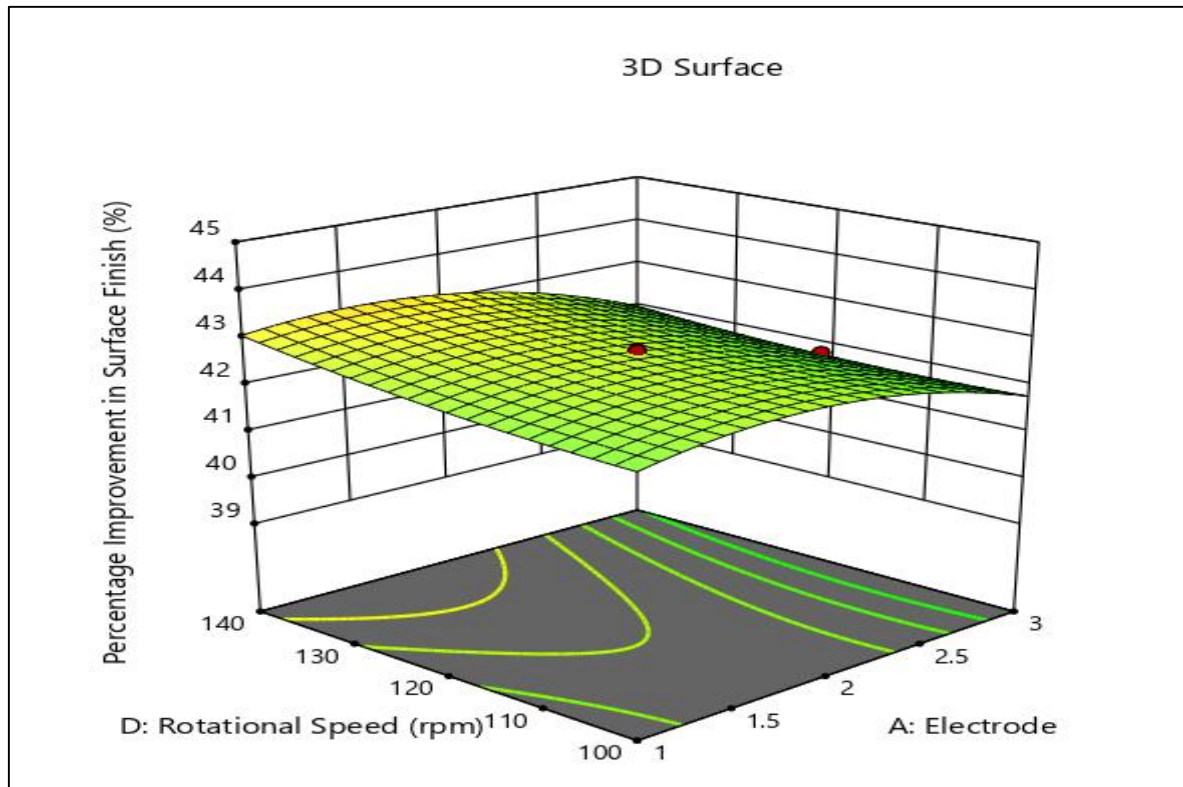


Figure 122 Effect of electrode and rotational speed on percentage improvement in surface finish

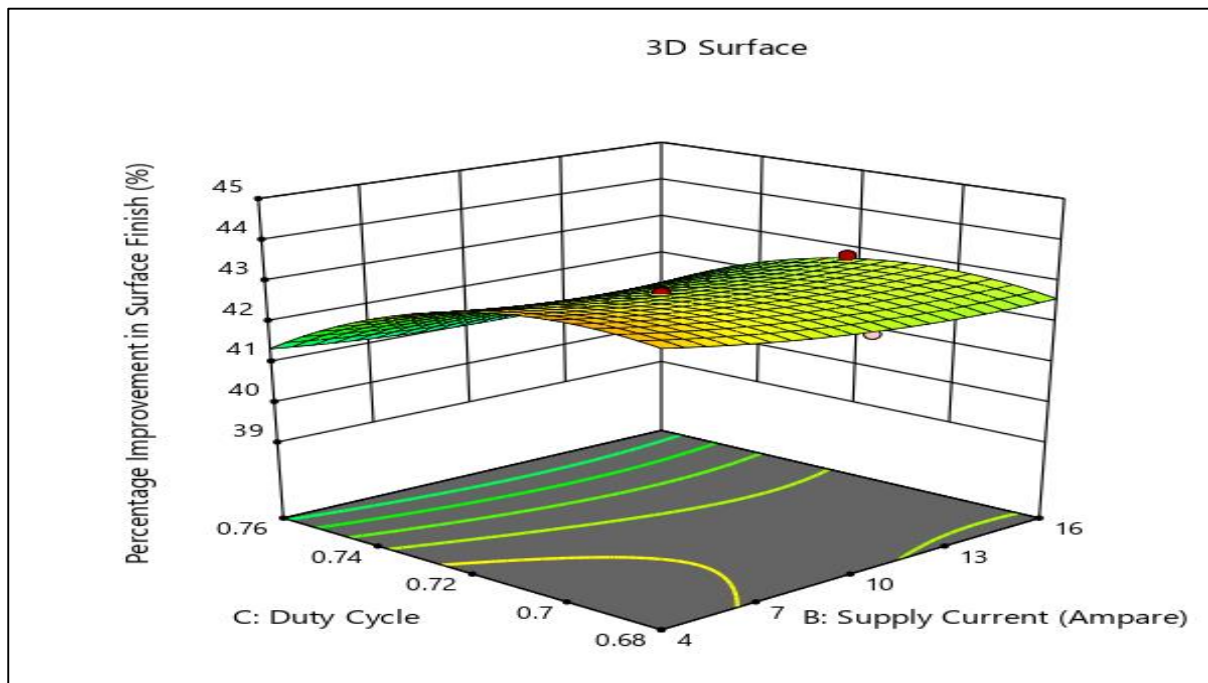


Figure 123 Effect of supply current and duty cycle in percentage improvement in surface finish

Figure 125 shows the effect of rotational speed and the current supply on $\% \Delta R_a$. The figure shows an increase in overall value of $\% \Delta R_a$ due to the effect of EDM and centrifugal action of the centrifugal force generating electrode (Ali et al 2020, walia et al 2006). Figure 26 shows the combine effect of duty cycle and rotational speed. The rotational speed results in the increase in $\% \Delta R_a$ due to the increase in the centrifugal action at the higher speed while the duty cycle results in the decrease in surface quality $\% \Delta R_a$ as it increases the MR (Ali et al 2020).

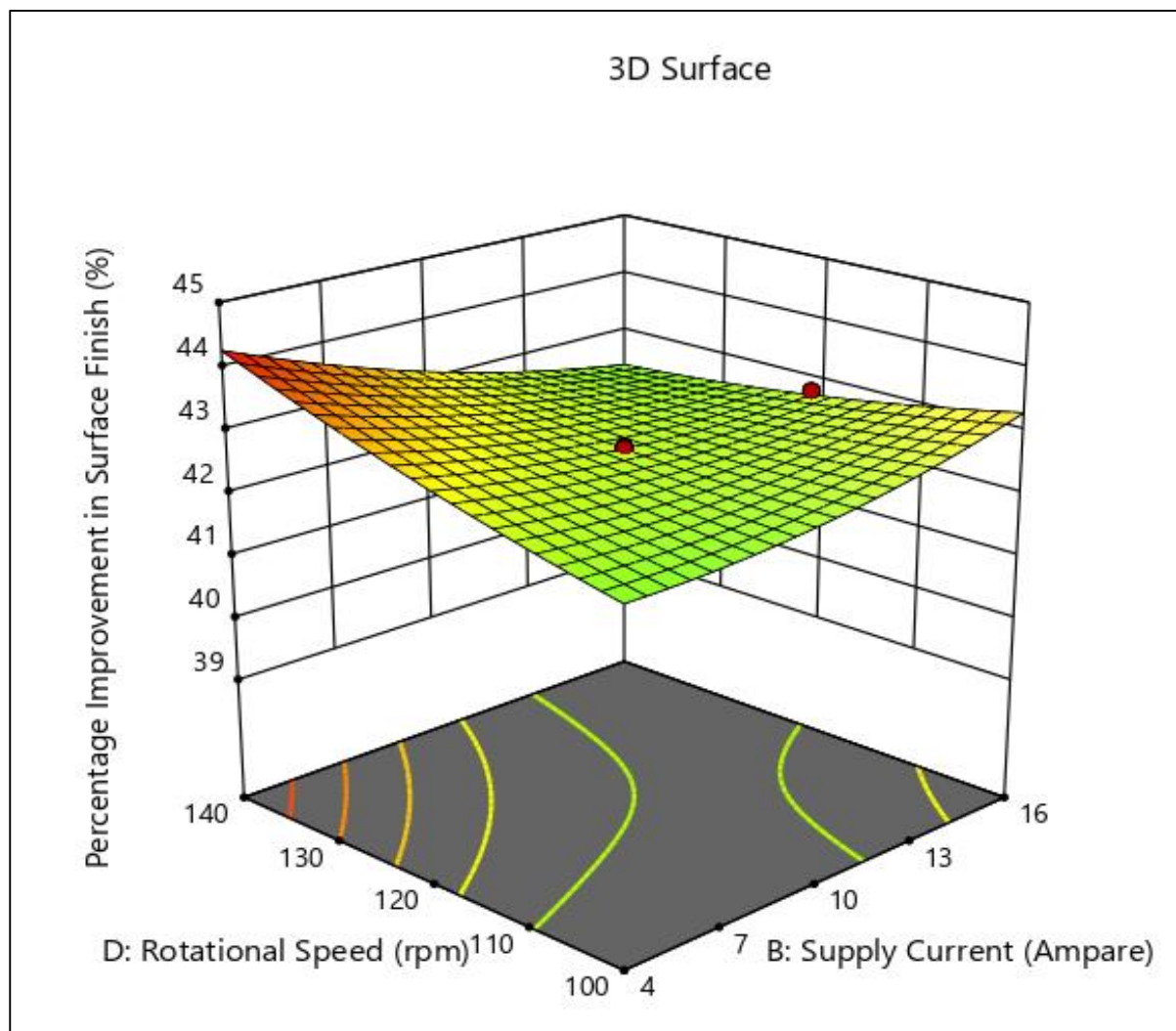


Figure 124 Effect of supply current and rotational speed on percentage improvement in surface finish

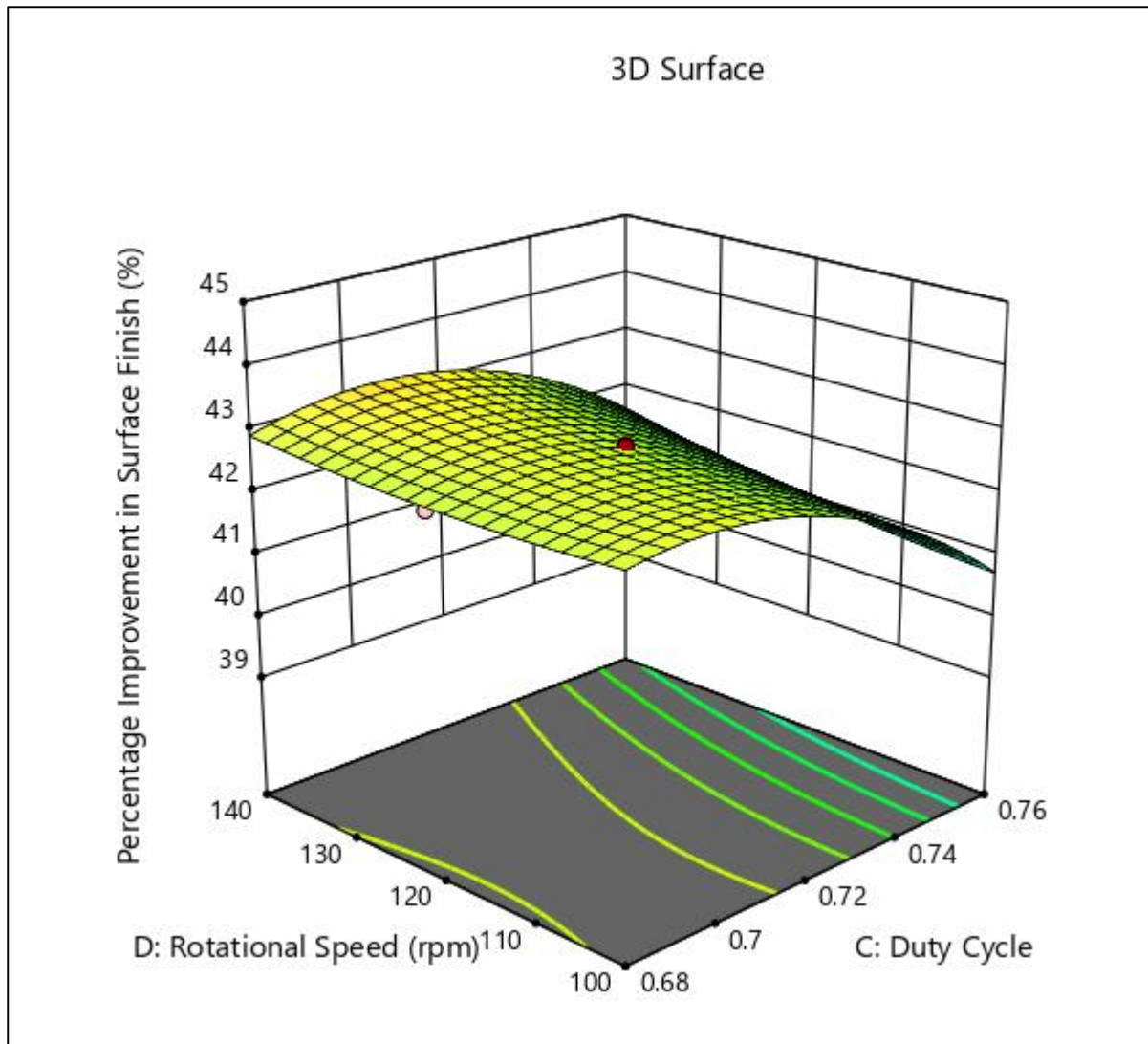


Figure 125 Effect of duty cycle and rotational speed on percentage improvement in surface finish

6.5. Confirmation Experiment

After the RSM CCD analysis the optimal values of the parameters are computed for the maximum value of material removal and percentage improvement in surface finish. The optimal value is taken at 95 percent confidence level and the values are recorded in the table 17. The table shows that the optimal value of electrode type is 1.73935 which is taken 2 for the confirmation experiments. The value of supply current is taken as 7.81556 A, which is consider as 8 A as it is difficult to enter the decimal value in the analog EDM controller. The value of supply current is supplied through buttons in whole number in the EDM controller.

The optimal value of duty cycle is 0.711518 and the rotational speed of 140 rpm are found as optimal value. The analysis shows that the predicted value is 51.369 mg for the material removal and shows the value of 43.6995 %.

The confirmation experiments were done on the optimal values to get the observed values for both MR and for the percentage improvement in surface roughness. The error obtained between the predicted value and the observed value in case of percentage improvement in surface finish is 0.65 percent for material removal and it is 1.58 percent for the percentage improvement in surface finish. The percentage error is less and acceptable considering the environmental factors and the non-automated process of the TACAFM process. The another sources of error are the leakage of media from the fixture joint as the media flows the with the high extrusion pressure which results in the atmospheric interaction with the media.

Table 17 Optimal Values and results

Response	A	B	C	D	P.V	O.V	% Error
Units	Type	Ampere		rpm			
(MR)	1.7393 5	7.81556	0.711518	140	51.369 mg	51.031 mg	0.65 %
(%ΔR_a)	1.7393 5	7.81556	0.711518	140	43.6995 %	43.009 %	1.58 %
<p>➤ A – Type of Electrode</p> <p>➤ B - Supply Current</p> <p>➤ C - Duty Cycle</p> <p>➤ D - Rotational Speed</p> <p>➤ MR - material removal</p> <p>➤ %ΔR_a – Percentage improvement in surface finish</p> <p>➤ P.V - Predicted value form software</p> <p>➤ O.V - Value obtained after experimentation based on optimal value obtained from software</p> <p>➤ % Error- Percentage error between the predicted and observed value. (Predicted Value- Observed value/ Predicted value)</p>							

SUMMARY

- 1. The finishing of internal surface is carried out using the TACAFM process with the different electrode geometry.**
- 2. The different shape of CFG electrode spline shape electrode with straight blade, spline shape electrode with the curved blade and the square shape electrode.**
- 3. RSM methodology is used to analyse the effect of electrode shape, rotational speed, duty cycle and the supply current on material removal and percentage improvement in surface finish of brass workpiece during the TACAFM process.**
- 4. All process parameters, their interactions and their square were significant with P values less than 0.05.**
- 5. The analysis shows that the value of material removal and the percentage improvement in surface finish shows the maximum value of the with the spline shape electrode with the curved blade, at 7.8 A current, 0.71 duty cycle and 140 rpm.**

Chapter 7. Results, Discussion and validation

The present chapter includes the results of the various tests performed on the finished workpiece machined by the TACAFM with the help of spline shape electrode with the curved blade. The chapter discuss the morphology of finished brass surface with the help of optical micrograph taken by optical microscope, surface roughness plot taken by Taylor Hobson tallysurf, SEM image taken from scanning electron microscope, X ray diffraction and the EDAX plot. The chapter also discuss the advantage of the new proposed CFG electrode with curved blade over the conventional spline shape electrode with straight blade and also validates the experimentation process.

7.1. Background

The present investigation studied the effect of geometry of CFG electrode on the material removal and on the percentage improvement in surface finish. The simulation and modelling along with the experimental validation shows that the proposed spline shape electrode with the curved blade gives an edge over the other CFG electrodes when material removal of the TACAFM process is discussed. The proposed electrode is little down when the percentage improvement in surface finish is observed but the overall functionality of the electrode is better compared to spline shape with straight blade and the square shape electrode. To prove this point, the separate experiments were performed on 8 samples with 3 different electrodes and keeping the optimal values of other parameter and the trends in the percentage improvement in surface finish and the material removal is observed. The comparison results of the analysis for the material removal and for the percentage improvement in surface finish is shown in the figure 1 and 2. Figure 126 shows the material removal of 8 different samples with 3 different electrodes performed at optimal parameters which are current supply as 8 A, duty cycle of 0.71 and the electrode of 140 RPM. It clearly highlights the dominance of spline shape electrode with the curved blade compare to other shape and the square shape CFG electrode showed very little MR, which proves the proposed electrode increases the efficiency of the TACAFM process. Figure 127 shows the comparison of the percentage improvement in the surface finish in TACAFM process with different electrode geometry. Here Square shape electrode showed a significant improvement as spline shape electrode with the curved blades slightly increases the MR which hampers the surface integrity of the finish surface. Thus the optimization is required to achieve maximum percentage improvement in surface finish along with the maximum material removal.

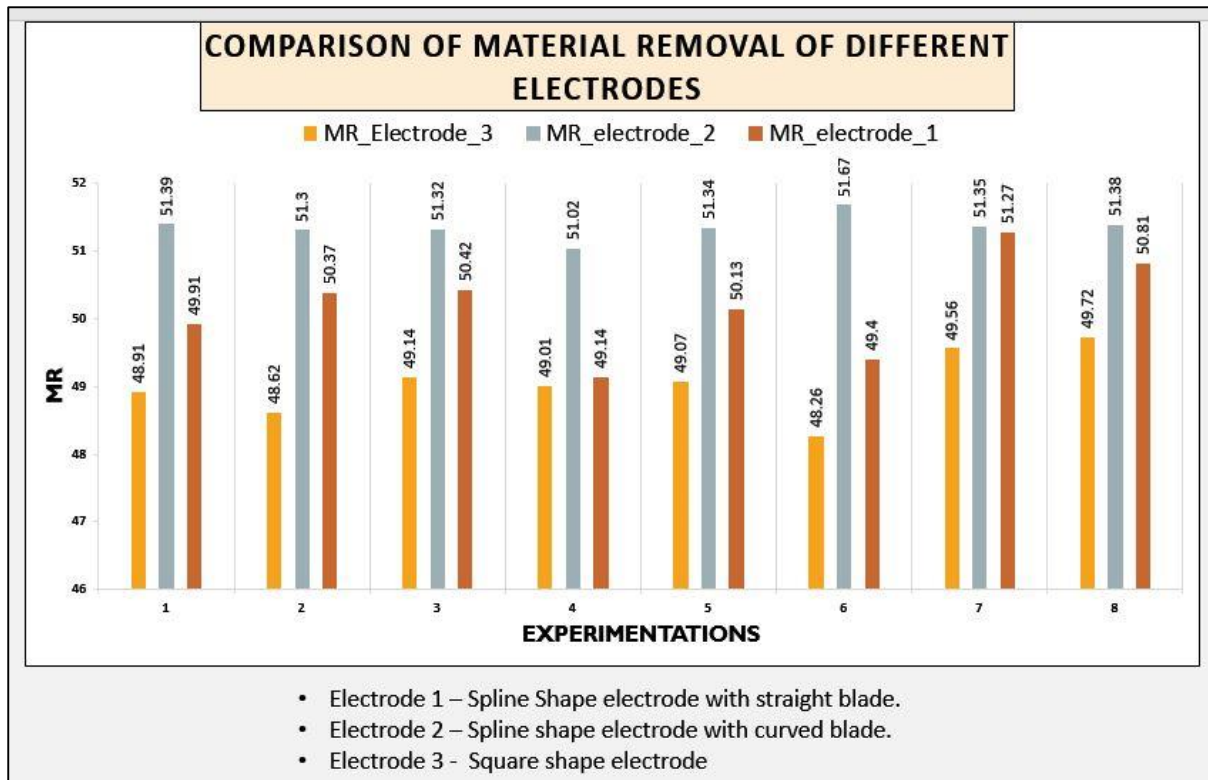


Figure 126 Comparison of material removal of TACAFM process with different shape of CFG electrodes

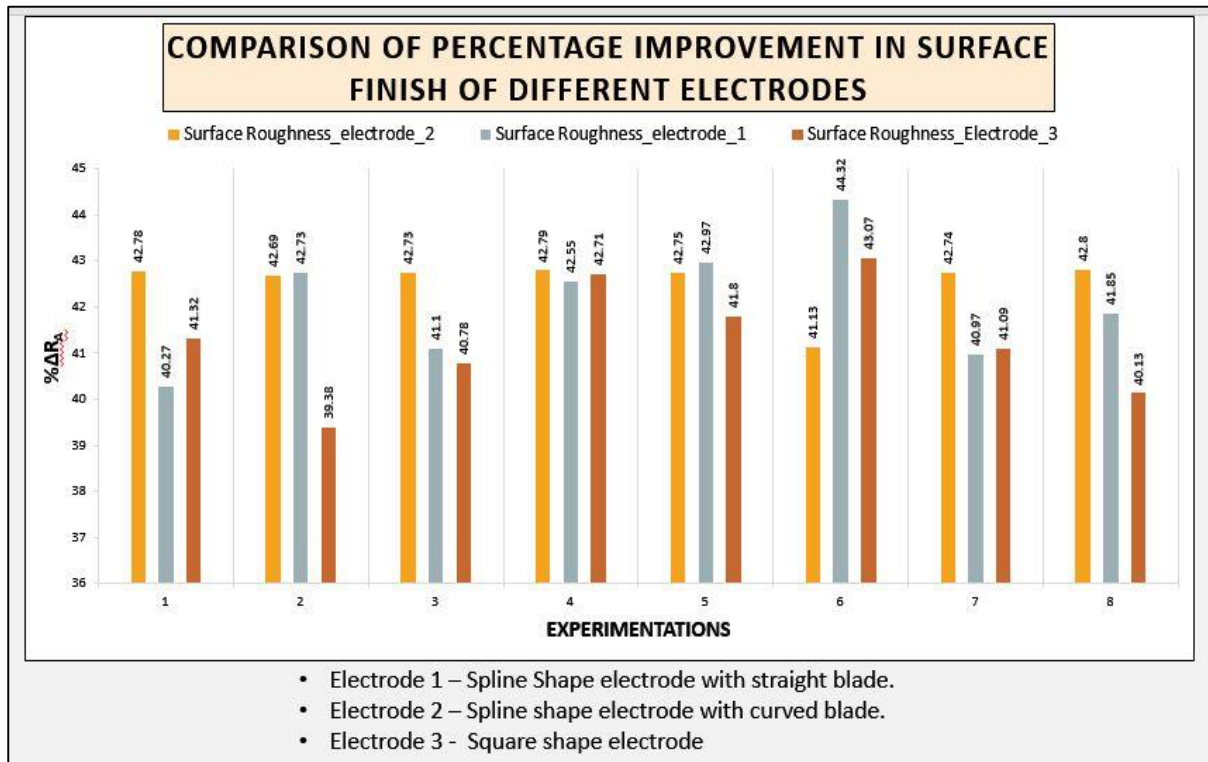


Figure 127 Comparison of percentage improvement in surface finish of TACAFM process with different geometry of CFG electrode

7.2. Morphology of Finished Brass Surface

The morphology of the finished surface is discussed with the help of micrograph and the SEM images. Further XRD and EDAX is also done for the finished workpiece to prove the validity of the spark formation in the TACAFM process.

7.2.1. Optical Micrograph

The TACAFM process involves the material removal mechanism through melting due to the heat produced by the spark and by the abrasion action of the abrasives over the surface of the workpiece because of the extrusion of laden media due to the pressure difference. The rotation of CFG electrode also directs the media particle towards the wall of the workpiece which enhances the dynamic number of abrasive particles near the wall which interns enhances the finishing process (Walia et al. 2006). Figure 128 shows the micrograph of the finished workpiece without polishing. The figure 128 (a) and 128 (b) are taken at 100 X magnification while the figure 128 (c) and 128 (d) are 200 magnifications. The figure highlights the machined surface with the spark proof. It is represented by the continuous dark band on the micrograph.

The figure 129 shows the micrograph of the polished surface at 100 X and 200X magnification. The figure 129 (a) shows the finished surface obtained after machining. The finished surface possesses abrasive marks due to abrasion action of abrasive particles present in the media with the wall of the workpiece. This abrasion action is due to the resultant force produced by the combination of centrifugal force (Coriolis + tangential) and axial (abrasive weight and axial force), which enhances MR compared to conventional abrasive flow machining process [Ali et al. 2020, walia et al. 2006]. The black marks shown in figure 129 (b) and figure 129 (c) shows the spark proof which is produced during the TACAFM process when the current is supplied between the electrode and the workpiece. Since the spark is involving in the machining process, there is a chance of oxidation of the workpiece surface also the heat produced by the spark initiates the melting of workpiece also which results in the accumulation of some molten metal which may be appeared on the surface of the finished workpiece. But due to continuous flow of media, the interaction of workpiece surface with atmosphere is cutoff which limits the formation of oxide layer, hence very less or negligible oxide layer would be seen on the surface of finished workpiece [Ali et al 2020]. Figure 129 (d) shows the surface of finished workpiece. Also as the number of extrusion cycle increases, the interaction of abrasive particle with the workpiece increases which results in the increase in the abrasion process. This interaction results in the removal of molten metal that is deposited on the finished surface due to melting and the oxide layer (if produce) during the spark action on the workpiece surface [patil et al

2023]. With the further increase in the number of cycle the abrasive present in the media will get blunt and abrasion process becomes weak. Thus the material removal takes place mostly due to thermal effect and media flowing over the workpiece acts as a polishing agent [Ali et al 2020].

Figure 130 shows the micrograph of finished brass workpiece with polishing and after application of etchant to view the grain structure and grain boundaries. The ferric chloride and nitric acid were used to produce an effective etchant and grain boundary were obtained. Figure 130 (a) and 130 (b) shows the spark proof and oxide layer at 100X and figure 130 (c) and 130 (d) shows the finished machined structure at 200X magnification. It is to be noted that the marks of the oxide layer and the spark are spotted which can be seen in figure 130 (d).

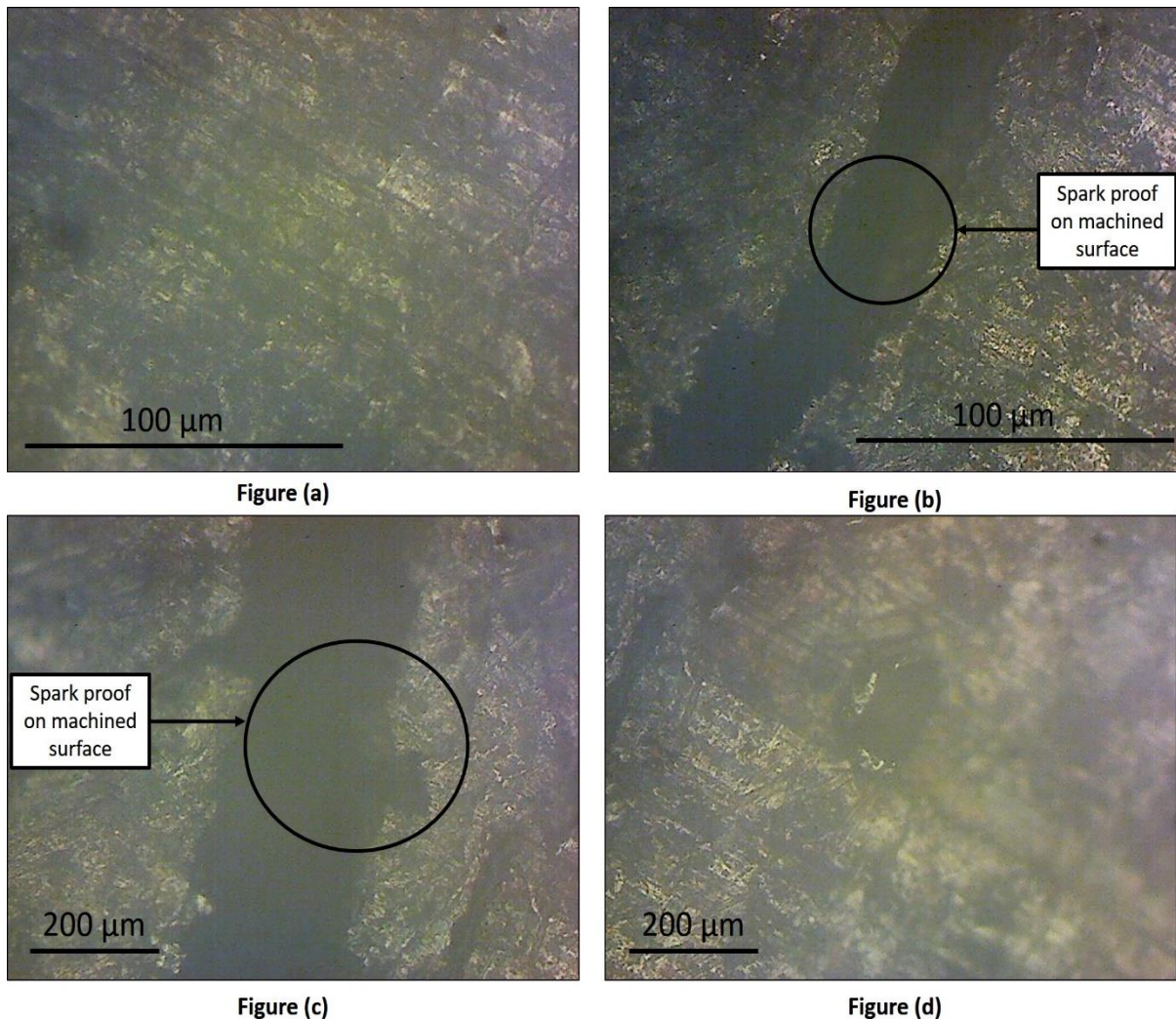


Figure 128 Micrograph without polishing (a) and (b) 100 X magnification, (c) and (d) 200 X magnification

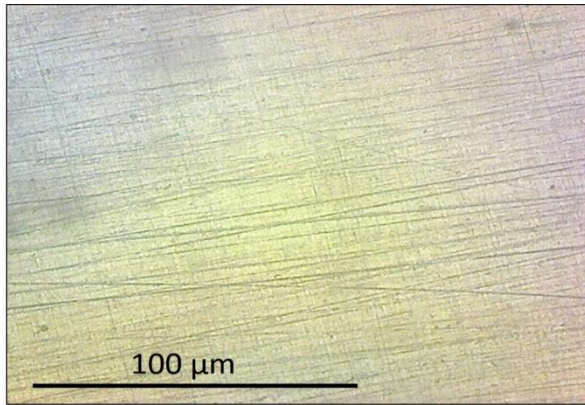


Figure (a)

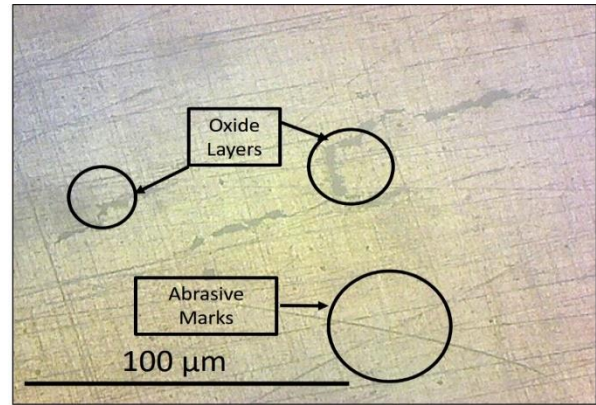


Figure (b)

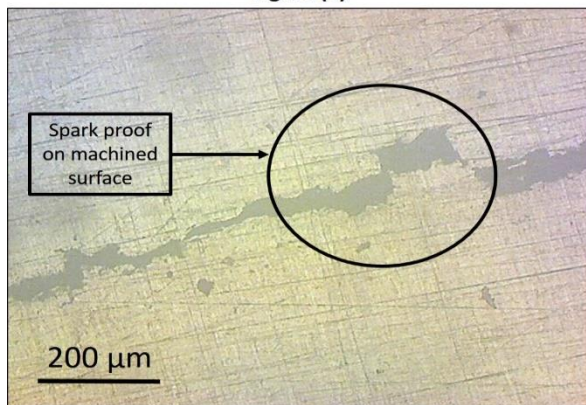


Figure (c)

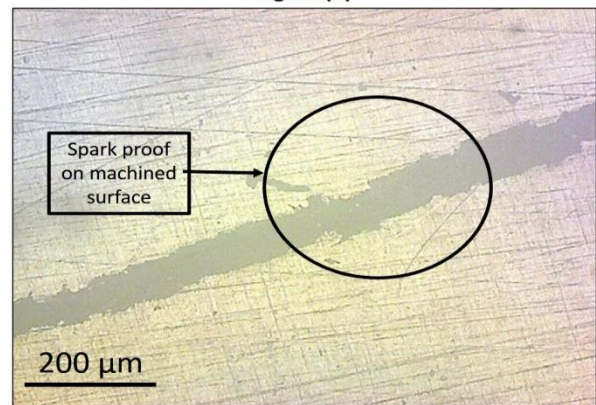


Figure (d)

Figure 129 Polished micrograph (a) and (b) 100 X magnification (c) and (d) 200 X magnification

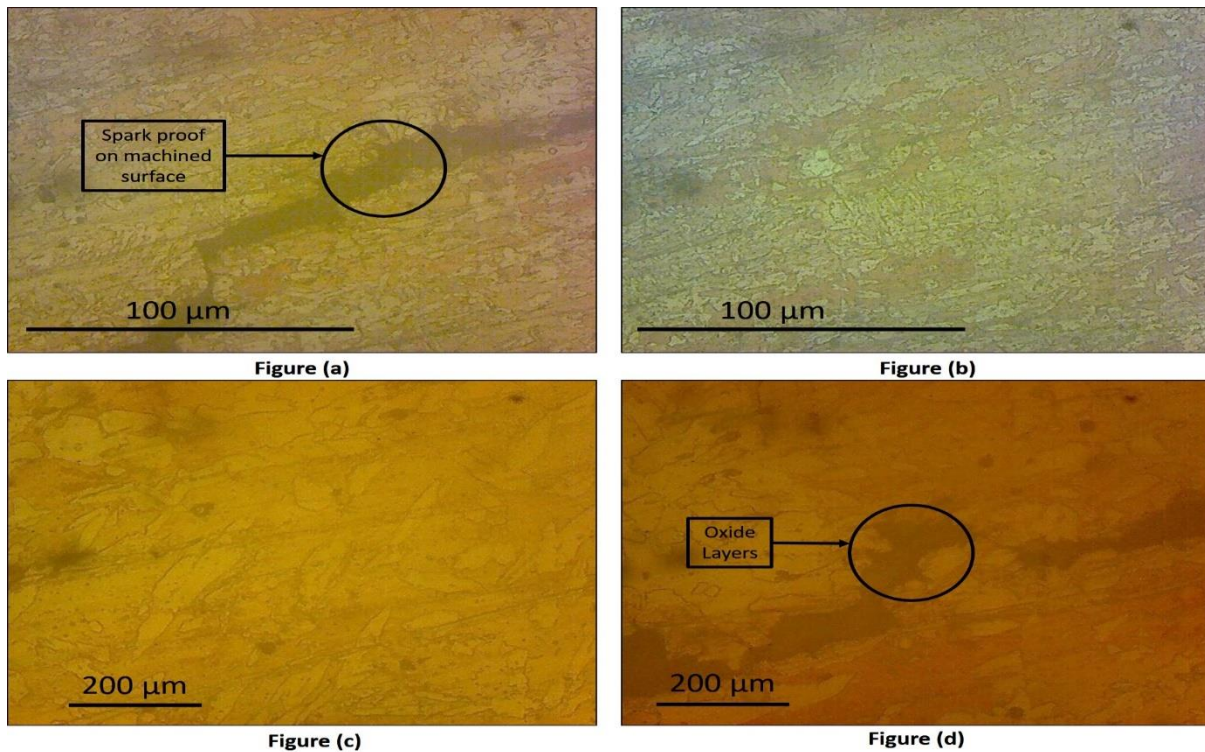


Figure 130 Polished Structure with etchant (a) and (b) 100X magnification (c) and (d) 200X magnification

7.2.2. SEM Images

In order to justify the morphology of the finished surface in more details, the SEM image of the finished surface was done. The optical microscope has limited resolution with smaller depth of field when compared with SEM. Also important phenomenon may be uncovered due to the reflection of light in the optical microscope. On the other hand, SEM provides the advantage of greater depth with sub-nanometre analysis of the sample and can analyse up to the higher magnification. Figure 131 shows the SEM images and XRD analysis of the finished surface. The figure 131 (i) shows the SEM image of the unfinished brass workpiece which highlights the presence of surface irregularities which needs to be finished. Figure 131 (ii) shows the oxide layer, molten metal and the random abrasive marks over the surface of the finished workpiece representing the involvement of abrasion and centrifugal action over the workpiece [Ali et al 2020]. The figure 131 (iii) shows the uniform parallel arrangement of the spark. This is because of the rotation of the CFG electrode inside the media. The spark produced between the electrode and the workpiece is uniformly travelled around the workpiece due to the rotation of the electrode [23,51]. Also as the number of cycles would increase the uniformity of surface would also increase. This is due to the fact with the increase in number of cycles the abrasive particles interaction with the workpiece surface increases resulting in higher MR also the media

carry away the removed workpiece particle with which also accelerates the abrasion process [walia et al 2006]. Figure 131 (iv) shows the smooth finished surface after TACAFM process.

7.2.3. X-Ray Diffraction

The further confirmation of the spark formation was done by considering the XRD of the brass workpiece before and after machining of the workpiece, shown in figure 132. The figure clearly indicates the difference in the XRD pattern before and after machining. The XRD pattern before machining represent the brass alloy and the change in the pattern after machining is due to the formation of oxide layer and molten metal which is possible due to the spark formation by the proposed novel electrode (Ali et al 2020). The XRD pattern for the un-machined workpiece is shown by red curve and the XRD pattern for the machined surface is shown with the black curve. The XRD results of the workpiece after machining shows the peak at the 2θ value of 42.32° which correlates with the copper oxide at (200) plane with cubic crystal system. Also the copper oxide peak may also be seen at the 2θ value of 36.44° corresponding to plane of (111) corresponding to cubic crystal system [23,60]. The confirmation of oxide layer may also be felt by the presence of zinc oxide which is found at the 2θ value of 63.102° which corresponds to the (103) plane corresponding to hexagonal crystal structure [23,61].

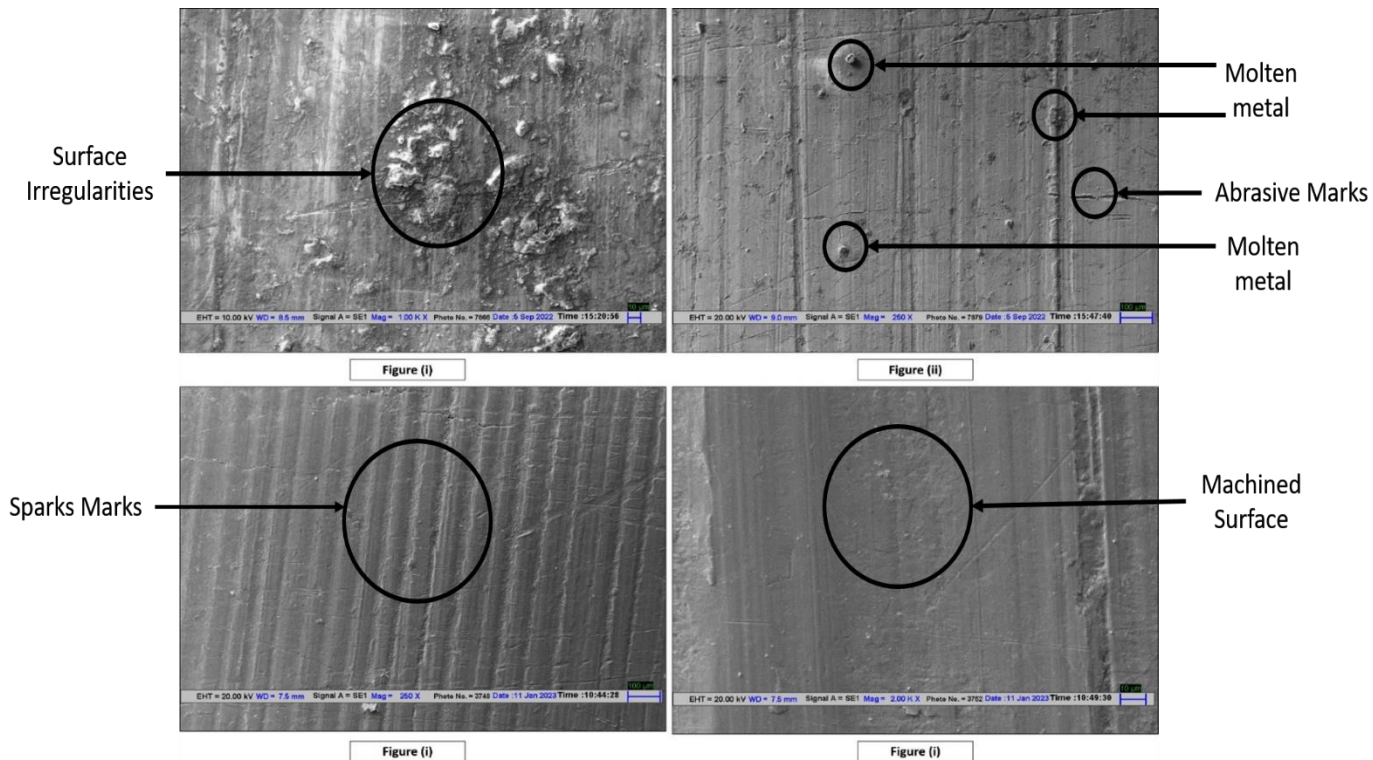


Figure 131 Image of Brass surface (i) Un finished Surface (ii) Finished surface (iii) Uniform Spark Marks (iv) Finished Surface

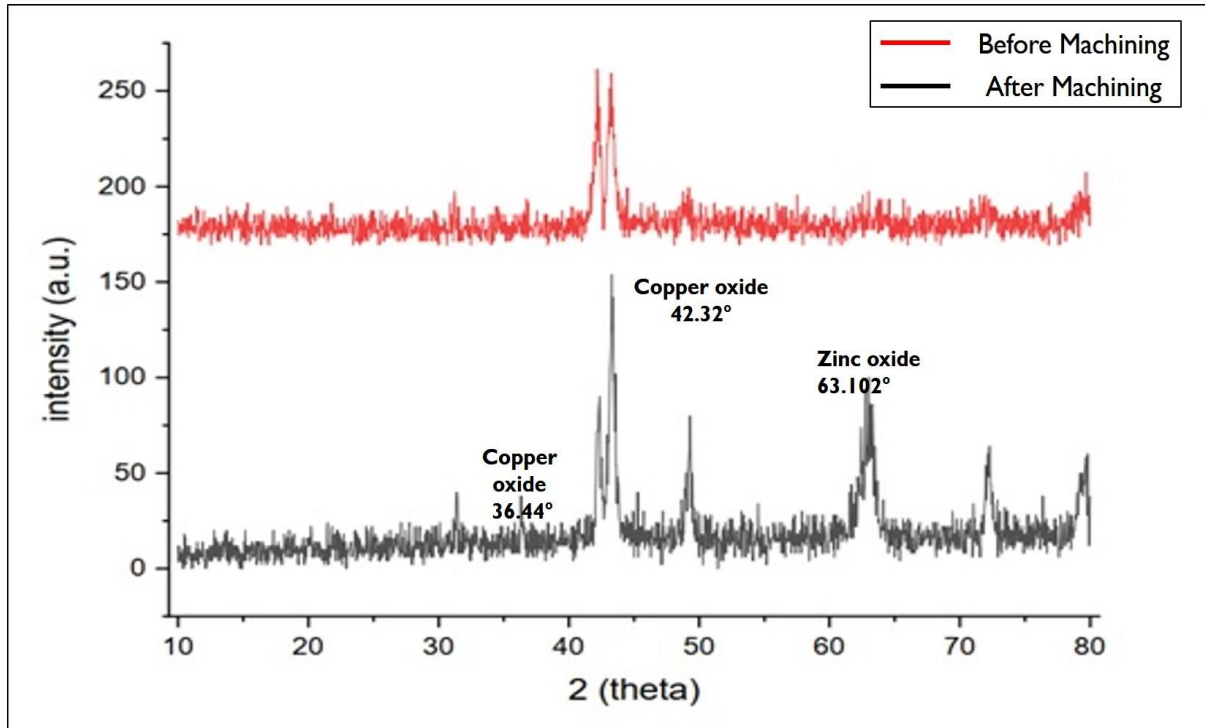


Figure 132 XRD Pattern of the workpiece (i) before finishing (ii) After finishing

7.2.4. EDAX analysis

EDAX stands for energy dispersive X ray analysis. In this technique a beam of electron directed towards the surface of the workpiece which produces X rays based on the nature and characteristic of the element present in the sample. In the present sample the availability of oxygen is to be checked which would occur due to the oxide layer present on the surface. The oxide layer will be formed by virtue of the spark which initiate the formation of copper and zinc oxide. Figure 8 shows the EDAX of the finished workpiece. Figure 133 (a) shows the area of consideration of the finished workpiece, figure 134 (b) shows the relevant graph highlighting the peak of elements. Figure 135 (c) shows the major component with their percentage and symbols. The EDAX clearly highlights the presence of oxygen which is formed due to the presence of oxide layer due to spark formation.

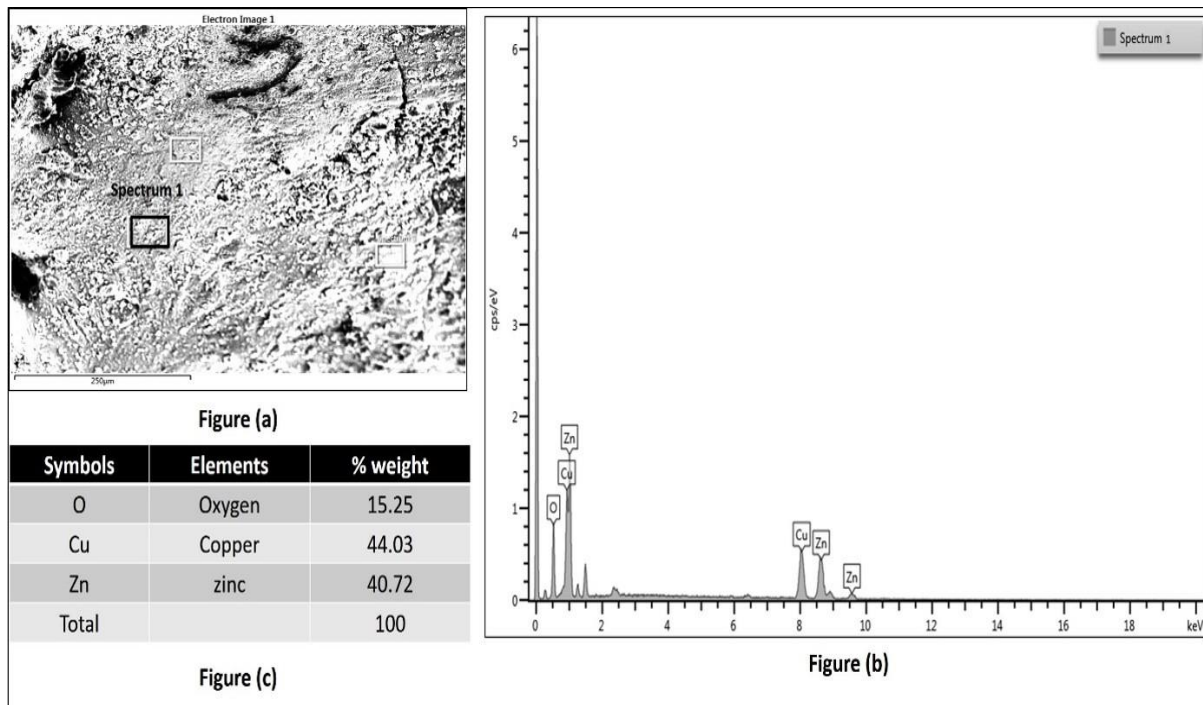


Figure 133 EDAX of the workpiece (a) Area of consideration (b) Graph highlighting the peak of the constituent element (c) table showing the weight percent of the constituent elements

7.3. Surface Roughness Plots

The TACAFM process shows the significant improvement in the material removal which may degrade the surface integrity thus a proper CFG electrode is used which provides an adequate surface finish along with the maximum material removal from the workpiece surface. For this purpose, the percentage improvement in surface finish is calculated for the spline shape electrode with the curved blade as it showed maximum MR in simulation and experimental results. The percentage improvement in surface finish is calculated based on initial surface finish of the sample based on R_a values using a tallysurf. Taylor Hobson tallysurf having the resolution of 0.01 micrometre and the maximum stroke length of 16 mm was used to compute the value of surface roughness. Since the target surface was curved and it was difficult to mark the specific location on the internal surface before and after the machining process, so the value of surface roughness was taken at 3 locations on the workpiece before and after finishing and the average was considered as a reading before and after finishing. Figure 134 shows the surface roughness curves of machined and un-machined workpiece.

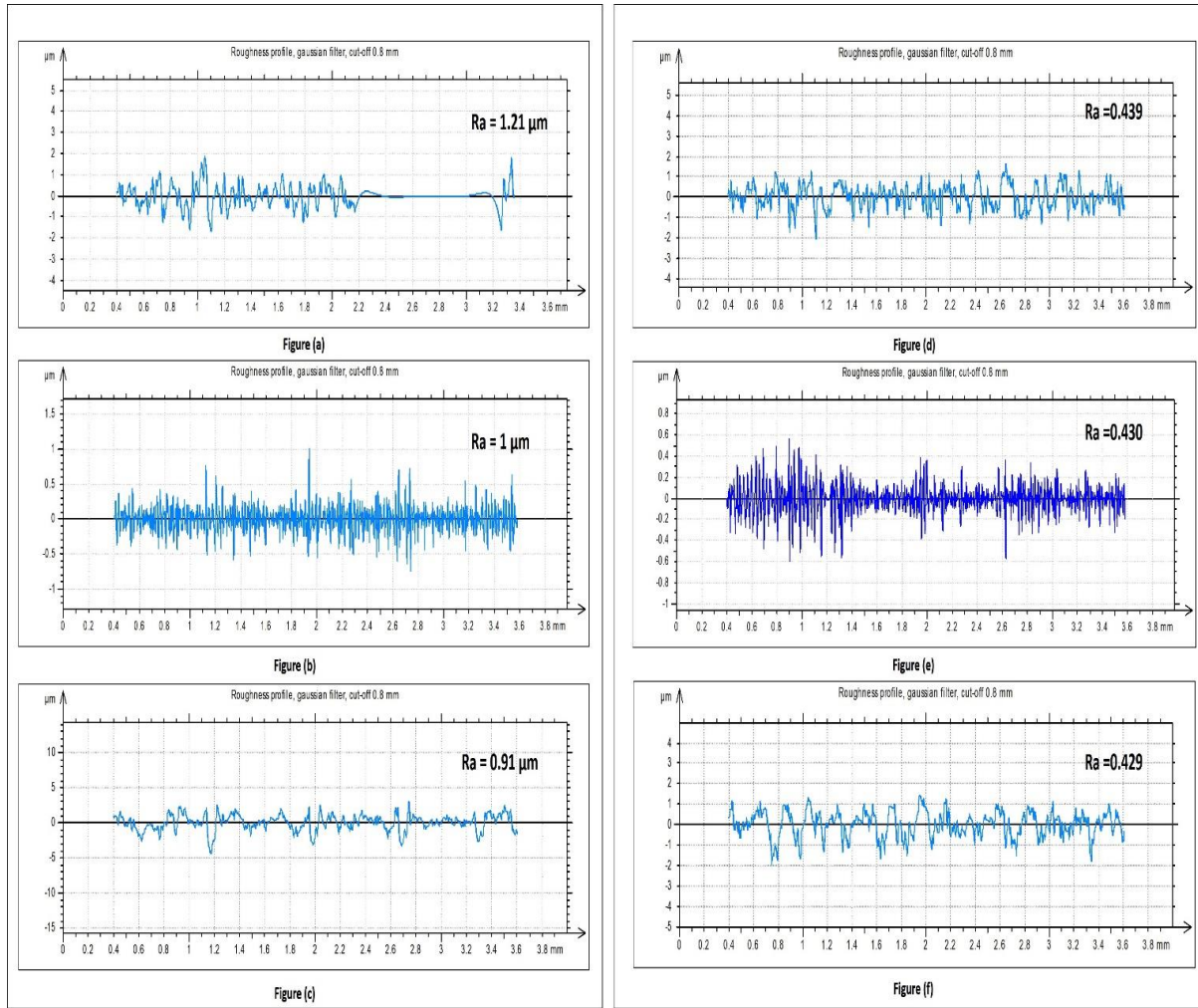


Figure 134 Surface roughness plots (a), (b) and (c) plots before machining (d),(e) and (f) plots after machining

Figure 134 shows the significant improvement in the value of R_a before and after finishing which highlights the surface finish capability of the TACAFM process using the proposed CFG electrode which is spline shape electrode with the curved blade that provides maximum MR with adequate surface finish.

7.4. Advantage of Curved spline shape electrode over straight blade

The experimental results show the increase in the MR and in $\%\Delta R_a$ when spline shape electrode with the curved blade is used in TACAFM process. This effect is observed due to the curvature of the blade present in proposed electrode. The machining in TACAFM process is observed due to the combine action of the thermal, centrifugal and conventional extrusion of the media within the internal surface of the workpiece. The thermal effect makes the material softening due to the spark formation which results in the deeper penetration of the abrasive particle over the surface of the workpiece. The total force exerted by the abrasive particle on the surface of

the workpiece is the combination of force extorted due to conventional extrusion, thermal effect and the Coriolis effect of CFAAFM process, which is given by equation (3) [Ali et al 2020]

$$F_{TACAFM \text{ by Abrasive}} = \left[\sum_{i=\theta_a}^0 (CA\sigma) \sin\theta_i \cdot N_d - F_{thermal} \right] \pm W \quad (3)$$

Where $F_{(TACAFM \text{ by abrasive})}$ is the total force acting on workpiece by the abrasive particle during TACAFM process, C is the flow constraint factor, A is projected area of abrasive particles, σ is uniaxial flow stress of the workpiece material, N_d is the number of dynamic active particle, $F_{(thermal)}$ is the force on abrasive due to the thermal effect and W is the weight of the abrasive particle. The negative and positive are used depending upon the direction of extrusion. Here θ_i is the approach angle by which the abrasive particle hits the workpiece due to the resultant force produced by the centrifugal and axial force. The curve blade present on the novel proposed electrode increases the centrifugal force on the media particle by providing circular motion to the media which increases Coriolis force [Ali et al 2020]. Due to this effect the approach angle increases which in turns increases total force exerted by the particle for indentation. Hence the proposed tool with curvature effect results in the increase in penetration compared to the primitive tool used in the investigation. Figure 10 shows the mechanism of propose spline shape electrode with curved blade compare to the traditional spline shape electrode with the straight blade used in the TACAFM process. Figure 135 (a) shows the top view of the primitive electrode and figure 135 (b) shows the forces acting on the abrasive during the penetration inside the work surface. The resultant force is the vector some of (centrifugal and Coriolis) and the axial force (extrusion and weight of the abrasive). This resultant force results in the angular impingement of abrasive particle on the workpiece surface. This angle is called approach angle denoted by θ in figure 135 (b). Figure 135 (c) top view of the proposed electrode Figure 135 (d) working mechanism of the proposed electrode.

Figure 135 (c) shows the top view of the proposed electrode inside the workpiece highlighting the curve blade of the electrode. It is evident from figure 135 (d) that due to the curvature of the rod the resultant force increases due to the increase in Coriolis and centrifugal force which increases the angle of impingement of the abrasive particle on the workpiece surface. Thus the approach angle ϕ is more than θ due to which total force exerted by the proposed electrode is greater than that of the conventional spline shape electrode. The MR by overall TACAFM process is given by equation 4 [Ali et al 2020]

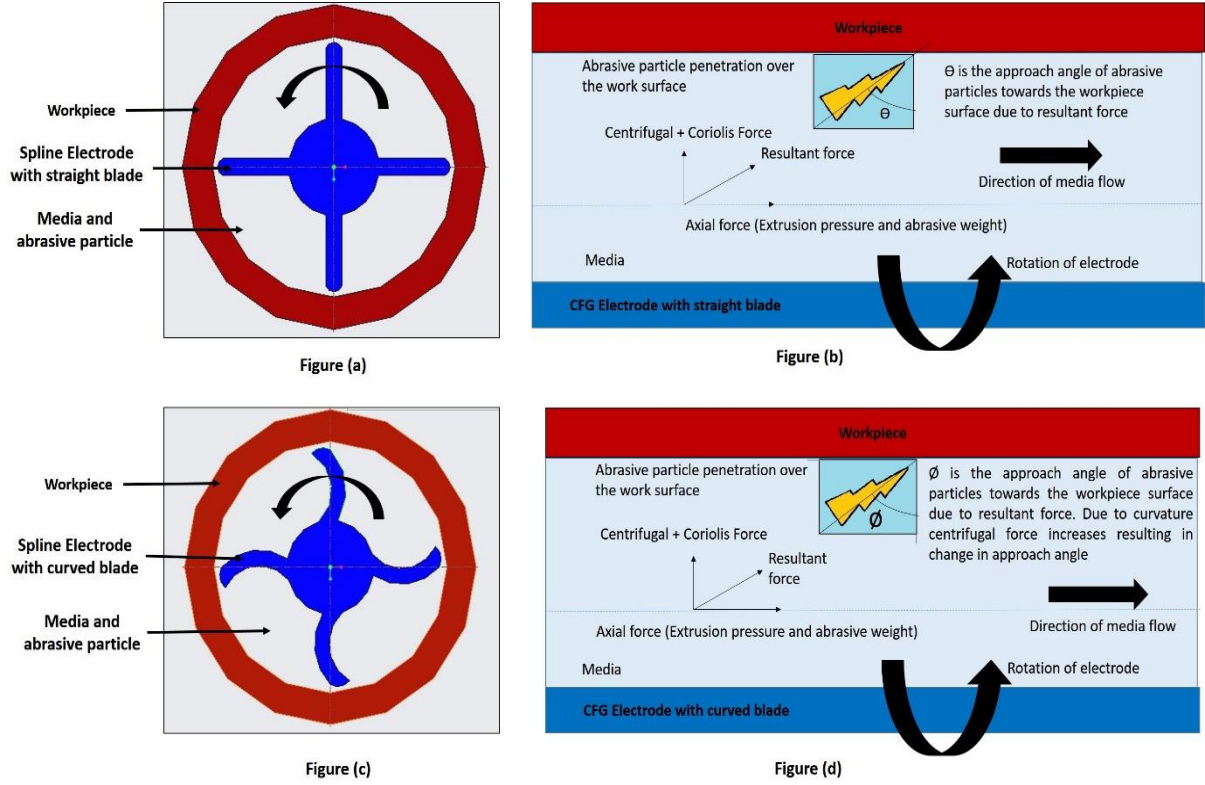


Figure 135 Material removal mechanism of electrode (a) spline shape electrode with straight blade (b) mechanism of material removal with primitive tool (c) Top view of the spline shape electrode with curve blade (d) Mechanism of material removal by proposed electrode

$$MR_{TACAFM} = \rho N \left[\frac{d_g^2}{4} \sin^{-1} \frac{2\sqrt{x \cdot (d_g - x)}}{d_g} - \sqrt{x \cdot (d_g - x)} \cdot \left(\frac{d_g}{2} - x \right) \right] \cdot \sum_{i=1}^{2n} \left[1 - \frac{R_a^f}{R_a^i} \right] \cdot L_w + K \cdot V \cdot I \cdot T_{on} \quad (4)$$

Where ρ is the density of the material, N represents the number of abrasive particle indenting on workpiece per stroke, d_g is the diameter of spherical abrasive particle and x is the length of penetration, n is the number of cycle, R_a^f and R_a^i represents the final and initial surface roughness after and before machining respectively, L_w is the length of workpiece, K is the constant, V is voltage, I is current and T_{on} is the pulse on time. Equation 4 shows the MR is a function of the ratio of final and initial surface roughness obtained after and before machining. The value $\left[1 - \frac{R_a^f}{R_a^i} \right]$ is less than 1 which results in the decrease in MR. Hence with significant increase in R_a value a marginal increase in MR is observed.

As discussed earlier the TACAFM process is combination of two machining process involving thermal and abrasion process. The thermal effect due to spark formation soften the work surface due to which less effort is required for the machining process by the abrasion mechanism. Thus

the desired surface finish and MR is achieved in less number of cycle compared to individual thermal and centrifugal effect where more number of cycles are required for desired machining which increase machining time. Thus the proposed spline shape CFG electrode with the curved blade makes the TACAFM process more efficient by increasing the MR and reducing the machining time.

Summary

- 1. TACAFM is a recent hybrid of AFM which improves MR and reduces machining time compared to the conventional AFM process by combining the advantage of spark energy, centrifugal action and conventional AFM process.**
- 2. The curved blade of the proposed novel electrode increases the centrifugal force on the media compared to straight spline electrode which enhances the MR and improves the surface finish due to increase in the effective number of dynamic abrasive particle on the work surface.**
- 3. The micrograph, SEM and XRD validates the spark generation and machining efficiency of the TACAFM process and justify the use of proposed electrode in the developed TACAFM process.**
- 4. The EDAX analysis shows the presence of oxygen element which verify the spark formation and validates the TACAFM process**

Chapter 8. Conclusion and Future Scope of Work

The present chapter includes the overall conclusions of the study and includes key points of the literature review, media preparation, modelling and simulation, experimental analysis and the results and validation section. The chapter also discussed about the future scope of the study in brief.

8.1. Conclusions

The present study highlights the effects of different geometrical shapes of the centrifugal force generating electrode along with other process parameters on the material removal and percentage improvement in surface finish on TACAFM Process. The ANSYS modelling was done to analyse the flow parameters with different electrode geometry and experiments were performed to compute the optimum values of the process parameters. The following point may be concluded after the simulation and modelling of the process.

1. The RSM result shows the process parameters (electrode type, supply current, duty cycle and rotational speed) are the significant parameters for the TACAFM process
2. The result shows that for computation of MR, electrode type is major contributing factor which contributes about 17.61 percent, followed by supply current 9.23 percent then duty cycle with 2.63 percent and rotational speed as least contributing factor.
3. The result shows that for $\% \Delta R_a$ duty cycle is major contributing factor which contributes about 35.26 percent followed by electrode type which contributes 7.80 percent, followed by supply current and rotational speed which contributes about 2.78 percent.
4. The experimental results show that the spline electrode with the curved blade significantly improves the MR and percentage improvement in surface finish.
5. The average experimental values for the material removal is 50.31 mg and the average experimental value for percentage improvement in surface finish is 42.096 percent.
6. The optimal value for the material removal based on response surface methodology is 51.368 mg and that of the percentage improvement in surface finish is 43.701 percent.
7. The observed value of MR and $\% \Delta R_a$ after the experimentation on optimum parameters are 51.0316 and 43.009 respectively.

8. The percentage error between the predicted and observed experimental value at optimum parameters for the MR is 0.65 percent and that for the percentage improvement in surface finish is 1.58 percent.
9. The percentage error between the predicted and average experimental value for the MR is 2.10 percent and that for the percentage improvement in surface finish is 3.81 percent.
10. The optimal value of parameters for the maximum value of material removal (MR) and the percentage improvement in surface finish ($\%\Delta R_a$) is by taking 2nd type of electrode which is spline shape electrode with the curved blade at the supply current of 7.809 ampere with duty cycle of 0.711 at the rotational speed of 140 rpm.
11. The SEM image shows the molten metal, abrasive and spark marks on the surface which highlights the material removal mechanism as the combination of melting and abrasion process.
12. The variation of XRD pattern of the workpiece before and after machining highlights the change over the workpiece during machining process which may be due to the generation of spark.
13. The Presence of oxygen in the EDAX analysis justify the spark generation during the machining process.
14. When thermal energy is used for material removal during finishing process, thermal energy is dominant in compare to concentration of abrasives which provides a significant material removal compare to AFM.
15. The centrifugal generating electrode (CFG) used in the TACAFM process does two works. Firstly, it provides centrifugal action in the media which directs the abrasive particle towards the wall of the workpiece. Secondly it acts as an anode which is a negative terminal when DC is supplied for the spark generation.
16. The spline shape electrode with straight blade is used in the initial TACAFM process. Different shapes of electrode provide different throwing ability of media hence there is a need to explore the different shape electrodes (straight spline electrode, curved spline electrode, triangular shape electrode, rectangular shape electrode) for the increasing the efficiency of the process.

17. The investigation proposes a new spline shape electrode with the curved blade which is used to increase the centrifugal force in the media which directs the abrasive particles towards the wall of the workpiece, which accelerates the abrasion process, increasing the material removal of the workpiece.
18. The fixture is specially design to cater the rotation of the proposed CFG electrode and to facilitates the spark formation for the combination of EDM and CFAAFM process. Special arrangement for the rotation of electrode and short circuit prevention is taken care during the fixture design.
19. The media used in the process is a mixture of abrasive, polymer and gel in which abrasive provides cutting action, gel provides the viscosity and polymer provides the fluidity to the media.
20. Viscosity is the most prominent property of the media as it holds the abrasive particle during the finishing process. A high viscosity media is desirable for the TACAFM process as the viscosity of media decreases with the increase in temperature. Thus viscosity of various gel (engine oil based gel, Transformer oil based gel, hydrocarbon oil based gel) were tested using rheometer.
21. Hydrocarbon based oil shows the increase in viscosity with the shear rate, compared to engine oil and transformer oil based gel, which can be compensated with the decrease in viscosity during the actual machining process when the thermal energy is added to the media during the spark formation. Hence media based on hydrocarbon oil is consider for experimentation.
22. The FTIR analysis of the media shows the property of dielectric along with the polymeric linkage which is desirable for EDM effect and abrasive flow machining process.
23. The simulation results highlight the feasibility of proposed electrodes in the TACAFM process as shown by the temperature distribution over the workpiece surface. The temperature generated near the edge of the workpiece represents the spark formation due to the EDM effect.
24. The simulation results show that the pressure distribution over the workpiece for TACAFM process is at higher range compare to that of the conventional AFM process

under same working pressure. This increase in pressure results in the increase in the cutting force which interns increase the material removal.

8.2. Future Scope

The present investigation studies the effect of the different geometrical shape of the CFG electrode on the material removal and the percentage improvement in surface finish of the brass workpiece. The study reveals that the spline shape electrode with the curved blade gives the improvement of TACAFM process which can be used in many finishing process. The Process can be directly used for the following future scope.

1. This process can be improved or automated by using servo control hydraulic units.
2. There is need to develop different types of media to obtain better machining effect.
3. The set up can be optimized for many other process parameters like different shapes of work materials, different abrasives, flow rate of media etc.
4. There is need to develop proper fixturing arrangement.
5. Process is limited to conductive materials only.

References

1. V.K. Jain, 2009, Magnetic field assisted abrasive based micro-/nano-finishing, *Journal of Materials Processing Technology*, Volume 209 (20) 6022-6038, <https://doi.org/10.1016/j.jmatprotec.2009.08.015>.
2. Bhardwaj Anant, Ali Parvesh, Walia R.S, Murtaza. Qasim, Pandey S.M, 2019 Development of Hybrid Forms of Abrasive Flow Machining Process: A Review. K. Shanker et al. (eds.), *Advances in Industrial and Production Engineering, Lecture Notes in Mechanical Engineering* pp 41–67. https://doi.org/10.1007/978-981-13-6412-9_5.
3. Walia RS, Shan HS, Kumar P 2006 Parametric optimisation of centrifugal force-assisted abrasive flow machining (CFAAFM) by the Taguchi method. *J Mater Manuf Processes* 21(4). <https://doi.org/10.1080/10426910500411645>
4. Brar B.S, Walia R.S, Singh V.P, Sharma M 2013 A robust helical abrasive flow machining process (HLX-AFM). *J Inst Eng India Ser C* 94(1) 21–29. <https://doi.org/10.1007/s40032-012-0054-9>.
5. Sharma A.K, Venkatesh G, Rajesha S 2015 Experimental investigations into ultrasonic-assisted abrasive flow machining (UAAFMM) process. *Int J Adv Manuf Technol* 80, 477–493. <https://doi.org/10.1007/s00170-015-7009-2>.
6. Sankar MR, Mondal S, Ramkumar J, Jain V 2009 K Experimental investigations and modelling of drill bit guided abrasive flow finishing (DBG-AFF) process. *International Journal of Advance Manufacturing Technology* 42(7–8) 678–688. <https://doi.org/10.1007/s00170-008-1642-y>.
7. Sankar M.K, Jain V.K, Ramkumar J 2010 Rotational abrasive flow finishing process and its effects on a finished surface. *Int J Mach Tools Manuf* 50 (7) 637–650. <https://doi.org/10.1016/j.ijmachtools.2010.03.007>.
8. Singh S, Shan H.S 2002 Development of magneto abrasive flow machining process. *Int J Mach Tools Manufacturing* 42:953–959. [https://doi.org/10.1016/S0890-6955\(02\)00021-4](https://doi.org/10.1016/S0890-6955(02)00021-4).
9. Dabrowski L, Marciniak M, Wieczarek W, Zygmunt A 2006 Advancement of abrasive flow machining using an anodic solution. *J New Mater Electrochem Syst* 9:439–445.
10. Singh R, Walia R.S, Suri N.M 2015 Parametric optimisation of a centrifugal-magnetic force assisted abrasive flow machining process using utility concept. *International Journal Research in Engineering and Technology* 4(8) 2321–2730.
11. Vaishya R, Walia R.S, Kalra P 2015 Design and development of hybrid electrochemical

- and centrifugal force assisted abrasive flow machining. 4th international conference on materials processing and characterisation. *Mater Today Proc* 2:3327–3341. <https://doi.org/10.1016/j.matpr.2015.07.158>.
12. Ali P, Walia RS, Murtaza Q, Singari Ranganath Muttanna 2020 Material removal analysis of hybrid EDM-assisted centrifugal abrasive flow machining process for performance enhancement. *J Braz. Soc. Mech. Sci. Eng.* 42 302. <https://doi.org/10.1007/s40430-020-02375-6>.
 13. Ali Parvesh, Walia R.S, Murtaza Qasim, Ranganath M.S 2020 Modeling and Analysis of developed Thermal Additive Centrifugal Abrasive Flow Machining process, *Surf. Topogr.: Metrol. Prop.* 8 035013. <https://doi.org/10.1088/2051-672X/abaffe>.
 14. Ali Parvesh, Walia RS, Murtaza Qasim, Ranganath Muttanna Singari 2022 Characterization of finished surface through thermal additive centrifugal abrasive flow machining for better surface integrity, *Indian Journal of Engineering & Materials Sciences*, Vol. 29, pp. 29-44. <http://op.niscair.res.in/index.php/IJEMS/article/view/63175/0>.
 15. Walia, R.S, Shan, H.S., Kumar, Pradeep., (2006) Parametric Optimization of Centrifugal Force-Assisted Abrasive Flow Machining (CFAAFM) by the Taguchi Method, *Materials and Manufacturing Processes*, 21:4, 375 382, DOI: [10.1080/10426910500411645](https://doi.org/10.1080/10426910500411645).
 16. Walia, R.S, Shan, H.S., Kumar, Pradeep., (2006) Abrasive flow machining with additional centrifugal force applied to the media, *Machining Science and Technology*, 10:3, 341-354, DOI: [10.1080/10910340600902157](https://doi.org/10.1080/10910340600902157).
 17. Walia, R.S., Shan, H.S. & Kumar, P. Determining dynamically active abrasive particles in the media used in centrifugal force assisted abrasive flow machining process. *Int J Adv Manuf Technol* 38, 1157–1164 (2008). <https://doi.org/10.1007/s00170-007-1184-8>.
 18. Crochet M. J, Davies A.R, Walters K, Numerical simulation of Non Newtonian Flow, *Journal of Non-Newtonian Fluid Mechanics*, (1985), 17, pp. 373-374.
 19. Williams R.E, Rajurkar K.P, Metal removal and surface finish characteristics in Abrasive Flow Machining, New York, U.S.A., American Society of Mechanical Engineers, (1989), 38, pp. 93-106.
 20. Rhoades L.J, Abrasive Flow Machining of cylinder heads and its positive effect on performance and cost characteristics, SAE Technical Paper Series [SAE International Motorsports Engineering Conference & Exposition, (1996), 1, pp. 49-53.

21. Petri Kimberly L, Billo Richerd E, Bidanda Bopaya, A neural network process model for abrasive flow machining operations, *Journal of manufacturing system*, (1998), 17.
22. Jain R K, Jain V K (a), Abrasive fine finishing processes – a review, *Int. J. Mf. Sci. Prod.* (1999), 2, pp. 61-69.
23. Singh S, Shan H.S, Development of magneto abrasive flow machining process, *International Journal of Machine Tool & Manufacture*, (2002), 42, pp. 953-959.
24. Singh S, Shan H. S, Kumar P, Effects of magnetic field on abrasive flow machining. *Proc. 12th Int. DAAAM Symposium Jena, Germany, October*, (2001)
25. Singh Sehijpal, Shan H. S, Kumar. P, Wear behavior of materials in magnetically assisted abrasive flow machining, *Journal of Materials Processing Technology*, (2002), 128, pp. 155–161.
26. Gorana V. K, Jain V. K, Lal G. K, Experimental investigation into cutting forces and active grain density during abrasive flow machining, *International Journal of Machine Tools & Manufacture*, (2004), 44, pp. 201–211.
27. Jain N.K, Jain V.K, Jha. S, Parametric optimization of advance fine finishing processes, *International Journal of Advanced Manufacturing Technology*, (2007), 34(11-12), pp. 1191-1213.
28. Singh S, Chhabra R, Shan H. S, Kumar P, Time series modeling of surfaces produced by flow of magnetic abrasives, *Proc SECTAS, D.E.I. Dayalbagh, Agra, India*, (2002), pp 450-455.
29. Singh S, Shan H. S, Kumar P, Effects of magnetic field on abrasive flow machining. *Proc. 12th Int. DAAAM Symposium Jena, Germany, October*, (2001).
30. Gorana V. K, Jain V. K, Lal G. K (a), Forces prediction during material deformation in Abrasive Flow Machining, *Wear*, (2006) , 260, pp. 128–139.
31. Gorana V. K, Jain V. K, Lal G. K (b), Prediction of surface roughness during Abrasive Flow Machining, *Int J Adv Manuf Technology*, (2006), 31, pp. 258–267.
32. Dabrowski L, Marciniak M, Szewczyk T , Analysis of abrasive flow machining with an electrochemical process aid, *Proc. Institution of Mechanical Engineers*, (2006), 220, pp. 397-403.
33. Tzeng Hsinn Jyh, Yan Biing-Hwa, Hsu Rong Tzong, Lin Yan Cherng, Self-modulating abrasive medium and its application to abrasive flow machining for finishing microchannel surface, *International journal of Advance manufacturing technology*, (2007), 32, pp. 1163–1169.

34. Wang A.C, Weng S.H, Developing the polymer abrasive gels in AFM process, *Journal of Materials Processing Technology*, (2007), 192–193, pp. 486–490.
35. Wani A. M, Yadava Vinod, Khatri Atul, Simulation for the prediction of surface roughness in magnetic abrasive flow finishing (MAFF), *Journal of Materials Processing Technology*, (2007), 190, pp. 282–290.
36. Fang Liang, Sun Kun, Cen Qihong, Particle movement patterns and their prediction in abrasive flow machining, *Tribotest*, (2007), 13, pp. 195–206.
37. Fang Liang, Zhao Jia, Sun Kun, Zheng Degang, Ma Dexin, Temperature as sensitive monitor for efficiency of work in abrasive flow machining, *Wear*, (2009), 266, pp. 678–687.
38. Das Manas, Jain V.K, Ghoshdastidar P.S, Fluid flow analysis of magnetorheological abrasive flow finishing (MRAFF) process, *International Journal of Machine Tools & Manufacture*, (2008), 48, 415–426.
39. Das Manas, Jain V.K, Ghoshdastidar P.S, Nanofinishing of flat workpieces using rotational–magnetorheological abrasive flow finishing (R-MRAFF) process, *The International Journal of Advanced Manufacturing Technology*, (2012), 62(1-4), pp. 405-420.
40. Walia R. S, Shan H. S, Kumar. P (a), Determining dynamically active abrasive particles in the media used in centrifugal force assisted abrasive flow machining process, *Int J Adv Manuf Technology*, (2008), 38, pp.1157–1164.
41. Walia R.S, Shan H. S, Kumar. P (a) Enhancing AFM process productivity through improved fixturing, *Int J Adv Manuf Technology*, (2009), 44, pp. 700–709.
42. Walia R. S, Shan H. S, Kumar. P (b), Morphology and integrity of surfaces finished by centrifugal force assisted abrasive flow machining, *Int J Adv Manuf Technology*, (2008), 39, pp.1171–1179.
43. Walia R S, Shan H S, Kumar P (b), Modelling of centrifugal-force-assisted abrasive flow machining, *Proc. IMechE, Part E: J. Process Mechanical Engineering*, (2009), 223, pp.195-204.
44. Sankar M.R, Jain V.K, Ramkumar J, Joshi Y.M, Rheological characterization of styrene-butadiene based medium and its finishing performance using rotational abrasive flow finishing process, *International Journal of Machine Tools & Manufacture*, (2011) ,51, pp. 947–957. 170.

45. Sankar M.R, Jain V.K, Ramkumar J, Rotational abrasive flow finishing process and its effects on finished surface, *International journal of machine tools and manufacture*, (2010), 50 (7), pp. 637-650.
46. Sankar M.R, Jain V.K, Ramkumar J, Abrasive Flow Machining (AFM): An Overview, *Indo-US Workshop on Smart Machine Tools, Intelligent Machining Systems and Multi-scale Manufacturing*, December, (2008).
47. Sankar M. R, Jain V. K, Ramkumar J, Experimental investigations into rotating workpiece abrasive flow finishing, *Wear*, (2009), 267 (1-4), pp. 43-51.
48. Uhlmann E, Modelling the AFM process on advanced ceramic materials. *Journal of materials processing technology*, (2009), 209 (20), pp. 6062-6066.
49. Uhlmann E, Mihotovic V, Roßkamp S, Dethlefs A, A pragmatic modelling approach in Abrasive Flow Machining for complex shaped automotive components, *7th HPC 2016 – CIRP Conference on High Performance Cutting, Procedia CIRP*, (2016), 46, pp. 51 – 54.
50. Wang A.C, Cheng K.C, Chen K.Y, Lin Y.C, Enhancing the Surface Precision for the Helical Passageways in Abrasive Flow Machining, *Materials and Manufacturing Processes*, (2014), 29, pp. 153–159.
51. Wang A.C, Lee S.J, Study the characteristics of Magnetic finishing with gel Abrasives, *International Journal of Machine Tools & Manufacture*, (2009), 49, pp. 1063–1069.
52. (a) Kar Kamal K, Ravikumar N. L, Kumar Piyush, Tailor B, Ramkumar J, Sathiyamoorthy D, Performance evaluation and rheological characterization of newly developed butyl rubber based media for abrasive flow machining process, *Journal of Materials Processing Technology*, (2009), 209 (4), pp. 2212-2221.
53. Kar K. K, Ravikumar N L, Tailor P.B, Ramkumar J, Saathiyamoorthy D, Preferential media for abrasive flow machining, *Journal of Manufacturing Science and Engineering*, (2009), 131(1), doi:10.1115/1.3046135.
54. Mali H.S, Manna Alakesh, Optimum selection of abrasive flow machining conditions during fine finishing of Al/15 wt.% Sic-MMC using Taguchi method, *International Journal of Advanced Manufacturing Technology*, (2010), 50, pp. 1013–1024.
55. Jang Kyung-In, Seok Jong won, Min Byung-Kwon, Lee Sang Jo, An electrochemomechanical polishing process using magnetorheological fluid, *International Journal of Machine Tools and Manufacture*, (2010), 50 (10), pp. 869-881.

56. Rajesha S, Venkatesh G, Sharma A.K, Kumar Pradeep, Performance study of a natural polymer based media for abrasive flow machining, *Indian Journal of engineering and Materials Sciences*, (2010), 17, pp. 407-413.
57. Sharma A. K, Kumar P, Rajesh S, An improved ultrasonic abrasive flow machining. Patent number 3578/DEL/201, India (2011).
58. Bähre, Dirk & Brünnet, Horst & Swat, Martin. (2012). Investigation of One-way Abrasive Flow Machining and In-process Measurement of Axial Forces. *Procedia CIRP*. 1. 419–424. 10.1016/j.procir.2012.04.075.
59. Brar B. S, Walia R. S, Singh V. P, Sharma M, A robust helical abrasive Flow machining process (HLX-AFM), *J. Inst. Eng. India Ser. C*, (2013), 94(1), pp. 21–29.
60. Howard Mitchell, Cheng Kai, An industrially feasible approach to process optimisation of abrasive flow machining and its implementation perspectives, *Proc. IMechE Part B: Journal of Engineering Manufacture*, (2013), 227 (11), pp. 1748-1752.
61. Gao H, Fu Y.Z, Zhu J.H, Wu M.Y, Sun Y.W, Study on the characteristics of new abrasive medium for Abrasive Flow Machining, *Advanced Materials Research*, (2013), 797, pp. 417-422.
62. Schmitt Joachim, Diebels Stefan, Simulation of the Abrasive Flow Machining process, *ZAMM · Z. Angew. Math. Mech.*, (2013), 93(2 – 3), pp. 147 – 153.
63. Wan S, Ang Y. J, Sato T, Lim G. C, Process modelling and CFD simulation of two-way abrasive flow machining, *International journal of Advance manufacturing technology*, (2014), 71, pp. 1077–1086.
64. Kenda J, Duhovnik J, Tavčar J, Kopač J, Abrasive flow machining applied to plastic gear matrix polishing, *The International Journal of Advanced Manufacturing Technology*, (2014), 71, (1–4), pp. 141–151.
65. Sooraj V. S, Radhakrishnan V, Fine finishing of internal surfaces using elastic abrasives *International Journal of Machine Tools and Manufacture*, (2014), 78, pp. 30-40.
66. Ibrahim Abbas F, Saad Kariem, Hamdan Wissam K, Studying Abrasive Flow Machining Conditions by Using Taguchi Method, *Eng&Tech. Journal*, (2014), 32 (4).
67. Swat Martin, Brunnet Horst, Lyubenova Nataliya, Schmitt Joachim, Diebels Stefan, Bahre Dirk, Improved process control and model of axial forces of one way Abrasive Flow Machining, 6th CIRP International Conference on High Performance Cutting, HPC2014, *Procedia CIRP*, (2014), 14, pp. 19 – 24.

68. Brar B. S, Walia R. S, Singh V. P, Electrochemical-aided abrasive flow machining (ECA2FM) process: a hybrid machining process, *Int J Adv Manuf Technology*, (2015), 79, pp. 329–342.
69. Gupta Ravi, Chahal Balinder, Investigation and Optimization of Process Parameters in Electrochemical Aid Abrasive Flow Machining, *International Journal of Scientific and Engineering Research*, (2015), 6.
70. Mittal Sushil, Kumar Vinod, Kumar Harmesh, Experimental Investigation and Optimization of Process Parameters of Al/Sic MMC Finished by Abrasive Flow Machining, *Materials and manufacturing processes*, (2015), 30 (7), pp. 902-911.
71. Venkatesh G, Sharma A. K, Kumar Pradeep (a), On ultrasonic assisted abrasive flow finishing of bevel gears, *International Journal of Machine Tools & Manufacture*, (2015), 89, pp. 29–38.
72. Venkatesh Gudipadu, Sharma A. K, Singh Nitish (b), Simulation of media behaviour in vibration assisted abrasive flow machining, *Simulation Modelling Practice and Theory*, (2015), 51, pp. 1–13.
73. Dong Zhiguo, Ya Gang, Liu Jiancheng, Study on machining mechanism of high viscoelastic abrasive flow machining for surface finishing, *Proc. IMechE Part B: Journal of Engineering Manufacture*, (2015), 231 (4), pp. 608-617.
74. Bremerstein Tina, Potthoff Annegret, Michaelis Alexander, Schmiedel Christian, Uhlmann Eckart, Blug Bernhard, Amann Tobias, Wear of abrasive media and its effect on Abrasive Flow Machining results, *Wear*, (2015), 342-343, pp. 44–51.
75. Fu Youzhi, Wan Xuanping, Gao Hang, Wei Haibo, Li Shichong, Blade Surface Uniformity of blisk finished by Abrasive Flow Machining, *Int J Adv Manuf Technology*, (2016), 84, pp. 1725–1735.
76. Singh Sachin, Raj Arjun A.S, Sankar M.R, Jain V.K, Finishing force analysis and simulation of nanosurface roughness in abrasive flow finishing process using medium rheological properties, *Int J Adv Manuf Technol*, (2016), 85, pp. 2163–2178.
77. Kumar Sonu, Murtaza Qasim, Walia R.S, Dhull S, Tyagi P. K, Synthesis CNTs Particle Based Abrasive Media for Abrasive Flow Machining Process, 5th National Conference on Processing and Characterization of Materials, Materials Science and Engineering, (2016), 115, doi:10.1088/1757-899X/115/1/012034.
78. Wu M.Y, Gao H, Experimental study on large size bearing ring raceway's precision polishing with Abrasive Flowing Machine (AFM) method, *Int J Adv Manuf Technology*, (2016), 83, pp.1927–1935.

79. Marzban Mohammad Ali, Hemmati Seyed Jalal, Modelling of abrasive flow rotary machining process by artificial neural network, *International Journal of Advanced Manufacturing Technology*, (2017), 89, pp.125–132.
80. Cheng Kai, Shao Yizhi, Bodenhurst Rodrigo, Jadv Mitul, Modeling and Simulation of Material Removal Rates and Profile Accuracy Control in Abrasive Flow Machining of the Integrally Bladed Rotor Blade and Experimental Perspectives, *J. Manuf. Sci. Eng.*, (2017), 139(12), doi: 10.1115/1.4038027.
81. Kheradmand Saeid, Esmailian Mojtaba, Fatahy A, Numerical simulation of the combination effect of external magnetic field and rotating workpiece on abrasive flow finishing, *Journal of Mechanical Science and Technology*, (2017), 31 (4), pp. 1835-1841.
82. Singh Sachin, Kumar Deepu, Sankar M.R., Experimental, Theoretical, and Simulation Comparative Study of Nano Surface Roughness Generated During Abrasive Flow Finishing Process, *J. Manuf. Sci. Eng.*, (2017), 139(6), doi: 10.1115/1.4035417.
83. Li Junye, Su Ningning, Weihong Zhao, Yi Yanlu, Hu Jinglie, Study on the polishing of curved pipe parts by solid liquid two phase abrasive flow, *Journal of Measurements in Engineering*, (2017), 5(2), pp. 59-67.
84. Mohammadian Neda, Turenne Sylvain, Brailovski Vladimir, Surface finish control of additively-manufactured Inconel 625 components using combined chemical-abrasive flow polishing, *Journal of Materials Processing Tech.*, (2018), 252, pp. 728–738.
85. Li Jun Ye, Wang Bin Yu, Wu Guiling, Hu Jing Lei, *Materials Science and Engineering*, (2018), 382, doi:10.1088/1757-899X/382/4/042003.
86. Wei Haibo, Peng Can, Gao Hang, Wang Xuanping, Wang Xuyue, On establishment and validation of a new predictive model for material removal in Abrasive Flow Machining, *International Journal of Machine Tools and Manufacture*, *International Journal of Machine Tools and Manufacture*, (2019), 138, pp. 66–79.
87. Ali, P., Walia, R. S., Rastogi, V., & Tyagi, M. (2016). Modelling of CNT particles based abrasive laden media used for abrasive flow machining. In *Proceedings of 6th International & 27th All India Manufacturing Technology, Design and Research Conference* (pp. 178-183).
88. Ali P, Pandey S.M, Ranganath M.S, Walia R.S, Murtaza Q 2020 Experimentation and modelling of CNT additive abrasive media for micro finishing, *Measurement*.15 1 107 133. <https://doi.org/10.1016/j.measurement.2019.107133>.

89. Basha SM, Venkaiah N, Sankar MR (2023) Development and performance evaluation of Galactomannan polymer based abrasive medium to finish atomic diffusion additively manufactured pure copper using abrasive flow finishing, additive Manufacturing 61 (2023) 103290. <https://doi.org/10.1016/j.addma.2022.103290>.
90. Yadav Pawan, Jayswal SC (2019) Study of Media in AFM and its Hybrid Processes. Materials Today, Proceedings 18 3017–3026. <https://doi.org/10.1016/j.matpr.2019.07.173>.
91. Dixit Nitin, Sharma Varun, Kumar Pradeep (2021) Development and characterisation of Xanthan Gum based abrasive media and performance analysis using abrasive flow machining. Journal of Manufacturing Processes 67 101–115. <https://doi.org/10.1016/j.jmapro.2021.04.053>.
92. Zhang, Zhenzhong, Zhang Xianpeng, Liu Xiao, Zhou Peifa, Yao Peng, Huang Chuanzhen, Liu Hanlian, Zhu Hongtao, Bin Zou (2020) Preparation and Application of a Novel Water-Based Viscoelastic Polishing Fluid for Abrasive Flow Machining. CIRP Bio Manufacturing Conference. <https://doi.org/10.1016/j.procir.2020.05.153>.
93. Ahmad S, Singari RM, Mishra RS (2021) Development of Al₂O₃-SiO₂ based magnetic abrasive by sintering method and its performance on Ti-6Al-4V during magnetic abrasive finishing. Transactions of the IMF, 99(2), 94-101. <https://doi.org/10.1080/00202967.2021.1865644>.
94. Zhang Baocai, Qiao Yu, Khiabani Nasim, Wang Xinchang. (2022) Study on rheological behaviors of media and material removal mechanism for abrasive flow machining (AFM) micro structures and corresponding simulations, Journal of Manufacturing Processes 73 248–259, <https://doi.org/10.1016/j.jmapro.2021.11.006>.
95. Li, Zhen., Liu, Xiaokang., Jia, Haili., Yu, Jianhong., Cai, Yujun., Li, Guohe (2023) Study on the temperature field in the cutting zone for machining monocrystalline silicon wafer using free abrasive multi-wire saw, Materials Science in Semiconductor Processing 161, 107481. <https://doi.org/10.1016/j.mssp.2023.107481>.
96. Basha, S.M., Sankar, M.R., Venkaiah, N (2023) Experimental investigation on deballing and surface finishing of selective laser melted 18Ni300 steel using polymer rheological abrasive medium, Wear 523 (2023) 204813. <https://doi.org/10.1016/j.wear.2023.204813>.
97. Zhuang, Kejia., Wan, Liyang., Weng, Jian., Wu, Zhizheng., Zhang, Yuhua., Tian, Chengjin., Yang, Yan (2023) A new elastic abrasive jet machining method for post–

treatment of tool coatings: A case study on TiAlN coated tools for titanium machining, *Tribology International* 185 (2023) 108533. <https://doi.org/10.1016/j.triboint.2023.108533>.

98. Feng, Ming., Wu, Yongbo., Wang, Youliang., Zeng, Jiang., Bitoh, Teruo., Nomura, Mitsuyoshi., Fujii, Tatsuya. Effect of the components of Magnetic Compound Fluid (MCF) slurry on polishing Characteristics in aspheric-surface Finishing With The doughnut-shaped MCF tool. *Precision Engineering* 65 (2020) 216–229. <https://doi.org/10.1016/j.precisioneng.2020.04.02>.
99. Srinivas, K., Murtaza, Q. and Aggarwal, A.K., 2019. Effect of Shape of Magnet on the Machining of Workpiece. *International Journal of Recent Technology and Engineering (IJRTE)*, ISSN, pp.2277-3878.
100. Srinivas, k., Murtaza, Q., Aggarwal, A.K 2019 Effect of permanent magnetic pole orientation on field strength in viscoelastic magnetic abrasive finishing process, *International Journal of Mechanical and Production Engineering Research and Development (IJMPERD)* ISSN (P): 2249–6890; ISSN (E): 2249–8001 Vol. 9, Issue 5, Oct 2019, 43–52.
101. Ansari, Irfan.Ahmad., Kar, Kamal. K., Ramkumar, J (2023) Effect of ground tire rubber media's viscoelasticity and flow passage geometry on the abrasive flow finishing of helical gear, *Journal of Manufacturing Processes* 101 (2023) 219–233. <https://doi.org/10.1016/j.jmapro.2023.06.012>.
102. Kuma CW, Wu CH, Wan S, Kang CW (2020) Prediction and compensation of material removal for AFM of additively manufactured metal components, *Journal of Materials Processing Tech.* <https://doi.org/10.1016/j.jmatprotec.2020.116704>.
103. A. Wahab Hashmi, H. Singh Mali, A. Meena (2022) Experimental investigation on AFM (AFM) of FDM printed hollow truncated cone parts, *Materials Today: Proceedings*. 56 1369–1375. <https://doi.org/10.1016/j.matpr.2021.11.428>.
104. Han Sangil, Ferdinando Salvatore, Joël Rech, Bajolet Julien (2020) AFM(AFM) finishing of conformal cooling channels created by selective laser melting (SLM). <https://doi.org/10.1016/j.precisioneng.2020.03.006>.
105. Han Sangil, Salvatorea Ferdinando, Recha Joël, Bajoletb Julien, Courbon Joël (2020). Effect of AFM (AFM) finish of selective laser melting (SLM) internal channels on fatigue performance, *Journal of Manufacturing Processes* <https://doi.org/10.1016/j.jmapro.2020.09.065>.

106. Ganesan, Narendran., Mallikarjuna, B., Nagesha, B.K., Gnanasekaran, N (2022) Experimental investigation on additive manufactured single and curved double layered microchannel heat sink with nano fluids, Heat and Mass Transfer. <https://doi.org/10.1007/s00231-022-03336-6>.
107. Goyal Aneesh, Singh Harvinder, Goyal Rachin, Singh Rajdeep, Singh Swarn (2022) Recent advancements in AFM and abrasive materials: A review, Materials Today: Proceedings 56 3065–3072. <https://doi.org/10.1016/j.matpr.2021.12.109>.
108. Singh Swarn, Kumar Harish, Kumar Santosh, Chaitanya Saurabh (2022) A systematic review on recent advancements in Abrasive Flow Machining (AFM). Materials Today: Proceedings 56 3108–3116. <https://doi.org/10.1016/j.matpr.2021.12.273>.
109. Mohseni-Mofidi S, Pastewka L, Teschner M, Bierwisch C (2022) Magnetic-assisted soft AFM studied with smoothed particle hydrodynamics, Applied Mathematical Modelling. 101 38–54. <https://doi.org/10.1016/j.apm.2021.07.015>
110. Manjunath M.A, Vinod, Prakash, N Balashanmugam, MR Sankar (2020) Abrasive flow finishing for surface roughness improvement of aluminium propeller: A case study. Materials Today: Proceedings, 26 1113–1118. <https://doi.org/10.1016/j.matpr.2020.02.223>.
111. Rajendra Baraiya, Atul, Babbar, Vivek Jain, Dheeraj Gupta (2020) In-situ simultaneous surface finishing using AFM via novel fixture. Journal of Manufacturing Processes, Journal of Manufacturing Processes, 50 266–278. <https://doi.org/10.1016/j.jmapro.2019.12.051>.
112. Fu Youzhi, Gao Hang, Yan Qiusheng, Wang Xuanping (2019) A new predictive method of the finished surface profile in abrasive flow machining process. Precision Engineering, 60 497–505. <https://doi.org/10.1016/j.precisioneng.2019.08.011>.
113. Ahmad S, Gangwar S, Yadav PC, Singh DK (2017) Optimisation of process parameters affecting surface roughness in magnetic abrasive finishing process. Materials and Manufacturing Processes, 32(15), 1723-1729. <https://doi.org/10.1080/10426914.2017.1279307>.
114. Anant. Bhardwaj, computational and experimental analysis of parameters in centrifugal force assisted abrasive flow machining process, Diss. 2019, Delhi Technological University.

115. Krishna Gautam G, N Jinesh (2020) Optimisation of process parameters in abrasive flow machining of SS 304L using Taguchi method and grey relation analysis. *Materials Today: Proceedings* 58, 335–338. <https://doi.org/10.1016/j.matpr.2022.02.240>.
116. Srinivas Krovvidi, Bharadwaj Anant (2018) Pressure Variation in Abrasive Flow Machining: Modelling and Simulation. *IJAPIE-2018-10-423*, ISSN: 2455–8419. Vol 3 (4), 15-19.
117. Srinivas K, Murtaza Q, Aggarwal A.K (2019). Modelling of Viscoelastic Fluid in Finishing Processes. *International journal of scientific & technology research* volume 8, ISSUE 09, ISSN 2277-8616.
118. Quacquarelli, A., Mollon, G., Commeau, T., Fillot, N (2022) Combining discrete and continuum mechanics to investigate local wear processes induced by an abrasive particle flow, *Tribology International* 179 (2023) 108126, <https://doi.org/10.1016/j.triboint.2022.108126>.
119. Kumar, Som., Singh, Karamjit., Brar, B.S., Kumar, Rakesh (2022) Effect of processing condition on abrasive flow machining process: A review, *Materials Today: Proceedings*, <https://doi.org/10.1016/j.matpr.2022.12.237>.
120. Malpotra, Anil., Singh, Beant, Singh, Lakhvir (2023) Electrolytic magnetic abrasive finishing process – A review, *Material today proceeding*, <https://doi.org/10.1016/j.matpr.2023.03.237>.
121. Ali, Parvesh., Ranganath, M.S., Walia, R.S., Murtaza, Q (2018) optimization of micro hardness of finished surface in spark assisted abrasive flow machining, *International Journal of Mechanical and Production Engineering Research and Development (IJMPERD)*, Vol. 9, Issue 2, 415-424.
122. Manikandan, R., Ponnusamy, Prasanth., Nanthakumar, S., Gowrishankar, A., Balambica, V., Girimurugan, R., Mayakannan, S (2023) Optimization and experimental investigation on AA6082/WC metal matrix composites by abrasive flow machining process, *Materials Today: Proceedings*, <https://doi.org/10.1016/j.matpr.2023.03.274>.
123. Bi, Guangyue., Li, Yuzhu., Lai, Min., Fang, Fengzhou (2023) Mechanism of polishing lutetium oxide single crystals with polyhedral diamond abrasive grains based on molecular dynamics simulation, *Applied Surface Science* 616 (2023) 156549. <https://doi.org/10.1016/j.apsusc.2023.156549>.
124. Sharma, Anushka., Chawla, Himagra., Srinivas, Krovvidi (2023) Prediction of Surface Roughness of Mild Steel finished with Viscoelastic Magnetic Abrasive Medium.

EVERGREEN Joint Journal of Novel Carbon Resource Sciences & Green Asia Strategy, Vol. 10, Issue 02, pp1061-1067.

125. Mehta, S., Gauba, P., Kaushal, S., Ali, P., Dhanda, M., Walia, R.S. (2023). Developments in Hybrid Abrasive Flow Machining: A Review on Models and Analyses. In: Maurya, A., Srivastava, A.K., Jha, P.K., Pandey, S.M. (eds) Recent Trends in Mechanical Engineering. Lecture Notes in Mechanical Engineering. Springer, Singapore. https://doi.org/10.1007/978-981-19-7709-1_38.
126. Ali Parvesh., Ranganath, M.S., Walia, R.S., Murtaza, Qasim., 2019 Various developments in Abrasive Flow Machining Process: A Review, IJAPIE-2019-04-234, Vol 4 (2), 20-26. <https://doi.org/10.35121/ijapie201904234>.
127. Choopani, Yahya., Razfar, Reza Mohammad., Khajehzadeh, Mohsen., Khosrojerdi, Mohammadreza. (2022) Design and development of ultrasonic assisted-rotational magnetorheological abrasive flow finishing (UA-RMRAFF) process, Applied Acoustics 197 108950. <https://doi.org/10.1016/j.apacoust.2022.108950>.
128. Kohut T (1988) Surface finishing with Abrasive flow machining, SME Technical Paper Proc. 4th International Aluminium extraction Technology seminar, Washington D.C. 35–42.
129. Gaurav, Purnashis Chakraborty, Vejendla, Prasad SB (2022) Deformation and annealing of brass. Materials Today: Proceedings 64 1380–1383, <https://doi.org/10.1016/j.matpr.2022.04.502>.
130. M.-A.H. Al-Akhras, M.K.H. Qaseer, B.A. Albiss, M.A. Alebrhim, U.S. Gezawa, Investigation of composition and structure of spongy and hard bone tissue using FTIR spectroscopy, XRD and SEM, IOP Conf. Ser.: Mater. Sci. Eng. 305 (2018) 012010. <https://doi.org/10.1088/1757-899X/305/1/012010>.
131. Liu Shixian, Kimura Shogo, Okada Akira, Kitamura Tomohiko (2022) Optimization of Dielectric Oil Viscosity for High-precision Wire EDM. Procedia CIRP 113 244–249. <https://creativecommons.org/licenses/by-nc-nd/4.0>.
132. Chen KY, Wang AC, Cheng KC, Chen HM, Lin YC (2020) Study of the Characteristics of EDM by using silicone oils as dielectric. Procedia CIRP 95 454–459. <http://creativecommons.org/licenses/by-nc-nd/4.0/>
133. Patil, suraj., Kulkarni, Raviraj., Patil, Maharudra., Malik, Vinayak. Raghunath. (2023) Investigations on material removal and tool wear rate of silver nanoparticles coated copper electrodes for electric discharge machining, Advances in Materials and Processing Technologies. DOI: [10.1080/2374068X.2023.2194519](https://doi.org/10.1080/2374068X.2023.2194519).

Research Publications in SCI/SCIE Journals

1. Bhardwaj, A., Srinivas, K. & Chaudhary, R. Novel electrode for thermal additive centrifugal force-assisted abrasive flow machining. **J Braz. Soc. Mech. Sci. Eng.** **45**, 583 (2023). <https://doi.org/10.1007/s40430-023-04504-3>.
2. Bhardwaj A, Srinivas K, Chaudhary R. Analysis of thermal additive centrifugal abrasive flow machining process with improved electrode geometry. **Proceedings of the Institution of Mechanical Engineers, Part E: Journal of Process Mechanical Engineering**. 2023;0(0). doi:[10.1177/09544089231195171](https://doi.org/10.1177/09544089231195171).
3. Bhardwaj, Anant., Srinivas, Krovvidi., Chaudhary, Rajiv. (2023). Analysis of Shapes of Centrifugal Force- Generating Rod in Centrifugal Force-Assisted Abrasive Flow Machining Process , **MAPAN-Journal of Metrology Society of India** (June 2023) 38(2):459–479 <https://doi.org/10.1007/s12647-023-00626-0>.
4. Bhardwaj, Anant., Srinivas, Krovvidi., Chaudhary, Rajiv. (2021). Modelling of Wind Turbine Magnet for magnetic force Finishing and Magnetic Force assisted Abrasive Flow Machining Process. **Journal of Engg. Research ICARI Special Issue** pp. 121-130. ISSN 2307-1877. <https://doi.org/10.36909/jer.ICARI.15291>.
5. Bhardwaj, A., Srinivas, K. & Chaudhary, R. Morphology of Finished Brass Surface by Thermal Additive Centrifugal Abrasive Flow Machining Process Using Novel Electrode. **JOM** (2023). <https://doi.org/10.1007/s11837-023-06220-8>

Publication in scopus/ peer review

1. Bhardwaj, Anant., Srinivas, Krovvidi. (2018). Pressure variation in Abrasive Flow Machining. **IJAPIE** ISSN 0972-3641-2018-10-423, Vol 3 (4), 15-19.
2. Bhardwaj, Anant., Srinivas, Krovvidi., Chaudhary, Rajiv. (2021). Modelling and Simulation of Abrasive Flow Machining. **IJAPIE**- ISSN 2455-8419-04-251, Vol 6 (2), 01-09, <https://doi.org/10.35121/ijapie202104251>.

Conferences attended

1. “International Conference On Recent Advances in Fluid Mechanics”, held at Manipal Institute of Technology, MAHE, Manipal, from 4 to 6th October 2022. Title of paper presented – Engine oil based polymer gel preparation for Thermal Additive Centrifugal Force Assisted Abrasive Flow Machining Process.
2. Fourth International Conference On “Computational Experimental Methods in

Mechanical Engineering”, dated 9 to 11 February 2023 organized by GL Bajaj Institute of Technology and Management, Greater Noida, UP India. Title of paper presented – Media Gel optimization for Thermal Additive Centrifugal Abrasive Flow Machining.

3. Second international conference on “Recent Innovations in Engineering Management and Pharmacy”, held on 24th and 25th February 2023 at IEC Group of Institutions, Greater Noida. Title of paper presented – Feasible shapes of centrifugal force generating electrode in thermal additive centrifugal Abrasive flow machining process.